

C 0165
A-617

2016 / Volume 54 / Number 2

ISSN 1641-4640

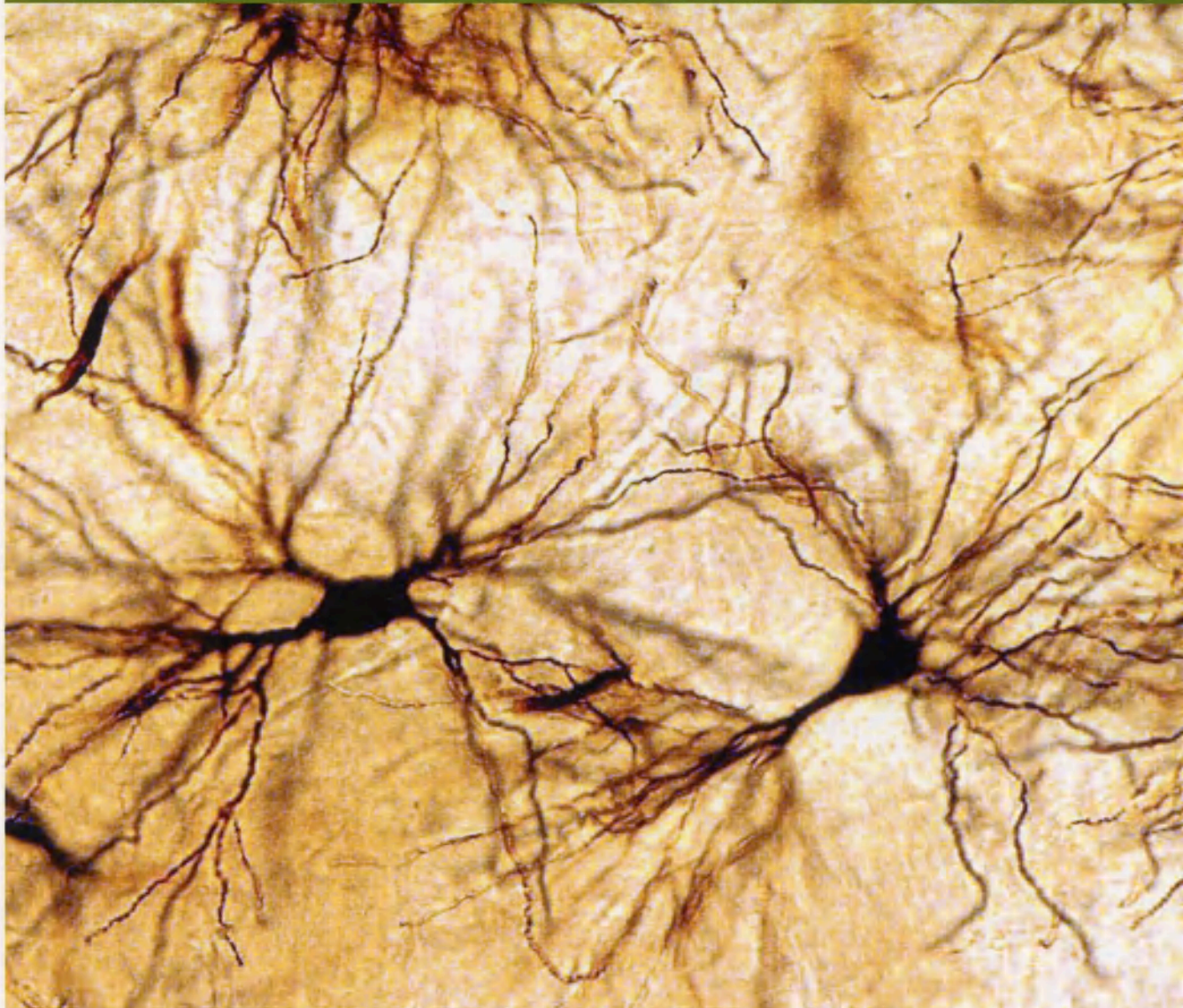


Folia

www.folianeuro.termedia.pl

NEUROPATHOLOGICA

Official Journal of Mossakowski Medical Research Centre Polish Academy of Sciences
and
Polish Association of Neuropathologists



ISSN 1641-4640



9 771641 464629

<http://rcin.org.pl>

w. 713

Folia

NEUROPATHOLOGICA

Folia

Neuropathologica



Editorial Board

Editor in Chief

Editorial Board

Associate Editor

Editorial Office

Neurological Medical Research Centre
The Academy of Medicine
ul. Krakowska 26
00-908 Warszawa
tel: +48 22 628260 00
fax: +48 22 628260 02

Editorial Board

- David A. Brown (Calgary)
- Robert Brown (London)
- Stanislaw Czerniak (Warsaw)
- Robert Darian (Warsaw)
- Wojciech Cwiklinski (Warsaw)
- Caroline Craft (Stockholm)
- Peter Dworkowski (Warsaw)
- Matti Haltia (Helsinki)
- Elisbeth Koga (New York)
- Andrzej Kościński (Warsaw)
- Pawel Kujawa (Gdansk)
- David Lewis (Boston, MA)
- Walter Linker (New Orleans)
- Arzy Łachowicz (Warsaw)
- Danuta Malinska (Warsaw)
- Janusz Maryl (Gdansk)
- Shun-ichi Nagamura (Kobe)
- Yngve Olsson (Uppsala)
- Wiesław Papierz (Gdansk)
- Jana Rafajová (Warsaw)
- Nikola Ruzić-Terzić (Belgrade)
- Harvey B. Sarnat (Calgary)
- Janina Strojnowska (Warsaw)
- Janina Szmal (Poznań)
- Hirotoshi Takamori (Kyoto)
- Xiaofei Wang (Indianapolis)
- Teresa Wroblewska (Gdansk)

Printed in partly biodegradable paper
by the Faculty of Science and Higher Education

Termedia

Advertising House
ul. Piłsudskiego 653 Poznań, Poland
tel: +48 61 822 77 01
fax: +48 61 822 77 01
e-mail: advertising@termedia.pl
www.termedia.pl

President of the Management Board
of the Termedia Publishing House
Janusz Michalak

Scientific Director
of the Termedia Publishing House
Małgorzata Ranała

Editor
Marcyna Jermolaj
e-mail: m.jermolaj@termedia.pl

Marketing and Advertising Department
Krzysztof Holata
phone: +48 61 822 77 61 ext. 508
e-mail: rozprawy@termedia.pl

Distribution/Subscription Department
Jolanta Janiszewska
phone: +48 61 822 77 00
e-mail: prenumerata@termedia.pl

TERMEDIA Publishing House

ul. Piłsudskiego 653 Poznań, Poland
tel: +48 61 822 77 01
fax: +48 61 822 77 01
e-mail: wartosc@termedia.pl

Indexed/abstracted in: Medline, Research Alert, PubMed, Research Alert, Chemical Abstracts, EMBASE/Excerpta Medica, Medical Bibliography, Index Medicus, etc.

Printed with support of the Ministry of Science and Higher Education

<http://rcin.org.pl>

This journal is registered at the Copyright Clearance Center, Inc., 222 Rosewood Drive, Danvers, MA 01923, USA. Organizations in the USA who are also registered with the Copyright Clearance Center may therefore copy material (beyond the limits permitted by sections 107 and 108 of US copyright law) subject to payment to CCC of the per copy fee of \$12.00. This consent does not extend to multiple copying for promotional or commercial purposes. ISI Tear Sheet Service, 3501 Market Street, Philadelphia, PA 19104, USA, is authorized to supply single copies of separate articles for private use only. For all other use, permission should be sought from Cambridge or the Cambridge University Press. This journal is registered with the Copyright Licensing Agency, 90 Tottenham Court Road, London W1P 0LP, UK. Organizations in the UK who are also registered with the Copyright Licensing Agency may therefore copy material (beyond the limits permitted by sections 107 and 108 of US copyright law) subject to payment to CLA of the per copy fee of £10.00. This journal is registered with the Copyright Clearance Center, Inc., 222 Rosewood Drive, Danvers, MA 01923, USA. Organizations in the USA who are also registered with the Copyright Clearance Center may therefore copy material (beyond the limits permitted by sections 107 and 108 of US copyright law) subject to payment to CCC of the per copy fee of \$12.00. This consent does not extend to multiple copying for promotional or commercial purposes. ISI Tear Sheet Service, 3501 Market Street, Philadelphia, PA 19104, USA, is authorized to supply single copies of separate articles for private use only. For all other use, permission should be sought from Cambridge or the Cambridge University Press. This journal is registered with the Copyright Licensing Agency, 90 Tottenham Court Road, London W1P 0LP, UK. Organizations in the UK who are also registered with the Copyright Licensing Agency may therefore copy material (beyond the limits permitted by sections 107 and 108 of US copyright law) subject to payment to CLA of the per copy fee of £10.00.



Official Journal of Mossakowski Medical Research Centre Polish Academy of Sciences
and Polish Association of Neuropathologists

Editor-in-Chief

Ewa Matyja
e-mail: ematyja@imdik.pan.pl

Associate Editor

Milena Laure-Kamionowska
e-mail: mkamionowska@imdik.pan.pl

Editorial Office

Mossakowski Medical Research Centre
Polish Academy of Sciences
5 Pawińskiego St.
02-106 Warsaw, Poland
phone: +48 22 608 65 03
fax: +48 22 608 65 02

Editorial Board

Mario Alberghina (Catania)
Stefan Angielski (Gdańsk)
Zbigniew Czernicki (Warsaw)
Isidro Ferrer (Barcelona)
Marek Gołębiowski (Warsaw)
Caroline Graff (Stockholm)
Paweł Grieb (Warsaw)
Matti Haltia (Helsinki)
Elżbieta Kida (New York)
Andrzej Kochański (Warsaw)
Paweł P. Liberski (Łódź)
David N. Louis (Boston, MA)
Walter J. Lukiw (New Orleans)
Jerzy Łazarewicz (Warsaw)
Danuta Maślińska (Warsaw)
Janusz Moryś (Gdańsk)
Shun-ichi Nakamura (Kobe)
Yngve Olsson (Uppsala)
Wielisław Papierz (Łódź)
Janina Rafałowska (Warsaw)
Nicola Rizzuto (Verona)
Harvey B. Sarnat (Calgary)
Joanna Strosznajder (Warsaw)
Janusz Szymaś (Poznań)
Hitoshi Takahashi (Niigata)
Xiaofei Wang (Indianapolis)
Teresa Wrzotkova (Gdańsk)

The journal is partly financially supported
by the Ministry of Science and Higher Education

termedia

Termedia Publishing House
Kleeberga 2, 61-615 Poznan, Poland
phone/fax: +48 61 822 77 81
e-mail: termedia@termedia.pl
www.termedia.pl
www.folianeuro.termedia.pl

Warsaw office
phone/fax: +48 22 827 75 14
e-mail: biuro.warszawa@termedia.pl

President of the Management Board
of the Termedia Publishing House
Janusz Michalak

Scientific Director
of the Termedia Publishing House
Maciej Banach

Production Editor
Marzena Demska
e-mail: m.demska@termedia.pl

Marketing and Advertising Department
Renata Dolata
phone: +48 61 822 77 81 ext. 508
e-mail: r.dolata@termedia.pl

Distribution Subscription Department
Jolanta Jankowiak
phone: +48 61 656 22 00
e-mail: prenumerata@termedia.pl

Impact Factor for Folia Neuropathologica equals 1.568
MNI^{SW} score for Folia Neuropathologica equals 20
Index Copernicus Value 2014 for Folia Neuropathologica equals 22.61 (154.82)
Position in Index Copernicus ranking systems available at <http://www.indexcopernicus.pl>

Abstracted and indexed in Index Medicus/MEDLINE, Neuroscience Citation Index, SciSearch, Research Alert, Chemical Abstracts, EMBASE/Excerpta Medica, Polish Medical Bibliography, Index Copernicus

The journal is financially supported by the Ministry of Sciences and Higher Education.

Print run: 450 copies

Copyright: © 2016 Mossakowski Medical Research Centre Polish Academy of Sciences and the Polish Association of Neuropathologists. This is an Open Access article distributed under the terms of the Creative Commons Attribution-NonCommercial-ShareAlike 4.0 International (CC BY-NC-SA 4.0) License (<http://creativecommons.org/licenses/by-nc-sa/4.0/>), allowing third parties to copy and redistribute the material in any medium or format and to remix, transform, and build upon the material, provided the original work is properly cited and states its license.



Contents

- Can neurodegenerative disease be defined by four 'primary determinants': anatomy, cells, molecules, and morphology?** 89
Richard A. Armstrong
- High expression of DNA methyltransferases in primary human medulloblastoma** 105
Tímea Pócza, Tibor Krenács, Eszter Turányi, János Csáthy, Zsuzsanna Jakab, Peter Hauser
- Assessment of candidate immunohistochemical prognostic markers of meningioma recurrence** 114
Tamás Csonka, Balázs Murányi, Rita Szepesi, János Bencze, László Bognár, Álmos Klekner, Tibor Hortobágyi
- Ultrastructural pathology of human peritumoural oedematous cerebellar cortex** 127
Orlando José Castejón
- Survival in the pre-senile dementia frontotemporal lobar degeneration with TDP-43 proteinopathy: effects of genetic, demographic and neuropathological variables** 137
Richard A. Armstrong
- The topography of cortical microbleeds in frontotemporal lobar degeneration: a post-mortem 7.0-tesla magnetic resonance study** 149
Jacques De Reuck, Florent Auger, Nicolas Durieux, Vincent Deramecourt, Claude-Alain Maurage, Florence Lebert, Didier Leys, Charlotte Cordonnier, Florence Pasquier, Régis Bordet
- Potent effects of alkaloid-rich extract from *Huperzia selago* against sodium nitroprusside-evoked PC12 cells damage via attenuation of oxidative stress and apoptosis** 156
Anna Magdalena Lenkiewicz, Grzegorz Arkadiusz Czapski, Henryk Jęsko, Anna Wilkaniec, Wojciech Szypuła, Agnieszka Pietrosiuk, Aneta Marta Uszyska, Agata Adamczyk
- Effects of diclofenac sodium on the hippocampus of rats with acute subdural hematoma: histological, stereological, and molecular approach** 167
Aysin Pinar Turkmen, Suleyman Kaplan, Abdurrahman Aksoy, Berrin Zuhul Altunkaynak, Kıymet Kübra Yurt, Ebru Elibol, Cengiz Çokluk, Mehmet Emin Onger
- Natural apoptosis in developing mice dopamine midbrain neurons and vermal Purkinje cells** 180
Joaquin Martí-Clua
- Lhermitte-Duclos disease with neurofibrillary tangles in heterotopic cerebral grey matter** 190
Daniel Rusiecki, Boleslaw Lach

Comment by the author

Dr D. Rusiecki, Department of Neurology, A. J. Offensky, Astor University, Birmingham, UK. Email: dr.lach@astor.edu.pl

doi: 10.1016/j.fneut.2016.01.001

Can neurodegenerative disease be defined by four ‘primary determinants’: anatomy, cells, molecules, and morphology?

Richard A. Armstrong

Vision Sciences, Aston University, Birmingham, United Kingdom

Folia Neuropathol 2016; 54 (2): 89-104

DOI: 10.5114/fn.2016.60438

Abstract

Traditional methods of describing and classifying neurodegenerative disease are based on the clinico-pathological concept supported by molecular pathological studies and defined by ‘consensus criteria’. Disease heterogeneity, overlap between disorders, and the presence of multiple co-pathologies, however, have questioned the validity and status of many traditional disorders. If cases of neurodegenerative disease are not easily classifiable into distinct entities, but more continuously distributed, then a new descriptive framework may be required. This review proposes that there are four key neuropathological features of neurodegenerative disease (the ‘primary determinants’) that could be used to provide such a framework, viz., the anatomical pathways affected by the disease (‘anatomy’), the cell populations affected (‘cells’), the molecular pathology of ‘signature’ pathological lesions (‘molecules’), and the morphological types of neurodegeneration (‘morphology’). This review first discusses the limitations of existing classificatory systems and second provides evidence that the four primary determinants could be used as axes to define all cases of neurodegenerative disease. To illustrate the methodology, the primary determinants were applied to the study of a group of closely related tauopathy cases and to heterogeneity within frontotemporal lobar degeneration with TDP-43 proteinopathy (FTLD-TDP).

Key words: neurodegenerative disease, primary determinants, anatomy, cells, molecules, neurodegeneration.

Introduction

Traditional methods of describing and classifying cases of neurodegenerative disease are based on the original clinico-pathological concept, viz., a distinct clinical profile in combination with ‘signature’ pathological lesions. This system was used to describe the first cases of Alzheimer’s disease (AD) [2], Pick’s disease (PiD) [139], dementia with Lewy bodies (DLB) [107], and Creutzfeldt-Jakob disease (CJD) [44,88]. Subsequently, these original descrip-

tions were refined and modified by molecular studies which resulted in the discovery of disease-specific antibodies and enabled the molecular signature of brain lesions to be established [20,59]. Ultimately, ‘consensus criteria’ have been established for the majority of disorders, e.g., AD [120,125,133,162], DLB [120], multiple system atrophy (MSA) [71,72], and progressive supranuclear palsy (PSP) [108,109], representing the coordinated views of experts in the field regarding the most important clinical and

Communicating author:

Dr Phil. Richard A. Armstrong, Vision Sciences, Aston University, Birmingham B4 7ET, United Kingdom, phone: 0121-204-4102, fax: 0121-204-4048, e-mail: R.A.Armstrong@aston.ac.uk

pathological features useful in diagnosis. As a result, neurodegenerative disorders have continued to be regarded as more or less distinct 'entities', neuropathologically defined by signature pathological lesions, and characterised by a specific molecular pathology [20,59].

Recent research, however, has revealed considerable heterogeneity within existing disorders [15,22], overlap between closely related entities [19,55,63,76], and the co-occurrence in individual cases of two or more co-pathologies [19,93,172]. Hence, in a recent comparative study of 1032 cases representing ten different disorders, 361 cases, approximately 35% of the sample, were excluded largely as a result of multiple pathology [25]. Not only do these exclusions ignore a large quantity of data, a bias is also created in favour of 'typical' or 'pure' examples of a disorder, thus ignoring potential intermediate, overlap, or multiple pathology cases. As a consequence, a reconsideration of existing disease entities and a new descriptive framework which can accommodate overlap and heterogeneity may be necessary [8,19,54,62, 128,137].

An alternative method of describing cases of neurodegenerative disease is to use a geometrical system based on 'ordination', i.e., by arranging individual cases with reference to a co-ordinate frame so that their similarities and differences can be spatially represented [8,15,22,140]. In such a system, there may be no attempt to name a disorder or to classify cases into any pre-existing groups, but only to plot individual cases with reference to the co-ordinate frame. Location of a case would reveal its similarities and differences to other cases, and proximity to similar cases may reveal underlying common pathological mechanisms. To define the axes of such a co-ordinate frame, however, would require quantitative measures of a range of neuropathological variables.

This review proposes that there are four key features of neurodegenerative disease (the 'primary determinants') which could be used to provide such a descriptive framework, viz., the anatomical pathways affected by the disease ('anatomy'), the cell populations affected ('cells'), the major molecular pathology of the 'signature' pathological lesions ('molecules'), and the morphological types of neurodegeneration ('morphology'). Hence, this review discusses: (1) limitations of existing classificatory systems, (2) evidence that the four primary determinants could provide a description of cases of neu-

rodegenerative disease, (3) whether the four determinants are 'independent' variables, (4) whether the four determinants should be differentially weighted, and (5) describes the application of the method to the study of a group of closely-related tauopathy cases and heterogeneity within fronto-temporal lobar degeneration with TDP-43 proteinopathy (FTLD-TDP) [22].

Limitations of existing classifications

Several studies have questioned whether neurodegenerative diseases are distinct or whether individual cases represent points in a 'continuum' of neuropathological change [8,19,20]. Hence, extensive overlap was observed between cases of AD and Parkinson's disease (PD), interpreted as the action of common pathogenic mechanisms within vulnerable neuronal populations [137]. The authors argued that currently defined disease entities failed to deal with disease overlap and that a new classification should be considered [137]. In addition, Forstl [62] argued that the traditional clinico-pathological concept often accommodates genetically and clinically diverse conditions within the same group and therefore may have outlived its usefulness. The frequent use by authors of such terms as 'complex syndrome', 'spectrum of disorders', 'multiple pathologies', or even 'continuum' testifies to the extent to which boundaries between different disorders are more indistinct than previously thought [8,38,68,160].

Central to the argument of how neurodegenerative disease should be classified has been the status of AD [101,118]. Alzheimer's disease is heterogeneous [145] and can be divided into clinically relevant subgroups such as sporadic AD (SAD), tangle only AD, and the various genetic subtypes of familial AD (FAD), but only one subgroup actually corresponds to the disease originally described by Alzheimer [169]. In addition, a number of descriptive terms are used to describe AD co-pathology, e.g., AD neuropathological change (ADNC), and neurofibrillary tangle (NFT)-only change in medial temporal lobe (NFT-MTL). Defining exact criteria for AD has always been difficult due to phenotypic heterogeneity, the absence of specific markers, and overlap of pathology with cognitively normal brain and related disorders [7,90]. Hence, the term 'AD' may describe disease subgroups with markedly different characteristics, and it has been suggested that the looser term 'Alzheimer syndrome'

could be used or the term 'AD' dispensed with altogether [169]. If AD was to disappear as an entity, it would have significant implications for the status of many closely related disorders such as argyrophilic grain disease (AGD) [32,163,178], vascular dementia (VD) [95,106], and DLB [120].

The status of many other classically defined disorders has been equally controversial. Pick's disease [139], for example, is defined pathologically by the presence of tau-immunoreactive Pick bodies (PB) and abnormally enlarged neurons ('Pick cells'), but many cases of clinically typical PiD are at variance with these classic neuropathological features [98], e.g., some clinically typical PiD cases may lack PB [83]. Moreover, there is no convincing evidence linking the clinical symptoms of PiD with its histology, a challenge to the original clinico-pathological concept [60]. Subsequently, PiD became subsumed within the concept of 'frontotemporal dementia' (FTD) [87], but this classification also resulted in a heterogeneous group of disorders with considerable overlap between its constituent members [19]. Subsequent genetic and molecular studies have led to considerable changes in the classification and nomenclature within FTD and its neuropathological variants, viz. fronto-temporal lobar degeneration (FTLD) [37,164]. Clinical variants of FTD include the behavioural variant (bvFTD), language variants, e.g., semantic dementia (SD) and primary progressive aphasia (PPA), and motor variants such as corticobasal syndrome (CBS) and motor neuron disease (MND). In addition, pathological variants of FTLD include those with tau, transactive response (TAR) DNA-binding protein of 43 kDa (TDP-43), and fused in sarcoma (FUS)-immunoreactive inclusions [37].

Discrimination between different FTLD entities is often only possible using neuropathological criteria, the majority of which are based on the morphology and molecular composition of 'signature' pathological inclusions such as neuronal cytoplasmic inclusions (NCI), neuronal intranuclear inclusions (NII), and glial inclusions (GI), the latter including oligodendroglial inclusions ('coiled bodies'), tufted astrocytes (TA), astrocytic tangles (AT), and astrocytic 'plaques' (AP) [130]. Nevertheless, the clinical features of FTD may not predict their pathology, and neuropathological features alone cannot establish a diagnosis of FTD. In addition, studies have questioned whether some members should even be classified within FTD. Hence, corticobasal degeneration (CBD) is a predo-

minantly extrapyramidal motor disorder in which there is poor correlation between neuropathology and clinical syndrome [119]. In addition, there are FTD cases that exhibit a frontal lobe type of dementia but accompanied by a typical MND-type pathology not typical of any currently described FTD entity [30]. Consequently, FTD may define a group of cases, loosely united by clinical presentation, but with heterogeneous pathologies and therefore not easily classifiable according to clinico-pathological or any other criteria [77,79,99].

Similar problems can be observed within CJD, which in the past was regarded as a doubtful disease entity [100]. The original CJD concept [44,88] was subsequently discarded in favour of the term 'prion disease' [1,41], but there still remain problems such as overlap between CJD and other disorders, most notably with AD [19,20,76]. In addition, the prion-like behaviour of such pathological proteins as tau and α -synuclein [74,155] further blurs the distinction between classic prion diseases, tauopathies, and synucleinopathies.

The four primary determinants

This review proposes four key features, viz. the 'primary determinants', to describe the neuropathology of neurodegenerative disease: (1) anatomical pathways affected by the disease ('anatomy'), (2) cell types affected ('cells'), (3) primary molecular pathology of 'signature' pathological lesions ('molecules'), and (4) morphological types of neurodegeneration ('morphology'). How currently defined disorders may be related to these variables is shown in Table I.

Anatomy

One of the first demonstrations that a neurodegenerative disease was related to the breakdown of specific anatomical pathways was in AD [45,136]. Hence, a major feature of the pathology of AD is the disruption of afferent and efferent connections between the hippocampal formation and the rest of the brain [45]. Alzheimer's disease pathology may initially affect the temporal pole, especially the entorhinal cortex (EC), before spreading to the posterior parahippocampal gyrus (PHG) and then in a stepwise fashion to the hippocampus and association cortex, leaving primary sensory areas unimpaired until later in the disease [31,58,91,136]. The pathology may

Table I. Description of the major neurodegenerative diseases according to the four primary determinants

Disorder	Primary determinants			
	Anatomy	Cells	Molecules	Morphology
AD	GC, L	N	A β , 3R/4R tau	SP, NFT
AGD	L	N, A, O	4R tau	P-NFT, NT, GR, EN, V
CBD	FT, M, SC	N, A	4R tau	NCI
CJD	GC	N	PrP ^{Sc}	SP, V
DLB	L, C	N	α -synuclein	LB, NT, EN
FTD-MND	MC, SC	N, O	tau	NCI, GI
FTLD-TDP	FT	N, O	TDP-43	NCI, GI, V
MSA	SC	O, N	α -synuclein	GCI
NIFID	FT, L, SC	N, O	FUS	NCI, GI
PD-Dem	L, MC, SC	N	α -synuclein	LB, LT, LG
PiD	FT	N	3R tau	PB, PC
PSP	SC	N, A	4R tau	NFT, GI, AP

Disorders: AD – Alzheimer's disease, AGD – argyrophilic grain disease, CBD – corticobasal degeneration, CJD – Creutzfeldt-Jakob disease, DLB – dementia with Lewy bodies, FTDP-17 – fronto-temporal dementia and parkinsonism linked to chromosome 17, FTD-MND – motor neuron disease with dementia, MND – motor neuron disease, MSA – multiple system atrophy, NIFID – neuronal intermediate filament inclusion disease, PiD – Pick's disease, PD – Parkinson's disease, PSP – progressive supranuclear palsy; *Anatomy:* GC – general cortical, L – limbic, FT – frontotemporal, SC – subcortical; *Cells:* N – neurons, A – astrocytes, O – oligodendrocytes; *Molecules:* A β – β -amyloid, PrP^{Sc} – disease form of prion protein, FUS – fused in sarcoma, TDP-43 – transactive response (TAR) DNA-binding protein of 43 kDa; *Degeneration:* AP – astrocytic plaque, SP – senile plaques, NCI – neuronal cytoplasmic inclusions, P-NFT – pre-tangles, NFT – neurofibrillary tangles, NT – neuropil threads, GCI – glial cytoplasmic inclusions, GR – grains, EN – abnormally enlarged neurons, LB – Lewy bodies, LT – Lewy neurites, LG – Lewy grains, PB – Pick bodies, PC – Pick cells, V – vacuolation

then spread among cortical gyri and to subcortical regions via cortico-cortical and cortical-subcortical pathways respectively [5,45,136]. This hypothesis is supported by studies of the spatial patterns of SP and NFT [6,13] and of transgenic mice, in which there is selective disruption of cortico-cortical pathways [47]. Furthermore, this pattern of neurodegeneration correlates with specific neurotransmitter deficits, e.g., acetylcholinesterase-immunoreactive neurites are present at the periphery of SP, which could represent the degeneration of ascending and cortical cholinergic pathways [157].

Although many authors continue to argue that AD is a distinct entity [118], it is highly heterogeneous [42,61], and cases exhibit considerable neuropathological variation [15,19]. Variation in the anatomical spread of disease from its origin in the MTL could account for many of these differences [15,33,45]. Consequently, there may be a close relationship between the distribution of the pathology and the clinical features of individual patients [67]. For example, MTL areas are relatively spared in aphasic cases of AD, while more severe occipito-parietal degeneration, also

termed posterior cortical atrophy (PCA), is often associated with visual-spatial deficits at presentation [67].

The second commonest form of dementia is DLB, accounting for up to a quarter of all cases [120]. An essential feature of the neuropathological diagnosis of DLB is the presence of LB in the cerebral cortex and/or brain stem. Nevertheless, DLB exists in a variety of forms including neocortical, limbic [144], cerebral, and brainstem types, the neocortical subtype being the most common [85]. Many cases of DLB also exhibit ADNC [48,70,78], and therefore each pathological subtype of DLB can be divided into a 'pure' or 'mixed' form based on the degree of AD co-pathology [85]. Some studies have suggested anatomical differences in the pathways affected in AD and DLB. Brain glucose metabolism studies, for example, indicate that hypometabolism of the primary visual cortex (area V1) is more marked in DLB, whereas reductions in the posterior/temporal cortex, posterior cingulate gyrus, and frontal cortex occur in both AD and DLB [122]. Studies of regional cerebral blood flow (rCBF) report similar results, i.e., occipital hyperperfusion may be more frequent in DLB [110].

The pattern of temporal lobe atrophy may also differ between AD and DLB, with less hippocampal atrophy in DLB, which could explain the preservation of memory function in DLB [126].

In FTLT, which accounts for approximately 20% of all pre-senile cases of dementia [159], the pathological changes are usually more circumscribed, affecting primarily frontal and temporal lobes [156]. Nevertheless, there is often selective anatomical degeneration within this group. For example, in FTLT with transactive response (TAR) DNA-binding protein of 43 kDa (TDP-43)-immunoreactive inclusions, atrophy of the frontal lobe and temporal pole is seen in 97% of cases, but the hippocampus and subcortical areas are less affected [11,22,69]. In FTD and parkinsonism linked to chromosome 17 (FTDP-17) and CBD, however, degeneration largely affects the globus pallidus and substantia nigra and is accompanied by pathological changes in the cerebral cortex and subcortical areas [143]. In MND, cortical pathology is even more restricted to the motor cortex, although the brain stem and spinal cord may also be affected [29].

A further group of disorders exhibit a predominantly subcortical pathology including MSA, PD lacking dementia, and PSP. Hence in MSA, the substantia nigra, striatum, inferior olivary nucleus, pontine nuclei, and cerebellum are affected [18,49,105]. In some cases, there may be progressive cerebral atrophy affecting the frontal lobes [103] and the motor/premotor areas [168], the limbic system also being affected, principally in longer duration cases [138]. Although MSA is regarded as a single entity, two main subtypes are now recognized [72], viz., the cerebellar subtype (MSA-C) and parkinsonian subtype (MSA-P). The most consistent clinical syndrome, however, is parkinsonism, followed by cerebellar ataxia, and pyramidal tract signs [171]. Similarly, the anatomical distribution of pathological changes in PD is largely subcortical but with two clinical subtypes, viz., an 'akinetic-rigid' form with cell losses in the ventrolateral substantia nigra and related motor systems and a 'tremor-dominant' form with cell losses in the medial substantia nigra [89]. In addition, in PD with dementia (PD-Dem), which may be indistinguishable from DLB [28], there is spread of pathology to affect the cortical regions and hippocampus [24]. Progressive supranuclear palsy exhibits a more restricted form of subcortical degeneration, often sparing the cerebral cortex entirely [113]. Two clin-

ical phenotypes have been identified, viz., Richardson's syndrome (RS) and PSP-parkinsonism (PSP-P), the two subtypes varying in disease duration and in tau isoforms [173]. In addition, there is loss of cholinergic innervation to the thalamus and cerebral cortex in PD, but only to the thalamus in PSP [153].

Cells

The developing pathology of neurodegenerative disease may target specific cell populations. In AD, for example, it is the larger cortical pyramidal cells that are most vulnerable, smaller neurons being more resistant [80]. In addition, labelling of damaged neurons in AD is most conspicuous in lamina III of the cerebral cortex early in the disease but becomes more widespread as the pathology progresses [165]. This observation suggests a specific loss of cortico-cortical connections in AD [136], many of which use glutamate as neurotransmitter. The disease may then spread in either an orthograde or retrograde direction [45], gradually involving other neuronal types and eventually glial cells. In AD there is also loss of neurons which express the 75 kD neurotrophic receptor p75NTR [174] which preferentially binds β -amyloid ($A\beta$), and hence cells that undergo apoptosis could be mediated by this reaction. By contrast, cultured hippocampal neurons immunoreactive to the calcium-binding protein calretinin are more resistant to degeneration associated with $A\beta$ [142]. Moreover in FTLT, glutamate-immunoreactive pyramidal cells as well as calbindin D-28 γ -aminobutyric acid (GABA) neurons are lost but parvalbumin-immunoreactive cells preserved [57], consistent with loss of the cortico-cortical connections in FTLT.

A distinctive pattern of hippocampal pathology is present in CJD involving selective vulnerability of GABA neurons [75]. Hence, parvalbumin-immunoreactive neurons are severely depleted while calbindin-immunoreactive cells, which represent an early loss of inhibitory neurons, are largely preserved [75].

In FTLT, GI can be observed in oligodendroglial cells in the hippocampus, PHG, and amygdala [134]. In addition, a fundamental cytoskeletal alteration of oligodendrocytes occurs in MSA [18,50,170] resulting in the formation of characteristic 'glial cytoplasmic inclusions' (GCI) [135] which can be observed in the substantia nigra, striatum, inferior olivary nucleus, pontine nuclei, and cerebellum [105]. A close association between GCI and microtubules has also been

demonstrated [129], aberrant or ectopic expression of cdk5 and MAPK leading to abnormal phosphorylation of microtubule cytoskeletal proteins and the formation of inclusions. In MSA cases with frontal lobe atrophy [103], there are cell losses in laminae V/VI of the cerebral cortex, and GCI are often found in white matter. In addition, inclusions are found in the granule cell layer of the dentate gyrus and pre-frontal cortex and 'dot-like' structures or grains in the PHG [4]. The GCI may represent a pathological change synchronous with or preceding that of neuronal loss in MSA [84]. In addition, TA [82,102,175] are present in the motor cortex and striatum in PSP [51]. Neurons affected in PSP also appear to be functionally related, NFT occurring in interconnected extrapyramidal and oculomotor structures [151]. The presence of astrocytic pathology is regarded as a diagnostic feature of PSP [82] which may distinguish the disorder from the closely related CBD [81,109].

Molecules

The molecular pathology of 'signature' pathological lesions has played a highly significant role in diagnosis, the identification of new disease entities, and the development of theories of pathogenesis [20,59]. Studies of pathological lesions, however, reveal considerable molecular diversity [20]. In AD, for example, A β exists in several forms, the most common being A $\beta_{42/43}$, found largely in SP, whereas the more soluble A β_{40} is also found in association with blood vessels [121,146] and may develop later in the disease [46]. In addition, A β deposits may be associated with a variety of additional molecular constituents [20] including apolipoprotein E (Apo E) [176], α -antichymotrypsin, sulphated glycosaminoglycans, and complement factors [166]. A β -immunoreactive deposits also occur in DLB, but the ratio between the isoforms may differ from AD. In DLB, the predominant form of A β is A $\beta_{42/43}$, as in AD, but the level of A β_{40} is reduced compared with AD [117].

The majority of disorders have either tau- or α -synuclein-immunoreactive pathology. Within the tauopathies, PiD is characterised by tau with three microtubule repeats (3R tau), while PSP and CBD are composed of four-repeat (4R) tau [50,127]. Cellular inclusions in these disorders, however, are also associated with additional molecular constituents. Hence, PB in PiD are immunoreactive to ubiquitin

and Alz-50 [111] and in the synucleinopathy DLB [27], LB are also reactive for intermediate filaments (IF) [65], neurofilament (NF) proteins [66], cyclin dependent kinase-5 [34], α -B crystallin [112], and polyubiquitinated chains [86]. Furthermore, aggregates of abnormal intermediate filaments (IF) immunoreactive for α -internexin have been identified as a component of inclusions in neuronal intermediate filament inclusion disease (NIFID), a rare subtype of FTLD [10,30,36,92]. Subsequently, 'fused in sarcoma' (FUS) protein was identified as a major pathological protein in this disorder [23,132,177]. In addition, a significant number of cases of FTLD are linked to the product of the transcriptional repressor gene (*TARDP*), viz. TDP-43 [131], suggesting that these diseases may form another molecular group, viz., the TDP-43 proteinopathies.

Morphology

There are six main types of morphological degeneration observed in neurodegenerative disease. First, extracellular protein deposits are deposited in the neuropil e.g., A β in AD [73] or the disease form of prion protein (PrP^{Sc}) in CJD [152]. Second, intracellular protein aggregates develop as inclusions in cell bodies, nuclei, and the processes of neurons and glial cells. These include the various types of NCI, including NFT in AD, LB in PD and DLB [120], PB in PiD [111], and tau-reactive neurons in CBD [81]. In addition, GI, including the GCI characteristic of MSA [135], occur in a variety of disorders including FTLD-TDP, AGD, and CBD. Third, some disorders exhibit extensive neuropil threads (NT) or dystrophic neurites (DN) in specific brain regions such as in FTLD-TDP [22] and PD-Dem [24,149]. Fourth, disorders such as PD-Dem also possess Lewy grains (LG) which are α -synuclein-immunoreactive and which resemble the tau-reactive argyrophilic grains (AG) commonly observed in AGD [32,163,178], AD [148], and elderly, cognitively normal brains [52,94].

Fifth, abnormally enlarged neurons (EN), defined as having an irregularly enlarged or swollen cell body in which the largest diameter of the perikarya is at least three times the nuclear diameter [9], are a common feature of many disorders including AD [64], PiD, CBD, and AGD [163]. Enlarged neurons are also present in CJD, especially in cases with severe white matter degeneration [17,96,104]. In PSP, however, EN are less numerous and where present confined to

limbic regions [124,167]. There are also different types of EN. Hence, in PiD and CBD [14,16], there is uniform swelling of the neuronal perikaryon resulting in the characteristic 'ballooned' neurons, these cells being referred to as either Pick cells (PC) in PiD or ballooned neurons (BN) in CBD [126]. In addition, there are swollen achromatic neurons (SAN) in which the cell body is more irregularly enlarged, the Nissl substance uniformly pale, powdery, and eosinophilic, and the cell nucleus displaced to the cell margin [113]. Finally, there are swollen cells which occur in inherited neurovisceral disorders such as Niemann-Pick disease type-C in which swelling of the cell is associated with abnormalities in lipid storage [35,53]. Hence, EN in neurodegenerative disease lack specificity to any particular disease [64] but may indicate particular types of pathological change. Ballooned neurons occur after infarction and could represent an attempt at regeneration following axonal damage [3]. Enlarged neurons could also be a stress response since many swollen neurons are immunoreactive to α -B-crystallin induced by neuronal stress and which may have a protective function [123]. In addition, peripheral nerve transection, which separates nerve cells from their targets, may also lead to EN [141].

Sixth, significant vacuolation is a feature of many disorders, most notably CJD ('spongiform change') [152], but also to varying degrees AD, DLB, and FTLD, the latter often present as microvacuolation in superficial cortical laminae [22]. In the sporadic subtype of CJD (sCJD), clustering of vacuoles occurs in association with either neuronal perikarya or PrP^{Sc} deposits [17], while in the cerebellum of the variant subtype of CJD (vCJD), clusters of vacuoles in the molecular layer are negatively correlated with surviving Purkinje cells [21]. Hence, the degree of vacuolation could be an indication of the extent of neuronal loss in a region.

Independence of primary determinants

An important consideration is whether the four primary determinants are independent variables. If variables are inter-correlated, however, degeneration of a specific anatomical pathway may predict cell type affected, molecular pathology, or type of neurodegeneration. If this hypothesis is correct, then only certain combinations of anatomy, cells, molecules, and morphology would define neurodegenerative disease. Hence, in AD, which has tau-immunoreactive NFT, LB may also be present, and there is a strong correla-

tion between the presence of cortical α -synuclein-immunoreactive LB and degeneration of the substantia nigra [97]. In addition, in FAD linked to the *APP*₇₁₇ mutation, extrapyramidal features were present in all members of a single family and LB were present in a proportion of individuals [147]. Moreover, cortical LB in DLB are composed of intermediate filaments (IF) and a granular matrix, while brain stem LB have an electron-dense core and radially oriented filaments [65]. These results suggest that it is degeneration of a specific anatomical pathway, e.g., the extrapyramidal system, that could determine the molecular pathology, e.g., in this case, α -synuclein-immunoreactive LB. However, there is no specific relationship between grains (GR) and molecular pathology, GR being α -synuclein- or tau-immunoreactive in PD-Dem [149] and AGD [32,163,178] respectively.

In AD, cortical and subcortical NFT are composed of morphologically similar paired helical filaments (PHF), but cortical and subcortical PHF have a different molecular composition [161]. In addition, within the tauopathies, diseases may have morphologically similar tau-immunoreactive inclusions [56] but exhibit regional differences in distribution, especially in PSP, PD and CBD, which could be associated with different types of tau abnormality. Furthermore, in Niemann-Pick disease, the clinical spectrum of the disease is heterogeneous, rapid progression being associated with axonal spheroids and slow progression with NFT and neuronal dystrophy [158]. The NFT have a similar composition to those of AD but a different morphology reflecting their regional origin. In addition, frontal lobe atrophy could occur in both PSP and DLB associated with either NFT or LB respectively [43]. Differences in the neuronal population affected in the frontal cortex or in patient genotype could account for these differences. Positive correlations have also been observed among the densities of LB, LN, and LG in PD-Dem, suggesting that they could result from degeneration of the same neurons, LB aggregating in cell bodies and LN and LG in adjacent neurites and synapses respectively [24].

Studies that directly correlate a molecular pathology with loss of a specific cell type are rare. However, McKenzie *et al.* [115] found that specific areas of MTL secreted large quantities of amyloid precursor protein (APP), and that more APP-immunoreactive neurons were found in these areas in head injury patients, which could explain the high density of SP in the temporal lobe in AD [12] and the subsequent

spread of pathology [45]. In PSP, tau mRNA isoforms containing 4R tau are increased in the brainstem but not in the frontal cortex or cerebellum, which could predict the eventual anatomical distribution of these inclusions [40].

Weighting of primary determinants

Of the four primary determinants, molecular pathology has had the most profound impact over the last 25 years [20,54]. Should therefore this variable be regarded as the most fundamental? Classification based on molecular pathology, however, is often at variance with more traditional concepts based on anatomy. For example, AD and DLB are closely related and overlap extensively in clinical and pathological features [20], but AD is a tauopathy and DLB a synucleinopathy and therefore different at the molecular level. In addition, PSP is a tauopathy, but also an example of 'atypical parkinsonism' and therefore clinically related to the synucleinopathies PD, MSA, and DLB [154]. Recent research has criticised the concentration on 'signature' pathological lesions and their

molecular determinants and has questioned whether this emphasis has been detrimental to the study of neurodegenerative disease as a whole [39]. Hence, given current uncertainties regarding which variables are 'important' or 'fundamental', it is suggested that all four determinants should be given equal weight.

Application

An important practical question concerns what categories of anatomy, cells, molecules, and neurodegeneration should be used to define the descriptive axes. The multiplicity of possible defining variables suggests the use of a multivariate data analysis method such as principal components analysis (PCA) [15,22]. Principal components analysis simplifies a description of cases based on multiple variables by selecting two or three axes which describe sources of maximum variation in the data, i.e., 'the principal components' (PC). Hence, a PCA enables the degree of similarity and dissimilarity between cases to be studied based on quantitative estimates of their neuropathological characteristics [15,22]. The result of a PCA is a scatter plot of cases in relation to the PC in which the distance between cases reflects their similarity or dissimilarity, based on the defining histological features. Each PC therefore accounts for a proportion of the total variance in the data, PC1 accounting for the greatest amount of the variance and remaining PCs for diminishing amounts of the remaining variance. Such a system appears to have the requisite multivariate geometry and simplicity necessary to provide a possible framework for describing neurodegenerative disease. The following examples are based on relatively small numbers of cases and a restricted range of descriptive variables to illustrate the methodology.

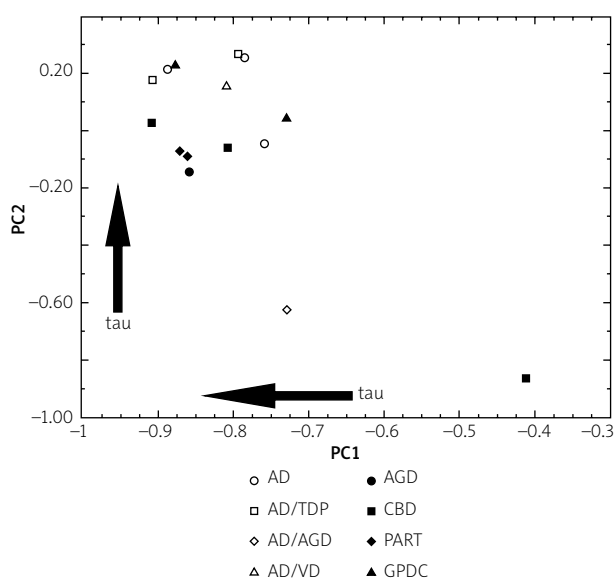


Fig. 1. Principal components analysis of 15 tauopathy cases (AD – Alzheimer's disease, AGD – argyrophilic grain disease, CBD – corticobasal degeneration, GPDC – Guamanian Parkinson's disease dementia complex [GPDC], PART – primary age-related tauopathy) using variables derived from the four primary determinants. A plot of the cases in relation to the first two principal components (PC 1 and 2 (Armstrong, unpublished data).

Example 1: Investigating the relationships between closely related tauopathies

The objective was to investigate similarities and differences among 15 closely related tauopathy cases traditionally classified as AD, AGD, CBD, Guamanian Parkinson's disease dementia complex (GPDC), or primary age-related tauopathy (PART). The defining variables include: (1) anatomy: frontal and temporal lobes and substantia nigra, (2) cells: neurons, astrocytes, oligodendrocytes, (3) molecules: tau, A β , and TDP-43, and (4) morphology: NCI, NT, GR, AT, GI, SP, EN, and

vacuolation. A plot of the 15 cases in relation to the first two principal components is shown in Figure 1.

Several features are evident from this plot. First, the majority of cases form a single cluster towards the upper left of the plot, the two remaining cases (AD/AGD, CBD) being more atypical. Second, within the main cluster, there is no obvious clustering of cases with similar co-pathology such as AD or TDP-43, although the two PART cases do occupy closely related positions. Third, several neuropathological variables are correlated with the factor loadings of the cases on the PC but overall there is a general increase in tau pathology with increasingly negative loadings on PC1 and positive loadings on PC2. Hence, if a new tauopathy case were to be added to this analysis, it would be possible to determine: (1) from its location, whether the new case was a typical or an atypical tauopathy, (2) the affinity of the new case relative to previous cases, and (3) the relative location of the case along a continuum of severity of tau pathology.

Example 2: Investigation of subtypes of FTLD-TDP

The second example is a study of neuropathological heterogeneity within FTLD with TDP-43-immunoreactive pathology (FTLD-TDP). These cases have a complex neuropathology comprising NCI, NII, GI, and DN. Four pathological subtypes of FTLD-TDP have been proposed [37,114,150] based on the type and regional distribution of the various types of inclusion. Hence, type 1 cases (Mackenzie-type 2) are characterized by long DN in superficial cortical laminae with few or no NCI or NII, type 2 (Mackenzie-type 3) by numerous NCI in superficial and deep cortical laminae with infrequent DN and sparse or no NII, type 3 (Mackenzie-type 1) by pathology predominantly affecting the superficial cortical laminae with numerous NCI, DN and varying numbers of NII, and type 4 by numerous NII, and infrequent NCI and DN especially in neocortical areas. The defining variables were: (1) anatomy: frontal and temporal lobes, (2) cells: neurons and oligodendroglia, (3) molecules: TDP-43, and (4) neurodegeneration: NCI, NII, DN, and GI. Hence, quantitative estimates of density of TDP-43-immunoreactive neuronal and glial inclusions were made in frontal and temporal regions of 94 cases of FTLD-TDP [22]. A PCA of the data is shown in Figure 2 and shows that cases representing the four subtypes exhibit considerable overlap, subtypes 1 and 4 being the most distinctive

and located towards the bottom and top of the plot respectively. Cases of subtype 2 and 3 were less distinct, with a greater degree of overlap. Hence, new cases could be added to the analysis over time and their location relative to PC1 and PC2, and therefore to all previous cases, established. Location of a new case would suggest to which subtype the case may belong. Hence, in Figure 2, new case A would be most likely to be an example of subtype 1 and case B of subtype 4. New cases C and D are more difficult to classify, although it is probable that they have more affinity with subtypes 2 and 3.

Further applications

More extensive applications of the methodology could include all cases of neurodegenerative disease from a single neuropathological centre and ultimately from several contributing centres. A major problem in attempting to apply this approach on a larger scale, however, is the lack of comparative quantitative data of sufficient scope, detail, quality, and consistency to define all possible cases. Most quan-

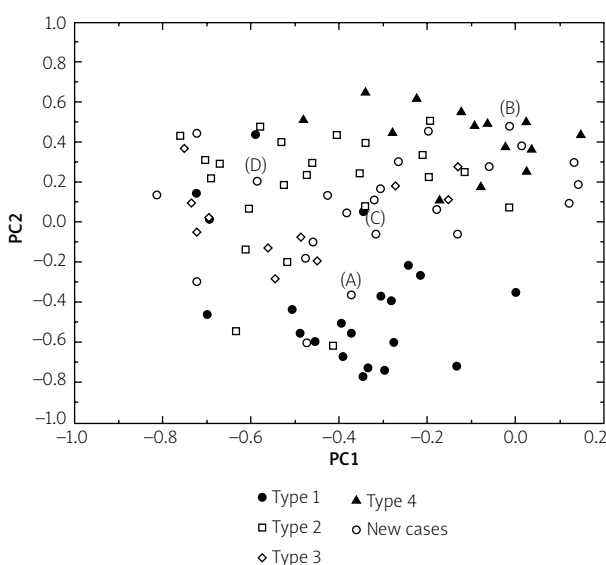


Fig. 2. Principal components analysis of 94 cases of frontotemporal lobar degeneration with TDP proteinopathy (FTLD-TDP) based on the densities of TDP-43 immunoreactive neuronal and glial inclusions in frontal and temporal cortex. Identified on the plot are the subtypes of disease based on the system of Cairns *et al.* (2007). Cases marked A, B, C, D are new cases added to the existing plot (data from Armstrong *et al.* 2010).

titative studies of a disorder quantify only signature pathological lesions [11], while others confine observations to a restricted number of anatomical regions or cell types, whereas all aspects of anatomy, cells, molecules, and morphology would need to be measured in each case. Nevertheless, the recent detailed comparative study of a large number of cases of ten neurodegenerative diseases, albeit using semi-quantitative data [25], demonstrates that it is feasible to collect comparative data across a large number of cases and disorders, enabling a descriptive system to be developed based on the four primary determinants.

Conclusions

This review proposes that four primary determinants could be used as the basis of a system to describe the neuropathology of neurodegenerative disease and which can take into account disease heterogeneity, overlap, and the presence of multiple pathologies. Such an approach has a number of advantages. First, it could describe all cases of neurodegenerative disease, not just those that may fit more traditional concepts. Second, it would emphasise the continuous nature of neurodegenerative disease by incorporating disease heterogeneity and overlap to their true extent [8,19]. Third, it would remove the necessity to classify new cases within an existing system, especially those which exhibit more complex multiple pathologies, as each case would be regarded as unique and would be located within a space defined by the primary determinants. Fourth, it potentially reveals the similarities and differences between cases included in the analysis, emphasising that common pathological mechanisms may be involved in different disorders. A major limiting factor in applying such a system on a large scale, however, is the current lack of detailed quantitative data of sufficient quality across cases and disorders [25].

Disclosure

Author reports no conflict of interest.

References

- Aguzzi A, Weissmann C. Prion research: the next frontier. *Nature* 1997; 389: 795-798.
- Alzheimer A. Über eine eigenartige Erkrankung der Hirnrinde. *Allge Zeitsch Psychiatr und Psychisch-Gerich Med* 1907; 64: 146-148.
- Aoki K, Uchihara T, Nakamura A, Komori T, Arai N, Mizutani T. Expression of apolipoprotein E in ballooned neurons: comparative immunohistochemical study in neurodegenerative disorders and infarctions. *Acta Neuropathol* 2003; 106: 436-440.
- Arai N, Papp MI, Lantos PL. New observations on ubiquitinated neurons in the cerebral cortex of multiple system atrophy (MSA). *Neurosci Lett* 1994; 182: 197-200.
- Armstrong RA. Alzheimer's disease: are cellular neurofibrillary tangles linked to β /A4 formation at projection sites? *Neurosci Res Commun* 1992; 11: 171-178.
- Armstrong RA. Is the clustering of neurofibrillary tangles in Alzheimer's patients related to the cells of origin of specific corticocortical projections? *Neurosci Lett* 1993; 160: 57-60.
- Armstrong RA. The interface between Alzheimer's disease, normal aging and related disorders. *Current Aging Science* 2008; 1: 122-132.
- Armstrong RA. On the classification of neurodegenerative disorders: discrete entities, overlap or continuum? *Folia Neuropathol* 2012; 50: 201-218.
- Armstrong RA. A quantitative study of abnormally enlarged neurons in cognitively normal brain and neurodegenerative disease. *Clin Neuropathol* 2013; 32: 128-134.
- Armstrong RA, Cairns NJ. Topography of α -internexin-positive neuronal aggregates in 10 patients with neuronal intermediate filament inclusion disease. *Eur J Neurol* 2006; 13: 528-532.
- Armstrong RA, Cairns NJ. Comparative quantitative study of 'signature' pathological lesions in the hippocampus and adjacent gyri of twelve neurodegenerative disorders. *J Neural Transm* 2015; 122: 1355-1367.
- Armstrong RA, Myers D, Smith CUM. The distribution of senile plaques, neurofibrillary tangles and β /A4 protein in the hippocampus in Alzheimer's disease. *Neurosci Res Commun* 1992; 10: 87-94.
- Armstrong RA, Myers D, Smith CUM. The spatial patterns of β /A4 deposit subtypes in Alzheimer's disease. *Acta Neuropathol* 1993; 86: 36-41.
- Armstrong RA, Cairns NJ, Lantos PL. The spatial pattern of Pick bodies, Pick cells and Alzheimer disease pathology in Pick's disease. *Neuropathology* 1999; 19: 64-70.
- Armstrong RA, Nochlin D, Bird TD. Neuropathological heterogeneity in Alzheimer's disease: a study of 80 cases using principal components analysis. *Neuropathology* 2000; 1: 31-37.
- Armstrong RA, Cairns NJ, Lantos PL. A quantitative study of the pathological lesions in the neocortex and hippocampus of 12 patients with corticobasal degeneration. *Exp Neurol* 2000; 163: 348-356.
- Armstrong RA, Lantos PL, Cairns NJ. Spatial correlations between the vacuolation, prion protein deposits, and surviving neurons in the cerebral cortex in sporadic Creutzfeldt-Jakob disease. *Neuropathology* 2001; 21: 266-271.
- Armstrong RA, Cairns NJ, Lantos PL. A quantitative study of the pathological changes in ten patients with multiple system atrophy (MSA). *J Neural Transm* 2004; 111: 485-495.
- Armstrong RA, Cairns NJ, Lantos PL. Overlap between neurodegenerative disorders. *Neuropathology* 2005; 25: 111-124.

20. Armstrong RA, Lantos PL, Cairns NJ. What determines the molecular composition of abnormal protein aggregates in neurodegenerative disease? *Neuropathology* 2008; 28: 351-365.
21. Armstrong RA, Ironside J, Lantos PL, Cairns NJ. A quantitative study of the pathological changes in the cerebellum of 15 cases of variant Creutzfeldt-Jakob disease. *Neuropathol Appl Neuro* 2009; 35: 36-45.
22. Armstrong RA, Ellis W, Hamilton RL, Mackenzie IRA, Hedreen J, Gearing M, Montine T, Vonsattel J-P, Head E, Lieberman AP, Cairns NJ. Neuropathological heterogeneity in frontotemporal lobar degeneration with TDP-43 proteinopathy: a quantitative study of 94 cases using principal components analysis. *J Neural Transm* 2010; 117: 227-239.
23. Armstrong RA, Gearing M, Bigio EH, Cruz-Sanchez FF, Duyckaerts C, Mackenzie IRA, Perry RH, Skullerud K, Yokoo H, Cairns NJ. The spectrum and severity of FUS-immunoreactive inclusions in the frontal and temporal lobes of ten cases of neuronal intermediate filament inclusion disease. *Acta Neuropathol* 2011; 121: 219-228.
24. Armstrong RA, Kotzbauer PT, Perlmutter JS, Campbell MC, Hurth KM, Schmidt RE, Cairns NJ. A quantitative study of α -synuclein pathology in fifteen cases of dementia associated with Parkinson disease. *J Neural Transm* 2014; 121: 171-181.
25. Arnold SE, Toledo JB, Appleby DH, Xie SX, Wang LS, Baek Y, Wolk DA, Lee EB, Miller BL, Lee VM, Trojanowski JQ. Comparative survey of the topographical distribution of signature molecular lesions in major neurodegenerative disease. *J Comp Neurol* 2013; 521: 4339-4353.
26. Barber R, McKeith IG, Ballard C, Gholkar A, O'Brien JT. A comparison of medial and lateral temporal lobe atrophy in dementia with Lewy bodies and Alzheimer's disease: magnetic resonance imaging volumetric study. *Dement Geriatr Cogn* 2001; 12: 198-205.
27. Bayer TA, Jakala P, Hartmann T, Harvas L, McLean C, Culvenor JG, Li QX, Masters CL, Falkai P, Beyreuther K. Alpha-synuclein accumulates in Lewy bodies in Parkinson's disease and dementia with Lewy bodies but not in Alzheimer's disease beta amyloid plaque cores. *Neurosci Lett* 1999; 266: 213-216.
28. Berg D, Postuma RB, Bloem B, Chan P, Dubois B, Gasser T, Goetz CG, Halliday GM, Hardy J, Lang AE, Litvan I, Marek K, Obeso J, Oertel W, Olanow CW, Poewe W, Stern M, Deuschl G. Time to redefine PD? Introductory statement of the MDS Task Force on the definition of Parkinson's disease. *Movement Disord* 2014; 29: 454-462.
29. Bergmann M, Kuchelmeister K, Schmid KW, Kretschmar HA, Schroder R. Different variants of FTD: a neuropathological and immunohistochemical study. *Acta Neuropathol* 1996; 92: 170-179.
30. Bigio EH, Lipton AM, White CL, Dickson DW, Hirano A. Frontotemporal dementia and motor neurone degeneration with neurofilament inclusion bodies: additional evidence for overlap between FTD and ALS. *Neuropathol Appl Neuro* 2003; 29: 239-253.
31. Braak H, Braak E, Bohl J. Retrosplenial region involvement in Alzheimer's disease. *Neurodegeneration* 1992; 1: 53-57.
32. Braak H, Braak E. Argyrophilic grain disease: frequency of occurrence in different age categories and neuropathologic diagnostic criteria. *J Neural Transm* 1998; 105: 801-819.
33. Braak H, Alafuzoff I, Arzberger T, Kretschmar H, Del Tredici K. Staging of Alzheimer disease-associated neurofibrillary pathology using paraffin sections and immunocytochemistry. *Acta Neuropathol* 2006; 112: 389-404.
34. Brion JP, Couk AM. Cortical and brain stem type Lewy bodies are immunoreactive for the cyclin dependent kinase-5. *Am J Pathol* 1995; 147: 1465-1476.
35. Bu B, Li J, Davies P, Vincent I. Deregulation of cdk5, hyperphosphorylated and cytoskeletal pathology in the Niemann-Pick type C murine model. *J Neurosci* 2002; 22: 6515-6525.
36. Cairns NJ, Perry RH, Jaros E, Burn D, McKeith IG, Lowe JS, Holton J, Rossor MN, Skullerud K, Duyckaerts C, Cruz-Sanchez FF, Lantos PL. Patients with a novel neurofilamentopathy: dementia with neurofilament inclusions. *Neurosci Lett* 2003; 341: 177-180.
37. Cairns NJ, Bigio EH, Mackenzie IRA, Neumann M, Lee VMY, Hatanpaa KJ, White CL, Schneider JA, Grinberg LT, Halliday G, Duyckaerts C, Lowe JS, Holm IE, Tolnay M, Okamoto K, Yokoo H, Murayama S, Woulfe J, Munoz DG, Dickson DW, Ince PG, Trojanowski JQ, Mann DMA. Neuropathologic diagnostic and nosological criteria for frontotemporal lobar degeneration: consensus of the Consortium for Frontotemporal Lobar Degeneration. *Acta Neuropathol* 2007; 114: 5-22.
38. Caselli RJ. Asymmetric cortical degeneration syndrome. *Curr Opin Neurol* 1996; 9: 276-280.
39. Castellani RJ, Perry G. Pathogenesis and disease-modifying therapy in Alzheimer's disease: the flat line of progress. *Arch Med Res* 2012; 43: 694-698.
40. Chambers CB, Lee JM, Troncoso JC, Reich S, Muma NA. Overexpression of four-repeat tau in RNA isoforms in progressive supranuclear palsy but not in Alzheimer's disease. *Ann Neurol* 1999; 46: 325-332.
41. Chesebro B. BSE and prions: uncertainties about the agent. *Science* 1998; 279: 42-43.
42. Chui HC, Teng EL, Henderson VW, Moy AC. Clinical subtypes of dementia of the Alzheimer type. *Neurology* 1985; 35: 1544-1550.
43. Cordato NJ, Halliday GM, Harding AJ, Hely MA, Morris JGL. Regional brain atrophy in progressive supranuclear palsy and Lewy body disease. *Ann Neurol* 2000; 47: 718-728.
44. Creutzfeldt HG. Uber eines eigenartige herd-formige Erkrankung des Zentralnervensystems. In: *Histologische und Histo-pathologische Arbeiten uber die Grosshirnrinde*. Nissl F, Alzheimer A (eds.). Gustav Fisher, Jena 1921; pp. 1-48.
45. De Lacoste M, White CL. The role of cortical connectivity in Alzheimer's disease: a review and model system. *Neurobiol Aging* 1993; 14: 1-16.
46. Delacourte A, Sergeant N, Champain D, Watzet A, Maurage CA, Lebert F, Pasquier F, David JP. Nonoverlapping but synergetic tau and amyloid precursor protein pathologies in sporadic Alzheimer's disease. *Neurology* 2002; 59: 398-407.
47. Delatour B, Blanchard V, Pradier L, Duyckaerts C. Alzheimer pathology disorganises cortico-cortical circuitry: direct evidence from a transgenic mouse model. *Neurobiol Dis* 2004; 16: 41-47.

48. Dickson DW, Ruan D, Crystal H, Mark MH, Davies P, Kress Y, Yen SH. Hippocampal degeneration differentiates diffuse Lewy body disease (DLBD) from Alzheimer's disease: light and electron microscope immunocytochemistry of CA2-3 neurites specific to DLBD. *Neurology* 1991; 41: 1402-1409.
49. Dickson DW, Lin WL, Liu WK, Yen SH. Multiple system atrophy: a sporadic synucleinopathy. *Brain Pathol* 1999; 9: 721-732.
50. Dickson DW, Liu WK, Hardy J, Farrer M, Melita N, Vitti R, Mark M, Zimmermann T, Gothe L, Sage J, Sima A, Damato C, Abin R, Gilman S, Yen SH. Widespread alterations of alpha-synuclein in multiple system atrophy. *Am J Pathol* 1999; 155: 1241-1251.
51. Dickson DW. Neuropathological differentiation of progressive supranuclear palsy and corticobasal degeneration. *J Neurol* 1999; 246: 6-15.
52. Ding ZT, Wang Y, Jiang YP, Hashizume Y, Yoshida M, Mimuro M, Inagaki T, Iwase T. Characteristics of alpha-synucleinopathy in centenarians. *Acta Neuropathol* 2006; 111: 450-458.
53. Distl R, Treiber-Held S, Albert F, Meske V, Harzer K, Ohm TG. Cholesterol storage and tau pathology in Nieman-Pick type C disease in the brain. *J Pathol* 2003; 200: 104-111.
54. Drouot B, Pincon-Raymond M, Chambaz J, Pillot T. Molecular basis of Alzheimer's disease. *Cell Mole Life Sci* 2000; 57: 705-715.
55. Feany MB, Dickson DW. Neurodegenerative disorders with extensive tau pathology: a comparative study and review. *Ann Neurol* 1996; 40: 139-148.
56. Feany MB, Mattiace LA, Dickson DW. Neuropathological overlap of progressive supranuclear palsy, Pick's disease and corticobasal degeneration. *J Neuropathol Exp Neuro* 1996; 55: 53-67.
57. Ferrer I. Neurons and their distribution in frontotemporal dementia. *Dement Geriatr Cogn* 1999; 10: 55-60.
58. Filey CM, Kleinschidtdemasters BK, Gross KF. Non-Alzheimer frontotemporal dementia: a neurobehavioural and pathological study. *Clin Neuropathol* 1994; 13: 109-116.
59. Forman MS, Trojanowski JQ, Lee VM-Y. Neurodegenerative diseases: a decade of discoveries paves the way for therapeutic breakthroughs. *Nat Med* 2004; 10: 1055-1063.
60. Forstl H, Baldwin B. Pick and the focal brain atrophies. *Fortschr Neurol Psych* 1994; 62: 345-355.
61. Forstl H, Fischer P. Diagnostic confirmation, severity and subtypes of Alzheimer's disease. *Eur Arch Psychiatry Clin Neurosci* 1994; 244: 252-260.
62. Forstl H. Alzheimer's disease: the size of the problem, clinical manifestation and heterogeneity. *J Neural Transm* 1998; 54: 1-8.
63. Forstl H. The Lewy body variant of Alzheimer's disease: clinical, pathophysiological and conceptual issues. *Eur Arch Psych Clin Neurol* 1999; 249: 64-67.
64. Fujino Y, Delucia MW, Davies P, Dickson DW. Ballooned neurons in the limbic lobe are associated with Alzheimer-type pathology and lack diagnostic specificity. *Neuropathol Appl Neuro* 2004; 30: 676-682.
65. Fukuda T, Tanaka J, Watabe K, Numoto RT, Minamitani M. Immunohistochemistry of neuronal inclusions in the cerebral cortex and brain stem in Lewy body dementia. *Acta Pathol Japon* 1993; 43: 545-551.
66. Gai WP, Blumbergs PC, Blessing WW. Microtubule-associated protein-5 is a component of Lewy bodies and Lewy body neurites in the brainstem and forebrain regions affected in Parkinson's disease. *Acta Neuropathol* 1996; 91: 78-81.
67. Galton CJ, Patterson K, Xuereb JH, Hodges JR. Atypical and typical presentations of Alzheimer's disease: a clinical, neuropsychological, neuroimaging and pathological study of 13 cases. *Brain* 2000; 123: 484-498.
68. Garraux G, Salmon E, Degueldre C, Lemaire C, Frank G. Medial temporal lobe metabolic impairment in dementia associated with motor neuron disease. *J Neurol Sci* 1999; 168: 145-150.
69. Giannakopoulos P, Hof PR, Bouras C. Dementia lacking distinctive histopathology: clinicopathological evaluation of 32 cases. *Acta Neuropathol* 1995; 89: 346-355.
70. Gibb WR, Luthert PJ, Janota I, Lantos PL. Cortical Lewy body dementia: clinical features and classification. *J Neurol Neurosurg Psychiatry* 1989; 52: 185-192.
71. Gilman S, Low PA, Quinn N, Albanese A, Ben-Schlomo Y, Fowler CJ, Kaufmann H, Klockgether T, Lang AE, Lantos PL, Livan I, Mathias CJ, Oliver E, Robertson D, Schatz I, Wenning GK. Consensus statement on the diagnosis of multiple system atrophy. *J Auton Nerv Syst* 1998; 74: 189-192.
72. Gilman S, Wenning GJK, Low PA, Brooks DJ, Mattias CJ, Trojanowski JQ, Wood NW, Colosima C, Durr A, Fowler CJ, Kaufmann H, Klockgether T, Lees A, Poese W, Quinn N, Revesz T, Robertson D, Sandroni T, Seppi K, Vidailhet M. Second consensus statement on the diagnosis of multiple system atrophy. *Neurology* 2008; 71: 670-676.
73. Glenner GG, Wong CW. Alzheimer's disease and Down's syndrome: sharing of a unique cerebrovascular amyloid fibril protein. *Biochem Bioph Res Commun* 1984; 122: 1131-1135.
74. Goedert M, Clavaguera F, Tolnay M. The propagation of prion-like protein inclusions in neurodegenerative diseases. *Trends Neurosci* 2010; 33: 317-325.
75. Guentchev M, Hainfellner JA, Trabattori GR, Budka H. Distribution of parvalbumin-immunoreactive neurons in brain correlates with hippocampal and temporal cortical pathology in Creutzfeldt-Jakob disease. *J Neuropathol Exp Neurol* 1997; 56: 1119-1124.
76. Hainfellner JA, Aanschutz J, Jellinger K, Liberski PP, Gullotta F, Budka H. Coexistence of Alzheimer type neuropathology in Creutzfeldt-Jakob disease. *Acta Neuropathol* 1998; 96: 116-122.
77. Hamilton RL, Bouser R. Alzheimer's disease pathology in amyotrophic lateral sclerosis. *Acta Neuropathol* 2004; 107: 515-522.
78. Harrington CR, Perry RH, Perry EK, Hurt J, McKeith JG, Roth M, Wischik CM. Senile dementia of the Lewy body type and Alzheimer type are biochemically distinct in terms of paired helical filaments and hyperphosphorylated tau proteins. *Dementia* 1994; 5: 215-228.
79. Hodges JR, Davies RR, Xuereb JH, Casey B, Broe M, Bak TH, Kril JJ, Halliday GM. Clinicopathological correlates in frontotemporal dementia. *Ann Neurol* 2004; 56: 399-406.
80. Hof PR, Morrison JH. Neocortical neuronal subpopulations labelled by a monoclonal antibody to calbindin exhibit differential vulnerability in Alzheimer's disease. *Exp Neurol* 1991; 111: 293-301.

81. Ikeda K. Basic pathology of corticobasal degeneration. *Neuropathology* 1997; 17: 127-133.
82. Ikeda K, Akiyama H, Kondo H, Haga C, Tanno E, Tokuda T, Ikeda S. Thorn-shaped astrocytes: possibly secondarily induced tau-positive glial fibrillary tangles. *Acta Neuropathol* 1995; 90: 620-625.
83. Ikeda K, Tsuchiya K. Motor neuron disease group accompanied by inclusions of unidentified protein signalled by ubiquitin. *Neuropathology* 2004; 24: 117-124.
84. Inoue M, Yagishita S, Ryo M, Hasegawa K, Amano N, Matsushita M. The distribution and dynamic density of oligodendroglial cytoplasmic inclusions (GCI) in multiple system atrophy: a correlation between the density of GCI and the degree of involvement of striatonigral and olivopontocerebellar systems. *Acta Neuropathol* 1997; 93: 585-591.
85. Iseki E, Marin W, Kosaka K, Kato M, Yamamoto T, Ueda K. Clinicopathological multiplicity of dementia with Lewy bodies. *Neuropathology* 1999; 19: 386-394.
86. Iwatsubo T, Yamaguchi H, Fujinuro M, Yokosawa H, Ihara Y, Trojanowski JQ, Lee VMY. Purification and characterisation of Lewy bodies from the brains of patients with diffuse Lewy body disease. *Am J Pathol* 1996; 148: 1517-1529.
87. Jackson M, Lowe J. The new neuropathology of degenerative frontotemporal dementias. *Acta Neuropathol* 1996; 91: 127-134.
88. Jakob A. Über eigenartige Erkrankungen des Zentralnervensystems mit bemerkenswerten anatomischen Befunden (spastische Pseudosklerose-Encephalomyelopathie mit disseminierten Degenerationsherden). *Dtsch Z Nervenheilk* 1921; 70: 132-146.
89. Jellinger KA, Bancher C. Neuropathology of Alzheimer's disease: a critical update. *J Neural Transm* 1998; 54: 77-95.
90. Jellinger KA. Recent developments in the pathology of Parkinson's disease. *J Neural Transm (Suppl)* 2002; 62: 347-376.
91. Jobst KA, Smith AD, Szatmari M, Molyneux A, Esiri MM, King E, Smith A, Jaskowski A, McDonald B, Wald N. Detection in life of confirmed Alzheimer's disease using a simple measurement of medial temporal lobe atrophy by computed tomography. *Lancet* 1992; 340: 1179-1183.
92. Josephs KA, Holton JL, Rossor MN, Braendgaard H, Ozawa T, Fox NC, Petersen RC, Pearl GS, Ganguly M, Rosa P, Laursen H, Parisi JE, Waldemar G, Quinn NP, Dickson DW, Revesz T. Neurofilament inclusion body disease: a new proteinopathy? *Brain* 2003; 126: 2291-2303.
93. Josephs KA, Knopman DS, Whitwell JL, Boeve BF, Parisi JE, Petersen RC, Dickson DW. Survival in the two variants of tau negative FTL: FTL-U versus FTL-MND. *Neurology* 2005; 65: 645-647.
94. Josephs KA, Whitwell JL, Parisi JE, Knopman DS, Boeve BF, Geda YE, Jack CR, Petersen RC, Dickson DW. Argrophilic grains: a distinct disease or an additive pathology? *Neurobiol Aging* 2008; 29: 566-573.
95. Kalaria RN. Comparison between Alzheimer's disease and vascular dementia: implications for treatment. *Neurol Res* 2003; 25: 661-664.
96. Kato S, Hirano A, Umahara T, Wena JF, Herz F, Ohama E. Ultrastructural and immunohistochemical studies on ballooned cortical neurons in Creutzfeldt-Jakob disease: expression of alpha-B-crystallin, ubiquitin and stress response protein-27. *Acta Neuropathol* 1992; 84: 443-448.
97. Kazee AM, Han LY. Cortical Lewy bodies in Alzheimer's disease. *Arch Pathol Lab Med* 1995; 119: 448-453.
98. Kertesz A, Kalvach P. Arnold Pick and German neuropsychiatry in Prague. *Arch Neurol* 1996; 53: 935-938.
99. Kertesz A, Davidson W, Munoz DG. Clinical and pathological overlap between fronto-temporal dementia, primary progressive aphasia and corticobasal degeneration: The Pick complex. *Dement Geriatr Cogn* 1999; 10: 46-49.
100. Kirschbaum WR. Jakob-Creutzfeldt Disease (spastic pseudosclerosis, A. Jakob; Heidenhain syndrome; subacute spongiform encephalopathy). Elsevier, New York 1968.
101. Knopman DS. An overview of common non-Alzheimer dementias. *Clin Geriatr Med* 2001; 17: 281-301.
102. Komori T. Tau positive glial inclusions in progressive supranuclear palsy, corticobasal degeneration and Pick's disease. *Brain Pathol* 1999; 9: 663-679.
103. Konogaya M, Sakai M, Matsuoka Y, Konogaya Y, Hashizume Y. Multiple system atrophy with remarkable frontal lobe atrophy. *Acta Neuropathol* 1999; 97: 423-428.
104. Kovacs GG, Voigtlander T, Hainfellner JA, Budka H. Distribution of intraneuronal immunoreactivity for the prion protein in human prion disease. *Acta Neuropathol* 2002; 104: 320-326.
105. Lantos PL. Cellular pathology of multiple system atrophy: a review. *J Neurol Neurosurg Psychiatry* 1994; 57: 129-133.
106. Lewis H, Beher D, Cookson N, Oakley A, Piggott M, Morris CM, Jaros E, Perry R, Ince P, Kenny RA, Ballard CG, Shearman MS, Kalaria RN. Quantification of Alzheimer pathology in ageing and dementia: age-related accumulation of amyloid beta(42) peptide in vascular dementia. *Neuropathol Appl Neurobiol* 2006; 32: 103-118.
107. Lewy FH. Paralysis agitans. I. Pathologische Anatomie. In: *Handbuch der Neurologie*. Lewandowsky M (ed.). Springer, Berlin 1912; pp. 920-933.
108. Litvan I, Agid Y, Calne D, Campbell G, Dubois B, Davoulen RC, Goetz CG, Golbe LI, Grafman J, Growden JH, Hallett M, Jankovic J, Quinn NP, Tolosa E, Zee DS, Chase TW, FitzGibbon EJ, Hall Z, Juncos J, Nelson KB, Oliver E, Pramstaller P, Reich SG, Verny M. Clinical research criteria for the diagnosis of progressive supranuclear palsy (Steele-Richardson-Olszewski syndrome): report of the NINDS-SPSP International Workshop. *Neurology* 1996; 47: 1-9.
109. Litvan I, Grimes DA, Lang AE, Jankovic J, McKee A, Verny M, Jellinger K, Chaudhuri KR, Pearce RKB. Clinical features differentiating patients with postmortem confirmed progressive supranuclear palsy and corticobasal degeneration. *J Neurol* 1999; 246: 1-5.
110. Lobotesis K, Fenwick JD, Phipps A, Ryman A, Swann A, Ballard C, McKeith IG, O'Brien JT. Occipital hypoperfusion on SPECT in dementia with Lewy bodies but not Alzheimer's disease. *Neurology* 2001; 56: 643-649.
111. Love S, Saitoh T, Quijada S, Cole GM, Terry RD. Ubiquitin and tau immunoreactivity of neurofibrillary tangles, Pick bodies and Lewy bodies. *J Neuropathol Exp Neuro* 1988; 47: 393-405.
112. Lowe J, Mayer RJ, Landon M. Ubiquitin in neurodegenerative diseases. *Brain Pathol* 1993; 3: 55-65.

113. Mackenzie IRA, Hudson LP. Achromatic neurons in the cortex of progressive supranuclear palsy. *Acta Neuropathol* 1995; 90: 615-619.
114. Mackenzie IR, Baborie A, Pickering-Brown S, Du Plessis D, Jaros E, Perry RH, Neary D, Snowden JS, Mann DMA. Heterogeneity of ubiquitin pathology in frontotemporal lobar degeneration: classification and relation to clinical phenotype. *Acta Neuropathol* 2006; 112: 539-549.
115. McKenzie JE, Gentleman SM, Roberts GW, Graham DI, Royston MC. Increased numbers of β APP-immunoreactive neurons in the entorhinal cortex after head injury. *Neuroreport* 1994; 6: 161-164.
116. Mann DMA. The topographic distribution of brain atrophy in Alzheimer's disease. *Acta Neuropathol* 1991; 83: 81-86.
117. Mann DMA, Brown SMP, Owen F, Baba M, Iwasubo T. Amyloid beta protein ($A\beta$) deposition in dementia with Lewy bodies: predominance of $A\beta$ 42/43 and a paucity of $A\beta$ 40 compared with sporadic Alzheimer's disease. *Neuropathol Appl Neuro* 1988; 24: 187-194.
118. Martinez-Martin P. Is AD a homogeneous entity? Yes. *J Neural Transm (Vienna)* 2013; 120: 1467-1473.
119. Mathuranath PS, Xureb JH, Bak T, Hodges JR. Corticobasal ganglionic degeneration and/or frontotemporal dementia? A report of two overlap cases and review of the literature. *J Neurol Neurosurg Psychiatry* 2000; 68: 304-312.
120. McKeith IG, Galasko D, Kosaka K, Perry EK, Dickson DW, Hansen LA, Salmon DP, Lowe J, Mirra SS, Byrne EJ, Lennox G, Quinn NP, Edwardson JA, Ince PG, Bergeron C, Burns A, Miller BL, Lovestone S, Collerton D, Jansen ENH, Ballard C, de Vos RAI, Wilcock GK, Jellinger KA, Perry RH. Consensus guidelines for the clinical and pathological diagnosis of dementia with Lewy bodies (DLB): report of the consortium on DLB international workshop. *Neurology* 1996; 47: 1113-1124.
121. Minoshima S, Foster NL, Sima AAF, Frey KA, Abin RL, Kuhl DE. Alzheimer's disease versus dementia with Lewy bodies: cerebral metabolic distinction with autopsy confirmation. *Ann Neurol* 2001; 50: 358-365.
122. Miller DL, Papayannopoulos IA, Styles J, Bobin SA, Lin YY, Biemann K, Iqbal K. Peptide compositions of the cerebrovascular and senile plaque core amyloid deposits of Alzheimer's disease. *Arch Biochem Biophys* 1993; 301: 41-52.
123. Minamu M, Mizutani T, Kawanishi R, Suzuki Y, Mori H. Neuronal expression of alpha B crystalline in cerebral infarction. *Acta Neuropathol* 2003; 105: 549-554.
124. Mizuno Y, Hori S, Kakizuka A, Okamoto K. Vacuole-creating protein in neurodegenerative diseases in humans. *Neurosci Lett* 2005; 343: 77-80.
125. Mirra SS, Heyman A, McKeel D, Sumi SM, Crain BJ, Brownlee LM, Vogel FS, Hughes JP, van Belle G, Berg L. The consortium to establish a registry for Alzheimer's disease (CERAD). Part II. Standardization of the neuropathologic assessment of Alzheimer's disease. *Neurology* 1991; 41: 479-486.
126. Mori H, Oda M. Ballooned neurons in corticobasal degeneration and progressive supranuclear palsy. *Neuropathology* 1997; 7: 248-252.
127. Morris HR, Baker M, Yasojima K, Khan NM, Wood NW, Hardy J, Grossman M, Trojanowski J, Revesz T, Bigio EH, Bergeron C, Janssen JC, McGeer PL, Rossor MN, Lees AJ, Lantos OL, Hutton M. Analysis of tau haplotypes in Pick's disease. *Neurology* 2002; 59: 443-445.
128. Morris JC. The nosology of dementia. *Neurol Clin* 2000; 18: 773.
129. Nakamura S, Kawamoto Y, Nakano S, Akiguchi I, Kimura J. Cyclin-dependent kinase 5 and nitrogen-activated protein kinase in glial cytoplasmic inclusions in multiple system atrophy. *J Neuropath Exp Neur* 1998; 57: 690-698.
130. Neumann M, Kretschmar HA. Pathology and biochemistry of frontotemporal dementias. *Nervenheilkunde* 2004; 23: 73-79.
131. Neumann M, Sampathu DM, Kwong LK, Truax AC, Micsenyi MC, Chou TT, Bruce J, Schuck T, Grossman M, Clarke CM, McCluskey LF, Miller BL, Masliah E, Mackenzie IR, Feldmen H, Feiden W, Kretschmar HA, Trojanowski JQ, Lee VMY. Ubiquitinated TDP-43 in frontotemporal lobar degeneration and amyotrophic lateral sclerosis. *Science* 2006; 314: 130-133.
132. Neumann M, Roeher S, Kretschmar HA, Rademakers R, Baker M, Mackenzie IRA. Abundant FUS-immunoreactive pathology in Neuronal intermediate filament inclusion disease (NIFID). *Acta Neuropathol* 2009; 118: 605-616.
133. Newell KL, Hyman BT, Growden JH, Hedley-Whyte ET. Application of the National Institute on Aging (NIA)-Reagan Institute criteria for the neuropathological diagnosis of Alzheimer's disease. *J Neuropathol Exp Neurol* 1999; 58: 1147-1155.
134. Noda K, Katayama S, Watanabe C, Yamamura Y, Nakamura S. Gallyas and tau positive glial structures in motor neuron disease with dementia. *Clin Neuropathol* 1999; 18: 218-225.
135. Papp MI, Lantos PL. The distribution of oligodendroglial inclusions in multiple system atrophy and its relevance to clinical symptomatology. *Brain* 1994; 117: 235-243.
136. Pearson RCA, Esiri MM, Hiorns RW, Wilcock GK, Powell TPS. Anatomical correlates of the distribution of the pathological changes in the neocortex in Alzheimer's disease. *Proc Natl Acad Sci U S A* 1985; 82: 4531-4534.
137. Perl DP, Olanow CW, Calne D. Alzheimer's disease and Parkinson's disease: distinct entities or extremes of a spectrum of neurodegeneration? *Ann Neurol* 1998; 44: S19-S31.
138. Piao YS, Hayashi S, Hasegawa M, Wakabayashi K, Yamada M, Yoshimoto M, Ishikawa A, Iwasubo T, Takahashi H. Co-localisation of α -synuclein and phosphorylated tau in neuronal and GCI in a patient with multiple system atrophy of long duration. *Acta Neuropathol* 2001; 101: 285-293.
139. Pick A. Über einen weiteren Symptomenkomplex im Rahmen der Dementia senilis, bedingt durch umschriebene stärkere Hirnatrophie (gemischte Apraxie). *Monat Psych Neurol* 1906; 19: 97-108.
140. Pielou EC. *An Introduction to Mathematical Ecology*. J. Wiley, New York, London, Sydney, Toronto 1969.
141. Pierucci A, de Oliveira AL. Increased sensory neuron apoptotic death two weeks after peripheral axotomy in C57BL/6J mice compared to A/J mice. *Neurosci Lett* 2006; 396: 127-131.
142. Pike CJ, Cotman CW. Calretinin-immunoreactive neurons are resistant to β -amyloid toxicity in vitro. *Brain Res* 1995; 671: 293-298.
143. Reed LA, Schmidt ML, Wszolek ZK, Balin BJ, Soontornniyomkij V, Lee VMY, Trojanowski JQ, Schelper RL. The neuropathology of a chromosome 17-linked autosomal dominant parkinson-

- sism and dementia ("pallidoponto-nigral degeneration"). *J Neuropath Exp Neur* 1998; 57: 588-601.
144. Rezaie P, Cairns NJ, Chadwick A, Lantos PL. Lewy bodies are located preferentially in limbic areas in diffuse Lewy body disease. *Neurosci Lett* 1996; 212: 111-114.
 145. Ritchie K, Touchon J. Heterogeneity in senile dementia of the Alzheimer type: individual differences, progressive deterioration or clinical subtypes? *J Clin Epidemiol* 1992; 45: 1391-1398.
 146. Roher AE, Lowenson JD, Clarke S, Wolkow W, Wang R, Cotter RJ, Reardon IM, Zurcherneely HA, Heinrikson RL, Ball MJ, Greenberg BD. Structural alterations in the peptide backbone of β -amyloid core protein may account for its deposition and stability in Alzheimer's disease. *J Biol Chem* 1993; 268: 3072-3073.
 147. Rosenberg CK, Pericak-Vance MA, Saunders AM, Gilbert JR, Gaskell PC, Hulette CM. Lewy body and Alzheimer pathology in a family with the amyloid-beta precursor protein APP717 gene mutation. *Acta Neuropathol* 2000; 100: 145-152.
 148. Sabbagh MN, Sandhu SS, Farlow MR, Veddeis L, Shell HA, Caviness JN, Connor DJ, Sue L, Adler CH, Beach TG. Correlation of clinical features with argyrophilic grains at autopsy. *Alz Dis Assoc Dis* 2009; 23: 229-233.
 149. Saito Y, Kawashima A, Ruberu NN, Fujiwara H, Koyama S, Sawaki M, Arai T, Nagura H, Yamanouchi H, Hasegawa M, Iwatsubo T, Murayama S. Accumulation of phosphorylated α -synuclein in aging human brain. *J Neuropath Exp Neurol* 2003; 62: 644-654.
 150. Sampathu DM, Neumann M, Kwong LK, Chou TT, Micsenyi M, Truax A, Bruce J, Grossman M, Trojanowski JQ, Lee VM. Pathological heterogeneity of frontotemporal lobar degeneration with ubiquitin-positive inclusions delineated by ubiquitin immunohistochemistry and novel monoclonal antibodies. *Am J Pathol* 2006; 169: 1343-1352.
 151. Saper CB, Wainer BH, German DC. Axonal and transneuronal transport in the transmission of neurological disease: potential role in system degenerations including Alzheimer's disease. *Neuroscience* 1987; 23: 389-398.
 152. Schulz-Schaeffer WJ, Giese A, Windl O, Kretschmar HA. Polymorphism at codon 129 of the prion protein gene determines cerebellar pathology in Creutzfeldt-Jakob disease. *Clin Neuropathol* 1996; 15: 353-357.
 153. Shinotoh H, Namba H, Yamaguchi M, Fukushi K, Nagatsuka S, Iyo M, Asahina M, Hattori T, Tanada S, Irie T. Positron emission tomographic measurement of acetylcholinesterase activity reveals differential loss of ascending cholinergic systems in Parkinson's disease and progressive supranuclear palsy. *Ann Neurol* 1999; 46: 62-69.
 154. Spillantini MG, Crowther RA, Jakes R, Cairns NJ, Lantos PL, Goedert M. Filamentous alpha-synuclein inclusions link multiple system atrophy with Parkinson's disease and dementia with Lewy bodies. *Neurosci Lett* 1998; 251: 205-208.
 155. Steiner JA, Angot E, Brunden P. A deadly spread: cellular mechanisms of α -synuclein transfer. *Cell Death Differ* 2011; 18: 1425-1433.
 156. Steinling M, Defebvire L, Duhamel A, Lecouffe P, Lavenu I, Pasquier F, Charpentier P. Is there a typical pattern of brain SPECT imaging in Alzheimer's disease? *Dement Geriatr Cogn* 2001; 12: 371-378.
 157. Struble RG, Powers RE, Casanova MF, Kitt CA, Brown EC, Price DL. Neuropeptidergic systems in plaques in Alzheimer's disease. *J Neuropath Exp Neurol* 1987; 46: 567-584.
 158. Suzuki K, Parker CC, Pentchev PG. Niemann-Pick disease type C: neuropathology revisited. *Dev Brain Dyst* 1997; 10: 306-320.
 159. Tabaton M, Perry G, Gambelli L, Manello V, Gambetti P. Influence of neuronal location on antigenic properties of neurofibrillary tangles. *Ann Neurol* 1988; 23: 604-610.
 160. Talbot P. Fronto-temporal dementia. *Alzheimer's Review* 1997; 6: 1-5.
 161. Talbot PR, Goulding PJ, Lloyd JJ, Snowden JS, Neary D, Testa HJ. Interrelation between classic motor neuron disease and frontotemporal dementia: neuropsychological and single-photon emission computed tomography study. *J Neurol Neurosurg Psychiatry* 1995; 58: 541-547.
 162. Tierney M, Fisher R, Lewis A, Zoritto M, Snow W, Reid D, Nieuwstraten P. The NINCDS-ADRDA work group criteria for the clinical diagnosis of probable Alzheimer's disease. *Neurology* 1988; 38: 359-364.
 163. Tolnay M, Monsch AU, Staehelin HB, Probst A. Argyrophilic grain disease: a disorder distinct from Alzheimer's disease. *Pathologie* 1999; 20: 159-168.
 164. Trojanowski JQ, Dickson D. Update on the neuropathological diagnosis of frontotemporal dementias. *J Neuropath Exp Neurol* 2001; 60: 1123-1126.
 165. Troncoso JC, Sukhov RR, Kawas CH, Koliatsos VE. In situ labeling of dying cortical neurons in normal aging and in Alzheimer's disease: correlations with senile plaques and disease progression. *J Neuropath Exp Neurol* 1996; 55: 1134-1142.
 166. Verga L, Frangione B, Tagliavini F, Giaccone G, Migheli A, Bugiani O. Alzheimer's and Down's patients: cerebral preamyloid deposits differ ultrastructurally and histochemically from the amyloid of senile plaques. *Neurosci Lett* 1989; 105: 294-299.
 167. Wakabayashi K, Takahashi H. Pathological heterogeneity in progressive supranuclear palsy and corticobasal degeneration. *Neuropathology* 2004; 24: 79-86.
 168. Wakabayashi K, Ikeuchi T, Ishikawa A, Takahashi H. Multiple system atrophy with severe involvement of the motor cortical areas and cerebral white matter. *J Neurol Sci* 1998; 156: 114-117.
 169. Wallin A, Blennow K. Clinical subgroups of Alzheimer's syndrome. *Acta Neurol Scand* 1996; 93: 51-57.
 170. Wenning GK, Quinn NP. Multiple system atrophy. *Baillieres Clin Neurol* 1997; 6: 187-204.
 171. Wenning GK, Tison F, Ben-Shlomo Y, Daniel SE, Quinn NP. Multiple system atrophy: a review of 203 pathologically proven cases. *Movement Disord* 1997; 12: 133-147.
 172. Whitwell JL, Jack CR, Senjern ML, Josephs KA. Patterns of atrophy in pathologically confirmed FTLD with or without motor neuron degeneration. *Neurology* 2006; 66: 102-104.
 173. Williams DR, de Silva R, Paviour DC, Pittman A, Watt HC, Kilford L, Holton JL, Revesz T, Lees AJ. Characteristics of two distinct clinical phenotypes in pathologically proven progressive

- supranuclear palsy: Richardson's syndrome and PSP-parkinsonism. *Brain* 2005; 128: 1247-1258.
174. Yaar M, Zhai S, Pilch PF, Doyle SM, Eisenhauer PB, Fine RE, Gilchrist BA. Binding of beta-amyloid to the p75 neurotrophic receptor induces apoptosis: a possible mechanism for Alzheimer's disease. *J Clin Invest* 1997; 100: 2333-2340.
175. Yamada T, McGeer PL, McGeer EG. Appearance of paired nucleated tau-positive glia in patients with progressive supranuclear palsy brain tissue. *Neurosci Lett* 1992; 135: 99-102.
176. Yamaguchi H, Ishiguro K, Sugihara S, Nakazato Y, Kawabayashi T, Sun XY, Hirai S. Presence of apolipoprotein ϵ on extracellular neurofibrillary tangles and on meningeal blood vessels precedes the Alzheimer β -amyloid deposition. *Acta Neuropathol* 1994; 88: 413-419.
177. Yokota O, Tsuchiya K, Terada S, Ishizu H, Uchikado H, Ikeda M, Oyenagi K, Nakamo I, Murayama S, Kuroda S, Akiyama H. Basophilic inclusion body disease and neuronal intermediate filament inclusion disease: a comparative clinicopathological study. *Acta Neuropathol* 2008; 115: 561-575.
178. Zhukareva V, Shah K, Uryu K, Braak H, del Tredici K, Sundarraj S, Clark C, Trojanowski JQ, Lee VMY. Biochemical analysis of tau proteins in argyrophilic grain disease, Alzheimer's disease and Pick's disease: a comparative study. *Am J Pathol* 2002; 161: 1135-1141.

High expression of DNA methyltransferases in primary human medulloblastoma

Tímea Pócza^{1,2}, Tibor Krenács^{3,4}, Eszter Turányi³, János Csáthy¹, Zsuzsanna Jakab¹, Peter Hauser¹

¹2nd Department of Pediatrics, Semmelweis University, Budapest, ²Department of Molecular Genetics, National Institute of Oncology, Budapest, ³1st Department of Pathology and Experimental Cancer Research, Semmelweis University, Budapest, ⁴Tumor Progression Research Group, Joint Research Organization of the Hungarian Academy of Sciences and Semmelweis University, Budapest, Hungary

Folia Neuropathol 2016; 54 (2): 105-113

DOI: 10.5114/fn.2016.60365

Abstract

Epigenetic alterations have been implicated in cancer development. DNA methylation modulates gene expression, which is catalyzed by DNA methyltransferases (DNMTs). The objective of our study was to evaluate expression of DNMTs in medulloblastoma and analyze its correlation with clinical features. Nuclear expression of DNMT1, DNMT3A and DNMT3B was analyzed in human primary medulloblastoma of 44 patients using immunohistochemistry. Correlation of expression of DNMT levels with classical histological subtypes, novel molecular subgroups and survival of patients was analyzed. Elevated expression of DNMT1, DNMT3A and DNMT3B was observed in 63.64%, 68.18% and 72.73% of all cases, respectively. None of them showed a correlation with classical histology or survival. Concerning molecular subtypes, significantly higher expression of DNMT1 was observed in the SHH group compared to non-SHH samples ($p = 0.02$), but without significant difference in DNMT3A or DNMT3B levels between any subtypes. In conclusion, DNMT1, DNMT3A and DNMT3B are highly expressed in human medulloblastoma samples, suggesting that promoter hypermethylation may play a role in medulloblastoma development. Demethylation of tumor suppressor gene promoters may be considered as a possible future target in therapy of medulloblastoma.

Key words: medulloblastoma, DNA methyltransferases, survival, SHH.

Introduction

Medulloblastoma (MB) is the most frequent malignant brain tumor in childhood, with various histological appearances. There are non-overlapping histological (classic, desmoplastic, extensive nodular, large cell/anaplastic) and molecular classifications (SHH, WNT, Group 3 and 4) for medulloblastoma [3,6,11,23,25,27,34]. Despite multimodal therapies, the 70-75% long-term survival rate has not been

exceeded yet in high-risk patients [13,29,34]. A more precise classification of patients would help to develop a more effective treatment strategy and reduce side effects [3,11,23].

There is emerging evidence that epigenetic changes contribute to carcinogenesis. The most important mechanisms of epigenetic alteration are DNA methylation, histone modification and microRNA regulation. DNA methyltransferases (DNMTs) are enzymes transferring methyl groups to cytosine in CpG dinu-

Communicating author:

Peter Hauser, 2nd Department of Pediatrics, Semmelweis University, Tűzoltó utca 7-9, H-1094 Budapest, Hungary, phone: +36(1)2151380, fax: +36(1)2151381, e-mail: hauserpeti@yahoo.com

cleotides, resulting in gene silencing. The DNMT family has three active members: DNMT1, DNMT3A and DNMT3B. DNMT3A and DNMT3B are regarded as *de novo* methyltransferases, whilst DNMT1 reacts on hemimethylated DNA, copying the methylation pattern during replication. Generally, tumor cells are characterized by global hypomethylation and hypermethylation of certain gene promoters. Therefore, repetitive elements are hypomethylated and specific tumor suppressor genes are repressed due to hypermethylation. These may contribute to chromosomal instability and abnormal gene silencing that could promote tumor-initializing steps [2,9,14,28,38]. Promoter hypermethylation of tumor suppressor genes and DNA repair genes has been observed in a wide variety of tumors, such as colorectal, breast cancer, glioma and medulloblastoma [19,22,36]. Overexpression of DNMTs was detected at the mRNA or protein level. Increased DNMT1 expression was described in gastric cancers, along with DNMT3A in breast and pancreatic cancer, or along with DNMT3B in glioma [8,16,30,38,39]. Although there is emerging evidence that epigenetic events play a remarkable role in the development of adult cancers, our knowledge about their role in pediatric brain tumors is still very limited.

DNA methylation studies in medulloblastoma have focused on the role of tumor suppressor genes in the development of brain tumors, and shed light on contradictory results in the majority of genes, except for RASSF1A [37]. Recent studies indicate that the DNA methylation profile can be used for MB subgrouping and disease risk assessment [18,35].

The aims of our study are to characterize the expression of DNMTs in human medulloblastoma samples and their potential prognostic role in survival of patients. Possible correlations of DNMT proteins and clinicopathological features are also analyzed.

Material and methods

Medulloblastoma tissue samples

Formalin-fixed, paraffin-embedded MB tumor samples were collected from the National Institute of Neurosciences (Budapest, Hungary) and 1st Institute of Pathology and Experimental Cancer Research, Semmelweis University (Budapest, Hungary). Forty-four primary medulloblastoma samples removed surgically between 2004 and 2010 and related clinical data of patients derived from the

Hungarian Pediatric Cancer Registry were used. The study was approved by the Ethics Committee of the Institutional Ethical Review Board of Semmelweis University (TUKEB No. 30/2015).

Tissue microarray (TMA) construction and immunohistochemistry

Hematoxylin and eosin (HE) stained sections were reviewed by a neuropathologist to select representative areas for producing TMA. TMA blocks were created by a computer-controlled TMA Master (3DHISTECH, Budapest, Hungary) instrument. Depending on sample quality one or two cores of representative areas with a diameter of 2 mm were taken from each tumor sample. From the TMA blocks 4 µm sections were created. Sections were deparaffinized, rehydrated, and endogenous peroxidase activity was blocked. Heat-induced antigen retrieval was performed with Tris-EDTA buffer (pH = 9.0) for 45 min in a microwave oven. Sections were incubated overnight using anti-DNMT1 antibody (dilution 1 : 200; Ab19905, Abcam, Cambridge, UK), anti-DNMT3A antibody (dilution 1 : 600; Ab13888, Abcam, Cambridge, UK) and anti-DNMT3B antibody (dilution 1 : 200; Ab13604, Abcam, Cambridge, UK) diluted in 5% BSA containing Tris-buffered saline (TBS; pH = 7.4). Antigen development was performed by Novolink Polymer Detection System (Novocastra, Wetzlar, Germany) following the manufacturer's instructions. Reactions were visualized by 3,3'-diaminobenzidine (DAB) (DAKO, Denmark) as a substrate, and then slides were counterstained by hematoxylin. Tonsil for DNMT1, and kidney for DNMT3A and DNMT3B were used as positive tissue controls.

For determination of the WNT subgroup anti-β-catenin antibody (dilution 1 : 150; M-3539, DAKO, Denmark) and of the SHH subgroup anti-secreted frizzled-related protein 1 (SFRP1) antibody (dilution 1 : 1500; ab-4193, Abcam, Cambridge, UK), characteristic proteins of these pathways, were applied. Immunohistochemical reactions were executed as described above, but antigen retrieval was performed in TE buffer boiled in a pressure cooker for 20 minutes.

Evaluation of immunostaining

Slides were digitalized by a Panoramic Scan instrument and examined by Panoramic Viewer

software (3DHISTECH, Budapest, Hungary). To evaluate DNMT expression only nuclear staining was considered. Intensity of staining and rate of positive cells were calculated from 1,000 cells in a representative area of each sample. According to the intensity of staining, four values were created: 0 (negative), 1 (weak), 2 (moderate) and 3 (strong). The proportion of positive cells was ranked in five groups: 0 (negative), 1 (1-25%), 2 (26-50%), 3 (51-75%) and 4 (76-100%). The products of the two values (0-12) were divided into two groups: 0-3 regarded as no/weak expression and 4-12 regarded as moderate/strong expression. Samples were classified into WNT or SHH subgroups when the proportion of positive cells with nuclear β -catenin or negative nuclear β -catenin and positive SFRP1 staining was above 10% [7,27].

Statistical analysis

All statistical analysis was performed using Statistica software (StatSoft Inc., Tulsa, OK, USA). Survival of patients was calculated by the Kaplan-Meier method. Correlation of expression of DNMTs and survival was examined by the log-rank test. Correlation of expression of each DNMT was analyzed by the Spearman rank order test. Correlation of expression of DNMTs and age, gender, histological subtype or molecular subgroups was examined by the Mann-Whitney *U*-test and Fisher's exact test, when appropriate. Results were considered statistically significant when the *p* value was less than 0.05.

Results

Patients' data

Demographic characteristics of the studied cohort are summarized in Table I. Median age of 44 patients was 8.5 years (range 1.1-28.7 years). The proportion of male patients was 55%. Histologically, 84.1%, 11.4% and 4.5% of patients showed classic, desmoplastic and large cell/anaplastic (L/A) type of medulloblastoma, respectively. Survival data were available in 40 patients (90.9%). Median follow-up time was 5.6 years (range 0-9.7 years). Patients were treated according to the Hungarian MBL2004/2008 schedules [15]. There is no standard treatment for adults with medulloblastoma in Hungary. Patients are treated according to the individual decision of each treating physician, and these treatment details are poorly accessible in Hungary. Therefore, adult patients were omitted from the survival analysis.

Expression of DNMTs in human medulloblastoma

Elevated (moderate/strong) expression of DNMT1, DNMT3A and DNMT3B was observed in 63.64%, 68.18% and 72.73% of patients, respectively (Table I). Representative stains are shown in Figure 1. The relationship of histology and DNMT expression was evaluated only in the classic and desmoplastic type. Moderate/strong expression of DNMT1 was detected in 62.2% of classic and 60.0% of desmoplastic, of DNMT3A in 70.3% of classic and 60.0% of desmoplastic, and of DNMT3B in 70.3% of classic and 80.0% of desmoplastic samples. We could analyze only two samples of L/A subtype. Both of them showed moderate/strong expression for DNMT1 and DNMT3B, but only one for DNMT3A.

Correlation between DNMT expression and patients' data

There was no correlation between the expression of DNMT1, DNMT3A and DNMT3B and age at disease onset or gender or histological subtype (Table II). Kaplan-Meier curves, based on different expression of DNMTs, did not show a significant difference in overall survival (Fig. 2). None of the DNMTs could be used as a prognostic marker for medulloblastoma in our cohort. DNMT1 and DNMT3A ($p = 0.08$), or DNMT1 and DNMT3B ($p = 0.17$) or DNMT3A and DNMT3B ($p = 0.69$) did not show a co-expression pattern. Expression of nuclear β -catenin was shown only in one patient (2.3%) with weak staining. There were 12 (27.3%) patients belonging to SHH subgroup according to their cytoplasmic, membranous or secreted SFRP1 expression and lack of nuclear β -catenin (Table I). Expression of DNMT1 in the SHH subgroup compared to the non-WNT/non-SHH subgroup of patients was significantly higher ($p = 0.02$), whereas expression of DNMT3A and DNMT3B did not differ significantly between different groups ($p = 0.78$ and $p = 0.17$, respectively, Table II).

Discussion

In recent years a new prognostic classification of medulloblastoma was introduced by molecular findings, whilst there are still several twists in this classification system. It is still motivating to find further prognostic markers [3,6,11,23,25,27,34]. Nowadays, an exact diagnosis of pediatric brain tumors can be established based on the methylation profile of dif-

Table I. Characteristics of patients and results of immunohistochemical staining of DNMTs, β -catenin, and SFRP1

	Gender	Histology	Age at disease onset (years)	State	Survival (years)	DNMT1*	DNMT3A*	DNMT3B*	β -catenin	SFRP1
1	F	Classic	1.18	Dead	0.18	0	0	0	Negative	Negative
2	M	L/A	7.84	Dead	1.47	9	4	6	Negative	Positive
3	F	Classic	5.99	Dead	4.56	4	9	3	Negative	Negative
4	F	Classic	14.04	Dead	0.00	4	6	8	Negative	Negative
5	M	Classic	10.81	Dead	7.98	4	8	8	Negative	Positive
6	F	Classic	3.31	Alive	9.38	6	8	12	Negative	Negative
7	M	Classic	13.54	Alive	9.74	8	12	12	Negative	Negative
8	M	Classic	17.09	Alive	8.99	2	0	8	Negative	Positive
9	F	Classic	10.09	Dead	3.07	2	8	8	Negative	Negative
10	M	Desmoplastic	14.54	Alive	9.08	1	2	3	Negative	Negative
11	M	Desmoplastic	5.14	Dead	0.59	4	4	6	Negative	Negative
12	F	Classic	17.90	Dead	5.02	4	2	8	Negative	Negative
13	M	Classic	3.11	Dead	0.92	2	1	4	Negative	Negative
14	F	Classic	4.71	Alive	8.54	4	6	12	Negative	Negative
15	M	Classic	15.30	Alive	7.80	2	4	2	Positive	Negative
16	F	Classic	8.48	Alive	7.24	12	2	2	Negative	Negative
17	F	Classic	14.28	Alive	8.09	4	8	8	Negative	Negative
18	M	Desmoplastic	6.63	Alive	7.90	3	12	8	Negative	Positive
19	M	L/A	13.84	Dead	1.94	4	3	12	Negative	Positive
20	M	Desmoplastic	4.34	Dead	0.09	9	12	4	Negative	Negative
21	M	Classic	8.56	Alive	7.00	2	4	12	Negative	Negative
22	M	Classic	15.46	Alive	6.52	2	8	12	Negative	Negative
23	M	Desmoplastic	2.59	Alive	6.52	4	2	4	Negative	Positive
24	M	Classic	4.50	Dead	1.92	4	12	3	Negative	Negative
25	F	Classic	9.30	Dead	5.54	8	12	12	Negative	Negative
26	M	Classic	6.81	Alive	6.63	4	2	3	Negative	Negative
27	F	Classic	8.50	Alive	6.07	8	0	12	Negative	Negative
28	M	Classic	7.70	Alive	6.02	2	8	8	Negative	Negative
29	F	Classic	1.77	Alive	6.76	9	8	8	Negative	Positive
30	F	Classic	4.92	Alive	6.56	6	8	6	Negative	Negative
31	M	Classic	22.90	NA	NA	6	4	8	Negative	Positive
32	M	Classic	10.76	Dead	5.22	2	2	4	Negative	Negative
33	F	Classic	21.43	NA	NA	6	0	12	Negative	Positive
34	F	Classic	16.71	Alive	5.67	2	12	1	Negative	Negative
35	M	Classic	7.92	Alive	5.48	1	1	4	Negative	Negative
36	F	Classic	10.75	Alive	5.65	4	4	3	Negative	Negative
37	F	Classic	1.78	Dead	0.48	2	8	6	Negative	Negative
38	M	Classic	4.63	Alive	4.99	4	3	4	Negative	Negative
39	M	Classic	28.25	NA	NA	9	4	6	Negative	Positive
40	F	Classic	1.07	Alive	3.23	6	12	3	Negative	Negative
41	F	Classic	2.84	Alive	3.12	2	8	2	Negative	Negative
42	M	Classic	13.18	Alive	2.80	2	8	8	Negative	Negative
43	F	Classic	28.69	NA	NA	9	12	2	Negative	Positive
44	M	Classic	9.68	Alive	2.12	9	12	12	Negative	Positive

*Product of intensity (0-3) and rate of positive cells (0-4), maximal value: 12 SFRP1 – secreted frizzled-related protein 1, DNMT – DNA methyltransferase, M – male, F – female, L/A – large cell/anaplastic, NA – not available

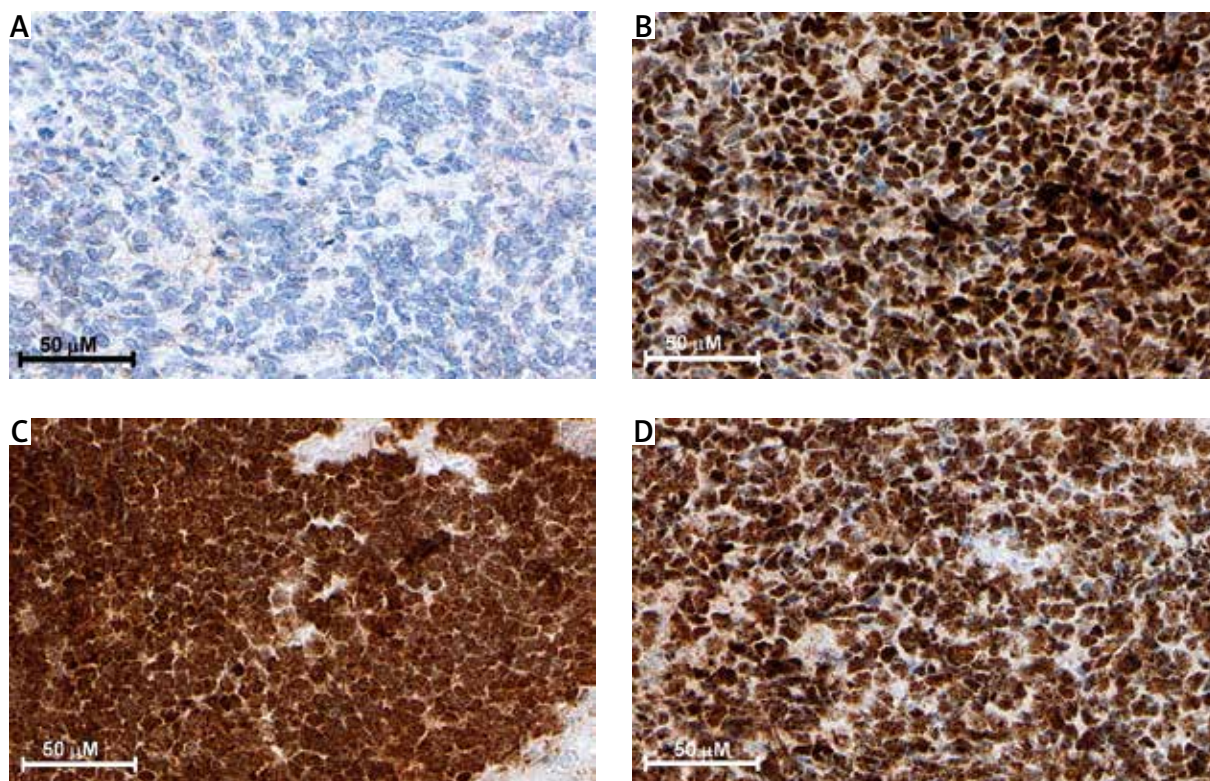


Fig. 1. Representative immunohistochemical staining of DNMTs in medulloblastoma. **A)** Negative staining of DNMT3A. **B, C, D)** Moderate/strong immunopositivity of DNMT1, DNMT3A and DNMT3B, respectively.

Table II. Evaluation of patients' characteristics and expression of different DNMTs. Correlation of DNMTs and clinical features are shown by probability value (*p*)

	All	DNMT1		<i>p</i>	DNMT3A		<i>p</i>	DNMT3B		<i>p</i>
		No/ Weak	Moderate/ Strong		No/ Weak	Moderate/ Strong		No/ Weak	Moderate/ Strong	
Number of patients	44	16 (36.36%)	28 (63.64%)	0.91 ^a	14 (31.82%)	30 (68.18%)	0.91 ^a	12 (27.27%)	32 (72.73%)	0.65 ^a
Median age of patients (years)	8.53	9.33	8.49		8.49	8.93		7.65	8.93	
Gender										
Male	24	11	13	0.21 ^b	9	15	0.52 ^b	4	20	0.10 ^b
Female	20	5	15		5	15		8	12	
Histological subtype										
Classic	37	14	23	1.00 ^b	11	26	0.64 ^b	11	26	1.00 ^b
Desmoplastic	5	2	3		2	3		1	4	
Large cell/anaplastic	2	0	2		#	1		1	#	
Molecular subtype										
Wnt	1	1	0	0.02 ^a *	0	1	0.78 ^a	1	0	#
Shh	12	2	10		4	8		1	11	
Non-Wnt/non-Shh	21	13	18		10	21		10	21	

^aMann-Whitney U-test, ^bFisher's exact test, two-tailed, # – not applicable, * – statistically significant

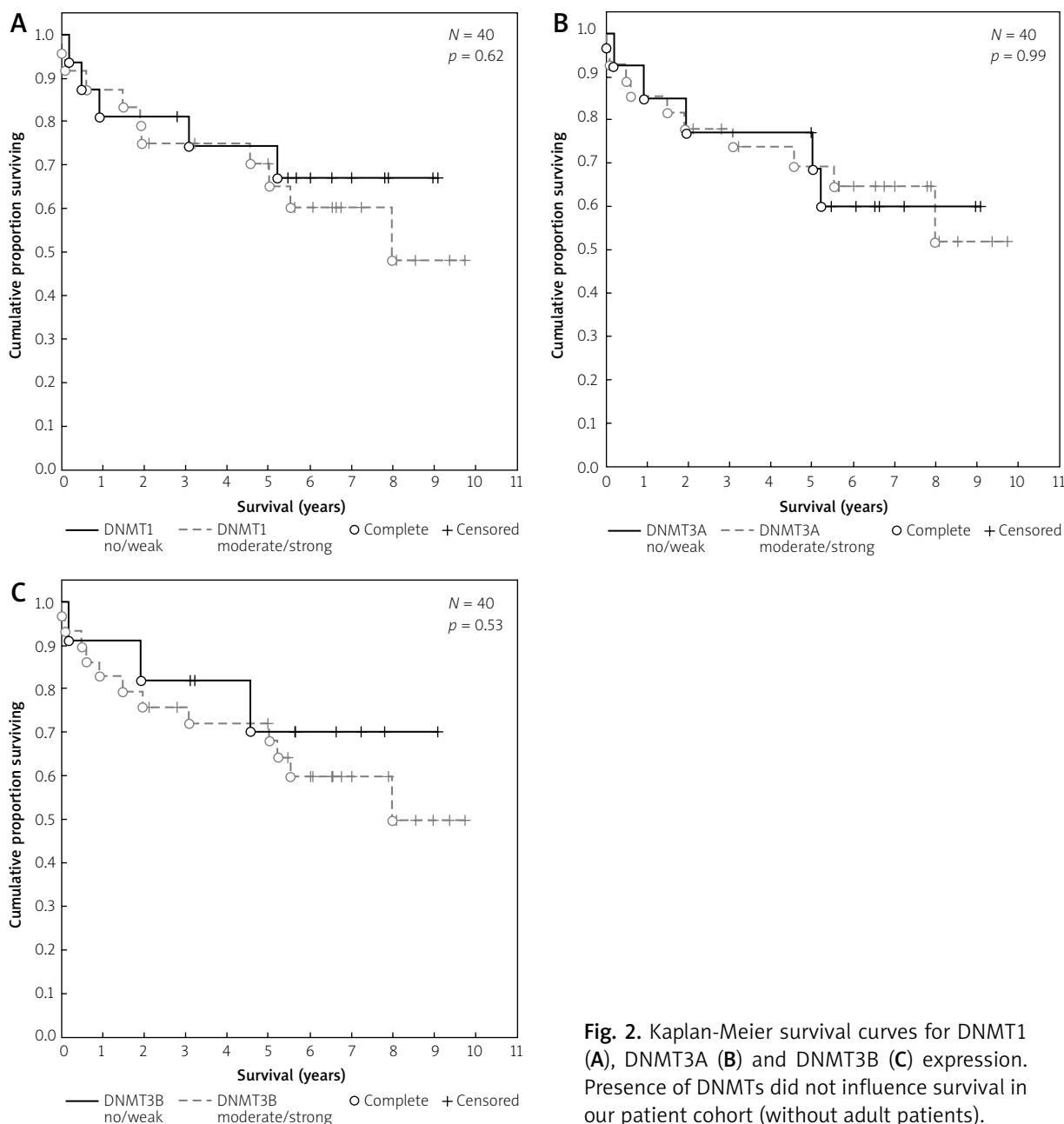


Fig. 2. Kaplan-Meier survival curves for DNMT1 (A), DNMT3A (B) and DNMT3B (C) expression. Presence of DNMTs did not influence survival in our patient cohort (without adult patients).

ferent tumor types [18,21,35]. DNMTs are responsible for DNA methylation, an important epigenetic regulation process, which contributes to development of cancer. DNMT1 is responsible for maintenance of methylation patterns during DNA replication. DNMT3A and DNMT3B are regarded as de novo methyl-transferases and abundantly expressed during embryonic development [2,9,14,19,22,28,38].

In our study, expression of three members of the DNMT family (DNMT1, DNMT3A, DNMT3B) in me-

dulloblastoma samples and their possible effect on disease outcome were examined. During the development and progression of MB, the biological role of DNMTs, crucial regulators of the methylation pattern, is not completely understood yet. In our study, the correlation of expression of these enzymes at the protein level and clinical data of MB patients were investigated.

In our experiments elevated expression of all DNMTs was observed in most of the MB samples.

Correlation of expression of DNMTs and histological subtype of MB, age at disease onset or gender was not proven in our experience. Increased DNMT1 expression indicates worse outcomes in several types of cancers, such as gastric cancer, hepatocellular carcinomas and pancreatic ductal adenocarcinoma [10,26,33]. In contrast, our analysis showed no difference in disease outcome when comparing patients with no/weak and moderate/strong expression of three DNMTs, so DNMTs are not predictive markers for medulloblastoma survival. The different result may be due to the different biological nature of medulloblastoma and above-mentioned tumor types. While there are some common dysregulated signaling pathways (WNT, SHH, Notch) in medulloblastoma and in these other cancer types, differences could also be observed in regulation of the following pathways: in gastric cancer altered EGFR, ErbB, mTOR, VEGF, HGF/MET pathways, etc.; in hepatocellular carcinoma altered Ras/Raf/MAPK, mTOR, etc.; and in pancreatic ductal adenocarcinoma FGF, Notch, TGF- β , EGF and retinoid signaling [1,31,32].

The SHH subgroup of MB is characterized by the expression of SFRP1 and lack of nuclear β -catenin [17,27]. Our results indicate that SHH pathway activation is associated with elevated DNMT1 expression, which could be a consequence of upregulation of DNMT1 by SHH in SHH-associated medulloblastomas. Similar observations were made in pancreatic cancer and in myelodysplastic syndrome (MDS) [16,40]. DNMT1 and DNMT3A could be regulated by Gli1, an effector of the SHH signaling pathway. The SHH pathway was inhibited in pancreatic cancer and MDS cell lines, resulting in decreased DNMT1 expression, whereas induction of the SHH pathway resulted in higher DNMT1 expression [16,40]. In contrast, DNMT1 inhibition resulted in increased expression of SFRP1 in MB cell lines [20]. One explanation could be that investigated MB cell lines do not belong to the SHH subgroup, since they showed lower levels of SFRP1 compared to the SHH subgroup. Among non-WNT/non-SHH patients, other mechanisms could result in DNMT1 activation. Further studies are needed to clarify the relationship between regulation of DNA methylation and SHH signaling pathway.

Theoretically, inhibition of DNA methylation is a therapeutic opportunity by reversing gene silencing [9,12,14,38]. An *in vitro* experiment showed that the DNMT inhibitor 5-aza-2'-deoxycytidine (decit-

abine) reactivates the tumor suppressor PTCH1 gene in the MB cell line [4]. A combination of DNMT and histone deacetylase (HDAC) inhibitors was effective to prevent MB development in *Ptch* knockout mice, while in advanced stage tumors this therapy was less efficient [5]. Epigenetic modulators combined with multi-kinase inhibitor could enhance apoptosis *in vitro* in medulloblastoma cells [24].

In conclusion, this is the first study to analyze DNMT expression in medulloblastoma in terms of expression level and correlation with clinical data. Elevated expression of DNMTs in human medulloblastoma, and association of DNMT1 and SHH subgroups were observed, without an effect on survival. Based on increased expression of DNMTs in medulloblastoma, their inhibition has potential for further investigation to optimize therapy of medulloblastoma.

Acknowledgments

We thank Edit Parsch and Zita Bratu for excellent technical assistance, Miklós Garami for assistance in performing experiments and Balázs Hauser for help in preparation of the manuscript.

Disclosure

Authors report no conflict of interest.

References

1. Chen C, Wang G. Mechanisms of hepatocellular carcinoma and challenges and opportunities for molecular targeted therapy. *World J Hepatol* 2015; 7: 1964-1970.
2. Choi JD, Lee JS. Interplay between epigenetics and genetics in Cancer. *Genomics Inform* 2013; 11: 164-173.
3. DeSouza RM, Jones BR, Lowis SP, Kurian KM. Pediatric medulloblastoma – update on molecular classification driving targeted therapies. *Front Oncol* 2014; 4: 176.
4. Diede SJ, Guenthoer J, Geng LN, Mahoney SE, Marotta M, Olson JM, Tanaka H, Tapscott SJ. DNA methylation of developmental genes in pediatric medulloblastomas identified by denaturation analysis of methylation differences. *Proc Natl Acad Sci U S A* 2010; 107: 234-239.
5. Ecke I, Petry F, Rosenberger A, Tauber S, Mönkemeyer S, Hess I, Dullin C, Kimmina S, Pirngruber J, Johnsen SA, Uhmanna A, Nitzki F, Wojnowski L, Schulz-Schaeffer W, Witt O, Hahn H. Antitumor effects of a combined 5-aza-2'-deoxycytidine and valproic acid treatment on rhabdomyosarcoma and medulloblastoma in *Ptch* mutant mice. *Cancer Res* 2009; 69: 887-895.
6. Ellison DW. Childhood medulloblastoma: novel approaches to the classification of a heterogeneous disease. *Acta Neuropathol* 2010; 120: 305-316.

7. Ellison DW, Dalton J, Kocak M, Nicholson SL, Fraga C, Neale G, Kenney AM, Brat DJ, Perry A, Yong WH, Taylor RE, Bailey S, Clifford SC, Gilbertson RJ. Medulloblastoma: clinicopathological correlates of SHH, WNT, and non-SHH/WNT molecular subgroups. *Acta Neuropathol* 2011; 121: 381-396.
8. Etoh T, Kanai Y, Ushijima S, Nakagawa T, Nakanishi Y, Sasako M, Kitano S, Hirohashi S. Increased DNA methyltransferase 1 DNMT1; protein expression correlates significantly with poorer tumor differentiation and frequent DNA hypermethylation of multiple CpG islands in gastric cancers. *Am J Pathol* 2004; 164: 689-699.
9. Gal-Yam EN, Saito Y, Egger G, Jones PA. Cancer epigenetics: modifications, screening, and therapy. *Annu Rev Med* 2008; 59: 267-280.
10. Gao J, Wang L, Xu J, Zheng J, Man X, Wu H, Jin J, Wang K, Xiao H, Li S, Li Z. Aberrant DNA methyltransferase expression in pancreatic ductal adenocarcinoma development and progression. *J Exp Clin Cancer Res* 2013; 32: 86.
11. Gerber NU, Mynarek M, von Hoff K, Friedrich C, Resch A, Rutkowski S. Recent developments and current concepts in medulloblastoma. *Cancer Treat Rev* 2014; 40: 356-365.
12. Goffin J, Eisenhauer E. DNA methyltransferase inhibitors-state of the art. *Ann Oncol* 2002; 13: 1699-1716.
13. Gottardo NG, Gajjar A. Chemotherapy for malignant brain tumors of childhood. *J Child Neurol* 2008; 23: 1149-1159.
14. Gros C, Fahy J, Halby L, Dufau I, Erdmann A, Gregoire JM, Ausseil F, Vispé S, Arimondo PB. DNA methylation inhibitors in cancer: recent and future approaches. *Biochimie* 2012; 94: 2280-2296.
15. Hauser P, Jakab Z, Kiss C, Szegedi I, Bárdi E, Batyik K, Ottóffy G, Kajtár P, Szűcs R, Nagy K, Cservák J, Masát P, Bálint K, Kordás M, Bognár L, Kocsis B, Vízkeleti J, Kriván G, Kállay K, Benyó G, Schuller D, Garami M. Előzetes eredmények a medulloblastoma/primitív neuroektodermális tumor PNET; kezelésében a magyar MBL 2004 kezelési sémával. *Magyar Belorvosi Archivum* 2009; 62: 196-201.
16. He S, Wang F, Yang L, Guo C, Wan R, Ke A, Xu L, Hu G, Xu X, Shen J, Wang X. Expression of DNMT1 and DNMT3a are regulated by GLL1 in human pancreatic cancer. *PLoS One* 2011; 6: e27684.
17. He J, Sheng T, Stelzer AA, Li C, Zhang X, Sinha M, Luxon BA, Xie J. Suppressing Wnt signaling by the hedgehog pathway through sFRP-1. *J Biol Chem* 2006; 281: 35598-35602.
18. Hovestadt V, Remke M, Kool M, Pietsch T, Northcott PA, Fischer R, Cavalli FM, Ramaswamy V, Zapatka M, Reifenberger G, Rutkowski S, Schick M, Bewerunge-Hudler M, Korshunov A, Lichter P, Taylor MD, Pfister SM, Jones DT. Robust molecular subgrouping and copy-number profiling of medulloblastoma from small amounts of archival tumour material using high-density DNA methylation arrays. *Acta Neuropathol* 2013; 125: 913-916.
19. Jin B, Robertson KD. DNA methyltransferases, DNA damage repair, and cancer. *Adv Exp Med Biol* 2013; 754: 3-29.
20. Kongkham PN, Northcott PA, Croul SE, Smith CA, Taylor MD, Rutka JT. The SFRP family of WNT inhibitors function as novel tumor suppressor genes epigenetically silenced in medulloblastoma. *Oncogene* 2010; 29: 3017-3024.
21. Korshunov A, Ryzhova M, Hovestadt V, Bender S, Sturm D, Capper D, Meyer J, Schrimpf D, Kool M, Northcott PA, Zheludkova O, Milde T, Witt O, Kulozik AE, Reifenberger G, Jabado N, Perry A, Lichter P, von Deimling A, Pfister SM, Jones DT. Integrated analysis of pediatric glioblastoma reveals a subset of biologically favorable tumors with associated molecular prognostic markers. *Acta Neuropathol* 2015; 129: 669-678.
22. Lahtz C, Pfeifer GP. Epigenetic changes of DNA repair genes in cancer. *J Mol Cell Biol* 2011; 3: 51-58.
23. Li KK, Lau KM, Ng HK. Signaling pathway and molecular subgroups of medulloblastoma. *Int J Clin Exp Pathol* 2013; 6: 1211-1222.
24. Marino AM, Frijhoff J, Calero R, Baryawno N, Ostman A, Johnsen JI. Effects of epigenetic modifiers in combination with small molecule inhibitors of receptor tyrosine kinases on medulloblastoma growth. *Biochem Biophys Res Commun* 2014; 450: 1600-1605.
25. Massimino M, Giangaspero F, Garrè ML, Gandola L, Poggi G, Biassoni V, Gatta G, Rutkowski S. Childhood medulloblastoma. *Crit Rev Oncol Hematol* 2011; 79: 65-83.
26. Mutze K, Langer R, Schumacher F, Becker K, Ott K, Novotny A, Hapfelmeier A, Höfler H, Keller G. DNA methyltransferase 1 as a predictive biomarker and potential therapeutic target for chemotherapy in gastric cancer. *Eur J Cancer* 2011; 47: 1817-1825.
27. Northcott PA, Korshunov A, Witt H, Hielscher T, Eberhart CG, Mack S, Bouffet E, Clifford SC, Hawkins CE, French P, Rutka JT, Pfister S, Taylor MD. Medulloblastoma comprises four distinct molecular variants. *J Clin Oncol* 2011; 29: 1408-1414.
28. Okano M, Bell DW, Haber DA, Li E. DNA methyltransferases Dnmt3a and Dnmt3b are essential for de novo methylation and mammalian development. *Cell* 1999; 99: 247-257.
29. Packer RJ, Zhou T, Holmes E, Vezina G, Gajjar A. Survival and secondary tumors in children with medulloblastoma receiving radiotherapy and adjuvant chemotherapy: results of Children's Oncology Group trial A9961. *Neuro Oncol* 2013; 15: 97-103.
30. Rajendran G, Shanmuganandam K, Bendre A, Muzumdar D, Mujumdar D, Goel A, Shiras A. Epigenetic regulation of DNA methyltransferases: DNMT1 and DNMT3B in gliomas. *J Neurooncol* 2011; 104: 483-494.
31. Rhim AD, Stanger BZ. Molecular biology of pancreatic ductal adenocarcinoma progression: aberrant activation of developmental pathways. *Prog Mol Biol Transl Sci* 2010; 97: 41-78.
32. Riquelme I, Saavedra K, Espinoza JA, Weber H, García P, Nervi B, Garrido M, Corvalán AH, Roa JC, Bizama C. Molecular classification of gastric cancer: towards a pathway driven targeted therapy. *Oncotarget* 2015; 6: 24750-24779.
33. Saito Y, Kanai Y, Nakagawa T, Sakamoto M, Saito H, Ishii H, Hirohashi S. Increased protein expression of DNA methyltransferase DNMT 1 is significantly correlated with the malignant potential and poor prognosis of human hepatocellular carcinomas. *Int J Cancer* 2003; 105: 527-532.
34. Schroeder K, Gururangan S. Molecular variants and mutations in medulloblastoma. *Pharmgenomics Pers Med* 2014; 7: 43-51.
35. Schwalbe EC, Williamson D, Lindsey JC, Hamilton D, Ryan SL, Megahed H, Garami M, Hauser P, Dembowska-Baginska B, Percek D, Northcott PA, Taylor MD, Taylor RE, Ellison DW, Bailey S, Clifford SC. DNA methylation profiling of medulloblastoma allows robust subclassification and improved outcome predic-

- tion using formalin-fixed biopsies. *Acta Neuropathol* 2013; 125: 359-371.
36. Sciuscio D, Hegi ME. Epigenetics and Brain Cancer. In: *Emerging Concepts in Neuro-Oncology*. Watts C (ed.). Springer-Verlag, London 2013; pp. 21-40.
 37. Sexton-Oates A, MacGregor D, Dodgshun A, Saffery R. The potential for epigenetic analysis of paediatric CNS tumours to improve diagnosis, treatment and prognosis. *Ann Oncol* 2015; 26: 1314-1324.
 38. Subramaniam D, Thombre R, Dhar A, Anant S. DNA methyltransferases: a novel target for prevention and therapy. *Front Oncol* 2014; 4: 80.
 39. Yu Z, Xiao Q, Zhao L, Ren J, Bai X, Sun M, Wu H, Liu X, Song Z, Yan Y, Mi X, Wang E, Jin F, Wei M. DNA methyltransferase 1/3a overexpression in sporadic breast cancer is associated with reduced expression of estrogen receptor-alpha/breast cancer susceptibility gene 1 and poor prognosis. *Mol Carcinog* 2015; 54: 707-719.
 40. Zou J, Hong Y, Tong Y, Wei J, Qin Y, Shao S, Wang C, Zhou K. Sonic hedgehog produced by bone marrow-derived mesenchymal stromal cells supports cell survival in myelodysplastic syndrome. *Stem Cells Int* 2015; 2015: 957502.

Assessment of candidate immunohistochemical prognostic markers of meningioma recurrence

Tamás Csonka¹, Balázs Murnyák¹, Rita Szepesi², János Bencze¹, László Bognár³, Álmos Klekner³, Tibor Hortobágyi¹

¹Division of Neuropathology, Institute of Pathology, ²Department of Neurology, ³Department of Neurosurgery, Faculty of Medicine, University of Debrecen, Debrecen, Hungary

Folia Neuropathol 2016; 54 (2): 114-126

DOI: 10.5114/fn.2016.60088

Abstract

Although tumour recurrence is an important and not infrequent event in meningiomas, predictive immunohistochemical markers have not been identified yet. The aim of this study was to address this clinically relevant problem by systematic retrospective analysis of surgically completely resected meningiomas with and without recurrence, including tumour samples from patients who underwent repeat surgeries. Three established immunohistochemical markers of routine pathological meningioma work-up have been assessed: the proliferative marker Ki-67 (clone Mib1), the tumour suppressor gene p53 and progesterone receptor (PR). All these proteins correlate with the tumour WHO grade, however the predictive value regarding recurrence and progression in tumour grade is unknown.

One hundred and fourteen surgical specimens of 70 meningioma patients (16 male and 54 female) in a 16 years' interval have been studied. All tumours had apparently complete surgical removal. On Mib1, PR and p53 immunostained sections, the percentage of labelled tumour cells, the staining intensity and the multiplied values of these parameters (the histoscore) was calculated. Results were statistically correlated with tumour WHO grade, (sub)type, recurrence and progression in WHO grade at subsequent biopsies.

Our results confirmed previous findings that the WHO grade is directly proportional to Mib1 and p53 and is inversely proportional to the PR immunostain. We have demonstrated that Mib1 and p53 have a significant correlation with and predictive value of relapse/recurrence irrespective of the histological subtype of the same WHO grade. As a quantitative marker, Mib1 has the best correlation with a percentage of labelled cells, whereas p53 with intensity and histoscore.

In conclusion, the immunohistochemical panel of PR, p53, Mib1 in parallel with applying standard diagnostic criteria based on H&E stained sections is sufficient and reliable to predict meningioma recurrence in surgically completely resected tumours.

Key words: immunohistochemistry, Ki-67, meningioma, p53, progesterone receptor, prognostic markers, tumour recurrence.

Introduction

Meningioma is one of the most frequent brain tumours [9]. According to the World Health Organization (WHO) classification, there are several subtypes like meningothelial, fibrous, transitional,

psammomatous, angiomatous, microcystic, secretory, lymphoplasmacyte-rich, metaplastic, choroid, clear cell, rhabdoid, papillary and other rare morphological phenotypes [6,21]. The assigned WHO grade I-III reflects the probable prognosis which is

Communicating author:

Tibor Hortobágyi, MD, PhD, FRCPath, EFN, Division of Neuropathology, Institute of Pathology, University of Debrecen, 98. Nagyerdeikrt. Debrecen, H-4032, Hungary, phone: +3652255248, e-mail: hortobagyi@med.unideb.hu; tibor.hortobagyi@kcl.ac.uk

determined by the subtype and/or specified morphological features such as mitotic rate, presence or absence of small geographic necrosis, nucleus-cytoplasm ratio and others [21]. Although tumour recurrence is an important and not infrequent event, our knowledge on predisposing factors is rather limited. The risk of recurrence increases with the WHO grade being 7-25% in WHO grade I, 30-50% in WHO grade II and 50-95% in WHO grade III [27,28,32,33]. The extent of resection assessed by the Simpson Grading System influences recurrence rates which is one reason of the wide range of probability [30]. The Simpson Grading System classifies the completeness of removal in a 5-tier scale ranging from macroscopically complete removal (grade I) to simple decompression with or without biopsy (grade V). Skull irradiation, inherited mutation of the NF2 gene (neurofibromatosis type 2) and epigenetic factors may also predispose to recurrence [22,23].

Another important phenomenon is tumour progression to a higher WHO grade. However, the risk and probability of progression remains rather unpredictable – even less so than tumour recurrence. Hence, there is a growing clinical need to identify additional and better predictors for recurrence and tumour progression than the currently used histological grade and extent of resection. Because immunohistochemistry has been routinely used in the pathological diagnostic practice for decades, the search for predictive immunohistochemical markers is of importance. In our study we focussed on 3 well-known immunohistochemical markers in routine pathological work-up of meningioma: the proliferative marker Ki-67 (clone Mib1), the tumour suppressor gene p53 and progesterone receptor. All these proteins have been studied in meningioma and the correlation with tumour grade has been confirmed by several studies. However, the predictive value regarding recurrence and progression in tumour grade remains unknown. The aim of this study is to address these clinically relevant questions by a systematic retrospective analysis of meningiomas with and without recurrence, with special emphasis on tumour samples from patients who underwent repeat surgeries due to tumour recurrence.

p53 is one of the major tumour suppressor proteins. The physiological functions of p53 are cell cycle regulation and conservation of the stability of the genome by preventing mutations, therefore it is called 'the guardian of the genome' [17]. More

than 50 percent of human tumours carries a deletion or mutation of the p53 genes (TP53) [13]. p53 can be activated by DNA damage, oxidative stress, osmotic shock, ribonucleotide depletion or oncogene expression. The activation is marked by an increase in the half-life of p53 and a change of its conformation [16], therefore shows increased Labelling Index (LI) with immunohistochemistry with the polyclonal antibodies routinely used in tumour diagnostics. The anticancer activity of p53 is through several mechanisms: it activates DNA repair proteins, induces growth arrest at the G1/S regulation point through p21 or initiates apoptosis if the DNA damage is irreversible [12]. It has been investigated also in meningioma and several studies showed a positive correlation with the grade and tumour recurrence [4,7,8,14,15,24,26], whereas authors reported the grade as an independent predictive factor of recurrences with high Mib1 and p53 LI being a supportive marker helpful in borderline cases [31].

Ki-67 is necessary for cellular proliferation; it is present during all active phases of the cell cycle, and absent from the G0 phase. Mib1 is the usually applied clone of the Ki-67 antibody which is widely used as a proliferative marker in the routine diagnostic work-up. The Mib1 LI shows a strong correlation with tumour growths, relapse/recurrence, length of disease free survival in various tumours [2,3,34] including meningioma [18,19].

Progesterone receptor (PR) is a steroid hormone receptor. It has been demonstrated that meningioma cells show positivity for PR; the ratio of the positive cells is inversely proportional to the WHO grade [18,27]. Also described earlier that the cellular biosynthesis of PR in meningioma is not oestrogen regulated as it is other sex steroid in tissues [5,7]. PR is encoded by the *PGR* gene on the long arm of chromosome 11. In a physiological situation after binding the progesterone hormone, the receptor undergoes a dimerization and is transported to the nucleus to bind to the DNA and induce transcription. Both forms (progesterone receptor A and progesterone receptor B) have a regulatory domain, a DNA binding domain, a hinge section and a ligand binding domain, but only the PR-B form possesses a transcription activation function.

The Mib1 antibody, p53 and PR are widely used immunohistochemical markers in meningioma diagnosis. In high-grade meningioma, the Mib1 LI is higher [1,4,28,29]. In our previous study we have reported

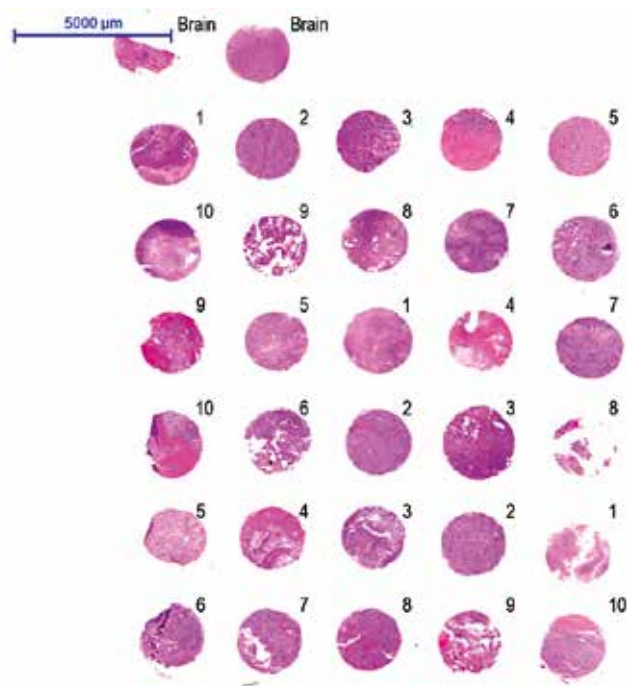


Fig. 1. Low magnification image of histological slide stained with haematoxylin-eosin, made from tissue microarray (TMA) paraffin block. In the upper left corner there are two tissue (brain) samples for guidance regarding localization. The numbers from 1 to 10 represent the individual cases. Every 'donor' case have 3 different samples in the 'recipient' block. Scale bar 5 mm.

a significant correlation between the frequency and intensity of p53 immunostaining and WHO grade [10]. The reduced of PR immunoreactivity is another known feature in the high grades of meningioma [18,20,25].

The aim of this study is to establish an easy-to-use immunohistochemical panel for the routine neuropathological use, which can predict meningioma relapse/recurrence. For validation we analysed the changes in immunohistochemical characteristics and expression patterns during relapse/recurrence and examined their relation to tumour grade.

Material and methods

One hundred and fourteen surgical specimens of 70 meningioma patients (16 male and 54 female) in a 16 years' interval have been retrospectively studied. All cases were revised by a consultant neuropathologist (TH) and divided into three grades and histological subtypes according to the WHO classification [21].

We established two study groups: patients with one or more recurrence/relapse(s) (R/R group) and

patients with meningioma without any radiological or post mortem evidence of recurrence/relapse (non-R/R group). Only cases with apparently complete surgical removal and no evidence of residual tumour on post-operative MRI were included.

After the surgical removal tissue samples were processed to generate sections from formalin fixed and paraffin embedded (FFPE) blocks which were stained with haematoxylin-eosin (H&E). One representative tissue block was selected per case. From these blocks tissue micro arrays (TMAs) were built. Each TMA contained samples from 10 cases (three samples from each cases) plus 2 normal brain tissue samples in the left upper corner as a reference to enable specimen identification in the TMA (Fig. 1). In total 12 TMA were built, containing tissue samples from 114 neurosurgical interventions.

Immunohistochemistry (IHC) was performed according to standardized methods. In brief, 4 μm thick sections from TMA blocks were stained with p53 mouse monoclonal antibody (clone DO-7, M7001, DAKO, Glostrup, Denmark); PR antibody (NCL-PGR-312, clone 16, Novocastra, Newcastle, UK) and anti-Ki-67 antibody (clone Mib1, M7240, DAKO,

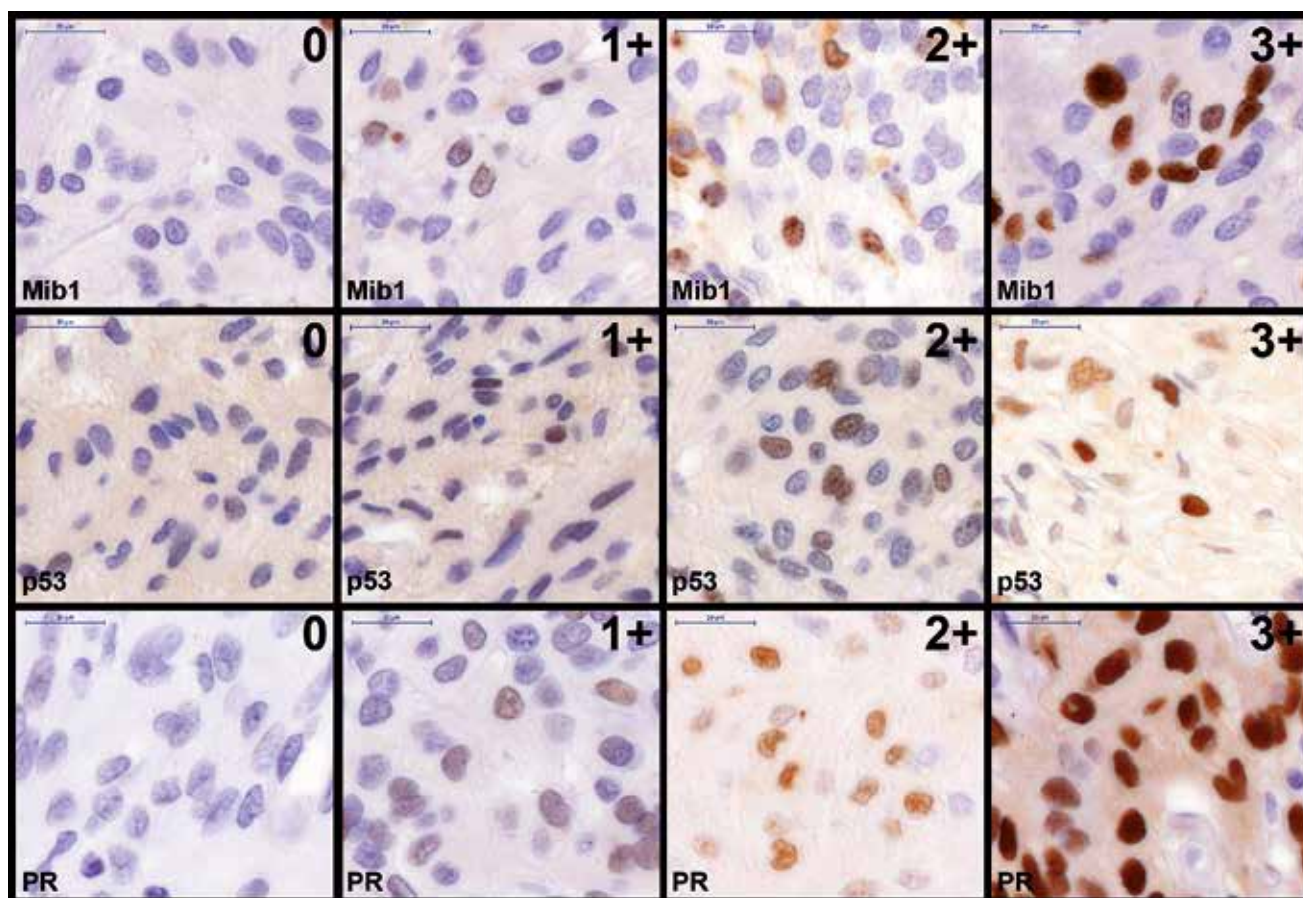


Fig. 2. Ki-67 (clone Mib1), p53, and progesterone receptor (PR) immunostain with representative images of the different immunolabeling intensities: negative (0), minimal positivity (1+), moderate positivity (2+), strong positivity (3+). Scale bar 20 μ m.

Glostrup, Denmark) according to the manufacturer's protocol with 1 : 100, 1 : 100 and 1 : 200 dilution for p53, PR and Ki-67, respectively. Sections were incubated with the primary antibody for 6 hours at room temperature; the visualization was performed with SuperSensitive™ One-step Polymer-HRP Detection System on Leica Bond Max™ fully automated IHC stainer with negative controls (omitting the primary antibody).

All of the H&E and immunostained TMA sections were scanned with a Panoramic Scanner (3DHistech, Budapest, Hungary). Two digital images were taken at 400 \times magnification from each tissue samples, in total 6 from each case. According to the intensity of nuclear staining of cells, 4 semi quantitative scores were applied: 0 (none), 1+ (weak), 2+ (moderate) and 3+ (strong) (Fig. 2).

Images in 10 reference cases were analysed quantitatively with ImageJ (NIH, Bethesda, USA) software Cell Counter function, to determine the exact percentage of immunopositive cells (Fig. 3). These images were used as reference cases to aid accurate semi-quantitative assessment in all cases. This is a method easily and reliably applicable in the routine pathological diagnostic practice, similarly to the assessment of percentage of immunopositive cells in other tumours.

Not only the percentage value of immunopositive cells but also the average labelling intensity score (0-3+; for reference images see Fig. 2) of the staining were calculated in each picture. Similarly to the histoscore of breast carcinoma i.e. the multiple of the percentage of the positive cells and the average

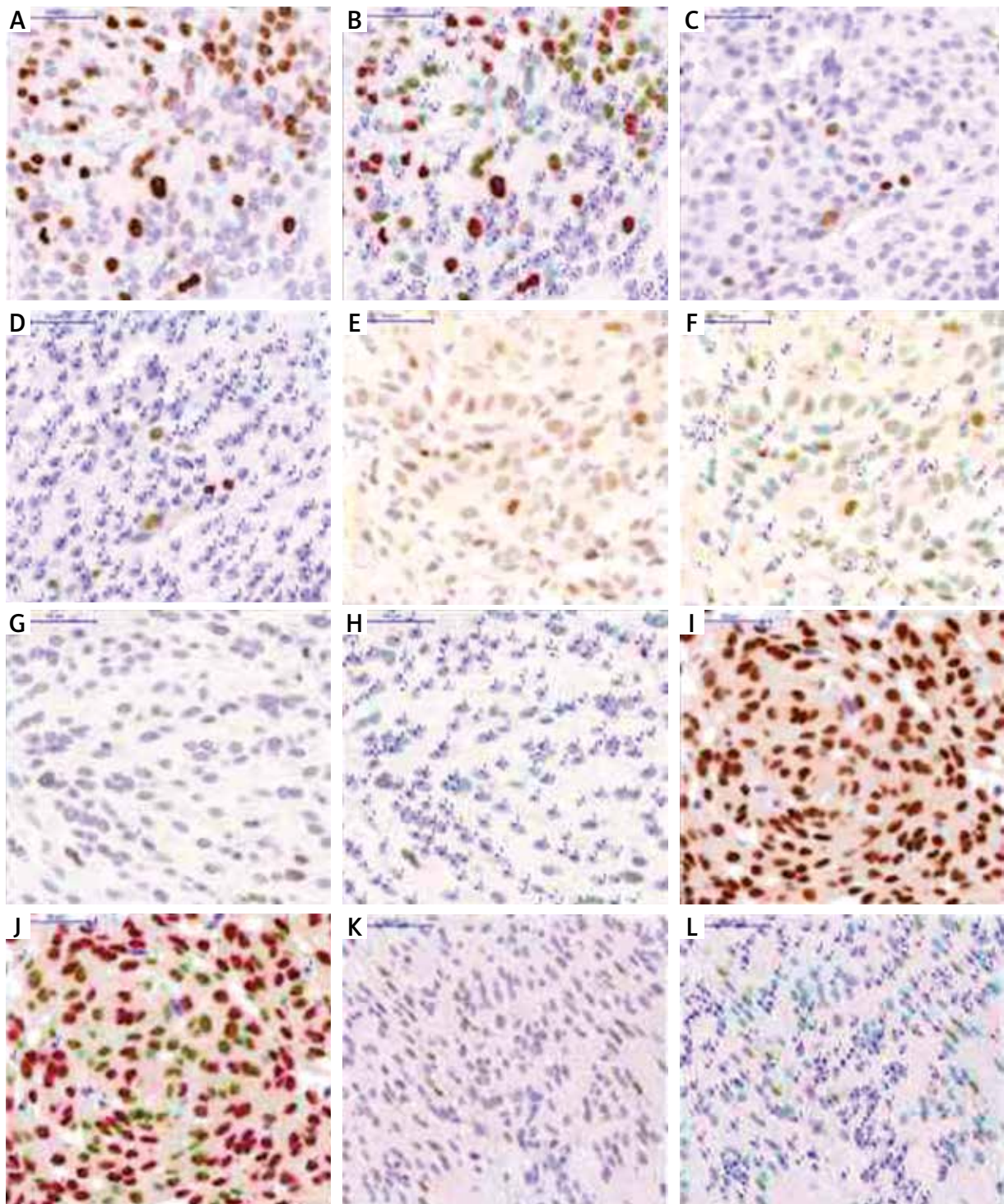


Fig. 3. Ki-67 (clone Mib1), p53 and progesterone receptor (PR) immunopositive cells counted using ImageJ software. **A, C, E, G, I, K** pictures are the originals, whereas **B, D, F, H, J, L** show cells numbered with ImageJ Cell Counter plug-in. The numbers from 1-4 stand for the negative, 1+, 2+ and 3+ cells, respectively. **A-B** pictures are immunostained for Mib1 (43.5% positivity). **C-D** pictures are immunostained for Mib1 (6.9% positive). **E-F** pictures are stained for p53 (58.9% positive). **G-H** pictures immunostained for p53 (9.8% positive). **I-J** pictures stained for PR (93.9% positive). **K-L** pictures immunostained for PR (31.3% positive).

intensity of the positive cell nuclei [11] were calculated.

Data were analysed with SPSS 22.0 for Windows (IBM, Armonk, NY, USA) statistical programme, using Kruskal-Wallis H-test, Mann-Whitney *U*-test and Wilcoxon signed ranks test. The patients were grouped by the grades (65 WHO grade I; 33 WHO grade II and 16 WHO grade III) and also based on the recurrence or relapse (R/R group) showed up at least 5 years after resection: patients without recurrence or relapse (non-R/R group), patients with definitive relapse or recurrence (R/R group).

The non-R/R cases were WHO grade I, while the R/R group have 18 WHO grade I, 9 WHO grade II and 2 WHO grade III tumour in the 1st histological sample.

Ethical approval has been obtained from the Institutional Research Ethics Committee (Number: DEOEC RKEB: 2437-2005).

Results

The 70 patients' average age was 56 years at the time of the first pathological examination. There were no significant differences between the R/R group and the non-R/R group. There were 16 patients (3 male and 13 female; average age 54 years) without recurrence or relapse (non-R/R group) with at least 5 years' survival after surgery and 31 patients (8 male and 23 female; average age 53 years, overall time of recurrence 19.6 months) with definitive relapse or recurrence (R/R group). Further 23 patients (5 male and 18 female, average age 59 years) were operated within 5 years without recurrence/relapse; however the time window was too short to include them in the non-R/R group. There were 65 WHO grade I cases, 33 WHO grade II cases and 16 WHO grade III cases. All of the non-R/R cases were WHO grade I. The R/R group contained 19 WHO grade I, 9 WHO grade II and three WHO grade III cases according to the 1st neuropathological diagnosis of the first surgical specimen. There were 8 patients whose subsequent surgical specimens had higher WHO grade than the first; 15 patients whose first and last cases both showed the same grade; and 6 patients who only had 1 histological sample and the recurrence/relapse was diagnosed by imaging techniques.

The histological subtypes were not statistically different between the R/R group and non-R/R group: there were 6 meningothelial, 5 transitional, 3 fibrous and 2 psammomatous in the non-R/R group, while

9 meningothelial, 6 transitional, 3 fibrous, one psammomatous, one clear cell, 8 atypical and 3 anaplastic in the R/R group. There was no increased tendency for recurrence for any WHO grade 1 subtype. Among grade 2-3 meningiomas, there was no specific subtype which had higher frequency of recurrence than the respective grade in general.

There is a significant correlation between WHO tumour grade and Mib1 LI (%) ($p < 0.001$), Mib1 staining intensity ($p = 0.001$), Mib1 histoscore ($p < 0.001$), p53 staining intensity ($p < 0.001$), p53 histoscore ($p = 0.031$), PR LI (%) ($p < 0.001$), PR intensity ($p < 0.001$) and PR histoscore ($p < 0.001$), respectively (Kruskal-Wallis test). Comparing only grade I and grade II tumours there is a significant correlation with Mib1 LI (%) ($p < 0.001$), Mib1 intensity ($p < 0.001$), Mib1 histoscore ($p < 0.001$), p53 intensity ($p = 0.001$), PR LI (%) ($p = 0.014$), PR intensity ($p = 0.029$) and PR histoscore ($p = 0.013$). Comparing grade II and grade III tumours there is a significant correlation with p53 intensity ($p = 0.049$), PR LI (%) ($p = 0.008$), PR intensity ($p = 0.008$) and PR histoscore ($p = 0.009$). When comparing grade I and grade III tumours there is a significant correlation of the higher grade with increased Mib1 LI (%) ($p < 0.001$), Mib1 histoscore ($p < 0.001$), p53 intensity ($p < 0.001$), p53 histoscore ($p = 0.023$), PR LI (%) ($p < 0.001$), PR intensity ($p < 0.001$), PR histoscore ($p < 0.001$) (Mann-Whitney test) (Table I, Fig. 4).

Irrespective of the grades of the R/R group, comparing the non-R/R and R/R groups there is a significant correlation with the Mib1 LI (%) ($p < 0.001$), Mib1 intensity ($p = 0.004$), Mib1 histoscore ($p < 0.001$), p53 LI (%) ($p = 0.027$), and the WHO grade ($p = 0.003$) (Fig. 5). In WHO grade I tumours in the R/R group there is a significant correlation with the Mib1 LI (%) ($p = 0.009$), Mib1 histoscore ($p = 0.029$), p53 LI (%) ($p = 0.032$), p53 histoscore ($p = 0.038$) (Table II, Fig. 6).

In the R/R groups when comparing the first case with the recurrent/relapsed cases there is a significant difference between the Mib1 LI (%) ($p = 0.002$), Mib1 histoscore ($p = 0.001$), p53 intensity ($p = 0.006$) and the grade ($p = 0.001$); and with Wilcoxon signed rank test when compared the first and last case of the same patient, there is a significant difference in the grade ($p = 0.007$), Mib1 LI (%) ($p = 0.042$), Mib1 histoscore ($p = 0.050$), and p53 LI (%) ($p = 0.042$) (Table III, Fig. 7).

Table I. Comparison of grade I, grade II and grade III cases with Kruskal-Wallis test, and the WHO grade pairs with Mann-Whitney test. Immunostain percentage, intensity (average intensity of cells: 0, 1, 2 or 3) and histoscore (intensity × percentage) for Mib1, p53 and progesterone receptor (PR)

	Mib1 Percentage	Mib1 Intensity	Mib1 Histoscore	p53 Percentage	p53 Intensity	p53 Histoscore	PR Percentage	PR Intensity	PR Histoscore
Kruskal-Wallis	0.000	0.001	0.000	0.316	0.000	0.031	0.000	0.000	0.000
Mann-Whitney grade I-II	0.000	0.000	0.000	0.272	0.001	0.065	0.014	0.029	0.013
Mann-Whitney grade II-III	0.449	0.320	0.831	0.654	0.049	0.376	0.008	0.008	0.009
Mann-Whitney grade I-III	0.000	0.086	0.000	0.198	0.000	0.023	0.000	0.000	0.000

Table II. Comparison of the non-recurrence/relapse (non-R/R) cases and recurrence/relapse (R/R) cases' first surgical specimens without regarding the grade (first row) and only in WHO grade I cases (second row)

	Grade	Mib1 Percentage	Mib1 Intensity	Mib1 Histoscore	p53 Percentage	p53 Intensity	p53 Histoscore	PR Percentage	PR Intensity	PR Histoscore
Mann-Whitney any grades	0.003	0.000	0.004	0.000	0.027	0.955	0.069	0.207	0.497	0.215
Mann-Whitney grade I	1.000b	0.009b	0.126b	0.029b	0.032b	0.195b	0.038b	0.708b	0.708b	0.858b

Table III. Comparison of the first and last surgical specimens of the recurrence/relapsed (R/R) cases with Mann-Whitney test (first row) and Wilcoxon signed rank test (second row). Immunostain percentage, intensity (average intensity of cells: 0, 1, 2 or 3) and histoscore (intensity × percentage) for Mib1, p53 and progesterone receptor (PR)

	Grade	Mib1 Percentage	Mib1 Intensity	Mib1 Histoscore	p53 Percentage	p53 Intensity	p53 Histoscore	PR Percentage	PR Intensity	PR Histoscore
Mann-Whitney progression	0.001	0.002	0.098	0.001	0.861	0.006	0.553	0.154	0.154	0.159
Wilcoxon progression	0.007	0.042	0.237	0.050	0.042	0.484	0.559	1.000	0.545	0.876

According to our data, the WHO grade has strong forward proportion to Mib1 and p53 and an inverse proportion to the PR immunostain (as shown in several previous papers). As a quantitative marker the Mib1 has a better correlation with percentage, whereas p53 with intensity and histoscore. Therefore, the panel of PR, p53, Mib1 is sufficient to

characterize meningioma immunohistochemically regarding the risk of recurrence as an integral part of the routine diagnostic histopathological practice.

Discussion

Meningioma is one of the most common intracranial tumours with high incidence in the neuro-

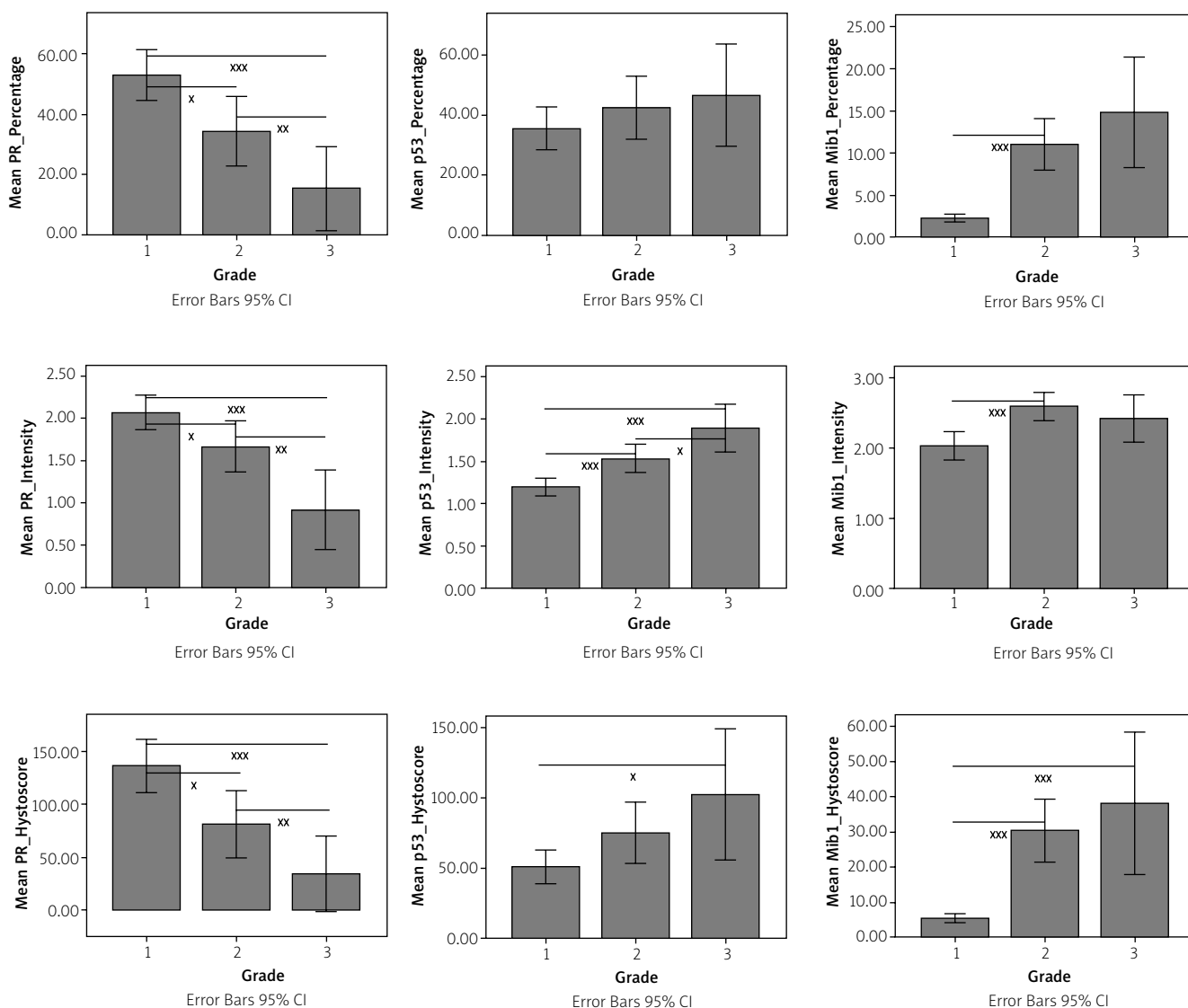


Fig. 4. Percentage (%), intensity (0, 1+, 2+, 3+) and histoscore (intensity × percentage) of immunostain with Ki-67 (clone Mib1), p53 and progesteron receptor (PR) for WHO grade I, II and III.

surgical practice. The histological subtypes are well characterised by the WHO, and the grading is based on these histological characteristics, morphological findings and the mitotic ratio. The Simpson Grading System also can provide further information of the probability of the recurrence [30].

The aim of this study was to establish an easy-to-use immunohistochemical panel for the routine neuropathological use, which can predict meningioma relapse/recurrence. This is particularly relevant

for tumours in problematic localization (e.g. falx meningiomas).

For validation we analysed the changes in immunohistochemical characteristics and expression patterns during relapse/recurrence and their relation to tumour grade.

Meningiomas usually are non-infiltrative neoplasms therefore complete surgical resection is curative. However, the tumour may spread laterally in small nests in the dura mater which could be a source of

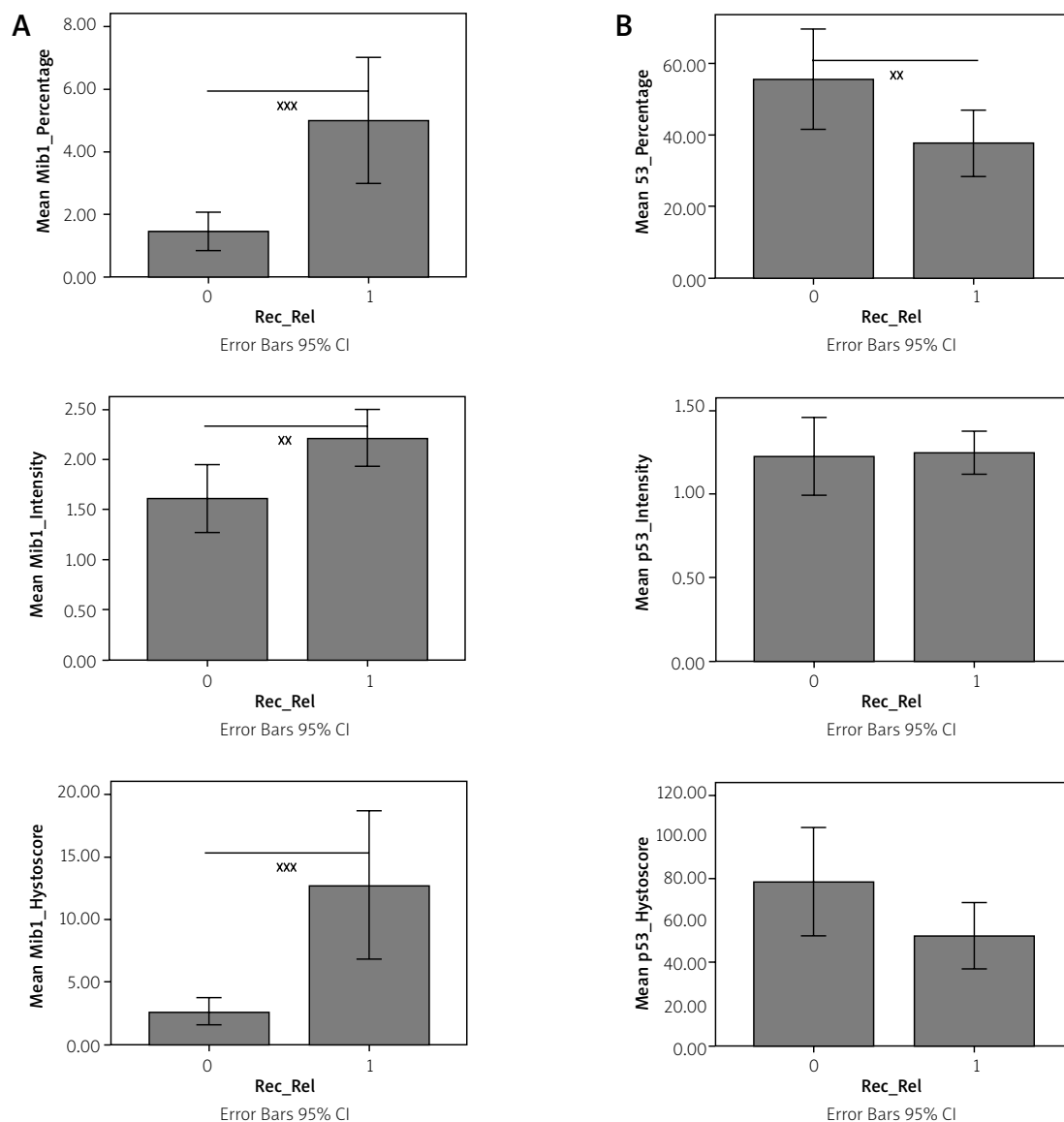


Fig. 5. Percentage (%), intensity (0, 1+, 2+, 3+) and histoscore (intensity × percentage) of immunostain with Ki-67 (clone Mib1) (A), and p53 (B) for non-recurrence/relapse (non-R/R) and recurrence/relapse (R/R) cases, without regarding the WHO grades.

recurrence. Hence no chemotherapy is effective even in high grade meningiomas – radiotherapy increases malignant transformation [33] – another argument for discovery of relatively simple predictive markers of tumour progression and recurrence.

Although the Mib1 labelling index can be different according to which laboratory-performed reaction [8], standardized method can help the data interpretation and comparison both for routine and experimental practice. In accordance with previous

studies the higher initial Mib1 LI has a predictive value regarding increased probability of recurrence. In R/R cases during evolution in time (i.e. time between 1st and last surgical procedure) there was an increase in Mib1 LI consistent with the known fact that tumour progression may occur over time which is reflected by increased proliferative potential and higher WHO grade.

The routinely used p53 antibody does not differentiate between the wild type and the mutant pro-

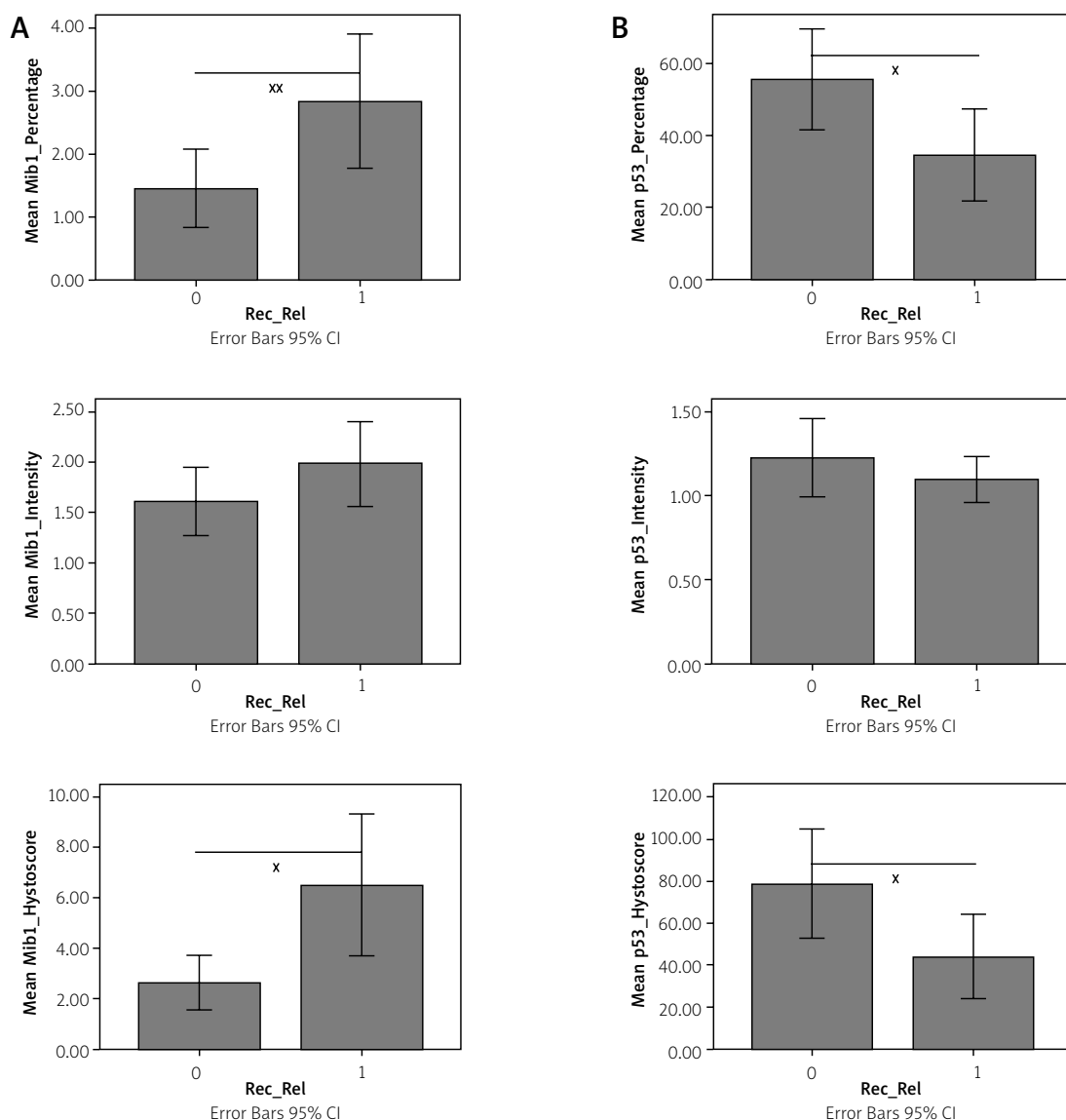


Fig. 6. Percentage (%), intensity (0, 1+, 2+, 3+) and histoscore (intensity x percentage) of immunostain with Ki-67 (clone Mib1) (A), and p53 (B) for non-recurrence/relapse (non-R/R) and WHO grade I of the recurrence/relapse (R/R) cases.

tein. Interestingly, the p53 LI and histoscore (but not the labelling intensity) has an inverse correlation with the chance of recurrence in the WHO grade I tumours in our study, but if we examine all the WHO grades, the increased staining in the higher grades, changes to forward proportion, similarly to prior studies [7,14,15]. This may be explained by the fact that the p53 immunoreactivity does not distinguish between the wild type (WT) and mutant protein; in non-recurrent cases increased normal protein may have

a beneficial effect as p53 is involved in DNA damage repair. In contrast, in recurrent cases p53 is more likely to be mutant and ineffective thereby contributing to tumour growth and recurrence. Mutation analysis could answer this problem, however, the focus of our study is on immunohistochemical markers, and therefore it is beyond the scope of the current project. Today the antibodies specific to mutated p53 are not routinely used therefore not applied in this study. The p53 LI and histoscore decreased during

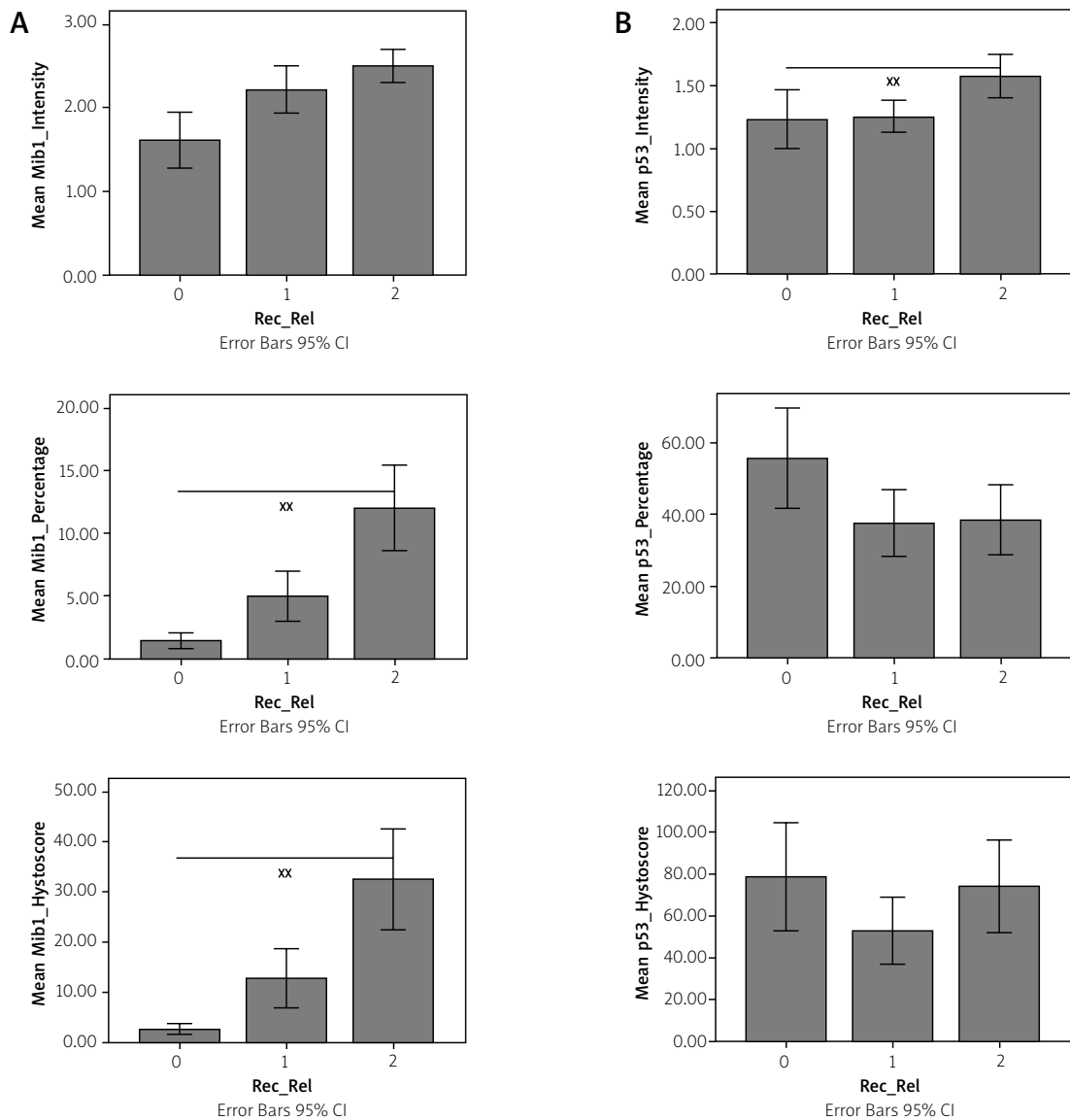


Fig. 7. Percentage (%), intensity (0, 1+, 2+, 3+) and histoscore (intensity x percentage) of immunostain with Ki-67 (clone Mib1) (A), and p53 (B) for the 1st, 2nd and last surgical specimens of the recurrence/replaced (R/R) cases.

time to recurrence which may indicate decreased levels of WT protein.

PR has an inverse relation with tumour grade in concert with previous reports [10,18,20,25] with no predictive value regarding recurrence.

Using p53 and Ki-67 molecular markers and the relatively simple and quick assessment method the increased risk of recurrence can be reliably predicted. However, it is foreseeable that the presented method has the potential for further improvement with the use of digitalized histological specimens,

because this enables automated quantitative image analysis as an integral component of the diagnostic process.

In summary, we have demonstrated a rather simple immunohistochemistry-based method with routinely used molecular markers to identify patients with increased risk of recurrence. Further work is needed to validate our work in more patients, multiple centres and in a prospective manner with long follow-up. The combination of histological, surgical and imaging markers may be a more sensitive tool

to predict recurrence and this can also be tested in future studies.

Acknowledgments

This work has been supported by the National Brain Research Program, Hungary (KTIA_13_NAP-A-II/7, and KTIA-NAP-13-1-2013-0001).

Disclosure

Authors report no conflict of interest.

References

- Abramovich CM, Prayson RA. Histopathologic features and MIB-1 labeling indices in recurrent and nonrecurrent meningiomas. *Arch Pathol Lab Med* 1999; 123: 793-800.
- Adamczyk A, Jesko H, Strosznajder RP. Alzheimer's disease related peptides affected cholinergic receptor mediated poly(ADP-ribose) polymerase activity in the hippocampus. *Folia Neuropathol* 2005; 43: 139-142.
- Affar EB, Shah RG, Dallaire AK, Castonguay V, Shah GM. Role of poly(ADP-ribose) polymerase in rapid intracellular acidification induced by alkylating DNA damage. *Proc Natl Acad Sci U S A* 2002; 99: 245-250.
- Amatya VJ, Takeshima Y, Sugiyama K, Kurisu K, Nishisaka T, Fukuhara T, Inai K. Immunohistochemical study of Ki-67 (MIB-1), p53 protein, p21WAF1, and p27KIP1 expression in benign, atypical, and anaplastic meningiomas. *Hum Pathol* 2001; 32: 970-975.
- Blankenstein M, Berns PM, Blaauw G, Mulder E, Thijssen JH. Presence of progesterone receptors and absence of oestrogen receptors in human intracranial meningioma cytosols. *Eur J Cancer and Clin Oncol* 1983; 19: 365-370.
- Bodi I, Hortobágyi T, Buk S. A 72-year-old woman with right frontal extra-axial mass. *Brain Pathol* 2008; 18: 279-282.
- Cho H, Ha SY, Park SH, Park K, Chae YS. Role of p53 gene mutation in tumor aggressiveness of intracranial meningiomas. *J Korean Med Sci* 1999; 14: 199-205.
- Chozick BS, Benzil DL, Stopa EG, Pezzullo JC, Knuckey NW, Epstein MH, Finkelstein SD, Finch PW. Immunohistochemical evaluation of erbB-2 and p53 protein expression in benign and atypical human meningiomas. *J Neurooncol* 1996; 27: 117-126.
- Claus EB, Bondy ML, Schildkraut JM, Wiemels JL, Wrensch M, Black PM. Epidemiology of intracranial meningioma. *Neurosurgery* 2005; 57: 1088-1095; discussion 1088-1095.
- Csonka T, Murnyák B, Szepesi R, Kurucz A, Klekner Á, Hortobágyi T. Poly(ADP-ribose) polymerase-1 (PARP1) and p53 labeling index correlates with tumour grade in meningiomas. *Folia Neuropathol* 2014; 52: 111-120.
- De Vos M, Schreiber V, Dantzer F. The diverse roles and clinical relevance of PARPs in DNA damage repair: current state of the art. *Biochem Pharmacol* 2012; 84: 137-146.
- el-Deiry WS, Tokino T, Velculescu VE, Levy DB, Parsons R, Trent JM, Lin D, Mercer WE, Kinzler KW, Vogelstein B. WAF1, a potential mediator of p53 tumor suppression. *Cell* 1993; 75: 817-825.
- Hollstein M, Sidransky D, Vogelstein B, Harris CC. p53 mutations in human cancers. *Science* 1991; 253: 49-53.
- Kamei Y, Watanabe M, Nakayama T, Kanamaru K, Waga S, Shiraiishi T. Prognostic significance of p53 and p21WAF1/CIP1 immunoreactivity and tumor micronecrosis for recurrence of meningiomas. *J Neurooncol* 2000; 46: 205-213.
- Karamitopoulou E, Perentes E, Tolnay M, Probst A. Prognostic significance of MIB-1, p53, and bcl-2 immunoreactivity in meningiomas. *Hum Pathol* 1998; 29: 140-145.
- Kastan MB, Kuerbitz SJ. Control of G1 arrest after DNA damage. *Environ Health Perspect* 1993; 101 Suppl 5: 55-58.
- Koshland DE Jr. Molecule of the year. *Science* 1993; 262: 1953.
- Kumar S, Kakkar A, Suri V, Kumar A, Bhagat U, Sharma MC, Singh M, Suri A, Sarkar C. Evaluation of 1p and 14q status, MIB-1 labeling index and progesterone receptor immunoreexpression in meningiomas: Adjuncts to histopathological grading and predictors of aggressive behavior. *Neurol India* 2014; 62: 376-382.
- Lanzafame S, Torrisi A, Barbagallo G, Emmanuele C, Alberio N, Albanese V. Correlation between histological grade, MIB-1, p53, and recurrence in 69 completely resected primary intracranial meningiomas with a 6 year mean follow-up. *Pathol Res Pract* 2000; 196: 483-488.
- Longstreth W, Dennis LK, McGuire VM, Drangsholt MT, Koepsell TD. Epidemiology of intracranial meningioma. *Cancer* 1993; 72: 639-648.
- Louis DN, Ohgaki H, Wiestler OD, Cavenee WK, Burger PC, Jouvet A, Scheithauer BW, Kleihues P. The 2007 WHO classification of tumours of the central nervous system. *Acta Neuropathol* 2007; 114: 97-109.
- Murnyak B, Bognár L, Klekner Á, Hortobágyi T. Epigenetics of Meningiomas. *Biomed Res Int* 2015; 2015: 532451.
- Murnyak B, Szepesi R, Hortobágyi T. Molecular genetics of familial tumour syndromes of the central nervous system. *Orv Hetil* 2015; 156: 171-177.
- Ohkoudo M, Sawa H, Hara M, Saruta K, Aiso T, Ohki R, Yamamoto H, Maemura E, Shiina Y, Fujii M, Saito I. Expression of p53, MDM2 protein and Ki-67 antigen in recurrent meningiomas. *J Neurooncol* 1998; 38: 41-49.
- Omulecka A, Papier W, Nawrocka-Kunecka A, Lewy-Trenda I. Immunohistochemical expression of progesterone and estrogen receptors in meningiomas. *Folia Neuropathol* 2006; 44: 111-115.
- Ozen O, Demirhan B, Altinors N. Correlation between histological grade and MIB-1 and p53 immunoreactivity in meningiomas. *Clin Neuropathol* 2005; 24: 219-224.
- Perry A, Cai DX, Scheithauer BW, Swanson PE, Lohse CM, Newsham IF, Weaver A, Gutmann DH. Merlin, DAL-1, and progesterone receptor expression in clinicopathologic subsets of meningioma: a correlative immunohistochemical study of 175 cases. *J Neuropathol Exp Neurol* 2000; 59: 872-879.
- Perry A, Scheithauer BW, Stafford SL, Lohse CM, Wollan PC. "Malignancy" in meningiomas: a clinicopathologic study of 116 patients, with grading implications. *Cancer* 1999; 85: 2046-2056.
- Perry A, Stafford SL, Scheithauer BW, Suman VJ, Lohse CM. The prognostic significance of MIB-1, p53, and DNA flow cytometry in completely resected primary meningiomas. *Cancer* 1998; 82: 2262-2269.

30. Simpson D. The recurrence of intracranial meningiomas after surgical treatment. *J Neurol Neurosurg Psychiatry* 1957; 20: 22-39.
31. Terzi A, Saglam EA, Barak A, Soylemezoglu F. The significance of immunohistochemical expression of Ki-67, p53, p21, and p16 in meningiomas tissue arrays. *Pathol Res Pract* 2008; 204: 305-314.
32. Touat M, Lombardi G, Farina P, Kalamarides M, Sanson M. Successful treatment of multiple intracranial meningiomas with the antiprogestosterone receptor agent mifepristone (RU486). *Acta Neurochir* 2014; 156: 1831-1835.
33. Umansky F, Shoshan Y, Rosenthal G, Fraifeld S, Spektor S. Radiation-induced meningioma. *Neurosurg Focus* 2008; 24: E7.
34. Wiemels J, Wrensch M, Claus EB. Epidemiology and etiology of meningioma. *J Neurooncol* 2010; 99: 307-314.

Ultrastructural pathology of human peritumoural oedematous cerebellar cortex

Orlando José Castejón

Biological Research Institute, Faculty of Medicine, Zulia University, Maracaibo, Venezuela

Folia Neuropathol 2016; 54 (2): 127-136

DOI: 10.5114/fn.2016.60057

Abstract

Cerebellar cortical biopsies of the peritumoural region of seven patients with cerebellar haemangioma, mesencephalic meningioma, cerebellopontine astrocytoma, cerebellopontine meningioma, and medulloblastoma of cerebellar vermis were examined by means of conventional transmission electron microscopy. Granule cells showed oedematous cytoplasm and mitochondria. Swollen Golgi cells exhibited lipofuscin granules and intranuclear inclusions. Both neuron cell types displayed swollen dendritic digits synapsing with afferent mossy fibre endings. Degenerated myelinated axons corresponding to afferent mossy and climbing fibres and efferent Purkinje cell axons were observed at the granular layer. Dense and clear ischaemic Purkinje cells established degenerated synapses with swollen parallel fibre synaptic varicosities. Degenerated Purkinje cell recurrent axonal collaterals were found at the molecular layer. Swollen and clear Bergmann glial cell cytoplasm was observed closely applied to the oedematous clear and dark Purkinje cell body, dendritic trunk, secondary and tertiary dendritic branches. Swollen climbing fibre endings featured by numerous microtubules and neurofilaments, and a decreased number of synaptic vesicles were observed making degenerated axo-spinodendritic synapses with clear and swollen dendritic spines from Purkinje, Golgi, basket and stellate cell dendrites. Swollen stellate neurons showed oedematous mitochondria. Lipofuscin-rich astrocytes and reactive phagocytic astrocytes were observed. The latter appeared engulfing haematogenous proteinaceous oedema fluid. All cerebellar neurons showed stress endoplasmic reticulum dysfunction featured by focal dilated cisterns and detachment of associated ribosomes. Myelin sheath degeneration was related with oligodendrocyte degenerating hydropic changes. The peritumoural ischaemic cerebellar nerve and glial cell abnormalities were related with neurobehavioral changes, tremor, nystagmus, dismetria and gait disturbance observed in the patients examined. The ultrastructural pathological changes were correlated with the biochemical cascade induced by vasogenic and cytotoxic oedema, altered calcium homeostasis, increased glutamate excitotoxicity, oxidative stress and DNA damage.

Key words: human cerebellum, cerebellar neurons, cerebellar oedema, cerebellar tumours, electron microscopy.

Introduction

Some earlier research investigations have been reported on ultrastructural biology and pathology of cerebellar tumours [14,15,16,27]. Axonal torpedoes on Purkinje cells of the cerebellum have been

observed at electron microscopic level in infantile neuroaxonal dystrophy, in two cases of brain tumours, and in a case of a 5-year-old boy suffering from juvenile astrocytoma [21,24,32]. The presence of intranuclear filamentous inclusions in cerebellar

Communicating author:

Prof. Orlando José Castejón, MD, Biological Research Institute, Faculty of Medicine, Zulia University, Maracaibo, Venezuela, fax: 58-261-7831611, e-mail: ocastejo@cantv.net

Golgi cells was reported by us in three patients with cerebellar tumours [4].

However, very few electron microscopic studies have been devoted to study the cortical biopsies of the cerebellar peritumoral region taken during neurosurgical treatment of human cerebellar, cerebello-pontine and mesencephalic tumours for systematically examining the alterations of cerebellar neurons and their abnormal intracortical circuits. This study is basically important to understand the pathogenesis of clinical cerebellar syndromes, such as gait disturbance, tremor, nystagmus, compression of cranial nerves, cognitive and neurobehavioural changes observed in the affected patients.

Material and methods

The present study describes the ultrastructural changes of focal peritumoural cerebellar cortex by means of cortical biopsies immediately taken during neurosurgical treatment of seven patients with cerebellar, cerebellopontine and mesencephalic tumours. Table I contains the clinical data, neuropathological features and localization of tumours. The neurosurgical study was performed and the cortical biopsies were taken according to basic principles of Helsinki. Cerebellar cortical biopsies of seven patients, ranging from 2- to 50-years old, with clinical diagnosis of cerebellar haemangioma, mesencephalic meningioma, cerebellopontine astrocytoma, cerebellopontine meningioma, and medulloblastoma of cerebellar vermis were examined by means of conventional transmission electron microscopy. Two to five mm thick cortical biopsies were immediately fixed in the surgical room in 4% glutaraldehyde-0.1M phosphate or cacodylate buffer, pH 7.4, at 4°C. After 2 hours' glutaraldehyde-fixation period, the cortical biopsies were divided into approximately 1 mm fragments

and observed under a stereoscopic microscope to check the quality of fixation of the sample, the glutaraldehyde diffusion rate, and the brownish coloration of the surface and deeper cortical regions, indicative of good glutaraldehyde fixation by immersion technique. Immersion in fresh glutaraldehyde solution of 1 mm slices was secondarily done for 2 hours after eliminating the remaining blood from the cortical biopsy by washing in similar 0.1 M phosphate or cacodylate buffer, pH 7.4 to avoid oxidation of the primary fixative solution. Secondary fixation in 1% osmium tetroxide-0.1 M phosphate buffer, pH 7.4, was carried out for 1-2 hours at 4°C. Black staining of the cortical slices also was observed under a stereoscopic microscope to check osmium tetroxide diffusion rate and quality of secondary fixation. They were then rinsed for 5 to 10 minutes in phosphate or cacodylate buffer of similar composition to that used in the fixative solution, dehydrated in increasing concentrations of ethanol, and embedded in Araldite or Epon. For proper orientation during the electron microscope study and observation of cortical layers, approximately 0.1 to 1 µm thick sections were stained with toluidine blue and examined with a Zeiss photomicroscope. Ultrathin sections, obtained with Porter-Blum and LKB ultramicrotomes, were stained with uranyl acetate and lead citrate, and observed in a JEOL 100B transmission electron microscope (TEM) at magnifications ranging from 20,000× to 90,000×. For each cortical biopsy, approximately 50 electron micrographs were systematically studied. Digital images were Photoshop analysed [7]. This paper was carried out according to the ethical principles of Helsinki Declaration, Ethical Committee of Biological Research Institute. The relative written consent was obtained in each case.

Table I. Neurosurgical study of oedematous human cerebellum

Case No. 1: MRR, 45 y, M	Tremor in upper and lower limbs, incoherent speech, gait disturbance, visual hallucinations, clouded sensorium, stupor	Medulloblastoma of cerebellar vermis
Case No. 2: ARM, 30 y, M	Headache, dismetry, gait disturbance and tremor	Cerebellopontine angle astrocytoma
Case No. 3: MIJ, 50 y, F	Headache, dismetry, tremor and ataxic gait	Cerebellar haemangioma cavernosum
Case No. 4: EJPV, 10 y, M	Dismetry, tremor, ataxic gait	Cerebellopontine angle meningioma
Case No. 5: GPRM, 2 y, F	Headache, vomits, nystagmus, paralysis of VI cranial nerve and ataxic gait	Medulloblastoma of cerebellar vermis
Case No. 6: FMQ, 9 y, F	Headache, tremor, nystagmus and ataxic gait	Cerebellopontine angle meningioma
Case No. 7: AML, 25 y, M	Headache, nystagmus, tremor and ataxia	Mesencephalic meningioma

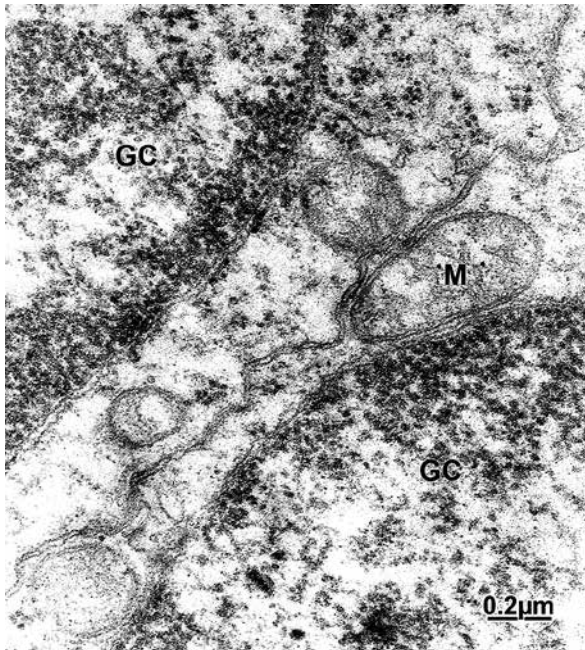


Fig. 1. Cerebellar medulloblastoma. Cerebellar cortex granular layer. Two swollen granule cells (GC) showing oedematous mitochondria (M). Note the twisted course of confronting limiting plasma membranes due to the expansive forces induced by the tumour.

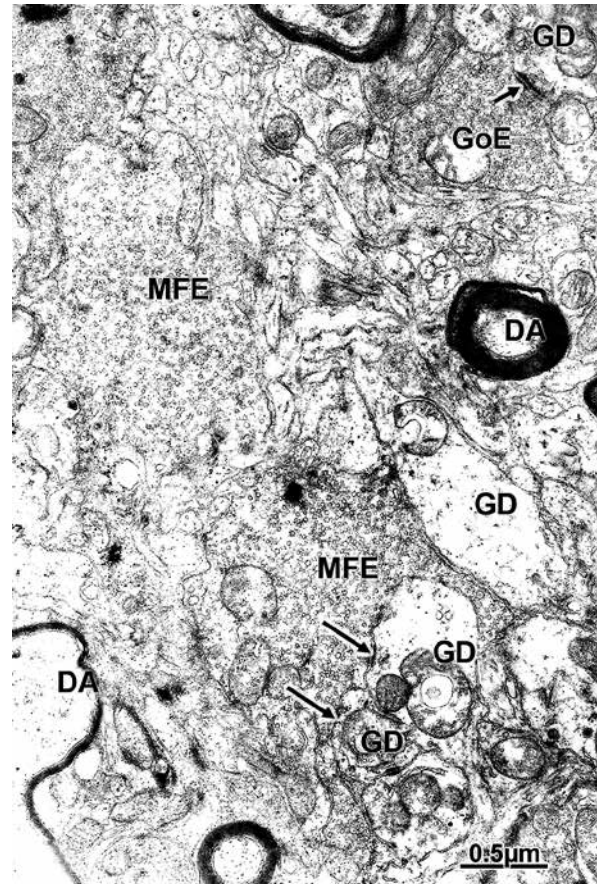


Fig. 2. Cerebellar meningioma. Cerebellar cortex granular layer. Notably swollen mossy fibre ending (MFE) containing a central core of oedematous mitochondria and numerous clear spheroidal synaptic vesicles. The long arrows indicate the synaptic contacts with granule cell dendritic tips (GD). A Golgi cell synaptic ending (GoE) localized at the periphery of cerebellar glomerulus appears making asymmetric synaptic contact (short arrow) with a granule dendrite (GD). Neighbouring degenerated myelinated axons (DA) corresponding to cerebellar afferent and/or efferent fibres also are distinguished.

Results

Close examination of cerebellar cortex showed at the level of granule cell layer, swollen granule cells characterized by an electron translucent cytoplasm and swollen mitochondria. There appeared closely apposed and their continuous limiting plasma membrane appeared separated by a 20 nm extracellular space (Fig. 1). The neighbouring mossy fibre glomerulus showed the oedematous afferent mossy fibre endings synapsing with swollen granule cell dendrites. Degenerated myelinated axons were observed at the granular layer. Some of these degenerated axons could correspond to the efferent Purkinje cell axons and the incoming afferent cerebellar mossy and climbing fibres (Fig. 2). Reactive astrocytes containing an increased amount of huge lipofuscin granules were found at the granular and molecular layers (Fig. 3).

The oedematous Golgi cell depicted an electron translucent cytoplasm, notably swollen mitochondria, dilated rough endoplasmic reticulum cisterns with focal detachment of associated ribosomes, enlarged

flattened cisterns of Golgi apparatus, numerous lipofuscin granules, and intranuclear inclusions (Fig. 4).

At the level of Purkinje cell layer, clear and dark ischaemic Purkinje cell bodies exhibited a dilated smooth and rough endoplasmic reticulum with focal detachment of membrane associated ribosomes (Figs. 5 and 6). The Purkinje cell bodies appeared covered by the swollen Bergmann glial cell cytoplasm. Dense Purkinje cell dendrites can be traced

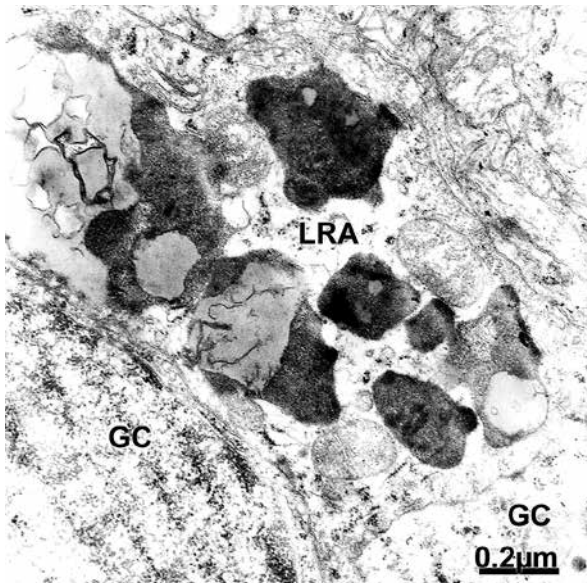


Fig. 3. Cerebellar meningioma. Cerebellar cortex granular layer. Lipofuscin-rich astrocyte (LRA) showing numerous and huge lipofuscin granules. The neighbouring swollen granule cells (GC) also are seen.

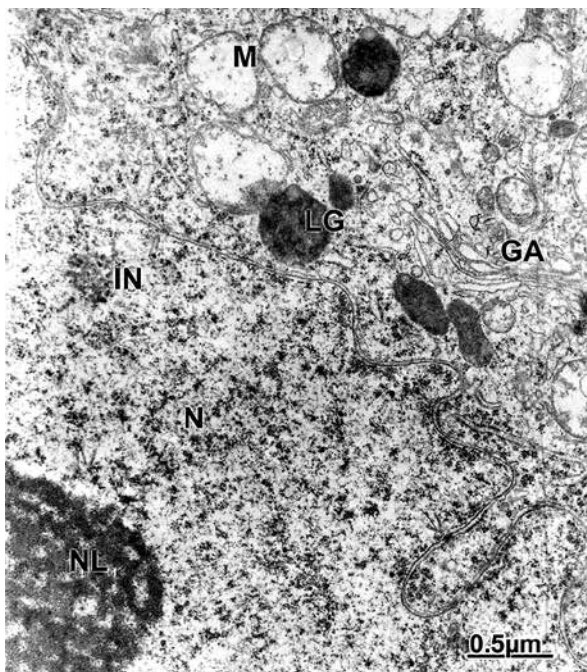


Fig. 4. Cerebellar haemangioma. Cerebellar cortex granular layer. Oedematous and clear Golgi cell soma (GC) exhibiting a lobulated nucleus and prominent nucleolus (NL), dilated rough endoplasmic reticulum (ER), and Golgi apparatus (GA), clustered free ribosomes and polyribosomes, lipofuscin granules (LG), and notably swollen mitochondria (M).

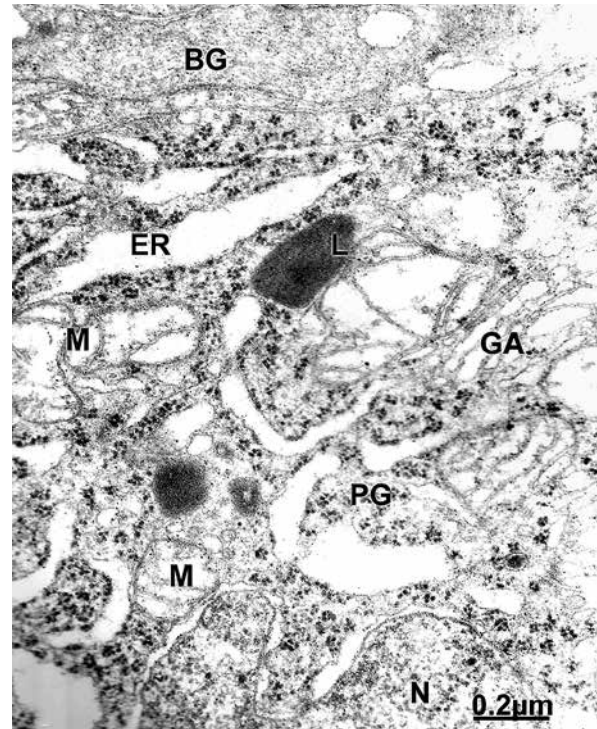


Fig. 5. Cerebellar meningioma. Cerebellar cortex Purkinje cell layer. Ischaemic and clear Purkinje cell body exhibiting a lobulated nucleus (N), and the irregularly dilated nuclear envelope, swollen rough (ER) endoplasmic reticulum with detachment of associated ribosomes, dense lysosomes (L), and swollen both mitochondria (M), and Golgi apparatus (GA), swollen mitochondria (M) and Golgi apparatus (GA), and lysosomes (L) with dark and fine granular matrix deposits. The satellite oedematous Bergmann glial cell (BG) is seen covering the Purkinje cell body.

throughout the width of molecular layer exhibiting the emergency sites of Purkinje dendritic spines, which establish axo-spino-dendritic synaptic contacts with the swollen synaptic varicosities of parallel fibres (Fig. 7). Oedematous Bergmann glial cells were observed containing swollen mitochondria and lipofuscin granules, and exhibiting the characteristic ascending Bergman fibres in the molecular layer (Fig. 8). The cytoplasm of Bergman glial cell also appeared surrounding the Purkinje recurrent axonal collaterals. In addition, swollen basket cells were found surrounding the Purkinje cell layer (Fig. 9).

The oedematous stellate neurons displayed swollen mitochondria, invaginated nuclear envelope, and

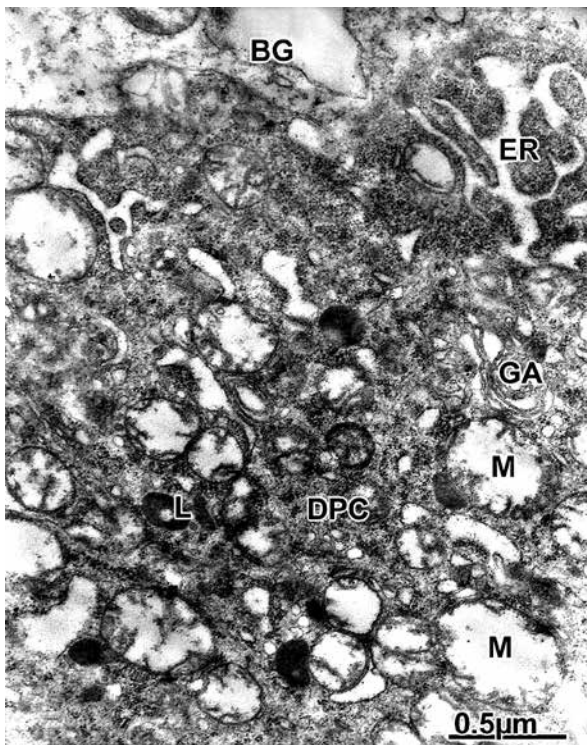


Fig. 6. Cerebellar meningeoma. Dark Purkinje cell (DPC) body showing the dense cytoplasmic matrix, tortuous aspect of rough endoplasmic reticulum (ER), the notably swollen mitochondria with fragmented cristae (M), oedematous Golgi apparatus (GA), vacuolated lysosomes (L). The oedematous and vacuolated Bergmann glial cell (BG) also is seen.

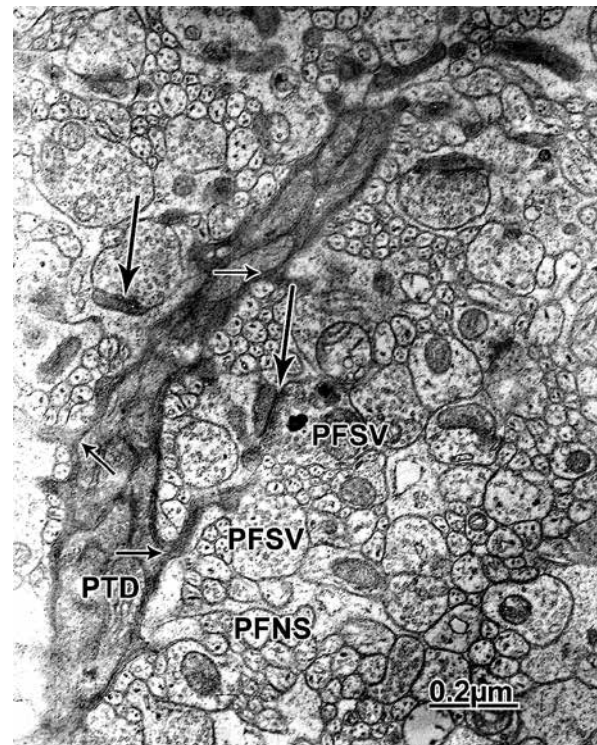


Fig. 7. Cerebellar meningeoma. Cerebellar molecular layer outer surface showing a dark tertiary Purkinje dendrite (PTD) showing the sites of emergency of dark dendritic spines (short arrows), and the degenerated axo-spinodendritic contacts of parallel fibre varicosities with Purkinje dark dendritic spines (long arrows). The cross sections of non-synaptic segments (PFNS) of parallel fibres also are distinguished.

enlarged rough endoplasmic reticulum with detachment of associated ribosomes (Fig. 10). Proteinaceous oedema fluid with fibrinous organization was found occupying the enlarged extracellular space of cerebellar molecular layer (Fig. 11).

Swollen longitudinal granule cell axons or parallel and climbing fibres were observed at the molecular layer alternating with the ascending and swollen Bergmann glial fibres, and clear dendritic processes of Golgi, basket and stellate cells. The parallel fibres were identified by the characteristic cross-sectioned bundles of parallel fibres and their degenerated “en passant” synaptic varicosities. In addition, the swollen cytoplasm of Bergmann glial cell closely surrounds the degenerated parallel fibre-Purkinje dendritic spine synapses. The latter appeared as dark degenerated structures (Fig. 12). Swollen climbing fibre branches appeared as electron translucent unmy-

elinated axons ascending in the molecular layer and containing numerous microtubules and neurofilaments. The large climbing fibre synaptic ending showed a decreased number of synaptic vesicles closely aggregated toward the presynaptic membrane. They appeared making synaptic contacts with clear and oedematous processes, presumably corresponding to ascending dendrites of Golgi, stellate and basket cell dendrites. Swollen and reactive Bergmann glial cells were observed surrounding climbing fibre endings (Fig. 13).

Swollen and dark microglial cells were observed engulfing haematogenous serum proteinaceous oedema fluid (Fig. 14). Some cerebellar capillaries showed a reduplicated basement membrane (Fig. 15), and open and apparently intact endothelial junctions. Similar findings also were reported by us in traumatic brain injuries [7].

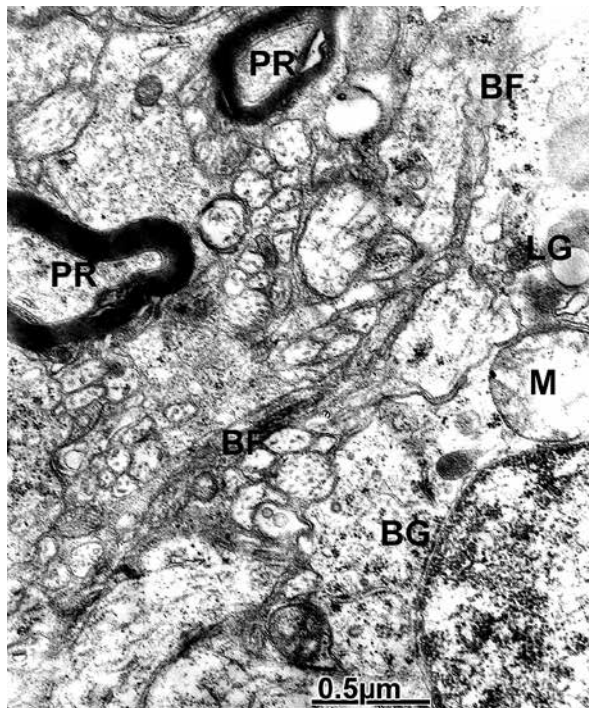


Fig. 8. Cerebellar medulloblastoma. Cerebellar Purkinje cell layer. Swollen Bergmann glial cell (BGC) showing oedematous mitochondria (M) and lipofuscin granules (LG). The ascending Bergmann fibres (BF) and Purkinje recurrent axonal collaterals (PR) also are seen.

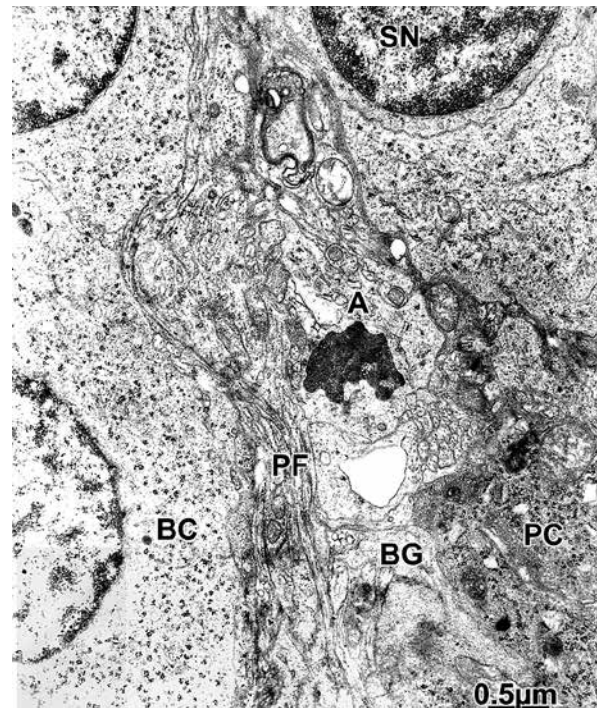


Fig. 9. Cerebellar meningioma. Cerebellar cortex Purkinje cell layer. Swollen basket cells (BC) surrounded by segments of swollen Bergmann glial cell (BG), dark Purkinje cell (PC) and lipofuscin-rich astrocyte (A) cytoplasm. The profile of parallel fibre bundles (PF) ascending toward the molecular layer, and the stellate neurons (SN) also are distinguished.

Discussion

The present study describes the oedematous intracellular changes and degenerated intracortical circuits of cerebellar neurons, and the reactive changes and neuroglial cells of cerebellar cortex in different cerebellar and brain stem tumours examined. Swollen clear granule, Golgi, Purkinje, stellate and basket cells, and Bergmann glial were found. On the contrary, some dark ischaemic Purkinje cells were observed suggesting a major vulnerability of Purkinje cells to the tumour expansion forces and the sustained ischaemic process. Similar results in cerebellar neurons, mainly dark Purkinje cells and Bergmann glial cells as described above, were also reported earlier by Sobaniec-Lotowska [28] in experimental encephalopathy induced by chronic application of valproate. According to this author, the general pattern of submicroscopic alterations of Purkinje cell perikarya suggested severe disorders in several intercellular biochemical extents, including

inhibition of oxidative phosphorylation and abnormal protein synthesis, both of which could lead to lethal damage. The enlargement of smooth and endoplasmic reticulum (ER) and the focal detachment of associated ribosomes suggest a form of stress-induced endoplasmic reticulum dysfunction [16]. According to Paschen [26], changes in neuronal calcium activity in the various subcellular compartments have divergent effects on affected cells. In the cytoplasm and mitochondria, where calcium activity is normally low, a prolonged excessive rise in free calcium levels is believed to be toxic. On the contrary, in the endoplasmic reticulum, calcium activity is relatively high and severe stress is caused by a depletion of ER calcium stores.

Dark Purkinje cell dendritic branches and dendritic spines were observed at the molecular layer. These findings herein interpreted as characterizing ischaemic Purkinje neurons, could also be due to acti-

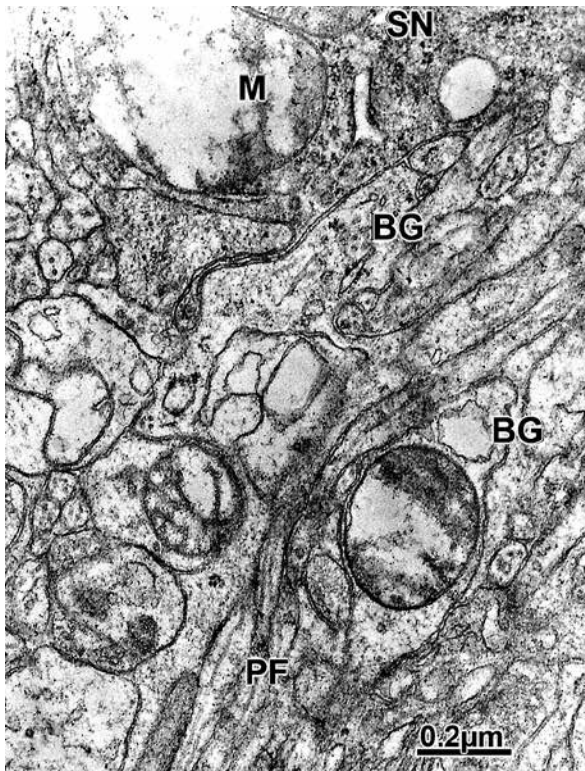


Fig. 10. Cerebellar hemangioma. Cerebellar molecular layer. Notably swollen stellate neuron (SN) with a degenerated mitochondrion (M), and surrounded by swollen and vacuolated Bergmann glial cell cytoplasm (BG) and ascending parallel fibre bundles (PF).

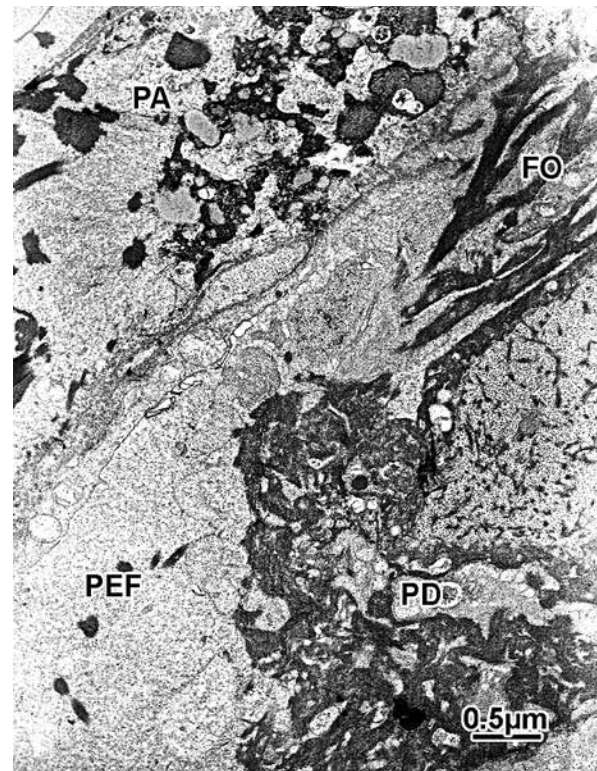


Fig. 11. Cerebellar cavernous haemangioma. Proteinaceous oedema fluid (PEF) deposited in the enlarged extracellular space exhibiting fibrinous organization (FO) and surrounded by a dark Purkinje cell degenerated dendrite (PD) and a phagocytic and lipofuscin-rich astrocyte (PA) containing deposits of fibrinous material.

vation of caspases and mitochondrial dysfunction [31], or hypoxia induced excitotoxic-type of dark cell degeneration [2]. Dark Purkinje dendritic arborisation and the degenerated parallel fibre and climbing Purkinje spines dendritic synapses could be related to the cognitive impairment and motor deficits of patients under study. Similar findings have been reported on dendritic Purkinje cells from human cerebellar vermis in Alzheimer's disease [25].

The presence of intranuclear filamentous inclusions in cerebellar Golgi cells was earlier reported by Castejon and Arismendi [4] in three patients with cerebellar tumours. They were related with stress conditions, excitotoxicity, damage of mitochondrial respiratory chain and impaired energy metabolism [18].

Degenerated cerebellar afferent and efferent myelinated axons were found in the granular and molecular layers of cerebellar cortex, which provide

evidence for myelin lipid dysfunction in the oedematous cerebellar cortex related with the oligodendrocyte degenerating hydropic changes [6,13]. Cytoskeletal disassembly and caspases are recently implicated in these processes highlighting the degenerating axonal processes in human hypoxic-ischaemic injury [29].

The presynaptic synaptic terminals of climbing fibres synapsing on Purkinje cell dendrites exhibited a decreased number of synaptic vesicles, indicating climbing fibre presynaptic degeneration [11]. Similar findings were reported by Baloyannis in vascular dementia [1].

We found lipofuscin-rich astrocyte which can be related with the associated ischaemic and degenerative processes. Similar observations have been reported by the present author in traumatic human brain injuries [9,10]. We also found reactive phagocytic astrocytes and microglial cells engulfing hae-

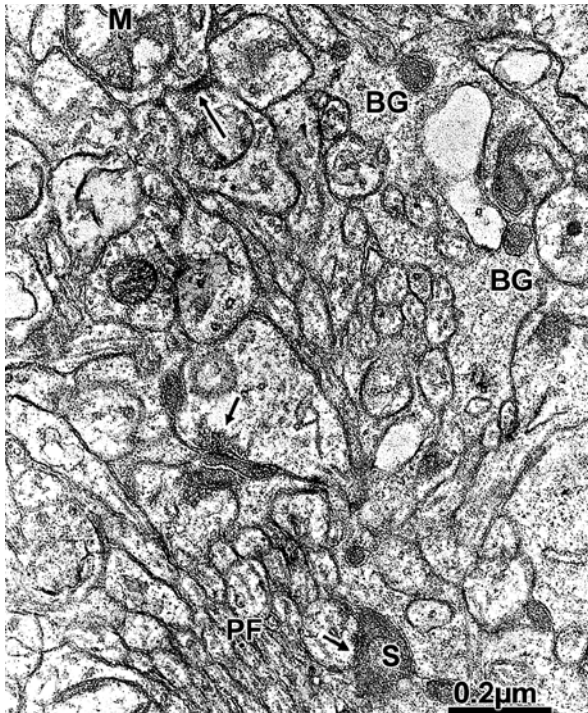


Fig. 12. Cerebellar meningioma. Cerebellar molecular layer showing the degenerated parallel fibre-dark Purkinje cell dendritic spine synapses (short arrows) and the degenerated climbing fibre-Purkinje dendrite synapses (long arrows). Protein-rich Bergmann glial cell (BG) swollen cytoplasm surrounds the molecular layer neuropil.

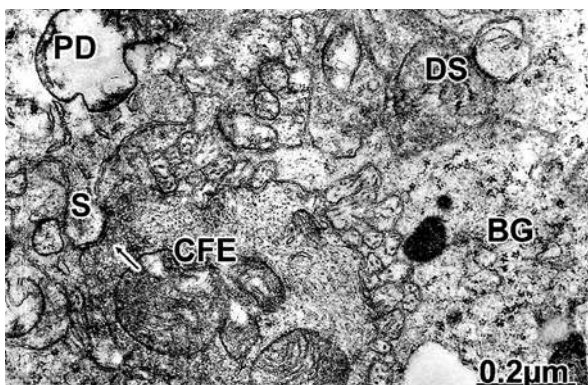


Fig. 13. Cerebellar hemangioma. Large and swollen climbing fibre ending (CFE) containing neurofilaments, swollen clear mitochondria and scarce synaptic vesicles making a swollen axo-spinodendritic contact (arrow) with a degenerated spine (S) of a swollen and clear Purkinje cell dendrite (PD). Note the enveloping perisynaptic Bergmann glial cell cytoplasm (BG). The upper right side of the figure shows degenerated presynaptic endings (DS).

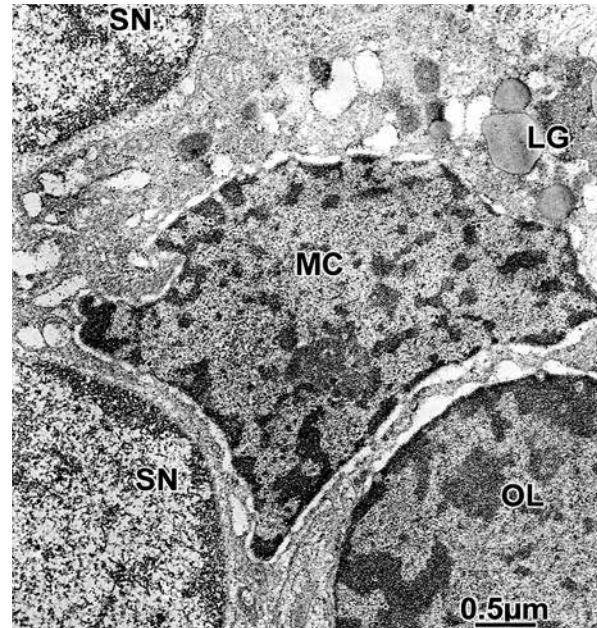


Fig. 14. Cerebellar meningioma. Cerebellar molecular layer showing a swollen and phagocytic microglial cell (MC) containing lipofuscin granules (LG) and phagocytic vacuoles, and a swollen oligodendrocyte (OL) intercalated among stellate neurons (SN).

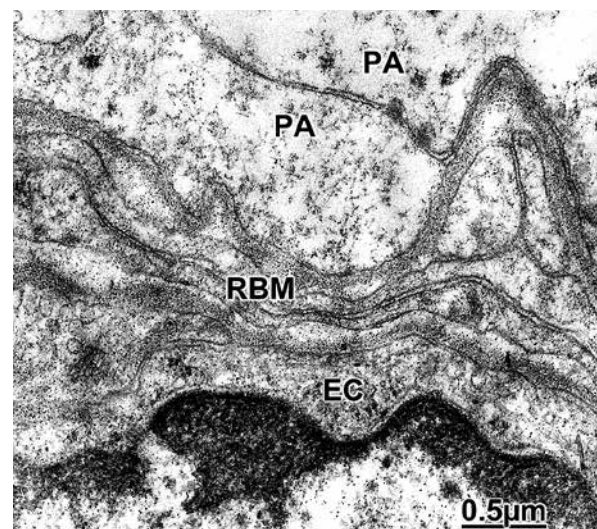


Fig. 15. Cerebellar meningioma. Cerebellar molecular layer. Cerebellar capillary showing the swollen abluminal cytoplasm of endothelial cell (EC), the reduplicated, swollen and vacuolated basement membrane (BM) exhibiting fine granular deposits of degraded glycoproteins basement matrix, and the oedematous perivascular astrocytic end-feet (PA). The swollen pericyte cytoplasm is observed between the basement membrane layering.

matogenous proteinaceous oedema fluid. These findings have been also described by Stoll *et al.* [30] in ischaemic brain lesions, and by us in severe traumatic and complicated human brain injuries [5,9,10].

Clinical correlates of peritumoural ischaemic process

The electron microscopic findings described herein and related with the oedematous microneurons (granule, basket, and stellate cells) and macroneurons (Golgi and Purkinje cells) of cerebella cortex, and their degenerated synaptic contacts in both granule cell and molecular layers with cerebellar afferent and intrinsic fibres could be related with the tremor, nystagmus, dismetry, gait disturbance and neurobehavioral changes observed in the patients examined. According to Louise [21], a cascade of biochemical and cellular events occurring in the Purkinje cell layer and its neuron neighbourhood, as well as the physiological effects of secondary remodelling/rewiring could be related with essential tremor. The derangement of neurons and intracortical circuits is in agreement with the hypothesis that cerebellar damage impairs executive control and monitoring of movement generation [3].

Some molecular considerations on peritumoural cerebellar ischaemic process

The peritumoural ischaemic process seems to include the detrimental biochemical events postulated by Hou and MacManus [17] for ischaemia-induced neuronal death, such as perturbation of calcium homeostasis leading to increased excitotoxicity, malfunction of endoplasmic reticulum and mitochondria, elevation of oxidative stress causing DNA damage, alteration in proapoptotic gene expression, and activation of the effector cysteine proteases (caspases) and endonucleases leading to the final degradation of the genome. The observed peritumoural cerebellar cell changes herein described also are similar to those described as permanent compression ischaemia [19]. A role of glutamate receptors in ischaemic process has been firmly established and a prominent characteristic of ischaemic insults is endoplasmic reticulum (ER) stress. In addition, a down-regulation of cell surface GABAB receptors has been postulated leading to diminished neuronal inhibition and contributing to excitotoxicity in

cerebral ischaemia [23]. Cerebellar Purkinje neurons are selectively vulnerable to AMPA (alpha-amino-3-hydroxy-5-methyl-4-isoxazolepropionic acid)-induced delayed neurotoxicity known as dark cell degeneration that is expressed as cytoplasmic and nuclear condensation, neuron shrinkage, and failure of physiology [31]. Sustained activation of N-methyl-D-aspartate (NMDA)-type glutamate receptors leads to excitotoxic neuronal death as observed in stroke, brain trauma, and neurodegenerative disorders. Superoxide production by NADPH oxidase is a requisite event in the process leading from NMDA receptor activation to excitotoxic death [20].

Alterations of cerebellar excitatory and inhibitory synaptic transmission may contribute to the ischaemia-induced neuronal degeneration [22]. We have observed swollen mitochondria indicating a decrease in high energy phosphate produced by ischaemia, which causes depletion of the materials necessary to produce this phosphate and strongly affecting the electron transport chain. The biochemical pathology of swollen mitochondria in brain oedema have been earlier analysed in detail by us in a previous publication [12].

The presence of extracellular electron dense deposits of proteinaceous oedema fluid and fibrinous organization, and the reduplicated capillary basement layering have also been described by us in severe traumatic brain injuries [7,8].

Acknowledgments

This paper has been carried out with a subvention obtained from CONDES-LUZ and Castejón Foundation. We deeply appreciate the technical digital help of Lic. Orlando Castejón de Pablos for preparation of electron micrographs.

Disclosure

Author reports no conflict of interest.

References

1. Baloyannis SJ. Pathological alterations of the climbing fibres of the cerebellum in vascular dementia: a Golgi and electron-microscope study. *J Neurol Sci* 2007; 257: 56-61.
2. Barenberg P, Strahlendorf H, Strahlendorf J. Hypoxia induces an excitotoxic-type of dark cell degeneration in cerebellar Purkinje neurons. *Neurosci Res* 2001; 40: 245-254.
3. Brunamonti E, Chiricozzi FR, Clausi S, Olivito G, Giusti MA, Molinari M, Ferraina S, Leggio M. Cerebellar damage impairs exec-

- utive control and monitoring of movement generation. *PLoS One* 2014; 9: e85997.
4. Castejón OJ, Arismendi GJ. Intranuclear filamentous inclusion in human oedematous cerebellar Golgi cells. *J Submicrosc Cytol Pathol* 2003; 35: 389-393.
 5. Castejón OJ. Electron microscopy of astrocyte changes and subtypes in traumatic human edematous cerebral cortex: a review. *Ultrastruct Pathol* 2013; 37: 417-424.
 6. Castejón OJ. Electron microscopic study of central axonal degeneration in traumatic human brain edema. *J Submicrosc Cytol* 1985; 17: 703-718.
 7. Castejón OJ, Valero C, Díaz M. Light and electron microscopy of nerve cells in traumatic oedematous human cerebral cortex. *Brain Inj* 1997; 11: 363-388.
 8. Castejón OJ. Ultrastructural alterations of human cortical capillary basement membrane in perifocal brain edema. A review. *Folia Neuropathol* 2014; 52: 10-21.
 9. Castejón OJ. Morphological astrocytic changes in complicated human brain trauma. A light and electron microscopic study. *Brain Inj* 1998; 12: 409-427.
 10. Castejón OJ. Astrocyte subtypes in the gray matter of injured human cerebral cortex. A transmission electron microscopic study. *Brain Inj* 1999; 13: 291-304.
 11. Castejón OJ, Valero C, Díaz M. Synaptic degenerative changes in human traumatic brain edema. *J Neurosurg Sci* 1995; 39: 47-65.
 12. Castejón OJ. Structural pattern of injured mitochondria in oedematous human cerebral cortex. *Brain Inj* 2004; 18: 1107-1126.
 13. Castejón OJ. Ultrastructural pathology of oligodendroglial cells in traumatic and hydrocephalic human brain edema: a review. *Ultrastruct Pathol* 2015; 39: 359-368.
 14. Chaudhry AP, Montes M, Cohn GA. Ultrastructure of cerebellar hemangioblastoma. *Cancer* 1978; 42: 1834-1850.
 15. Ferrer I, Isamat F, Acebes J. A Golgi and electron microscopic study of a dysplastic gangliocytoma of the cerebellum. *Acta Neuropathol* 1979; 47: 163-165.
 16. Ho KL. Ultrastructure of cerebellar capillary hemangioblastoma. IV. Pericytes and their relationship to endothelial cells. *Acta Neuropathol* 1985; 67: 2542-2564.
 17. Hou ST, MacManus JP. Molecular mechanisms of cerebral ischemia-induced neuronal death. *Int Rev Cytol* 2002; 221: 93-148.
 18. Iijima T. Mitochondrial membrane potential and ischemic neuronal death. *Neurosci Res* 2006; 55: 234-243.
 19. Kalimo H, Paljärvi L, Vapalahti M. The early ultrastructural alterations in the rabbit cerebral and cerebellar cortex after compression ischaemia. *Neuropathol Appl Neurobiol* 1979; 5: 211-223.
 20. Lam TI, Brennan-Minnella AM, Won SJ, Shen Y, Hefner C, Shi Y, Sun D, Swanson RA. Intracellular pH reduction prevents excitotoxic and ischemic neuronal death by inhibiting NADPH oxidase. *Proc Natl Acad Sci U S A* 2013; 110: 362-368.
 21. Louis ED. From neurons to neuron neighborhoods: the rewiring of the cerebellar cortex in essential tremor. *Cerebellum* 2014; 13: 501-512.
 22. Liang R, Pang ZP, Deng P, Xu ZC. Transient enhancement of inhibitory synaptic transmission in hippocampal CA1 pyramidal neurons after cerebral ischemia. *Neuroscience* 2009; 160: 412-418.
 23. Maier PJ, Zemoura K, Acuña MA, Yévenes GE, Zeilhofer HU, Benke D. Ischemia-like oxygen and glucose deprivation mediates down-regulation of cell surface γ -aminobutyric acidB receptors via the endoplasmic reticulum (ER) stress-induced transcription factor CCAAT/enhancer-binding protein (C/EBP)-homologous protein (CHOP). *J Biol Chem* 2014; 289: 12896-12907.
 24. Mann DM, Stamp JE, Yates PQ, Bannister CM. The fine structure of the axonal torpedo in Purkinje cells of the human cerebellum. *Neurol Res* 1980; 1: 369-378.
 25. Mavroudis IA, Manani MG, Petrides F, Petsoglou K, Njau SD, Costa VG, Baloyannis SJ. Dendritic and spinal pathology of the Purkinje cells from the human cerebellar vermis in Alzheimer's disease. *Psychiatr Danub* 2013; 25: 221-226.
 26. Paschen W. Endoplasmic reticulum: a primary target in various acute disorders and degenerative diseases of the brain. *Cell Calcium* 2003; 34: 365-383.
 27. Probst A, Ulrich J, Zdrojewski B, Hirt HR. Cerebellar ganglioglioma in a child. *J Neuropathol Exp Neurol* 1979; 38: 57-71.
 28. Sobaniec-Lotowska ME. Ultrastructure of Purkinje cell perikarya and their dendritic processes in the rat cerebellar cortex in experimental encephalopathy induced by chronic application of valproate. *Int J Exp Pathol* 2001; 82: 337-348.
 29. Sokolowski JD, Gamage KK, Heffron DS, Leblanc AC, Deppmann CD, Mandell JW. Caspase-mediated cleavage of actin and tubulin is a common feature and sensitive marker of axonal degeneration in neural development and injury. *Acta Neuropathol Commun* 2014; 2: 16.
 30. Stoll G, Jander S, Schroeter M. Inflammation and glial responses in ischemic brain lesions. *Prog Neurobiol* 1998; 56: 149-171.
 31. Strahlendorf J, Box C, Attridge J, Diertien J, Finckbone V, Henne WM, Medina MS, Miles R, Oomman S, Schneider M, Singh H, Veliyaparambil M, Strahlendorf H. AMPA-induced dark cell degeneration of cerebellar Purkinje neurons involves activation of caspases and apparent mitochondrial dysfunction. *Brain Res* 2003; 994: 146-159.
 32. Yagishita S. Morphological investigations on axonal swellings and spheroids in various human diseases. *Virchows Arch A Pathol Anat Histol* 1978; 378: 181-197.

Survival in the pre-senile dementia frontotemporal lobar degeneration with TDP-43 proteinopathy: effects of genetic, demographic and neuropathological variables

Richard A. Armstrong

Vision Sciences, Aston University, Birmingham, United Kingdom

Folia Neuropathol 2016; 54 (2): 137-148

DOI: 10.5114/fn.2016.60391

Abstract

Factors associated with survival were studied in 84 neuropathologically documented cases of the pre-senile dementia frontotemporal lobar degeneration (FTLD) with transactive response (TAR) DNA-binding protein of 43 kDa (TDP-43) proteinopathy (FTLD-TDP). Kaplan-Meier survival analysis estimated mean survival as 7.9 years (range: 1-19 years, SD = 4.64). Familial and sporadic cases exhibited similar survival, including progranulin (GRN) gene mutation cases. No significant differences in survival were associated with sex, disease onset, Braak disease stage, or disease subtype, but higher survival was associated with lower post-mortem brain weight. Survival was significantly reduced in cases with associated motor neuron disease (FTLD-MND) but increased with Alzheimer's disease (AD) or hippocampal sclerosis (HS) co-morbidity. Cox regression analysis suggested that reduced survival was associated with increased densities of neuronal cytoplasmic inclusions (NCI) while increased survival was associated with greater densities of enlarged neurons (EN) in the frontal and temporal lobes. The data suggest that: (1) survival in FTLD-TDP is more prolonged than typical in pre-senile dementia but shorter than some clinical subtypes such as the semantic variant of primary progressive aphasia (svPPA), (2) MND co-morbidity predicts poor survival, and (3) NCI may develop early and EN later in the disease. The data have implications for both neuropathological characterization and subtyping of FTLD-TDP.

Key words: frontotemporal dementia lobar degeneration (FTLD), survival, Kaplan-Meier estimator.

Introduction

Studies of the life expectancy of patients with dementia are important in calculating prevalence rates, while identifying factors that influence survival is useful both in counseling patients and their families and in public health planning [14,60]. However, there have been relatively few studies of survival especially in the pre-senile dementias [36] includ-

ing frontotemporal dementia (FTD), the second most common form of cortical dementia of early-onset after Alzheimer's disease (AD) [55,59]. Frontotemporal dementia is associated with a variety of clinical syndromes including FTD-motor neuron disease (FTD-MND), behavioral variant FTD (bvFTD), non-fluent variant of primary progressive aphasia (nfPPA), and the semantic variant of PPA (svPPA) [12].

Communicating author:

Dr Phil. Richard A. Armstrong, Vision Sciences, Aston University, Birmingham B4 7ET, United Kingdom, phone: +441212044102, e-mail: R.A.Armstrong@aston.ac.uk

Frontotemporal dementia is a clinical diagnosis, and pathological variants of the disease are termed frontotemporal lobar degeneration (FTLD). A specific pathological subtype of FTLD, viz., FTLD with transactive response (TAR) DNA-binding protein of 43 kDa (TDP-43) proteinopathy (FTLD-TDP), previously called FTLD with ubiquitin-immunoreactive inclusions (FTLD-U) [38,64], is characterized by a variable neocortical and allocortical atrophy principally affecting the frontal and temporal lobes. In addition, there is neuronal loss, microvacuolation of superficial cortical laminae, and a reactive astrocytosis [10,19]. A variety of TDP-43-immunoreactive inclusions are present in these cases including neuronal cytoplasmic inclusions (NCI), neuronal intranuclear inclusions (NII), dystrophic neurites (DN), and glial inclusions (GI) [10].

FTLD-TDP exhibits considerable pathological heterogeneity which may affect survival [10]. First, various genetic defects have been identified, the majority being caused by mutation of the progranulin (*GRN*) gene (FTLD-TDP-GRN) [11,13,23,46,51,61]. A less prevalent disorder, FTLD with valosin-containing protein (*VCP*) gene mutation [28], also has TDP-43 immunoreactive inclusions, and familial cases have also been shown to be caused by the chromosome 9 open reading frame 72 (*C9ORF72*) gene [39,52]. Second, FTLD is associated with various co-morbidities including MND (FTLD-MND), such cases being associated with a more localized pattern of frontal lobe atrophy [63] and with hippocampal sclerosis (HS) [1], in which significant neuronal loss occurs in the subiculum and sector CA1 of the hippocampus [35]. In addition, cases of later onset exhibit AD neuropathological change (ADNC), viz. senile plaques (SP) and neurofibrillary tangles (NFT) [10]. Third, various subtypes of FTLD-TDP have been proposed based on pathological criteria [20,40,53]. Using the system proposed by Cairns *et al.* [20]: type 1 cases are characterized by long DN in superficial cortical laminae with few or no NCI or NII, type 2 by numerous NCI in superficial and deep cortical laminae with infrequent DN and sparse or no NII, type 3 by pathology predominantly affecting the superficial cortical laminae with numerous NCI, DN and varying numbers of NII, and type 4 by numerous NII, and infrequent NCI and DN especially in neocortical areas [20].

Many published studies suggest that survival rates in the dementias vary considerably and may depend on numerous factors [17]. Hence, survival

may depend on age at diagnosis, sex, disease subtype, and severity of progression [5]. The objective of the present study was to investigate the influence of genetics, demographic variables, co-morbidity, and neuropathology on survival, as measured by duration of dementia, in a sample of well-documented FTLD-TDP cases [10]. Kaplan-Meier survival analysis was used to determine whether survival was influenced by genetics, demographic factors, or co-morbidity, while Cox regression analysis was used to determine whether there were correlations between survival and predictor variables such as the densities of TDP-43-reactive inclusions in various brain regions [33,48,66].

Material and methods

Cases

Eighty-four cases of FTLD-TDP (see Table I) were obtained from dementia centers in the USA and Canada: (1) Washington University School of Medicine, St. Louis, MO, USA; (2) University of California, Davis, CA, USA; (3) University of Pittsburgh, Pittsburgh, PA, USA; (4) Vancouver General Hospital, Vancouver, Canada; (5) Harvard Brain Tissue Resource Center, Belmont, MA, Emory University, Atlanta, GA, USA; (6) University of Washington, Seattle, WA, USA; (7) Columbia University, New York, NY, USA; (8) University of California, Irvine, CA, USA and (9) University of Michigan, Ann Arbor, MI, USA. All cases exhibited FTD with neuronal loss, microvacuolation in the superficial cortical laminae, and reactive astrocytosis consistent with diagnostic criteria for FTLD-TDP [19,39]. A variety of TDP-43-immunoreactive inclusions were present in these cases including NCI, NII, DN, and GI. Of the 84 cases, 39 (46%) were familial (one or more first degree relatives affected) and of these, 16 cases (19%) had *GRN* mutations [11,13,23,46,51,61], one had a *VCP* gene mutation [28], and one case was associated with *C9ORF72* [39,52]. The genetic defects in the remaining familial cases have not been identified to date. Nine of the cases (11%) had coexisting MND (FTLD-MND) [34,37] and seven (8%) were identified as having associated HS (FTLD-HS). Twelve cases (14%) were identified as having ADNC greater than expected from normal aging [44]. Braak staging was based on the density and distribution of β -amyloid ($A\beta$) deposits and NFT [15,16] and cases were also assigned to the four pathological subtypes [20].

Table I. Demographic details of the 84 cases of frontotemporal dementia lobar degeneration (FTLD) with TDP-43 proteinopathy (FTLD-TDP) used in the study. Data for age at death, survival, and disease onset are means with standard deviations (SD) in parentheses

Patient group	N	Death (years)	Onset (years)	Mean survival (years)
Sporadic cases	45 (22 M,23 F)	71.02 (1.49)	63.31 (1.43)	7.54 (0.80)
GRN mutation	16 (9 M,7 F)	70.33 (2.55)	61.27 (2.45)	7.61 (0.79)
Other familial cases	23 (11 M,12 F)	68.45 (2.10)	60.82 (2.02)	9.07 (1.01)

N – number of cases, *GRN* – progranulin, *M* – male, *F* – female

Case records

The following data were obtained from case and post-mortem records: (1) family history, (2) the presence of MND, HS, or AD co-morbidity, (3) age at death, (4) disease duration, measured from the onset of dementia symptoms, determined by clinical assessment, and defined as cognitive dysfunction sufficiently severe to impair activities of daily living, and (5) total brain weight.

Histological methods

After death, consent of the next-of-kin was obtained for brain removal, following local Ethical Committee procedures and the 1995 Declaration of Helsinki (as modified in Edinburgh, 2000). Tissue blocks were taken from the frontal lobe at the level of the genu of the corpus callosum to study the middle frontal gyrus (MFG) and temporal lobe at the level of the lateral geniculate body to study the inferior temporal gyrus (ITG), parahippocampal gyrus (PHG), CA1/2 sectors of the hippocampus, and dentate gyrus (DG). Tissue was fixed in 10% phosphate-buffered formal saline and embedded in paraffin wax. Immunohistochemistry (IHC) was performed on 4 to 10 μm sections with a rabbit polyclonal antibody that recognizes TDP-43 epitopes (dilution 1 : 1000; ProteinTech Inc., Chicago, IL). Sections were counterstained with hematoxylin.

Quantitative analysis of neuropathology

In the MFG, ITG, and PHG of each case, histological features were counted along strips of tissue (1600 to 3200 μm in length) located parallel to the pia mater, using 250 \times 50 μm sample fields arranged contiguously [3]. The sample fields were located in both the upper and lower cortex, the short edge of the field being orientated parallel with the pia

mater and aligned with guidelines marked on the slide. Between 32 and 64 fields were used to quantify each region. In the majority of cases, the upper and lower fields quantified lesions in lamina II and part of lamina III and in laminae V/VI respectively. In the hippocampus, the features were counted in the cornu ammonis (CA) in a region extending from the prosubiculum/CA boundary to the maximum point of curvature of the pyramidal layer before it extends to join the dentate fascia via CA3 and CA4. Hence, the region sampled encompassed approximately sectors CA1 and CA2, the short dimension of the contiguous field being aligned with the alveus. Little pathology was observed to extend into CA3/4 in these cases [10]. To quantify pathology in the dentate gyrus [38,41,64], the sample field was aligned with the upper edge of the granule cell layer. The NCI are rounded, spicular, or skein-like in shape [24,65], while the GI morphologically resemble the 'coiled bodies' reported in various tauopathies such as corticobasal degeneration (CBD), progressive supranuclear palsy (PSP), and argyrophilic grain disease (AGD). The NII are lenticular or spindle-shaped [50] and the DN characteristically long and contorted [31]. Small spherical or asymmetrical nuclei without cytoplasm but with the presence of a thicker nuclear membrane and more heterogeneous chromatin were identified as glial cells [2]. Abnormally enlarged neurons (EN) had enlarged perikarya, lacked NCI, had a shrunken nucleus displaced to the periphery of the cell, and the maximum cell diameter was at least three times the nucleus diameter [2,4]. The number of discrete vacuoles greater than 5 μm in diameter was also recorded in each field [9].

Data analysis

First, the survival data as a whole were tested for normality using the Kolmogorov-Smirnov and chi-square (χ^2) goodness of fit tests. The degree of skew

in the data was also tested. Second, the Kaplan-Meier 'product limit estimator' was used to study the overall pattern of survival among the 84 cases and is the fraction of cases which survive for a certain period after disease onset. In typical applications, the cases can also be grouped according to a categorical predictor variable and the effect of the variable on survival tested. Where two groups were present, e.g., familial/sporadic, male/female, presence/absence of co-morbidity, survival was compared using the log-rank test which determines whether the hazard ratio (HR) is significantly different from unity [5]. An assumption of this analysis is that the HR is relatively constant across time intervals ('proportionality assumption'). This assumption was tested by two methods: (1) by examining changes in the HR over time and (2) by fitting a model that includes, in addition to a fixed covariate group, a time-dependent variable. If the time-dependent covariate is not significant, then proportionality can be assumed and a model with the single fixed covariate is likely to be appropriate. Where more than two groups were present, survival was compared using the chi-square (χ^2) test. In addition, a life table analysis was performed to predict the life expectancy of FTLTDP patients at each age. Third, Cox regression was used to study the relationship between survival and vari-

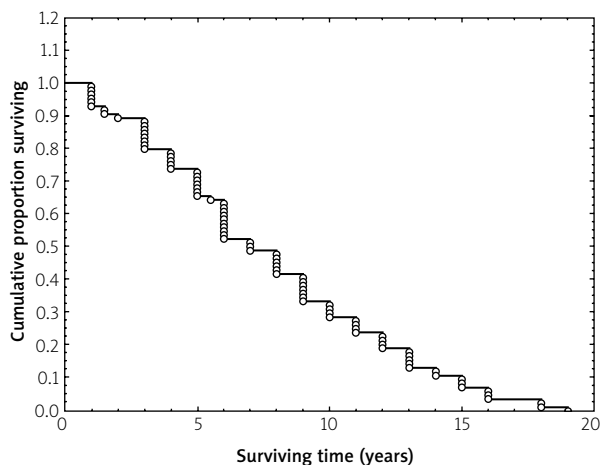


Fig. 1. Kaplan-Meier survival analysis of all 84 frontotemporal dementia lobar degeneration with transactive response (TAR) DNA-binding protein of 43 kDa (TDP-43) proteinopathy (FTLTDP) cases. Survival data are plotted as the proportion of individuals surviving at each time and at the upper limit of each yearly time interval.

ous predictor variables. Two such groups of variables were tested: (1) demographic variables such as age at death, and disease onset, and gross neuropathological assessments such as brain weight, Braak stage and disease subtype and (2) quantitative estimates of density of histological features. In each of these analyses, variables were modeled individually and were corrected for gender and age. Statistical significance in these tests was based on t and the Wald statistic [5].

Results

The distribution of the data as a whole did not deviate from normality (KS $d = 0.13$, $p > 0.05$; $\chi^2 = 9.52$, $DF = 5$, $p > 0.05$; Skew = 0.45, SE = 0.26). Mean disease duration of the 84 FTLTDP cases was 7.9 years (median: 7.0, range: 1-19 years, SD = 4.64). The survival function for all cases is shown in Figure 1, suggesting that 25% of cases died within four years, 50% within 6.9 years, and 75% within 10 years after onset of dementia. In addition, the data are summarized as a 'life table' (Table II), suggesting that median life expectancy was 7.58 years

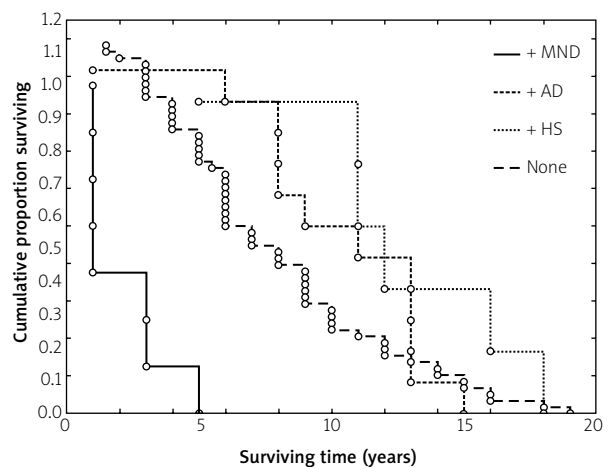


Fig. 2. Kaplan-Meier survival analysis of the data grouped into those FTLTDP patients with no co-morbidity (None), and those with associated Alzheimer's disease (AD) (HR = 0.51, CI = 0.30), hippocampal sclerosis (HS) (HR = 0.35, CI = 0.30), or motor neuron disease (MND) (HR = 2.23, CI = 0.18) (comparison between groups: $\chi^2 = 6.83$, $p < 0.05$). Survival data are plotted as the proportion of individuals surviving at each time and at the upper limit of each yearly time interval.

Table II. Life table for 84 frontotemporal dementia lobar degeneration with transactive response (TAR) DNA-binding protein of 43 kDa (TDP-43) proteinopathy (FTLD-TDP) cases

Interval (mid-point)	Number entering	Number dying	Proportion dying	Hazard rate	Median LE
0.5	84	0	0	0	7.58
1.5	84	8	0.10	0.10	6.67
2.5	76	1	0.01	0.01	6.50
3.5	75	8	0.12	0.11	5.58
4.5	67	5	0.07	0.08	5.21
5.5	62	8	0.13	0.14	4.57
6.5	54	10	0.19	0.20	4.25
7.5	44	3	0.07	0.07	4.50
8.5	41	6	0.15	0.16	3.87
9.5	35	7	0.20	0.22	3.63
10.5	28	4	0.14	0.15	3.40
11.5	24	4	0.17	0.18	2.80
12.5	20	4	0.20	0.22	2.50
13.5	16	5	0.31	0.37	2.33
14.5	11	2	0.18	0.20	2.17
15.5	9	3	0.33	0.40	1.50
16.5	6	3	0.50	0.67	1.00
17.5	3	0	0.17	0.18	1.60
18.5	3	2	0.67	1.00	0.75
19	1	1	0.50	–	–

LE – life expectancy

immediately after diagnosis, 3.4 years 10 years after, and 0.75 years 18 years after diagnosis.

The effect of various categorical predictor variables on survival is shown in Table III. The data suggest no significant differences in survival between familial and sporadic cases (log rank = 0.03, $p > 0.05$) or among cases divided into sporadic, GRN mutation, and remaining familial cases ($\chi^2 = 1.81$, DF = 2, $p > 0.05$). In addition, there were no significant differences in survival in males and females (log rank = 0.68, $p > 0.05$). However, significant effects of comorbidity on survival were evident ($\chi^2 = 22.70$, DF = 3, $p < 0.001$), cases with associated MND exhibiting reduced survival compared with those without copathology (HR = 2.23, CI = 0.18) and those with associated AD (HR = 0.51, CI = 0.30) and HS (HR = 0.51, CI = 0.35) showing increased survival ($\chi^2 = 6.83$, DF = 2,

Table III. Comparison of survival among various groups of cases of frontotemporal dementia lobar degeneration (FTLD) with TDP-43 proteinopathy (FTLD-TDP) using the Kaplan-Meier estimator

Grouping factor	Log-rank test	χ^2	p
Familial/Sporadic cases	0.03	–	> 0.05
Familial/GRN/Sporadic	–	1.81	> 0.05
Gender	0.68	–	> 0.05
Co-morbidity all groups	–	22.70	< 0.001
Co-morbidity: None, MND	2.33	–	< 0.01
Co-morbidity: None, AD, HS	–	6.83	< 0.05
Co-morbidity: AD, HS	–	0.80	> 0.05

P – probability, GRN – progranulin, MND – motor neuron disease, AD – Alzheimer's disease, HS – hippocampal sclerosis

Table IV. Analysis of the influence of demographic variables, brain weight, Braak stage, and disease subtype on survival using Cox regression (β – regression coefficient, SE – standard error, p – probability, $**p < 0.01$). Each variable was modeled individually and adjusted for gender

Variable	β	SE	t	Wald statistic	p
Patient age	-0.03	0.01	2.73	7.48	< 0.01
Disease onset	0.01	0.01	1.07	1.14	> 0.05
Brain weight	0.01	0.01	3.07	9.43	< 0.01
Braak A β stage	-0.06	0.19	0.33	0.10	> 0.05
Braak tangle stage	-0.06	0.08	0.74	0.55	> 0.05
Disease subtype	0.09	0.11	0.77	0.59	> 0.05

Table V. Analysis of the influence of the densities of neuropathological variables (NCI – neuronal cytoplasmic inclusions, GI – glial inclusions, NII – neuronal intranuclear inclusions, DN – dystrophic neurites, SN – surviving neurons, EN – abnormally enlarged neurons, Vac – vacuolation) on survival in various brain regions (MFG – middle frontal gyrus, ITG – inferior temporal gyrus, PHG – parahippocampal gyrus, HC – CA1/2 sectors of hippocampus, DG – dentate gyrus) (β – regression coefficient, SE – standard error, p – probability). Variables were modeled in groups for each brain region and adjusted for gender.

Region	Histology	β	SE	t	Wald	p
MFG(U)	NCI	0.60	0.79	0.74	0.56	> 0.05
	GI	0.68	1.89	0.36	0.13	> 0.05
	NII	-0.33	0.83	0.59	0.35	> 0.05
	DN	-0.36	0.36	0.93	0.88	> 0.05
	EN	-0.16	1.14	0.32	0.10	> 0.05
	N	-0.01	0.09	1.83	3.34	> 0.05
	Vac	-0.04	0.02	1.89	3.50	> 0.05
MFG(L)	NCI	1.81	1.07	1.67	2.80	> 0.05
	GI	-3.85	1.75	2.19	4.82	< 0.05
	NII	0.42	0.76	0.56	0.31	> 0.05
	DN	0.005	0.36	0.01	0.02	> 0.05
	EN	0.81	1.42	0.57	0.31	> 0.05
	N	0.24	0.10	2.54	6.45	< 0.05
	Vac	0.05	0.03	1.91	3.64	> 0.05
ITG(U)	NCI	1.46	0.48	3.56	12.69	< 0.001
	GI	-3.36	1.48	2.26	5.12	< 0.05
	NII	-0.44	0.82	0.53	0.29	> 0.05
	DN	-0.80	0.25	2.21	4.88	< 0.05
	EN	-0.73	2.19	0.33	0.11	> 0.05
	N	-0.19	0.07	2.86	8.21	< 0.001
	Vac	-0.03	0.03	1.15	1.33	> 0.05

Table V. Cont.

Region	Histology	β	SE	t	Wald	p
ITG(L)	NCI	0.52	0.73	0.71	0.51	> 0.05
	GI	-0.91	1.58	0.57	0.33	> 0.05
	NII	-0.14	0.72	0.20	0.04	> 0.05
	DN	-0.64	0.70	0.91	0.84	> 0.05
	EN	-1.52	1.09	1.40	1.95	> 0.05
	N	-0.19	0.08	2.39	5.75	< 0.05
	Vac	0.03	0.04	0.86	0.75	> 0.05
PHG(U)	NCI	0.72	0.63	1.14	1.31	> 0.05
	GI	1.85	1.88	0.98	0.97	> 0.05
	NII	0.46	0.88	0.52	0.28	> 0.05
	DN	-0.15	1.19	0.43	0.18	> 0.05
	EN	1.18	1.19	0.99	0.99	> 0.05
	N	-0.20	0.08	2.47	6.13	< 0.05
	Vac	-0.10	0.03	3.26	10.67	< 0.001
PHG(L)	NCI	-1.35	0.89	1.51	2.28	< 0.05
	GI	0.57	1.91	0.29	0.09	> 0.05
	NII	-1.07	0.74	1.45	2.10	> 0.05
	DN	-0.76	0.49	1.55	2.42	> 0.05
	EN	-3.17	1.37	2.31	5.37	< 0.05
	N	0.09	0.09	0.99	0.98	> 0.05
	Vac	-0.76	0.03	1.92	3.69	> 0.05
HC	NCI	3.68	1.38	2.67	7.11	< 0.05
	GI	-0.90	1.97	0.45	0.21	> 0.05
	NII	-0.27	0.60	0.44	0.20	> 0.05
	DN	-0.05	0.70	0.06	0.01	> 0.05
	EN	-1.83	1.04	1.77	3.11	> 0.05
	N	-0.06	0.11	0.55	0.31	> 0.05
	Vac	-0.09	0.03	0.69	0.03	> 0.05
DG	NCI	0.09	0.33	0.29	0.08	> 0.05
	NII	-1.06	1.62	0.65	0.43	> 0.05
	DN	-2.53	4.32	0.59	0.34	> 0.05
	EN	-2.95	15.94	0.18	0.03	> 0.05
	N	-0.12	0.05	2.31	5.32	< 0.05
	Vac	-0.07	0.05	0.59	1.67	> 0.05

$p < 0.05$). The HR for MND and HS were relatively constant across time intervals and the time-dependent covariates non-significant, suggesting that the proportionality assumption was valid. However, HR for AD varied between time intervals, and the time-dependent covariate was significant ($t = 2.23$, $p < 0.05$), thus violating the assumption of proportionality.

The results of the Cox regression analysis, corrected for gender, which included the demographic variables, brain weight, Braak staging, and pathological disease subtype, are shown in Table IV. The data suggest: (1) a relationship between patient age and survival ($t = 8.81$, $p < 0.01$), better survival being associated with a later age at death, (2) no significant association between survival and disease onset ($t = 0.79$, $p > 0.05$), (3) a significant relationship with brain weight ($t = 3.07$, $p < 0.01$), lower brain weight being associated with increased survival, and (3) no significant association between survival and Braak stages (A β : $t = 0.33$, $p > 0.05$; NFT: $t = 0.75$, $p > 0.05$), or disease subtype ($t = 0.82$, $p > 0.05$).

The results of the Cox regression analysis, corrected for gender, applied to the quantitative neuropathological variables measured in each brain region, are shown in Table V. Some histological features were associated with increased survival, including GI in the MFG ($t = 2.19$, $p < 0.05$), DN in the ITG ($t = 2.21$, $p < 0.05$), EN in the PHG ($t = 2.31$, $p < 0.05$), neurons in the MFG ($t = 2.54$, $p < 0.05$) and ITG ($t = 2.86$, $p < 0.001$), and vacuoles in the PHG ($t = 3.26$, $p < 0.001$). By contrast, density of NCI was associated with poorer survival in the ITG ($t = 3.56$, $p < 0.001$) and HC ($t = 2.67$, $p < 0.05$). A similar pattern of relationships was seen when the analysis was corrected for patient age. Only correlations between NCI in the ITG and EN in the PHG remained significant in these analyses after Bonferroni correction.

Discussion

Mean survival of the 84 FTLD-TDP cases was 7.9 years, similar to the 7.1 years recorded in a recent study of 102 AD cases [5], but longer than the 5.2 years and 6.5 years in AD estimated by Doody *et al.* [26] and Feldman *et al.* [27] respectively. Mean survival was also greater than the 6.08 years reported for a large sample of pre-senile dementia cases in the north of England, UK, but which comprised largely AD and vascular dementia (VD) [36]. Survival was increased compared with that reported for a specif-

ic group of AD cases, which had vascular disease co-morbidity, in which mean survival was less than five years [27]. This difference probably reflects the relative ages of the cases, vascular disease co-morbidity being less of a factor in pre-senile dementia. Median survival of the group (7 years), however, was similar to that of 61 pathologically confirmed FTLD patients [32]. Survival was reduced compared with a specific clinical subtype of FTLD, viz. svPPA, in which 50% of patients survived more than 12.8 years [33].

Two distinct subtypes of dementia progression have been identified, especially in AD [47,54,58], cases having either a very short (median survival 10 months) or a significantly longer survival and which may reflect education level [18,21]. Short survival cases were also evident in the present sample of FTLD-TDP, nine cases surviving for two years or less. A multiple discriminant analysis (MDA) [6] which compared these cases with the remaining FTLD-TDP cases suggested that reduced survival was not associated with different ages at death, disease onset, brain weight at post-mortem, difference in quantitative neuropathology, or co-morbidity.

No significant difference in survival was observed between males and females with FTLD-TDP, contrasting with some studies which show poorer survival in males with dementia [21,26,29]. In addition, the data suggested that survival was similar in familial and sporadic FTLD-TDP. This result contrasts with AD in which familial cases in general and cases specifically linked to presenilin 1 (*PSEN1*) mutation exhibited increased survival [5].

The data suggest that the presence of co-morbidity had a significant effect on survival, associated MND significantly shortening the lifespan. This result is similar to that previously reported for FTD-MND, which exhibited substantially reduced survival (median survival 3 years) [33]. Similarly in AD, the presence of at least one co-morbidity decreased survival [5,67] and the presence of combined co-morbidity and functional disability was an important predictor of lower survival [66]. In FTLD-TDP, however, the presence of associated AD or HS increased survival, suggesting possible synergistic interactions between competing pathologies. Consistent with this suggestion, Hodges *et al.* [32] found that the presence of tau pathology in FTLD improved prognosis (median survival 9.07). However, caution is necessary in interpreting these results as, first, HR for

AD varied between time intervals and the time-dependent covariate was significant ($t = 2.23, p < 0.05$), thus violating the assumption of proportionality, and, second, numbers of patients were small. Bowen *et al.* [14] also found a strong association between decreased survival in AD and cardiovascular disease (CVD), regarded as a significant determinant of progression to dementia. No effect of CVD or hypertension on survival, however, has been observed in other studies of AD [62] or in Down's syndrome (DS) patients [22], who frequently develop AD-type pathology [42,43,45]. Accurate quantitative data on CVD load, e.g., lacunar infarcts, micro-infarcts, and atherosclerosis of large vessels, were not available for many of the FTLD-TDP cases studied, but available data from some cases suggested that CVD load was significantly lower than in AD [5].

Whether brain weight significantly changes over the course of dementia has been controversial [5]. There are limitations in studying this complex variable post-mortem as many factors can influence brain weight, including body height and weight and the presence of systemic disease such as osteoporosis [5]. In the present study, lower brain weights were associated with better survival consistent with a gradual loss of brain volume in FTLD-TDP with disease progression. By contrast, in one study of AD, poorer survival was associated with lower gray matter volume, and smaller volume reductions in brain predicted better survival [56].

Cox regression analysis incorporating Bonferroni correction suggested that the density of NCI was positively associated with decreased survival in the ITG, suggesting either that abundant NCI could shorten survival times or that NCI could be characteristic of the early stages of the disease, being lost as the disease progresses. By contrast, the density of EN in the PHG was negatively associated with decreased survival, suggesting either that EN developed later in the disease or they could represent the earliest affected regions exposed to accumulating pathology over time. Studies suggest that pathological proteins in various neurodegenerative disorders may spread through the brain via anatomical connections [7,30,57]. In AD, for example, this spread frequently occurs from an origin in the medial temporal lobe to the cortical association areas and hippocampus, and then to the primary sensory areas [8,25,49]. Pathogenic TDP-43 may also exhibit this property, and therefore changes in density with duration in specif-

ic areas could reflect this spread. That the density of a 'signature' pathological change, viz., NCI, may vary with degree of survival has implications for both the neuropathological characterization and subtyping of FTLD-TDP, which rely on the relative density and distribution of TDP-43-reactive inclusions [20].

In conclusion, factors associated with survival were studied in 84 cases of pre-senile dementia frontotemporal dementia lobar degeneration (FTLD) with transactive response (TAR) DNA-binding protein of 43 kDa (TDP-43) proteinopathy (FTLD-TDP). The data suggested that survival in FTLD-TDP was greater than typical for the pre-senile dementias but shorter than some clinical subtypes such as SD. In addition, MND co-morbidity is a predictor of shorter survival times. There are also changes in the density of some neuropathological changes with survival, and hence the data may have implications for both diagnosis and subtyping of FTLD-TDP.

Acknowledgments

I thank the following for making tissue sections available for this study: Knight Alzheimer's Disease Research Center, Washington University School of Medicine, St. Louis, MO, USA, William Ellis (Department of Pathology, University of California, Davis, Sacramento, CA, USA), Ronald L. Hamilton (Department of Pathology, University of Pittsburgh, Pittsburgh, PA, USA), Ian R. A. Mackenzie (Department of Pathology, Vancouver General Hospital, Vancouver, Canada), E. Tessa Hedley-Whyte (Massachusetts General Hospital and Harvard Brain Tissue Resource Center, Belmont, MA, USA), Marla Gearing (Center for Neurodegenerative Disease, Emory University, Atlanta, GA, USA).

Disclosure

Author reports no conflict of interest.

References

1. Amandor-Ortiz C, Lin WL, Ahmed Z, Personett D, Davies P, Dua-ra R, Graff-Radford NR, Hutton ML, Dickson DW. TDP-43 immunoreactivity in hippocampal sclerosis and Alzheimer's disease. *Ann Neurol* 2007; 61: 435-445.
2. Armstrong RA. Correlations between the morphology of diffuse and primitive β -amyloid (A β) deposits and the frequency of associated cells in Down's syndrome. *Neuropath Appl Neurobiol* 1996; 22: 527-530.

3. Armstrong RA. Quantifying the pathology of neurodegenerative disorders: quantitative measurements, sampling strategies and data analysis. *Histopathology* 2003; 42: 521-529.
4. Armstrong RA. A quantitative study of abnormally enlarged neurons in cognitively normal brain and neurodegenerative disease. *Clin Neuropathol* 2013; 32: 128-134.
5. Armstrong RA. Factors determining disease duration in Alzheimer's disease: A postmortem study of 103 cases using the Kaplan-Meier estimator and Cox regression. *Biomed Intern* 2014; Article ID: 623487.
6. Armstrong RA, Hilton AC. *Statistical analysis in microbiology: Statnotes*. Wiley-Blackwell, Hoboken, New Jersey 2011.
7. Armstrong RA, Cairns NJ. Different molecular pathologies result in similar spatial patterns of cellular inclusions in neurodegenerative disease: a comparative study of eight disorders. *J Neural Transm* 2012; 119: 1551-1560.
8. Armstrong RA, Myers D, Smith CUM. Alzheimer's disease: size class frequency distributions of senile plaques: do they indicate when a brain tissue was affected? *Neurosci Lett* 1991; 127: 223-226.
9. Armstrong RA, Ironside J, Lantos PL, Cairns NJ. A quantitative study of the pathological changes in the cerebellum of 15 cases of variant Creutzfeldt-Jakob disease. *Neuropathol Appl Neurobiol* 2009; 35: 36-45.
10. Armstrong RA, Ellis W, Hamilton RL, Mackenzie IRA, Hedreen J, Gearing M, Montine T, Vonsattel J-P, Head E, Lieberman AP, Cairns NJ. Neuropathological heterogeneity in frontotemporal lobar degeneration with TDP-43 proteinopathy: a quantitative study of 94 cases using principal components analysis. *J Neural Transm* 2010; 117: 227-239.
11. Baker M, Mackenzie IR, Pickering-Brown SM, Gass J, Rademakers R, Lindholm C, Snowden J, Adamson J, Sadovnick AD, Rollinson S, Cannon A, Dwosh E, Neary D, Melquist S, Richardson A, Dickson D, Berger Z, Eriksen J, Robinson T, Zehr C, Dickey CA, Crook R, McGowan E, Mann D, Boeve B, Feldman H, Hutton M. Mutations in progranulin cause tau-negative frontotemporal dementia linked to chromosome 17. *Nature* 2006; 442: 916-919.
12. Bang J, Spina S, Miller BL. Frontotemporal dementia. *Lancet* 2015; 386: 1672-1682.
13. Behrens MI, Mukherjee O, Tu PH, Liscic RM, Grinberg LT, Carter D, Paulsmeyer K, Taylor-Reinwald L, Gitcho M, Norton JB, Chakraverty S, Goate AM, Morris JC, Cairns NJ. Neuropathologic heterogeneity in HDDD1: a familial frontotemporal lobar degeneration with ubiquitin-positive inclusions and progranulin mutation. *Alz Dis Assoc Disord* 2007; 21: 1-7.
14. Bowen JD, Malter AD, Shepperd L, Kukull WA, McCormick WC, Teri L, Larson EB. Predictors of mortality in patients diagnosed with probable Alzheimer's disease. *Neurology* 1996; 47: 433-439.
15. Braak H, Braak E. Neuropathological staging of Alzheimer-related changes. *Acta Neuropathol* 1991; 82: 239-259.
16. Braak H, Alafuzoff I, Arzberger T, Kretschmar H, Del Tredici K. Staging of Alzheimer disease-associated neurofibrillary pathology using paraffin sections and immunocytochemistry. *Acta Neuropathol* 2006; 112: 389-404.
17. Brodaty H, K. Seeher K, Gibson L. Dementia time to death: a systematic literature review on survival time and years of life lost in people with dementia. *Intern Psychogeriatr* 2012; 24: 1034-1045.
18. Bruandet A, Richard F, Bombois S, Maurage CA, Masse I, Amouyel P, Pasquier F. Cognitive decline and survival in Alzheimer's disease according to education level. *Dement Cog Geriatr* 2008; 25: 74-80.
19. Cairns NJ, Neumann M, Bigio EH, Holm IE, Troost D, Hatanpaa KJ, Foong C, White CL III, Schneider JA, Kretschmar HA, Carter D, Taylor-Reinwald L, Paulsmeyer K, Strider J, Gitcho M, Goate AM, Morris JC, Mishra M, Kwong LK, Steiber A, Xu Y, Forman MS, Trojanowski JQ, Lee VMY, Mackenzie IRA. TDP-43 familial and sporadic frontotemporal lobar degeneration with ubiquitin inclusions. *Am J Pathol* 2007; 171: 227-240.
20. Cairns NJ, Bigio EH, Mackenzie IRA, Neumann M, Lee VMY, Hatanpaa KJ, White CL, Schneider JA, Grinberg LT, Halliday G, Duyckaerts C, Lowe JS, Holm IE, Tolnay M, Okamoto K, Yokoo H, Murayama S, Woulfe J, Munoz DG, Dickson DW, Ince PG, Trojanowski JQ, Mann DMA. Neuropathologic diagnostic and nosological criteria for frontotemporal lobar degeneration: consensus of the Consortium for Frontotemporal Lobar Degeneration. *Acta Neuropathol* 2007; 114: 5-22.
21. Claus JJ, van Gool WA, Teunisse S, Walstra GJM, Kwa VIH, Hijdra A, Verbeeten B, Koelman JHTM, Bour LJ, De Visser BWO. Predicting survival in patients with early Alzheimer's disease. *Dem Cogn Geriatr* 1998; 9: 284-293.
22. Coppus AMW, Evenhuis HM, Verberne GJ, Visser FE, Oostra BA, Eikelenboom P, van Gool WA, Janssens ACJW, van Duijn CM. Survival in elderly persons with Down's syndrome. *Am Geriatr Soc* 2008; 6: 2311-2316.
23. Cruts M, Gijselink I, van der ZJ, Engelborgs S, Wils H, Pirci D, Rademakers R, Vandenberghe R, Dermaut B, Martin JJ, van Duijn C, Peeters K, Sciot R, Santens P, De pooter T, Mattheijssens M, van den BM, Cuijt I, Vennekens K, De Deyn PP, Kumar-Singh S, Van Broeckhoven C. Null mutations in progranulin cause ubiquitin-positive frontotemporal dementia linked to chromosome 17q21. *Nature* 2006; 442: 920-924.
24. Davidson Y, Kelley T, Mackenzie IRA, Pickering Brown S, Du Plessis D, Neary D, Snowden JS, Mann DMA. Ubiquitinated pathological lesions in frontotemporal lobar degeneration contain TAR DNA-binding protein, TDP-43. *Acta Neuropathol* 2007; 113: 521-533.
25. De Lacoste M, White CL. The role of cortical connectivity in Alzheimer's disease pathogenesis: a review and model system. *Neurobiol Aging* 1993; 14: 1-16.
26. Doody R, Pavlik V, Massman P, Kenan M, Yeh S, Powell S, Cooke N, Dyer C, demirovic J, waring S, Chan WY. Changing patient characteristics and survival experience in an Alzheimer's center patient cohort. *Dem Cogn Geriatr* 2005; 20: 198-208.
27. Feldman HH, Pirttila T, Dartigues JF, Everitt B, van Baelen B, Brashear HR, Berlin JA, Battisti WP, Kavanagh S. Analysis of mortality risk in patients with dementia treated with galantamine. *Acta Neurol Scand* 2009; 119: 22-31.
28. Forman MS, Mackenzie IR, Cairns NJ, Swanson E, Boyer PJ, Drachman DA, Jhaveri BS, Karlawish JH, Pestrvik A, Smith TN, Tu PH, Watts GDJ, Markesbery WR, Smith CD, Kimonis VE. Novel ubiquitin neuropathology in frontotemporal dementia with valosin-containing protein gene mutations. *J Neuropathol Exp Neurol* 2006; 65: 571-581.

29. Gambassi G, Lapane KL, Landi F, Sgaderi A, Mor V, Bernabei R. Sex differences in the relation between co-morbidity and mortality of patients with Alzheimer's disease. *Neurology* 1999; 53: 508-516.
30. Goedert M, Clavaguera F, Tolnay M. The propagation of prion-like protein inclusions in neurodegenerative diseases. *Trends Neurosci* 2010; 33: 317-325.
31. Hatanpaa KJ, Bigio EH, Cairns NJ, Womack KB, Weintraub S, Morris JC, Foong C, Xiao GH, Hladik C, Mantanona TY, White CL. TAR DNA-binding protein 43 immunohistochemistry reveals extensive neuritic pathology in FTLD-U: A Midwest-Southwest Consortium for FTLD-U study. *J Neuropathol Exp Neurol* 2008; 67: 271-279.
32. Hodges JR, Davies R, Xuereb J, Kril J, Halliday G. Survival in frontotemporal dementia. *Neurology* 2003; 61: 349-354.
33. Hodges JR, Mitchell J, Dawson K, Spillantini MG, Xuereb JH, McMonagle P, Nestor PJ, Patterson K. Semantic dementia: demography, familial factors and survival in a consecutive series of 100 cases. *Brain* 2010; 133: 300-306.
34. Josephs KA, Knopman DS, Whitwell JL, Boeve BF, Parisi JE, Petersen RC, Dickson DW. Survival in the two variants of tau negative FTLD: FTLD-U versus FTLD-MND. *Neurology* 2005; 65: 645-647.
35. Josephs KA, Whitwell JL, Jack CR, Parisi JE, Dickson DW. Frontotemporal lobar degeneration without lobar atrophy. *Arch Neurol* 2006; 63: 1632-1638.
36. Kay DWK, Forster DP, Newens AJ. Long-term survival, place of death, and death certification in clinically diagnosed pre-senile dementia in northern England: follow-up after 8-12 years. *Brit J Psychiatr* 2000; 177: 156-162.
37. Kersaitis C, Holliday GM, Xuereb JH, Pamphlett R, Bak TH, Hodges JR, Kril JJ. Ubiquitin-positive inclusions and progression of pathology in FTD and MND identifies a group with mainly early pathology. *Neuropathol Appl Neurobiol* 2006; 32: 83-91.
38. Kovari E, Gold G, Giannakopoulos P, Bouras C. Cortical ubiquitin positive inclusions in frontotemporal dementia without motor neuron disease: a quantitative immunocytochemical study. *Acta Neuropathol* 2004; 108: 207-212.
39. Luty AA, Kwok JBJ, Thompson EM, Blumsbergs P, Brooks WS, Loy CT, Dobson-Stone C, Panegyres PK, Hecker J, Nicholson GA, Halliday GM, Schofield PR. Pedigree with frontotemporal lobar degeneration-motor neuron disease and Tar DNA binding protein-43 positive neuropathology: genetic linkage to chromosome 9. *BMC Neurology* 2008; 8: 32.
40. Mackenzie IR, Baborie A, Pickering-Brown S, Du Plessis D, Jaros E, Perry RH, Neary D, Snowden JS, Mann DMA. Heterogeneity of ubiquitin pathology in frontotemporal lobar degeneration: classification and relation to clinical phenotype. *Acta Neuropathol* 2006; 112: 539-549.
41. Mackenzie IRA, Baker M, Pickering-Brown S, Hsinnig GYR, Lindholm C, Dwosh E, Cannon A, Rademakers R, Hutton M, Feldman HH. The neuropathology of frontotemporal lobar degeneration caused by mutations in the progranulin gene. *Brain* 2006; 129: 3081-3090.
42. Mann DMA, Esiri MM. The pattern of acquisition of plaques and tangles in the brains of patients under 50 years of age with Down's syndrome. *J Neurol Sci* 1989; 89: 169-179.
43. Mann DMA, Younis N, Jones D, Stoddart RW. The time course of the pathological events in Down's syndrome with particular reference to the involvement of microglial cells and deposits of β /A4. *Neurodegeneration* 1992; 1: 201-215.
44. Mirra SS, Heyman A, McKeel D, Sumi SM, Crain BJ, Brownlee LM, Vogel FS, Hughes JP, van Belle G, Berg L et al. The consortium to establish a registry for Alzheimer's disease (CERAD). II. Standardisation of the neuropathologic assessment of Alzheimer's disease. *Neurology* 1991; 41: 479-486.
45. Motte J, Williams RS. Age-related changes in the density and morphology of plaques and neurofibrillary tangles in Down syndrome brain. *Acta Neuropathol* 1989; 77: 535-546.
46. Mukherjee O, Pastor P, Cairns NJ, Chakraverty S, Kauwe JSK, Shears S, Behrens MI, Budde J, Hinrichs AL, Norton J, Levitch D, Taylor-Reinwald L, Gitcho M, Tu PH, Grinberg LT, Liscic RM, Armendariz J, Morris JC, Goate AM. HDDD2 is a familial frontotemporal lobar degeneration with ubiquitin-positive tau-negative inclusions caused by a missense mutation in the signal peptide of progranulin. *Ann Neurol* 2006; 60: 314-322.
47. Musicco M, Salamone G, Caltagirone C, Cravello L, Fadda L, Lupio F, Mosti S, Perri R, Palmer K. Neuropsychological predictors of rapidly progressing patients with Alzheimer's disease. *Dem Cogn Geriatr* 2010; 30: 219-228.
48. Nitrini R, Caramelli P, Herrera E, de Castro I, Bahia VS, Anghinah R, Caixeta LF, Radanovic M, Charchat-Fichman H, Porto CS, Carthery MT, Hartmann APJ, Huang N, Smid J, Lima EP, Takahashi DY, Takada LT. Mortality from dementia in a community dwelling Brazilian population. *Int J Geriatr Psych* 2005; 20: 247-253.
49. Pearson RCA, Esiri MM, Hiorns RW, Wilcock GK, Powell TPS. Anatomical correlates of the distribution of the pathological changes in the neocortex in Alzheimer's disease. *Proc Natl Acad Sci U S A* 1985; 82: 4531-4534.
50. Pirici D, Vandenberghe R, Rademakers R, Dermant B, Cruts M, Vennekens K, Cuijt I, Lubke U, Centerick C, Martin JJ, Van Broeckhoven C, Kumar-Singh S. Characterization of ubiquitinated intraneuronal inclusions in a novel Belgian frontotemporal lobar degeneration family. *J Neuropathol Exp Neurol* 2006; 65: 289-301.
51. Rademakers R, Hutton M. The genetics of frontotemporal lobar degeneration. *Curr Neurol Neurosci Rep* 2007; 7: 434-442.
52. Renton AE, Majounie E, Waite A, Simón-Sánchez J, Rollinson S, Gibbs JR, Schymick JC, Laaksovirta H, van Swieten JC, Myllykangas L, Kalimo H, Paetou A, Abramzon Y, Remes AM, Kaganovitch A, Scholz SW, Duckworth J, Ding J, Harmer DW, Hernandez DG, Johnson JO, Mok K, Rytan M, Trabzuni D, Guerreiro RJ, Orrell RW, Neal J, Murray A, Pearson J, Jansen IE, Sondervan D, Seelaar H, Blake D, Young K, Halliwell N, Callister JB, Toulson G, Ricahrdsen A, Gerhard A, Snowden J, Mann D, Neary D, Nalls MA, Peuralinna T, Jansson L, Isoviita VM, Kalvorinne AL, Hölttä-Vuori M, Ikonen E, Sulkava R, Benatar M, Wu J, chio A, Restagno G, Borghero G, Sabatelli M, The ITALSGEN Consortium, Heckerman D, Rogaeva E, Zinman L, Rothstein JD, Sendtner M, Drepper C, Eichler EE, Alkan C, Abdullaev Z, Pack SD, Dutra A, Pak E, Hardy J, Singleton A, Williams NM, Heutink P, Pickering-Brown S, Morris HR, Tienari PJ, Traynor BJ. A hexanucleotide repeat expansion in C9ORF72 is

- the cause of chromosome 9p21-linked ALS-FTD. *Neuron* 2011; 72: 257-268.
53. Sampathu DM, Neumann M, Kwong LK, Chou TT, Micsenyi M, Truax A, Bruce J, Grossman M, Trojanowski JQ, Lee VM. Pathological heterogeneity of frontotemporal lobar degeneration with ubiquitin-positive inclusions delineated by ubiquitin immunohistochemistry and novel monoclonal antibodies. *Am J Pathol* 2006; 189: 1343-1352.
 54. Schmidt C, Haik S, Satoh K, Rabano A, Martinez-Martin P, Roerber S, Brandel JP, de Pedro-Cuesta J, Laplanche JL, Kretzschmar H, Zerr I. Rapidly progressive Alzheimer's disease: a multicenter update. *J Alz Dis* 2010; 30: 751-756.
 55. Snowden J, Neary D, Mann D. Frontotemporal lobar degeneration: clinical and pathological relationships. *Acta Neuropathol* 2007; 114: 31-38.
 56. Staff RT, Murray AD, Ahearn T, Salarirad S, Mowat D, Starr JM, Deary IJ, Lemmon H, Whalley LJ. Brain volume and survival from age 78 to 85: the contribution of Alzheimer-type magnetic resonance imaging findings. *J Am Geriatr* 2010; 58: 688-695.
 57. Steiner JA, Angot E, Brunden P. A deadly spread: cellular mechanisms of α -synuclein transfer. *Cell Death Differ* 2011; 18: 1425-1433.
 58. Thalhauser CJ, Komarova NL. Alzheimer's disease: rapid and slow progression. *J Roy Soc* 2012; 9: 119-126.
 59. Tolnay M, Probst A. Frontotemporal lobar degeneration – tau as a pied piper? *Neurogenetics* 2002; 4: 63-75.
 60. Ueki A, Shinjo H, Shimode H, Nakajima T, Morita Y. Factors associated with mortality in patients with early-onset Alzheimer's disease: a five year longitudinal study. *Int J Geriatr Psych* 2001; 16: 810-815.
 61. Van Deerlin VM, Wood EM, Moore P, Yuan W, Forman MS, Clark CM, Neumann M, Kwong LK, Trojanowski JQ, Lee VM, Grossman M. Clinical, genetic and pathologic characteristics of patients with frontotemporal dementia and progranulin mutation. *Arch Neurol* 2007; 64: 1148-1153.
 62. Weiner MF, Risser RC. Effect of educational attainment on survival in Alzheimer's disease. *Alzheim Rep* 1998; 1: 369-374.
 63. Whitwell JL, Jack CR, Serijeni ML, Josephs KA. Patterns of atrophy in pathologically confirmed FTLN with or without motor neuron degeneration. *Neurology* 2006; 66: 102-104.
 64. Woulfe J, Kertesz A, Munoz DG. Frontotemporal dementia with ubiquitinated cytoplasmic and intranuclear inclusions. *Acta Neuropathol* 2001; 102: 94-102.
 65. Yaguchi M, Fujita Y, Amari M, Takatama M, Al-Sarraj S, Leigh PN, Okamoto K. Morphological differences of intraneural ubiquitin positive inclusions in the dentate gyrus and parahippocampal gyrus of motor neuron disease with dementia. *Neuropathology* 2004; 24: 296-301.
 66. Zekry D, Herrmann FR, C.E. Graf CE, Gianelli S, Michel JP, Gold G, Krause KH. High levels of co-morbidity and disability cancel out the dementia effect in predictions of long-term mortality after discharge in the very old. *Dem Cogn Geriatr* 2011; 32: 103-110.
 67. Zhou B, Zhao QH, Teramukai S, Ding D, Guo QH, Fukushima M. Executive function predicts survival in Alzheimer's disease. *J Alz Dis* 2010; 22: 673-682.

The topography of cortical microbleeds in frontotemporal lobar degeneration: a post-mortem 7.0-tesla magnetic resonance study

Jacques De Reuck¹, Florent Auger^{1,2}, Nicolas Durieux^{1,2}, Vincent Deramecourt^{1,3,4}, Claude-Alain Muraige^{1,3}, Florence Lebert^{1,4}, Didier Leys^{1,5}, Charlotte Cordonnier^{1,5}, Florence Pasquier^{1,4}, Regis Bordet^{1,6}

¹Université de Lille, INSERM U1171, ²Imaging Platform, Research Pole, ³Department of Pathology, ⁴Memory Clinic,

⁵Stroke Department, ⁶Pharmacological Department, Lille, France

Folia Neuropathol 2016; 54 (2): 149-155

DOI: 10.5114/fn.2016.60364

Abstract

Introduction: Cerebrovascular lesions are rare in frontotemporal lobar degeneration (FTLD), in contrast to other neurodegenerative diseases. Cortical microbleeds (CoMBs) are frequent in Alzheimer's disease, in particular in cases associated with cerebral amyloid angiopathy. The present study investigates the gyral topographic distribution of CoMBs in post-mortem FTLD brains with 7.0-tesla magnetic resonance imaging.

Material and methods: The distribution of CoMBs in 11 post-mortem FTLD brains and in 12 control brains was compared on T2*-GRE MRI of six coronal sections of a cerebral hemisphere. The mean values of CoMBs were determined in twenty-two different gyri. The findings were correlated to those separately observed on neuropathological examination.

Results: As a whole there was a trend of more CoMBs in the prefrontal section of FTLD as well as of the control brains. CoMBs were significantly increased in the superior frontal gyrus and the insular cortex ($p \leq 0.001$) and also in the inferior frontal gyrus and the superior temporal gyrus ($p \leq 0.01$).

Conclusions: CoMBs in FTLD are only increased in the regions mainly affected by the neurodegenerative lesions. They probably do not reflect additional cerebrovascular disease.

Key words: 7.0-tesla magnetic resonance imaging, topography of post-mortem cortical microbleeds, frontotemporal lobar degeneration, neurodegenerative diseases.

Introduction

Frontotemporal lobar degeneration (FTLD) is a heterogeneous disorder with various clinical and histological subtypes [22]. FTLD is the second most common cause of presenile dementia with differ-

ent genetic subtypes [20]. Despite the fact that most cases have a presenile onset, FTLD is not rare amongst elderly patients [3]. A recent neuropathological study showed that age together with vascular and Alzheimer-related co-pathology contributes

Communicating author:

J.L. De Reuck, Leopold II laan 96, BE-9000, Ghent, Belgium, phone: +32 9 2218844, fax: +32 9 3324971, e-mail: dereuck.j@gmail.com

to the morphological appearance of FTLD-tau [23]. In our recent neuropathological assessment of small cerebrovascular lesions, only a prevalence of white matter changes was observed in the FTLD brains, compared to age-matched controls [10]. These findings are in contrast to the high incidence of macro- and micro-infarcts, and hematomas and small cerebral bleeds observed in brains of patients with Alzheimer's disease (AD), in particular in those with associated cerebral amyloid angiopathy (CAA) [6,7].

Cerebral microbleeds (CMBs) are frequently detected on T2*-weighted gradient-echo magnetic resonance imaging (MRI) of patients with small-vessel diseases [26]. They are also found in asymptomatic patients as well as in those with various degrees of cognitive impairment [5]. The number of CMBs detected during life depends on the MRI characteristics, such as pulse sequence, sequence parameters, spatial resolution, magnetic field strength and image post-processing [17]. 7.0-tesla T2*-weighted gradient-echo MRI is able to detect reliably even the smallest bleeds in the cerebral cortex (CoMBs) on post-mortem brain sections [8]. This technique allows to determine the topographic distribution and to quantify the number of CoMBs on a large number of brain sections [25]. In our previous study we have demonstrated a significant prevalence of CoMBs in the deep cortical layers of the frontal cortex in FTLD [9]. However this frontal predominance of CoMBs is also observed in AD brains with and without CAA and in controls [14].

The aim of the present post-mortem MRI study is to compare the prevalence of CoMBs in twenty-two different cortical gyri of pure FTLD versus controls in order to determine their eventual clinical impact.

Material and methods

Twenty-three patients, followed-up at the Lille University Hospital underwent an autopsy. The cohorts consisted of 11 patients with FTLD and 12 controls who had no clinical history of dementia or stroke. The vascular risk factors were registered from the clinical files. The median age at disease onset of the FTLD patients was 54 (interquartile range of 46-64) years. The clinical phenotype of the FTLD patients was the behavioral variant in 9 and semantic dementia in 2. Two patients had in addition amyotrophic lateral sclerosis. None of them had on neuropathological examination Alzheimer features

or some degree of amyloid angiopathy. The post-mortem diagnosis of FTLD was made according to the neuropathological diagnostic and the nosological criteria of the Consortium for FTLD [4]. The main histological subtypes were FTLD-Tau in 3, FTLD-TDP-A in 1, FTLD-TDP-B in 3, FTLD-TDP-C in 3 brains and FTLD-FUS in 1 brain.

Previously obtained informed consent of the patients or from the nearest family allowed an autopsy for diagnostic and scientific purposes. The brain tissue samples were acquired from the Lille Neuro-Bank of the Lille University, federated to the Centre de Ressources Biologiques that acted as an institutional review board.

One fresh cerebral hemisphere was deeply frozen for biochemical examination. The remaining hemisphere, the brainstem and most of the cerebellum were fixed in formalin for 3 weeks.

The patients with FTLD were compared concerning the incidence of CoMBs to the control group.

Neuropathological examination

The diagnosis of FTLD was made according to a standard procedure examining samples from the primary motor cortex, the associated frontal, temporal and parietal cortex, the primary and secondary visual cortex, the cingulate gyrus, the basal nucleus of Meynert, the amygdaloid body, the hippocampus, basal ganglia, mesencephalon, pons, medulla and cerebellum. Slides from paraffin-embedded sections were immune-stained for protein tau, β -amyloid, α -synuclein, prion protein and TDP-43. FUS histochemistry was performed in Tau and TDP negative cases.

A quantitative evaluation of the cerebrovascular lesions was performed on a standard coronal section of a cerebral hemisphere, at the level of the mammillary body according to a previously described method [6].

MRI examination

Six coronal sections of a cerebral hemisphere from each brain were submitted to MRI: one at the prefrontal level in front of the frontal horn, one of the frontal lobe at the level of the head of the caudate nucleus, a central one near the mammillary body, a post-central one, a parietal one at the level of the splenium corporis callosi and one at the level of the occipital lobe.

Table I. Brain regions and gyri of interest on magnetic resonance imaging

Frontal lobe	Temporal lobe	Parietal lobe	Occipital lobe
Frontalis inferior	Temporalis inferior	Postcentralis	Lingualis
Frontalis medius	Temporalis medius	Insula	Precuneus
Frontalis superior	Temporalis superior	Parietalis inferior	Cuneus
Precentralis	Hippocampus	Parietalis medius	Occipitotemporalls
Rectus	Dentatus	Parietalis superior	
Orbitalis	Parahippocampalis	Cinguli	

We used a 7.0-tesla MRI Bruker BioSpin SA with an issuer-receiver cylinder coil of 72 mm inner diameter (Ettlingen, Germany), according to a previously described method [8]. The brain sections, previously cleaned from formalin, were placed in a plastic box filled with salt-free water, the size of which did not allow significant tissue movements. Three MRI sequences were used: a positioning sequence, a T2 sequence and a T2* sequence. The positioning sequence allowed determination of the three-direc-

tional position of the brain section inside the magnet. The thickness of the T2 images was 1 mm. The field of view was a 9 cm-square slide that was coded by a 256 matrix giving a voxel size of 0.352 × 0.352 × 1 mm. T2 weighted images were obtained by using RARE sequence (Rapid Acquisition with Relaxation Enhancement) with repetition time (TR), echo time (TE) and RARE factor of 2,500 ms, 33 ms and 8, respectively. The acquisition time of this sequence was 80 s. The thickness of the T2* images was 0.20 mm.

Table II. Comparison of the patients' characteristics, vascular risk factors and ranking values of the different neuropathological lesions in the control brains and those with frontotemporal lobar degeneration (FTLD)

Items	Control (n = 12)	FTLD (n = 11)	p value
Median age in years (IQR) at decease	67 (58-78)	67 (62-68)	0.52
Gender (% of males)	42	27	0.67
Vascular risk factors (%)			
Arterial hypertension	17	18	1.0
Diabetes	17	18	1.0
Hypercholesterolemia	17	18	1.0
Smoking	0	0	1.0
Antithrombotic drug use	25	18	1.0
Neuropathological lesions: ranking scores (standard deviations)			
White matter changes	0.3 (0.8)	1.5 (1.1)	0.01
Lacunar infarcts	0.0 (0.0)	0.2 (0.7)	0.70
Territorial infarcts	0.0 (0.0)	0.0 (0.0)	1.0
Haematomas	0.1 (0.3)	0.0 (0.0)	0.70
Cortical microinfarcts	0.1 (0.3)	0.1 (0.3)	0.60
Cortical microbleeds	0.1 (0.3)	0.9 (0.8)	0.04

IQR – interquartile range

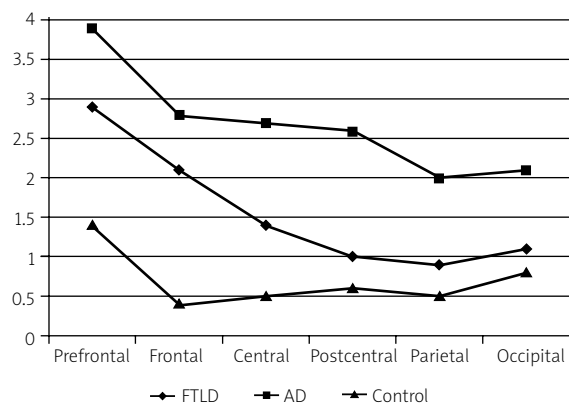


Fig. 1. Mean values of cortical microbleeds in the six coronal sections on T2*-weighted gradient-echo (GRE) magnetic resonance imaging of brains with frontotemporal lobar degeneration compared to those with Alzheimer's disease and to controls. Although their numbers are different between the three groups, they all display a similar anterior-posterior decreasing gradient of cortical microbleeds.

The field of view was also a 9 cm². It was coded by a 512 matrix, giving a voxel size of 0.176 × 0.176 × 0.2 mm. The slice thickness corresponded to the upper part of the brain section. This sequence was a GRE sequence with a short TR of 60 ms and TE of

22 ms, a flip angle of 30° and number of excitation of 20. The acquisition time of the sequence was 10 minutes.

The total number and the location of CoMBs was determined in 22 gyri of each brain (Table I) by consensus evaluation by three observers (JDR, FA, ND) blinded to the neuropathological diagnosis and based on comparison of brain sections of an anatomical atlas [19]. The inter-rater reliability resulted in an interclass correlation coefficient of 0.79. The mean values of CoMBs in FTLD brains were compared to the controls.

Statistical analyses

Univariate comparisons of unpaired groups were performed with the Fisher's exact test for categorical data. The non-parametric Mann-Whitney *U*-test was used to compare continuous variables. The significance level, two-tailed, was set at ≤ 0.01 for significant and ≤ 0.001 for highly significant. Values set at ≤ 0.05 and more than > 0.01 were considered as marginal significant and not included as relevant due to the relative small sample sizes.

Results

The FTLD and control groups did not show any statistical differences according to age, gender distribution and vascular risk factors. However, on the

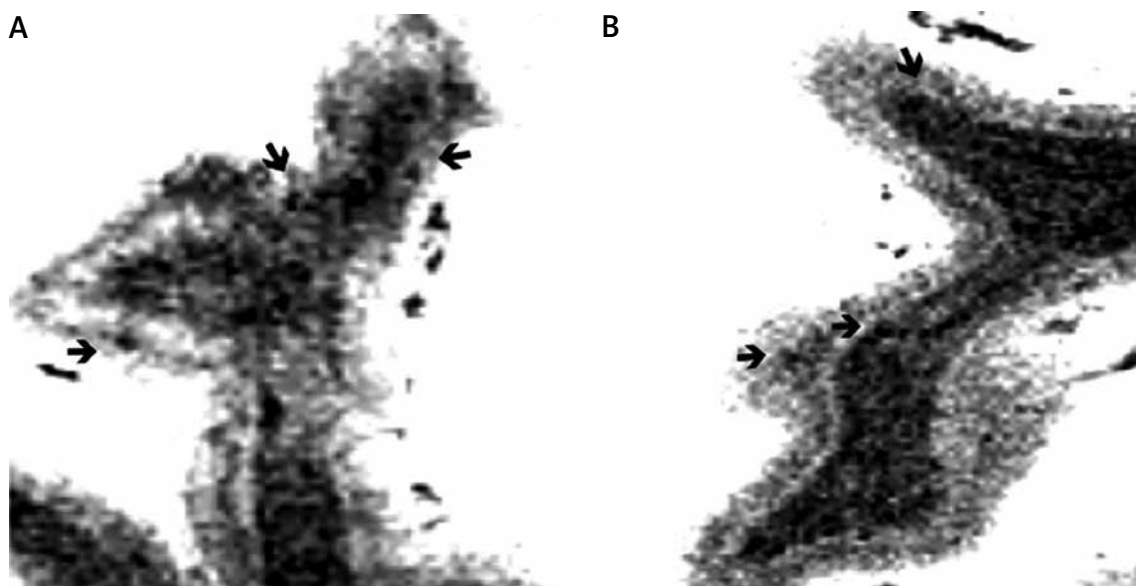


Fig. 2. Cortical microbleeds (arrows) on T2*-weighted gradient-echo (GRE) magnetic resonance imaging in the gyrus frontalis superior (A) and in the gyrus frontalis inferior (B).

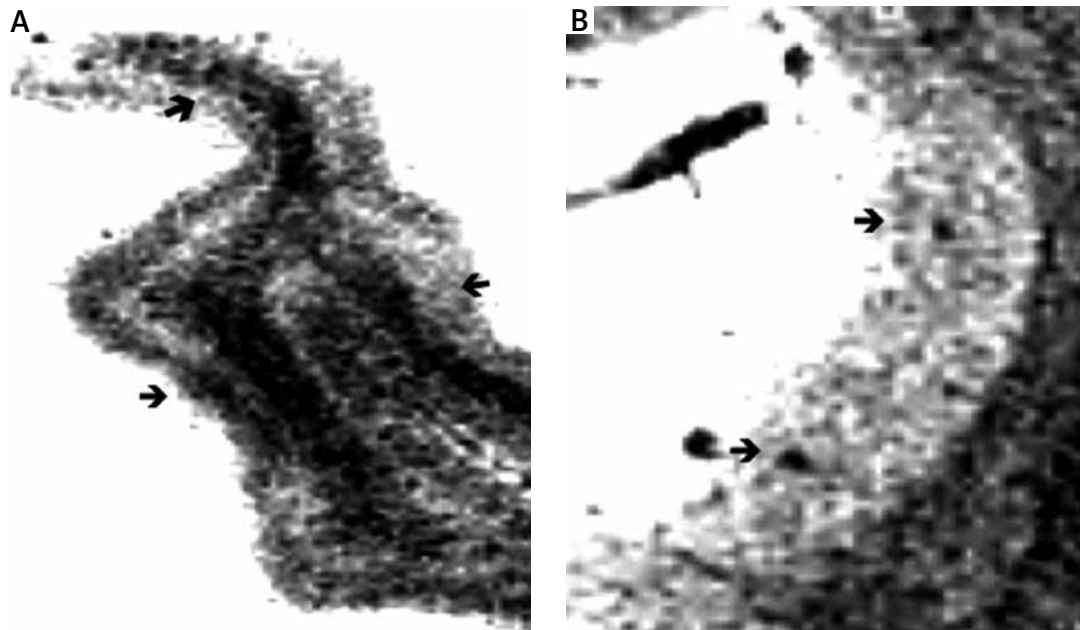


Fig. 3. Cortical microbleeds (arrows) on T2*-weighted gradient-echo (GRE) magnetic resonance imaging of the gyrus temporalis superior (A) and in the insular cortex (B).

neuropathological examination, white matter changes were significantly increased in the FTLD group compared to the control group ($p = 0.01$), while only marginally increased for the CoMBs. The other cerebrovascular lesions were rare and not statistically different between both groups (Table II).

When comparing on MRI the mean values of CoMBs in the six coronal sections on T2* GRE MRI an anterior-posterior decreasing gradient was observed in the FTLD as well as in the AD and the control brains (Fig. 1).

The mean values of CMBs in FTLD brains were significantly higher in the frontal superior gyrus and in the insular cortex ($p \leq 0.001$) (Fig. 2) and significantly in the frontal inferior and the temporal superior gyri ($p \leq 0.01$) (Fig. 3), compared to the control brains (Table III).

Discussion

The present study confirms that associated cerebrovascular lesions are rare in FTLD due to tau, TAR DNA-binding protein 43 and FUS [24]. Although in brains of elderly patients suffering from neurodegenerative diseases multiple pathologies are usually present [2], our series consist of pure types of FTLD allowing to determine more exactly the topography

of CoMBs related to this disease spectrum. Despite a similar global bleeding load in FTLD and in age-matched control brains [11], a similar anterior-posterior decreasing gradient of CoMBs is observed on the sequential hemispheric sections. This is also common to AD brains with or without CAA [14]. This similarity is probably related to the larger development of the frontal lobe compared to the parietal and occipital lobes [21].

However, the main findings in this study are that the CoMBs predominate in the superior and inferior frontal gyri, the superior temporal gyrus and the insular cortex, regions that are most affected by the neurodegenerative process [1].

The findings in FTLD share similarity with those observed in our post-mortem 7.0-tesla MRI study in progressive supranuclear palsy, in which small bleeds are mainly found around the dentate nucleus of the cerebellum and in the tegmentum pontis, where also the major neurodegenerative changes occur [12].

There is no evidence for increased angiogenesis and microglial activation in the neuropathologically most affected regions of different neurodegenerative diseases such as in Alzheimer, Parkinson, progressive supranuclear palsy, and incidental Lewy body disease. Such neo-angiogenic vessels could contribute

Table III. Comparison of the mean values (standard deviations) of cortical microbleeds between different gyri of frontotemporal lobar degeneration (FTLD) and controls

Gyrus	C (n = 12)	FTLD (n = 11)	p value
Frontalis inferior	0.8 (0.9)	2.4 (1.6)	< 0.01
Frontalis medius	1.2 (1.4)	2.7 (1.7)	0.04
Frontalis superior	1.2 (1.4)	3.8 (1.6)	< 0.001
Precentralis	1.1 (1.5)	1.9 (1.2)	0.10
Rectus	0.4 (0.7)	1.0 (0.8)	0.04
Orbitalis	0.8 (1.1)	1.3 (1.1)	0.24
Temporalis inferior	0.4 (1.0)	1.2 (1.2)	0.03
Temporalis medius	0.5 (0.8)	1.3 (0.9)	0.02
Temporalis superior	0.6 (1.1)	1.7 (0.8)	< 0.01
Hippocampus	0.4 (0.8)	0.4 (0.6)	0.45
Dentatus	0.5 (1.1)	0.9 (1.3)	0.09
Parahippocampalis	0.7 (1.2)	1.5 (1.1)	0.04
Postcentralis	0.7 (0.9)	1.4 (1.0)	0.03
Insula	0.0 (0.0)	1.3 (1.3)	< 0.001
Parietalis inferior	0.3 (0.4)	0.9 (0.9)	0.13
Parietalis medius	1.2 (1.4)	0.9 (0.9)	0.93
Parietalis superior	0.6 (0.5)	1.2 (1.1)	0.24
Cinguli	0.4 (0.6)	0.7 (0.5)	0.15
Lingualis	0.3 (0.9)	0.7 (1.2)	0.08
Precuneus	0.5 (0.8)	0.6 (0.9)	0.74
Cuneus	0.5 (0.9)	0.8 (1.5)	0.56
Occipitotemporalis	0.6 (1.0)	1.5 (1.1)	0.03

to neuroinflammation and lead to disruption of the blood-brain barrier [15,16]. The prevalence of CoMBs and the white matter changes in FTLD brains should not be considered as the hallmark of cerebrovascular diseases. Also the increased iron accumulation observed in the basal ganglia of brains with FTLD should not be related to small-vessel ischemic disease [13] as recently proposed [18].

The fact that the CoMBs prevail in the regions with the most prominent neurodegenerative lesions indicates that blood-brain barrier impairments may interact with the severity of the neurodegeneration

in FTLD and are secondary phenomena without impact on the clinical features of the disease.

Disclosure

Authors report no conflict of interest.

References

1. Agusta F, Canu E, Sarro L, Comi G, Filippi M. Neuroimaging findings in frontotemporal lobar degeneration spectrum of disorders. *Cortex* 2012; 48: 389-413.
2. Attems J, Jellinger K. Neuropathological correlates of cerebral multimorbidity. *Curr Alzheimer Res* 2013; 10: 569-577.
3. Baborie A, Griffiths TD, Jaros E, et al. Frontotemporal dementia in elderly individuals. *Arch Neurol* 2012; 69: 1052-1060.
4. Cairns NJ, Bigio EH, Mackenzie IR, et al. Consortium for Frontotemporal Lobar Degeneration. Neuropathologic diagnostic and nosologic criteria for frontotemporal lobar degeneration: consensus of the Consortium for Frontotemporal Lobar Degeneration. *Acta Neuropathol* 2007; 114: 5-22.
5. Cordonnier C, Al-Shahi Salman R, Wardlaw J. Spontaneous brain microbleeds, systematic review, subgroup analyses and standards for study design and reporting. *Brain* 2007; 130: 1988-2003.
6. De Reuck J, Deramecourt V, Cordonnier C, Leys D, Pasquier F, Maurage CA. Prevalence of small cerebral bleeds in patients with a neurodegenerative dementia: a neuropathological study. *J Neurol Sci* 2011; 300: 63-66.
7. De Reuck J, Deramecourt V, Cordonnier C, Leys D, Maurage CA, Pasquier F. The impact of cerebral amyloid angiopathy on the occurrence of cerebrovascular lesions in demented patients with Alzheimer features: a neuropathological study. *Eur J Neurol* 2011; 18: 313-318.
8. De Reuck J, Auger F, Cordonnier C, Deramecourt V, Durieux N, Pasquier F, Bordet R, Maurage CA, Leys D. Comparison of 7.0-T T2*-magnetic resonance imaging of cerebral bleeds in post-mortem brain sections of Alzheimer patients with their neuropathological correlates. *Cerebrovasc Dis* 2011; 31: 511-517.
9. De Reuck J, Deramecourt V, Cordonnier C, Auger F, Durieux N, Bordet R, Maurage CA, Leys D, Pasquier F. Detection of microbleeds in post-mortem brains of patients with frontotemporal lobar degeneration: a 7.0-Tesla magnetic resonance study with neuropathological correlates. *Eur J Neurol* 2012; 19: 1355-1360.
10. De Reuck J, Deramecourt V, Cordonnier C, Leys D, Pasquier F, Maurage CA. Cerebrovascular lesions in patients with frontotemporal lobar degeneration: a neuropathological study. *Neurodegenerative Dis* 2012; 9: 170-175.
11. De Reuck J. The significance of small cerebral bleeds in neurodegenerative dementia syndromes. *Aging Dis* 2012; 3: 307-312.
12. De Reuck J, Caparros-Lefebvre D, Deramecourt V, et al. Prevalence of small cerebral bleeds in patients with progressive supranuclear palsy: a neuropathological study with 7.0-Tesla magnetic resonance imaging correlates. *Folia Neuropathol* 2014; 52: 421-427.
13. De Reuck J, Deramecourt V, Auger F, Durieux N, Cordonnier C, Devos D, Defebvre L, Moreau C, Caparros-Lefebvre D, Leys D,

- Maurage CA, Pasquier F, Bordet R. Iron deposits in post-mortem brains of patients with neurodegenerative and cerebrovascular diseases: a semi-quantitative 7.0 T magnetic resonance imaging study. *Eur J Neurol* 2014; 21: 1026-1031.
14. De Reuck J, Auger F, Durieux N, Deramecourt V, Cordonnier C, Pasquier F, Maurage CA, Leys D, Bordet R. Topography of cortical microbleeds in Alzheimer's disease with and without cerebral amyloid angiopathy: A post-mortem 7.0-Tesla magnetic resonance imaging study. *Aging Dis* 2015; 6: 437-443.
 15. Desai BS, Schneider JA, Li JL, Carvey PM, Hendey B. Evidence of angiogenetic vessels in Alzheimer's disease. *J Neural Transm* 2009; 116: 587-579.
 16. Desai B, Patel A, Schneider JA, Carvey PM, Hendey B. Evidence of angiogenesis in Parkinson's disease, incidental Lewy body disease, and progressive supranuclear palsy. *J Neural Transm* 2012; 119: 59-71.
 17. Greenberg SM, Vernooij MW, Cordonnier C, Viswanathan A, Al-Shahi Salman R, Warach S, Launer LJ, Van Buchem MA, Breteler MM; Microbleed Study Group. Cerebral microbleeds: a guide to detection and interpretation. *Lancet Neurol* 2009; 8: 165-174.
 18. Janaway BM, Simpson JE, Hoggard N, Highley JR, Forster G, Drew D, Gebril OH, Matthews FE, Brayne C, Wharton SB, Ince PG; MRC Cognitive Function and Ageing Neuropathology Study. MRC Cognitive Function and Ageing Neuropathology Study. Brain haemosiderin in older people: pathological evidence for an ischaemic origin of magnetic resonance imaging (MRI) microbleeds. *Neuropathol Appl Neurobiol* 2014; 40: 258-269.
 19. Roberts M, Hanaway J. Atlas of the human brain in section. Lea & Febiger, Philadelphia 1970.
 20. Seelaar H, Kamphorst W, Rosso SM, et al. Distinct genetic forms of frontotemporal dementia. *Neurology* 2008; 71: 1220-1226.
 21. Semendeferi K, Damasio H, Frank R. The evolution of the frontal lobes: a volumetric analysis based on three-dimensional reconstructions of magnetic resonance scans of human and ape brains. *J Hum Evol* 1997; 32: 375-388.
 22. Sieben A, Van Langenhove T, Engelborghs S, Azmani A, Masdjedi R, de Koning I, Maat-Kievit JA, Anar B, Donker Kaat L, Breedveld GJ, Dooijes D, Rozemuller JM, Bronner IF, Rizzu P, van Swieten JC. The genetic and neuropathology of frontotemporal lobar degeneration. *Acta Neuropathol* 2012; 124: 353-372.
 23. Thal DR, von Armin CA, Griffin WS, Mrak RE, Walker L, Attems J, Arzberger T. Frontotemporal lobar degeneration FTLD-tau: pre-clinical lesions, vascular and Alzheimer-related co-pathologies. *J Neural Transm* 2015; 122: 1007-1018.
 24. Toledo JB, Arnold SE, Raible K, Brettschneider J, Xie SX, Grossman M, Monsell SE, Kukull WA, Trojanowski JQ. Contribution of cerebrovascular disease in autopsy confirmed neurodegenerative disease cases in the National Alzheimer's Coordinating Centre. *Brain* 2013; 136: 2697-2706.
 25. Wardlaw JM. Post-mortem MR brain imaging comparison with macro- and histopathology: useful, important and underused. *Cerebrovasc Dis* 2011; 31: 518-519.
 26. Werring DJ, Frazer DW, Coward LJ, Losseff NA, Watt H, Cipolotti L, Brown MM, Jäger HR. Cognitive dysfunction in patients with cerebral microbleeds on T2*-weighted gradient-echo MRI. *Brain* 2004; 127: 2265-2275.

Potent effects of alkaloid-rich extract from *Huperzia selago* against sodium nitroprusside-evoked PC12 cells damage via attenuation of oxidative stress and apoptosis

Anna Magdalena Lenkiewicz¹, Grzegorz Arkadiusz Czapski¹, Henryk Jęsko¹, Anna Wilkaniec¹, Wojciech Szypuła², Agnieszka Pietrosiuk², Aneta Marta Uszyńska¹, Agata Adamczyk¹

¹Mossakowski Medical Research Centre, Polish Academy of Sciences, Warsaw, ²Medical University of Warsaw, Poland

Folia Neuropathol 2016; 54 (2): 156-166

DOI: 10.5114/fn.2016.60361

Abstract

Imbalance between production and scavenging of free radicals and other reactive oxygen species (ROS) is a component of many diseases, but it is especially important in aging-related diseases of the central nervous system. Oxidative stress-induced neuronal dysfunction plays an important role in the pathomechanism of neurodegenerative disorders, including Alzheimer's and Parkinson's disease. Experimental data showed that free radical scavengers may protect the brain against oxidative modifications. The need for efficient and safe antioxidants with therapeutic potential stimulated the rise of interest in the medicinal plant products, which are a rich source of phytochemicals possessing biological activity. In our studies we focused on alkaloid fractions (AFs) isolated from club moss, *Huperzia selago* and *Diphasiastrum complanatum*, due to their beneficial activity and exclusive chemical structure. Our previous study demonstrated that selected alkaloids from *Huperzia selago* effectively protect macromolecules from oxidative damage. Therefore, in the present study we investigated the effects and mechanisms of action of AFs isolated from *Huperzia selago* and *Diphasiastrum complanatum* against sodium nitroprusside (SNP)-induced oxidative injury in PC12 cells. The results demonstrated that the selected AFs via reduction of nitric oxide (NO) liberation protected cells against oxidative stress, DNA and mitochondrial damage, as well as apoptosis caused by SNP. Selected AF notably decreased SNP-evoked mitochondrial polymerase γ (Polg) up-regulation. Furthermore, AF which contains Lycopodine, Serratidine, Lycoposerramine-G and (probably) Cermizine B completely inhibited the SNP-induced expression of interferon- γ (Ifng) and cyclooxygenase 2 (Ptgs2) as well as significantly down-regulated the expression of 12/15-lipoxygenase (Alox12) and tended to decrease the mRNA level of interleukin-6 gene (Il6). In conclusion, these results suggest that the AFs from *Huperzia selago* effectively protect PC12 cells against SNP-induced oxidative damage by adjusting the level of reactive nitrogen species, suppression of apoptosis and down-regulation of pro-inflammatory genes. The compounds present in these AFs could be potential candidates to develop successful drugs preventing oxidative damage and apoptosis in age-related neurodegenerative disorders.

Key words: oxidative stress, apoptosis, cell death, cytoprotection, *Huperzia selago*, *Diphasiastrum complanatum*.

Communicating author:

Agata Adamczyk, Mossakowski Medical Research Centre, Polish Academy of Sciences, 5 Pawińskiego St., 02-106 Warsaw, Poland, e-mail: agataadamczyk72@gmail.com

Introduction

Oxidative stress is an important component of pathophysiology of countless human diseases, but it is especially important in the pathomechanism of neurodegenerative disorders, such as Alzheimer's (AD) and Parkinson's (PD) disease, multiple sclerosis (MS), amyotrophic lateral sclerosis (ALS) and other age-related diseases [15]. Neuronal cells need large amounts of ATP for maintaining a high rate of metabolic activity, and they pay a high price for their extraordinary energy demand – they are highly vulnerable to oxidative stress [19]. Neurons are, comparing with other cell types, mostly dependent on oxidative phosphorylation as an energy source, therefore they are exposed to high oxygen concentration. Moreover, neuronal cells are rich in polyunsaturated fatty acids (PUFA) that are prone to oxidation [2]. In addition, brain contains relatively poor mechanisms of antioxidant defense, for example low levels of catalase and glutathione peroxidase [32]. Neurons are enriched in metal ions, which accumulate in the brain during aging and may catalyze reactive oxygen species (ROS) formation [31]. Therefore, it is suggested that oxidative stress that increases during brain aging is an important factor making the aged brain especially susceptible to neurodegenerative processes [8]. Excessive generation of ROS is responsible for macromolecules modification, including lipid peroxidation, as well as protein and DNA oxidation which in consequence could lead to activation of apoptotic signaling and cell death [29]. Furthermore, oxidative stress is a deleterious process that can affect cellular Ca^{2+} homeostasis, composition of cellular membranes and mitochondria function. Moreover, oxidative stress is a factor stimulating protein misfolding in neurodegenerative diseases, it can trigger and/or accelerate aggregation of amyloid β peptides ($A\beta$) and α -synuclein (ASN) [38] that are critical in the pathogenesis of AD and PD, respectively. Accumulating data suggest that antioxidant supplementation may be effective in the prevention and treatment of neurodegenerative diseases [28,30] and several natural compounds with antioxidant properties are being investigated for treatment of AD and PD. Some natural products including quercetin [4], curcumin [10], caffeic acid [12] and resveratrol [14] have been shown to be neuroprotective against oxidative injury. In addition, the antioxidant activities of various alkaloids, like berberine and huperzine A, have been investigated [33,40] and it has been shown

that early, regular usage of phytochemicals and their derivatives can delay the onset and progression of AD [16]. *Huperzia selago* (L.) Bernh. ex Schrank et Mart., a source of huperzine A (HupA) and other alkaloids commonly known as fir club moss (family *Huperziaceae*), is a plant of great interest that is used in combating a wide variety of diseases in European and Asian countries [5,22,36]. Plants of the *Diphasiastrum complanatum* (L.) Holub (*Lycopodiaceae* sensu stricto) do not contain HupA but they are rich in alkaloids, mostly lycopodine and its derivatives [7]. Our previous *in vitro* studies have shown that some alkaloids of *H. selago* exhibit potent antioxidative properties, scavenge free radicals and prevent lipid and protein oxidation [7]. However, the cytoprotective activity of these extracts against ROS-induced cell damage has never been studied. Therefore, in this study, we analyzed whether alkaloid fractions (AFs) isolated from *H. selago* and *D. complanatum* may protect cells against ROS-evoked death and what mechanism may be responsible for protective effects of AFs. Sodium nitroprusside (SNP) was used to induce oxidative stress in rat pheochromocytoma PC12 cells. This cell line exhibits unique sensitivity to oxidants and is widely used as a cellular model to study the mechanisms of oxidative stress and apoptosis, as well as a model for studying antioxidative and cytoprotective properties of various antioxidants [24,39,41]. For example, studies on PC12 cells have shown that amyloidogenic proteins, $A\beta$ and ASN induce cytotoxicity and also elicit excessive free radical production [1,11,18], mitochondrial dysfunction [11], apoptosis and cell death [20]. Here, we demonstrate that AFs prevent or at least markedly attenuate SNP-induced oxidative stress and protect PC12 cells from ROS-induced injury.

Material and methods

Chemicals

LDH-cytotoxicity Assay Kit II was purchased from BioVision (Mountain View, CA, USA), APO-DIRECT kit from BD Biosciences (San Jose, CA, USA), Dulbecco's Modified Eagle's Medium (DMEM), Fetal Bovine Serum (FBS), Horse Serum (HS), penicillin, streptomycin, glutamine, deoxyribonuclease I, 3-(4,5-dimethyl-2-tiazolilo)-2,5-diphenyl-2H-tetrazolium bromide (MTT), Hoechst 33342, DTT, polyethylenimine (PEI), Pluronic, dimethyl sulfoxide (DMSO), TRI-reagent, DNase I and all other common reagents were from

Sigma-Aldrich (St. Louis, MO, USA). High Capacity cDNA Reverse Transcription Kit and TaqMan Gene Expression Master Mix were from Applied Biosystems (Foster City, CA, USA). DAF-2 DA was purchased from Cayman Chemical Company (Michigan, USA). Fluo-4 AM and Rhod-2 AM was purchased from Thermo Fischer Scientific Inc. HPLC grade water was purchased from Merck KGaA, Darmstadt, Germany. Huperzine A was purchased from ChromaDex, Inc. (Laguna Hills, CA). The reference compounds, lycopodium and annotinine, were obtained from the Department of Pharmacognosy and Molecular Basis of Phytotherapy, Medical University of Warsaw.

Preparation of alkaloid fractions (AFs)

Plant material

Aerial parts of *H. selago* were collected in The Babia Gora Biosphere Reserve (Poland) in September 2010. Aerial parts of *D. complanatum* were collected in The Masurian Lake District (Poland). Material was identified and authenticated by one of the authors. Voucher specimens have been deposited in the herbarium of the Department of Pharmaceutical Biology and Medicinal Plant Biotechnology, Medical University of Warsaw.

Preparation and extracts purification

Alkaloid fractions were obtained by a conventional procedure from MeOH extract and examined using TLC and HPLC-DAD as previously reported by Czapski *et al.* [7].

Preparation of standard and sample solution of alkaloids

Standard solutions of HupA, lycopodium and annotinine as well as isolated AFs were dissolved in DMSO at a concentration 25 mg/ml which roughly corresponds to molar concentration of approximately 100 μ M for this group of alkaloids. Then dilutions were prepared in the same DMSO concentration, and AFs were used in final concentrations of 0.25 μ g/ml (approximately 1 μ M), 2.5 μ g/ml (approximately 10 μ M) and 6.25 μ g/ml (approximately 25 μ M).

Cell culture

Rat pheochromocytoma PC12 cells were a kind gift from Professor A. Eckert (University of Basel, Basel, Switzerland). The cells were cultured in DMEM

supplemented with 10% heat-inactivated fetal bovine serum, 5% heat-inactivated horse serum, 2 mM L-glutamine, 50 U/ml penicillin, 50 mg/ml streptomycin in 5% CO₂ atmosphere at 37°C.

Cell treatment protocols

Equal PC12 cell numbers were seeded into culture dishes, and after 24 h growth medium was changed to low-serum medium (DMEM supplemented with 2% heat-inactivated fetal bovine serum, 2 mM L-glutamine, 50 U/ml penicillin, 50 mg/ml streptomycin). Then, tested compounds were added to PC12 cells for 8-48 h. Freshly prepared sodium nitroprusside (SNP) at a concentration of 0.5 mM was used as an inducer of oxidative stress and apoptosis. The appropriate controls with DMSO, as a vehicle, were also prepared.

Determination of cell viability

For analysis of the effect of treatment on the mitochondrial function and cell survival MTT assay was performed. After 24-48 h incubation in the presence of tested compounds, the medium was changed to serum-free DMEM, MTT (0.25 mg/ml) was added and cells were incubated for 2 h. Then, medium was removed, cells were dissolved in DMSO and absorbance at 595 nm was measured on Bio-Rad model 680 microplate reader.

Determination of necrotic cell death

For analysis of necrotic cell death LDH assay was performed by using commercial LDH-cytotoxicity Assay Kit II (BioVision, CA, USA). Shortly, after 24 h incubation in the presence of tested compounds, the whole medium was collected, mixed and centrifuged at 600 × g for 10 min. Samples of supernatant were mixed with reaction buffer containing WST substrate and absorbance at 450 nm (reference 655 nm) was measured every 5 min for 30 min on Bio-Rad model 680 microplate reader. Data from the linear increase phase were used for calculations.

Determination of nitric oxide level by DAF-2 staining

Measurement of the nitric oxide level was carried out using fluorescent indicator DAF-2 DA (Cayman Chemical Company). PC12 cells were loaded with 10 μ M DAF-2 in the presence of pluronic (0.02%),

washed, and incubated in pluronic-supplemented HBSS without (control) or with SNP (0.5 mM). DAF-2 fluorescence was measured after 8 h.

Analysis of gene expression by quantitative real time polymerase chain reaction (qRT-PCR)

Cultured cells were washed two times with ice-cold phosphate-buffered saline (PBS), scraped down and collected by centrifugation (3 min, 1000 × g). RNA was isolated with TRI-reagent and DNA remainings were digested with DNase I according to the manufacturer's protocols (Sigma-Aldrich). Quantity and purity of RNA was measured spectroscopically at 260 and 280 nm wave lengths. Reverse transcription was performed using High Capacity cDNA Reverse Transcription Kit according to the manufacturer's protocol (Applied Biosystems, Foster City, CA, USA). The level of mRNA for *Polg* was analyzed using SYBR Green JumpStart Taq ReadyMix, using the primer pair: forward 5'-CGGCTGACCTAATCCCTTG-3', reverse 5'-CACTAACTGTTCTGCCAATCCT-3'. The levels of mRNA for *Ifng*, *Il6*, *Ptgs2*, *Alox12* and *Actb*, as a reference gene, were analyzed using TaqMan Gene Expression Assays (Rn00594078_m1, Rn01410330_m1, Rn01483828_m1, Rn01461082 and 4352340E, respectively) and TaqMan Gene Expression Master Mix (Applied Biosystems). Plates were analyzed on ABI PRISM 7500 apparatus (Applied Biosystems, Foster City, CA, USA). The relative levels of mRNA were calculated using the $\Delta\Delta C_t$ method. Specificity of PCR reaction was verified by analyzing melting profiles – each profile contained only a single peak representing the specific product.

Determination of DNA damage by TUNEL staining

The presence of DNA damage in cells was determined by TdT-mediated dUTP-FITC nick end labeling (TUNEL) followed by flow cytometric detection. Shortly, after incubation in the presence of tested compounds for 12 h, cells were fixed and stained by using APO-DIRECT Kit according to the manufacturer's protocol (BD Biosciences, San Jose, CA, USA). This method allows staining of damaged DNA by FITC, and total DNA with propidium iodide (PI). Samples were analysed on flow cytometer FACS Canto II.

Determination of apoptosis by Hoechst 33342 staining

The apoptotic body formation was determined by microscopic analysis of the cells stained with Hoechst 33342. Shortly, after 12 h incubation in the presence of tested compounds, the cells were fixed, stained and examined under a fluorescence microscope (Olympus BX51, Japan). Images were taken with a digital camera (Olympus DP70, Japan). A minimum of 200 cells/experimental group were counted in each experiment. Cells with typical apoptotic nuclear morphology (nuclear shrinkage, condensation) were identified as apoptotic and counted using randomly selected 30 fields for each experimental group. The results were expressed as % of apoptotic cells according to the equation: % of apoptotic cells = (apoptotic cells)/(all cells) × 100.

Statistical analysis

Data are expressed as mean values ± S.E.M. Normality of distribution of individual variables was checked with Anderson-Darling normality test. Two group comparisons were done using Student's *t*-test. Multiple comparisons were analyzed by one-way analysis of variance ANOVA with Tukey post-hoc test. Expression data for IFN- γ and IL-6 are not normally distributed. Therefore, Kruskal-Wallis non-parametric test with Dunn's multiple comparisons post-hoc test was used to assess the statistical significance of obtained results. The statistical analyses were performed by using Graph Pad Prism version 5.0 (Graph Pad Software, San Diego, CA). Statistical significance was accepted at $p < 0.05$.

Results

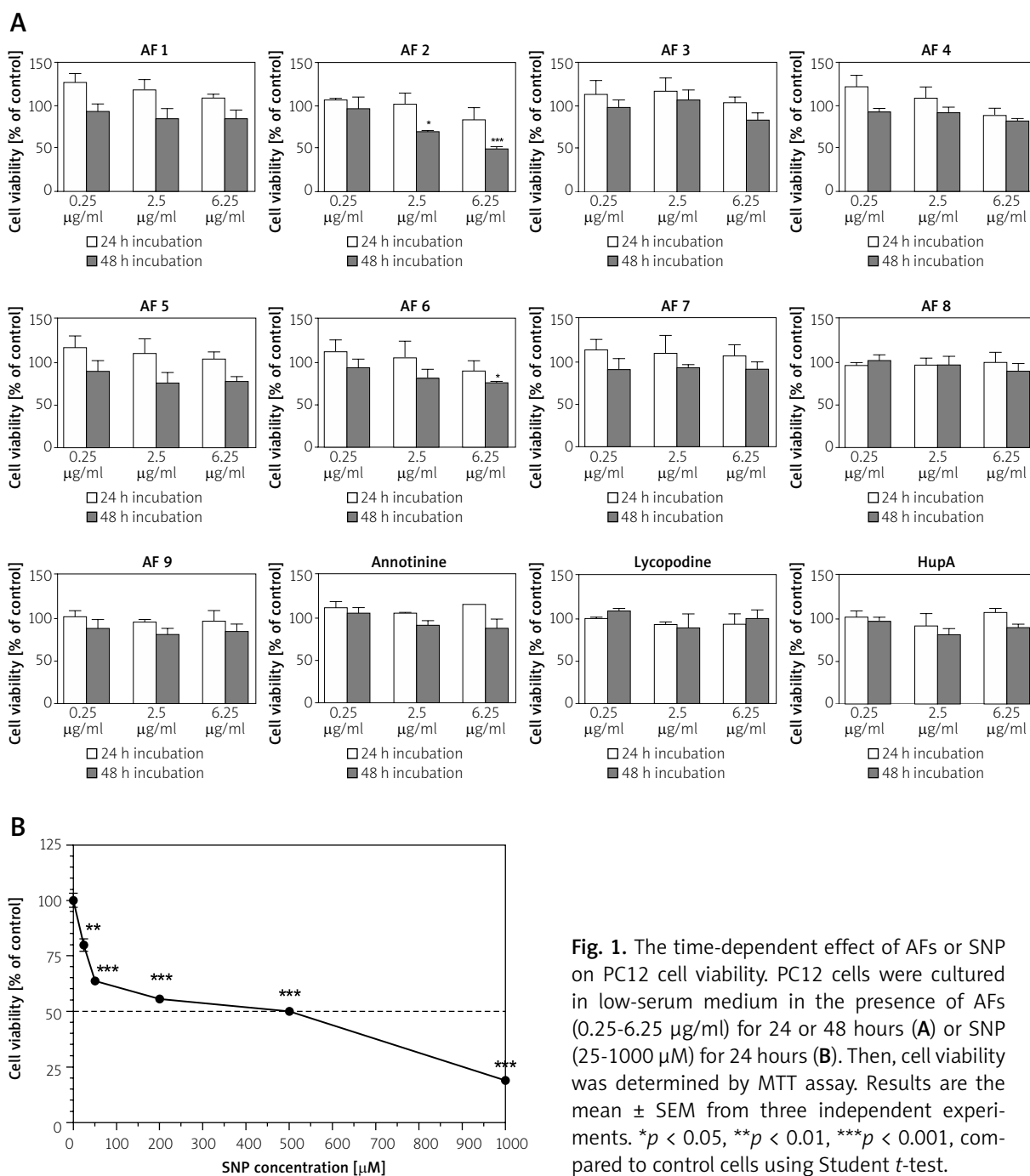
Our previous studies have shown that selected AFs isolated from *H. selago* and *D. complanatum* scavenge free radicals and effectively protect macromolecules from oxidative damage [7]. In the current study we investigate the possible cytoprotective properties of these compounds during oxidative stress *in vitro*. SNP, a donor of NO and other ROS, was used to generate oxidative stress and evoke cell death in PC12 cell line.

The initial aim was to define the optimal experimental conditions. First, we checked whether analyzed AFs possess any cytotoxic properties in our experimental system. The PC12 cells were incubated

in the presence of AFs at concentration range 0.25-6.25 $\mu\text{g/ml}$ (approximately 1-25 μM) for 24 h and 48 h. It was found that after 24 h of incubation the AFs did not affect the viability of PC12 cells. Exclusively two fractions, AF2 and AF6 at a concentration $\geq 2.5 \mu\text{g/ml}$, exerted a cytotoxic effect when the time of incubation was increased to 48 h (Fig. 1A). To determine the optimal concentration of SNP to induce oxidative

stress and cell death during 24 h treatment, cells were incubated in the presence of SNP in a concentration range of 25-1000 μM . The results showed that SNP reduced PC12 cell viability. Exposure to 500 μM SNP for 24 h decreased the viability of PC12 cells to 50% compared with the control group (Fig. 1B).

Therefore, further studies were carried out in the presence of AFs at 2.5 $\mu\text{g/ml}$ (approximately



10 μ M) concentration in oxidative stress evoked by incubation with 500 μ M SNP up to 24 h. The MTT assay revealed that several AFs demonstrated the tendency to protect cells against SNP-evoked damage, whereas, a statistically significant effect was observed exclusively in the presence of two extract fractions, AF4 and AF5 (Fig. 2A). However, none of the compounds tested had any effect on SNP-

induced release of lactate dehydrogenase (LDH) (Fig. 2B). Based on this observation in further experiments we focused on AF4 and AF5.

To analyze the mechanism of cytoprotection evoked by AF4 and AF5 during SNP-induced stress, cells were incubated with SNP in the presence of AF4 and AF5 for 8 h. The exposure of PC12 cells to SNP produced a marked increase in the NO level, as ana-

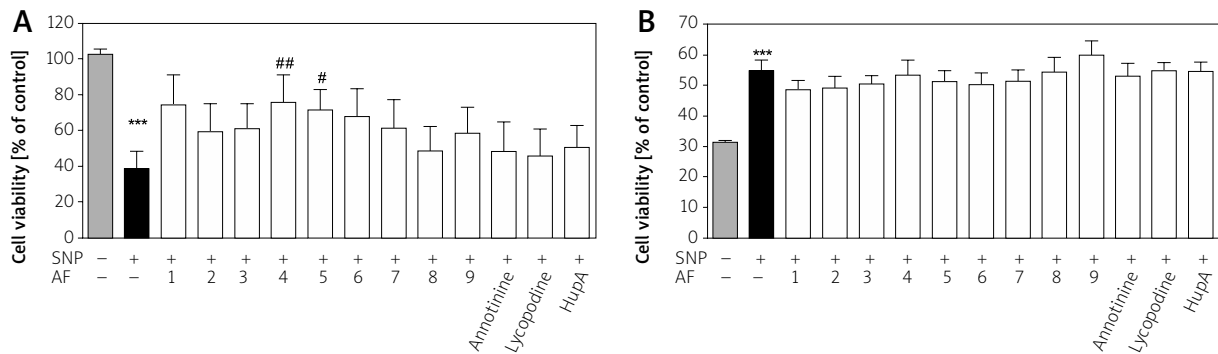


Fig. 2. The effect of AFs on SNP-evoked PC12 cell death. PC12 cells were cultured in low-serum medium in the presence of AFs (2.5 μ g/ml) and SNP (0.5 mM) for 24 h. The effect of tested compounds on cell viability or necrotic cell death were analyzed using MTT assay (A) and LDH leakage assay (B), respectively. Data represent the mean value \pm SEM for 4 independent experiments. *** p < 0.001, compared to control cells; # p < 0.05, ## p < 0.01, compared to SNP-treated cells using one-way ANOVA followed by the Tukey post-hoc test.

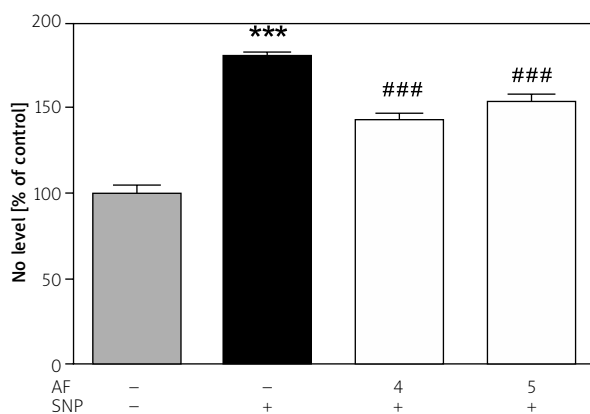


Fig. 3. The effect of AFs on SNP-evoked nitric oxide (NO) production. PC12 cells were loaded with 10 μ M DAF-2 in the presence of pluronic, washed, and incubated in pluronic-supplemented HBSS with AFs (2.5 μ g/ml) and SNP (0.5 mM). DAF-2 fluorescence was measured after 8 h. Data represent the mean value \pm S.E.M. for 3 independent experiments. *** p < 0.001, compared to the control cells; ### p < 0.001, compared to the SNP-treated cells using a one-way ANOVA followed by the Tukey post-hoc test.

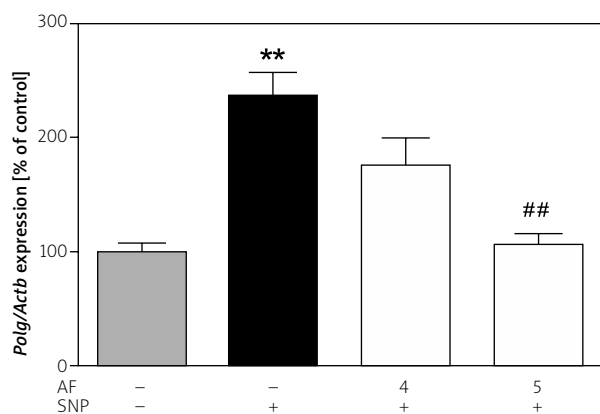


Fig. 4. The effect of AFs on SNP-evoked changes in *Polg* gene expression. PC12 cells were cultured in low-serum medium in the presence of AFs (2.5 μ g/ml) and SNP (0.5 mM) for 24 h. The *Polg* gene expression was determined as described in the Methods section by qRT-PCR. Data represent the mean value \pm S.E.M. for 3 independent experiments. ** p < 0.01, compared to the control cells; ## p < 0.01, compared to the SNP-treated cells using a one-way ANOVA followed by the Tukey post-hoc test.

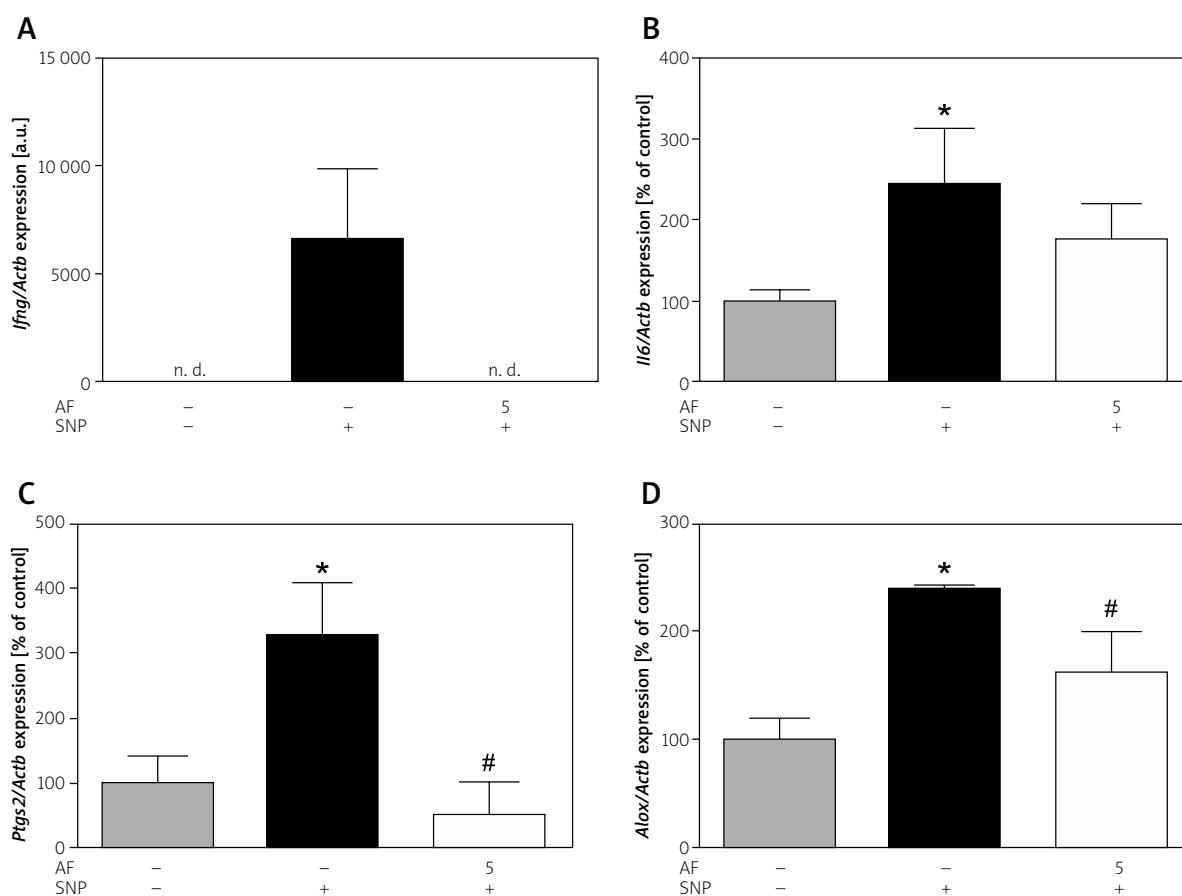


Fig. 5. The effect of AF on SNP-evoked changes in expression of genes encoding pro-inflammatory and pro-oxidative proteins. PC12 cells were cultured in low-serum medium in the presence of AF (2.5 μ g/ml) and SNP (0.5 mM) for 24 h. The expression of genes encoding pro-inflammatory cytokines: IFN- γ (A) and IL-6 (B) and pro-oxidative proteins: COX-2 (C) and 12/15-LOX (D) was determined as described in the Material and methods section by qRT-PCR. Data represent the mean value \pm S.E.M. for 3 independent experiments. * $p < 0.05$, compared to the control cells; # $p < 0.05$, compared to the SNP-treated cells using nonparametric Kruskal-Wallis followed by Dunn's multiple comparisons post-hoc test or one-way ANOVA followed by Tukey post-hoc test for genes encoding cytokines and pro-oxidative proteins, respectively.

lysed by fluorogenic probe DAF-2. The co-treatment with AF4 or AF5 led to a significant decrease in the NO level, by about 20% and 15%, respectively, when compared with the SNP-treated cells (Fig. 3). These data suggest that the possible mechanism of AF4 and/or AF5 action may be related to their NO-scavenging properties. Excessive amounts of NO and its metabolites are capable of altering gene expression as well as can impact the mitochondria function that is relevant to cell death. Here, we show that incubation of PC12 cells with SNP for 24 h evoked significant up-regulation of the expression of the gene for DNA polymerase γ (*Polg*) that is responsible for replication of mitochondrial DNA and its repair processes

(Fig. 4). In the presence of AF5, SNP did not increase the expression of *Polg*. Moreover, as shown in Figure 5, the expression of inflammation-related genes for IFN- γ (*Ifng*), IL-6 (*Il6*), COX-2 (*Ptgs2*) and 12/15-LOX (*Alox12*) was increased in SNP-treated cells after 24 h incubation, comparing with the control group. AF5 completely protected cells against SNP-evoked induction of *Ifng* expression (Fig. 5A), significantly down-regulated the expression of *Ptgs2* and *Alox12* (Fig. 5C and D) and tends to decrease the mRNA level of *Il6* (Fig. 5B). AF4 had no effect on the SNP-evoked induction of inflammation-related genes (data not shown).

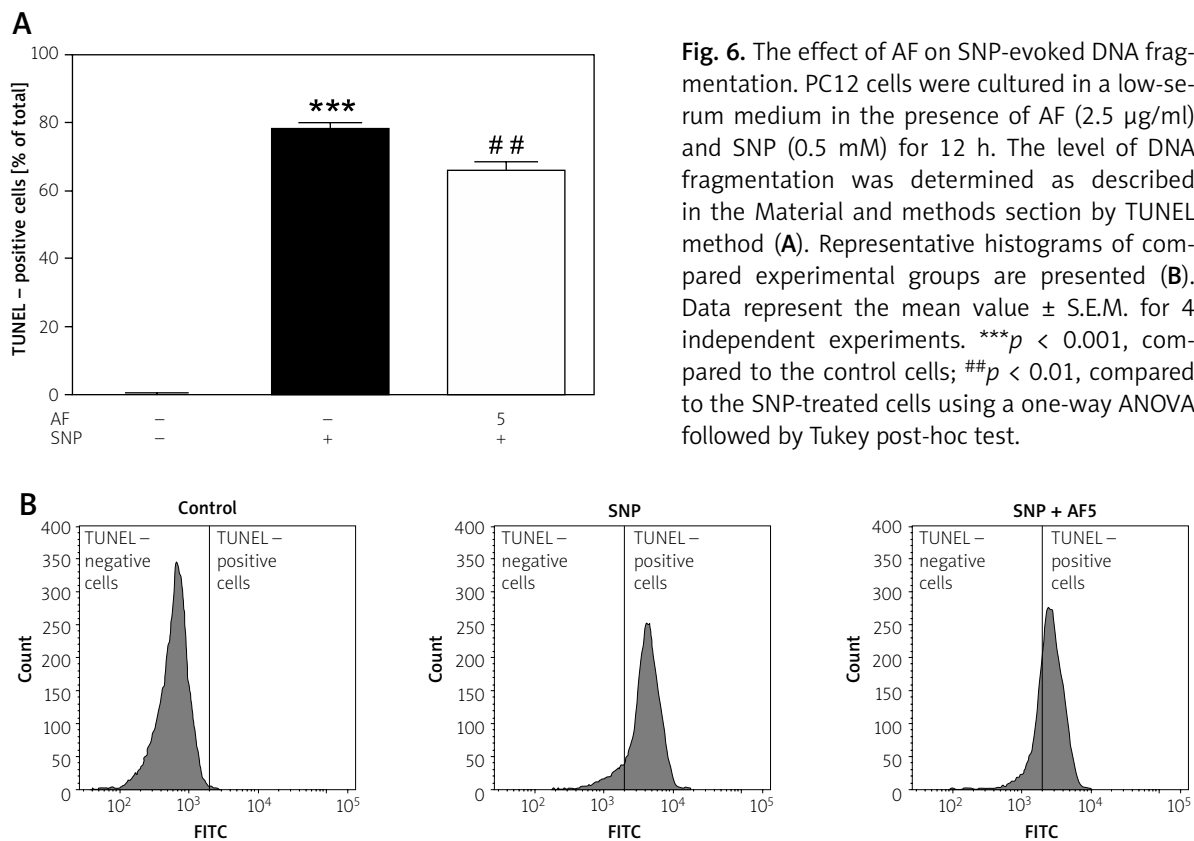


Fig. 6. The effect of AF on SNP-evoked DNA fragmentation. PC12 cells were cultured in a low-serum medium in the presence of AF (2.5 $\mu\text{g}/\text{ml}$) and SNP (0.5 mM) for 12 h. The level of DNA fragmentation was determined as described in the Material and methods section by TUNEL method (**A**). Representative histograms of compared experimental groups are presented (**B**). Data represent the mean value \pm S.E.M. for 4 independent experiments. *** $p < 0.001$, compared to the control cells; ## $p < 0.01$, compared to the SNP-treated cells using a one-way ANOVA followed by Tukey post-hoc test.

Furthermore, we analyzed the effect of AF5 on SNP-evoked loss of DNA integrity by using TUNEL method (TdT-mediated dUTP-FITC nick end labelling). SNP evoked an increase in the number of TUNEL-positive cells, indicating that the level of DNA fragmentation was elevated and AF5 reduced the percentage of cells classified as TUNEL-positive (Fig. 6A and B). The percentage of DNA fragmentation in PC12 cells exhibits a direct correlation with the percentage of apoptotic nuclei measured with Hoechst 33342 staining. SNP evoked typical hallmarks of apoptosis including chromatin aggregation and nuclear fragmentation, whereas AF5 effectively reduced SNP-evoked apoptotic processes (Fig. 7A and B).

Discussion

Oxidative stress is recognized as an important component of the pathomechanism of several neurodegenerative disorders [15]. Therefore, in the last few years many studies focused on the search for new effective antioxidants with neuroprotective properties. Many plant extracts or even single compounds exert their protective effect via removal of

free radicals or by the prevention of ROS generation. However, it appears that very often natural antioxidants, even if they show a beneficial protective effect in cell culture, have no or just limited effect in clinical trials [13]. Therefore, there is still an urgent need for new natural effective pharmaceuticals with antioxidant and cytoprotective properties. Our previous results indicated that alkaloid extracts from *H. selago* possess potent antioxidative properties, scavenge free radicals and prevent lipid and protein oxidation [13]. In the present work, the cytoprotective effects of alkaloid extracts from *H. selago* and *D. complanatum* on PC12 cells were tested. We found that the selected AFs, which were shown to have antioxidative properties, also exert a cytoprotective effect against SNP-induced oxidative stress.

Exposure to SNP *in vitro* partially mimics the oxidative stress observed in the brains of patients with neurodegenerative disorders [25, 27]. Excessive NO production plays a critical role in the pathomechanism of neurodegenerative and other neurological disorders. It has been shown that in degenerative conditions characterized by oxidative stress,

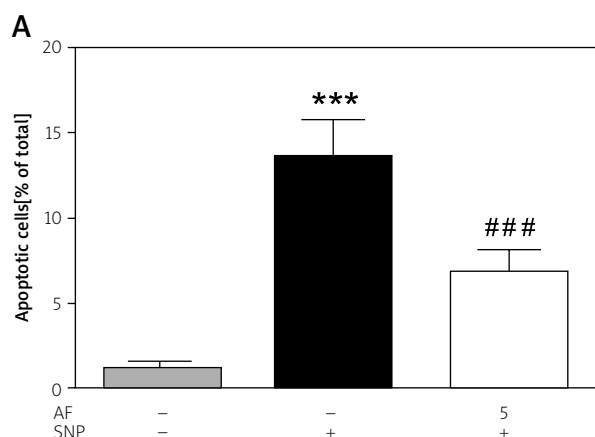
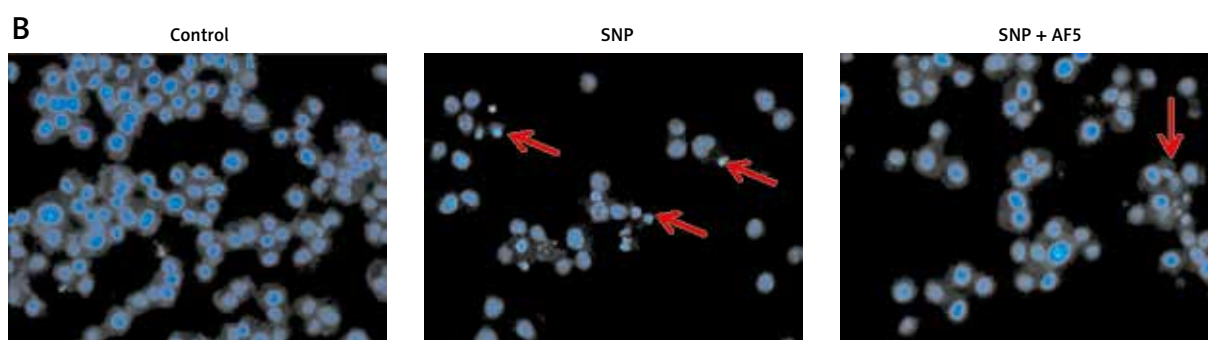


Fig. 7. The effect of AF on SNP-evoked apoptosis. PC12 cells were cultured in a low-serum medium in the presence of AF (2.5 µg/ml) and SNP (0.5 mM) for 12 h. The level of apoptosis was determined as described in the Material and methods section by Hoechst staining (A). Representative images are presented (B). Red arrows indicate nuclei with typical apoptotic features. Data represent the mean value ± S.E.M. for 4 independent experiments. *** $p < 0.001$, compared to the control cells; ### $p < 0.001$, compared to the SNP-treated cells using a one-way ANOVA followed by Tukey post-hoc test.



increased levels of NO lead to aberrant S-nitrosylation of proteins that contributes to the pathology of the disease [25]. Excessive liberation of NO and enhanced S-nitrosylation affects the mitochondrial function, proteostasis, transcriptional regulation, synaptic activity, and cell survival [26]. In the present work, the level of intracellular NO in PC12 cells was remarkably increased by SNP. However, co-treatment with AF4 or AF5 led to a reduction in the NO level. In the previous work we identified components of fractions AF4 and AF5. AF4 contains 6-β-hydroxyhuperzine, Huperzine A, Huperzine B, Lycoposerramine-L or Lycoposerramine-M, Lycopodine, Lycoposerramine-G, probable 8b-Hydroxylycoposerramine K and Lyconadin [13]. The identified components of AF5 were Lycopodine, Serratidine, Lycoposerramine-G and probably Cermizine B [7]. Therefore, these alkaloids might be responsible for antioxidative and cytoprotective properties of analyzed fractions. An elevated NO level induces mitochondrial failure including alterations in calcium homeostasis, mitochondrial energy, ROS generation and promotes mitochondrial DNA damage [3].

Because polymerase γ is the only DNA polymerase present in mitochondria, it is necessarily implicated in all DNA repair processes, therefore activation of this enzyme is considered as an indicator of mitochondrial DNA damage. In the present study we suggest that SNP evokes mitochondrial DNA damage leading to polymerase γ activation for DNA repair. Activation of this enzyme was not observed in the presence of AF5 fraction, indicating that components of AF5 effectively protected PC12 cells against SNP-induced mitochondrial injury. Till now, cytoprotective potential of these specific compounds has not been tested.

Oxidative stress affects many cellular signaling pathways, including alterations of gene expression, for example activation of transcription of inflammation-related IFN-γ, IL-6, IL-1β, and TNF-α [23]. Our work showed that AF5 attenuated transcription of inflammation-related genes activated by oxidative stress. AF5 completely prevented the SNP-evoked induction of *Ifnγ* and tends to down-regulate the expression of *Il6* in PC12 cells. Down-regulation of pro-oxidative/pro-inflammatory genes could be

an important mechanism of cytoprotection, because the inflammatory processes are involved in the pathomechanism of a wide range of neurodegenerative diseases, including AD and PD [9]. Especially intriguing is the effect of AF5 on expression of genes *Ptgs2* and *Alox12*, which contribute to synthesis of arachidonic acid (AA)-derived lipid mediators. Arachidonic acid is a free fatty acid that is released from the cell membrane in response to various stimuli [21]. There are two most important families of enzymes involved in the oxidative metabolism of AA, lipoxygenases (LOXs), which produce leukotrienes and the cyclooxygenases (COXs) COX-1 and COX-2, which produce prostaglandins. Recent work has highlighted the potential role of 12/15-LOX as well as COX-2 in the pathogenesis of neurodegenerative disorders [6]. Modulation of the expression and activity of LOX and COX might offer an effective disease-modifying strategy for therapy of neurodegenerative disorders. In the current study, we found that cell treatment with AF5 prevented SNP-induced upregulation of *Alox12* as well as *Ptgs2* expression. These data are in agreement with those obtained by Wang *et al.*, who showed that Huperzine A, an alkaloid compound found primarily in other firmoss, *H. serrata*, suppressed overexpression of inflammatory genes and improved learning and memory in rats [37]. Moreover, a lot of other alkaloids demonstrated significant anti-inflammatory properties [35]. The fragmentation of DNA is one of the most characteristic phenomena of apoptosis [34]. TUNEL assay, which was initially developed to detect apoptosis-related DNA degradation, labels DNA strand breaks, including the 3'OH termini of single strand breaks and all forms of double strand breaks. Therefore, it may indicate also other types of DNA degradation, for example evoked by oxidative damage. Here, using TUNEL method we showed that SNP induced DNA fragmentation and AF5 reduced the percentage of cells with damaged DNA. To specifically detect apoptotic fragmentation of DNA we used Hoechst 33342 staining, which allows identifying late apoptotic cells by morphological characterization of typical changes in nuclear chromatin aggregation and fragmentation. Our data indicated that SNP significantly increased the number of apoptotic cells, and AF5 efficiently reduced the number of cells with apoptotic morphology.

In conclusion, our data demonstrated that only selected alkaloid fractions of *H. selago* contain some

compounds having potent cytoprotective properties. They might be particularly promising compounds for discovering and developing novel clinical drugs in the treatment of neurodegenerative disorders.

Acknowledgments

Financial support was provided by National Science Centre Grant no. 2012/05/B/NZ3/ 02047 and by the project "Advanced methods, pharmaceuticals and therapies for health protection and economy in the 21st century: interdisciplinary studies in biomedical sciences at university second and third level", no. POKL.04.03.00-00-060/12. The project was co-financed by the European Union from the European Social Fund under the Operational Programme Human Capital, and by a grant from the Polish Ministry of Science and Higher Education, grant no. NN 405 362237.

Disclosure

Authors report no conflict of interest.

References

- Adamczyk A, Kazmierczak A, Czapski GA, Strosznajder JB. α -Synuclein induced cell death in mouse hippocampal (HT22) cells is mediated by nitric oxide-dependent activation of caspase-3. *FEBS Lett* 2010; 584: 3504-3508.
- Bazinet RP, Layé S. Polyunsaturated fatty acids and their metabolites in brain function and disease. *Nat Rev Neuro* 2014; 15: 771-785.
- Bolaños JP, Almeida A, Stewart V, Peuchen S, Land JM, Clark JB, Heales SJR. Nitric Oxide-Mediated Mitochondrial Damage in the Brain: Mechanisms and Implications for Neurodegenerative Diseases. *J Neurochem* 1997; 68: 2227-2240.
- Bournival J, Quessy P, Martinoli MG. Protective Effects of Resveratrol and Quercetin Against MPP⁺-Induced Oxidative Stress Act by Modulating Markers of Apoptotic Death in Dopaminergic Neurons. *Cell Mol Neurobiol* 2009; 29: 1169-1180.
- Czapski GA, Avram D, Sakharov DV, Wirtz KW, Strosznajder JB, Pap EHW. Activated neutrophils oxidize extracellular proteins of endothelial cells in culture: effect of nitric oxide donors. *Biochem J* 2002; 365: 897-902.
- Czapski GA, Gassowska M, Wilkaniec A, Chalimoniuk M, Strosznajder JB, Adamczyk A. The mechanisms regulating cyclin-dependent kinase 5 in hippocampus during systemic inflammatory response: The effect on inflammatory gene expression. *Neurochem Int* 2016; 93: 103-112.
- Czapski G, Szypula W, Kudlik M, Wilenska B, Kania M, Danikiewicz W, Adamczyk A. Assessment of antioxidative activity of alkaloids from *Huperzia selago* and *Diphysastrum complanatum* using in vitro systems. *Folia Neuropathol* 2014; 52: 1-13.

8. Dixon SJ, Stockwell BR. The role of iron and reactive oxygen species in cell death. *Nat Chem Biol* 2014; 10: 9-17.
9. Ferencik M, Novak M, Rovensky J, Rybar I. Alzheimer's disease inflammation and non-steroidal anti-inflammatory drugs. *Bratisl Lek Listy* 2001; 102: 123-132.
10. Fu XY, Yang MF, Cao MZ, Li DW, Yang XY, Sun JY, Zhang ZY, Mao LL, Zhang S, Wang FZ, Zhang F, Fan CD, Sun BL. Strategy to Suppress Oxidative Damage-Induced Neurotoxicity in PC12 Cells by Curcumin: the Role of ROS-Mediated DNA Damage and the MAPK and AKT Pathways. *Mol Neurobiol* 2014; 53: 369-378.
11. Gao X, Tang XC. Huperzine A attenuates mitochondrial dysfunction in beta-amyloid-treated PC12 cells by reducing oxygen free radicals accumulation and improving mitochondrial energy metabolism. *J Neurosci Res* 2006; 83: 1048-1057.
12. Gülçin I. Antioxidant activity of caffeic acid (3,4-dihydroxycinnamic acid). *Toxicology* 2006; 217: 213-220.
13. Halliwell B. Free radicals and antioxidants – quo vadis? *Trends Pharmacol Sci* 2011; 32: 125-130.
14. Jang JH, Surh YJ. Protective effect of resveratrol on β -amyloid-induced oxidative PC12 cell death. *Free Radic Biol Med* 2003; 34: 1100-1110.
15. Kim GH, Kim JE, Rhie SJ, Yoon S. The Role of Oxidative Stress in Neurodegenerative Diseases. *Exp Neurobiol* 2015; 24: 325-340.
16. Kim J, Lee HJ, Lee KW. Naturally occurring phytochemicals for the prevention of Alzheimer's disease. *J Neurochem* 2010; 112: 1415-1430.
18. Koh SH, Kwon H, Park KH, Ko JK, Kim JH, Hwang MS, Yum YN, Kim OH, Kim J, Kim HT, Do BR, Kim KS, Kim H, Roh H, Yu HJ, Jung HK, Kim SH. Protective effect of diallyl disulfide on oxidative stress-injured neuronally differentiated PC12 cells. *Brain Res Mol Brain Res* 2005; 133: 176-186.
19. Li J, O W, Li W, Jiang ZG, Ghanbari HA. Oxidative Stress and Neurodegenerative Disorders. *Int J Mol Sci* 2013; 14: 24438-24475.
20. Lin YH, Liu AH, Wu HL, Westenbroek C, Song QL, Yu HM, Ter Horst GJ, Li XJ. Salvianolic acid B, an antioxidant from *Salvia miltiorrhiza*, prevents Abeta(25–35)-induced reduction in BPRP in PC12 cells. *Biochem Biophys Res Commun* 2006; 348: 593-599.
21. Liscovitch M. Crosstalk among multiple signal-activated phospholipases. *Trends Biochem Sci* 1992; 17: 393-399.
22. Ma X, Gang DR. The Lycopodium alkaloids. *Nat Prod Rep* 2004; 21: 752-772.
23. Mukhopadhyay P, Rajesh M, Horváth B, Bátkai S, Park O, Tanchian G, Gao RY, Patel V, Wink DA, Liaudet L, Haskóe G, Mechoulam R, Pachera P. Cannabidiol protects against hepatic ischemia/reperfusion injury by attenuating inflammatory signaling and response, oxidative/nitrative stress, and cell death. *Free Radic Biol Med* 2011; 50: 1368-1381.
24. Muthaiyah B, Essa MM, Chauhan V, Chauhan A. Protective effects of walnut extract against amyloid beta peptide induced cell death and oxidative stress in PC12 cells. *Neurochem Res* 2011; 36: 2096-2103.
25. Nakamura T, Prikhodko OA, Pirie E, Nagar S, Akhtar MW, Oh CK, McKercher SR, Ambasudhan R, Okamoto S, Lipton SA. Aberrant protein S-nitrosylation contributes to the pathophysiology of neurodegenerative diseases. *Neurobiol Dis* 2015; 84: 99-108.
26. Nakamura T, Lipton SA. Protein S-Nitrosylation as a Therapeutic Target for Neurodegenerative Diseases. *Trends Pharmacol Sci* 2016; 37: 73-84.
27. Pytlowany M, Strosznajder JB, Jęsko H, Cąkała M, Strosznajder RP. Molecular mechanism of PC12 cell death evoked by sodium nitroprusside, a nitric oxide donor. *Acta Biochim Pol* 2008; 55: 339-347.
28. Rajendran P, Nandakumar N, Rengarajan T, Palaniswami R, Gnanadhas EN, Lakshminarasaiah U, Gopas J, Nishigaki I. Antioxidants and human diseases. *Clin Chim Acta* 2014; 436: 332-347.
29. Ramalingam M, Kim SJ. Reactive oxygen/nitrogen species and their functional correlations in neurodegenerative diseases. *J Neural Transm* 2012; 119: 891-910.
30. Ramassamy C. Emerging role of polyphenolic compounds in the treatment of neurodegenerative diseases: A review of their intracellular targets. *Eur J Pharmacol* 2006; 545: 51-64.
31. Ray PD, Huang BW, Tsuji Y. Reactive oxygen species (ROS) homeostasis and redox regulation in cellular signaling. *Cell Signal* 2012; 24: 981-990.
32. Ruskiewicz J, Albrecht J. Changes in the mitochondrial antioxidant systems in neurodegenerative diseases and acute brain disorders. *Neurochem Int* 2015; 88: 66-72.
33. Sarna LK, Wu N, Hwang SY, Siow YL, Karmin O. Berberine inhibits NADPH oxidase mediated superoxide anion production in macrophages. *Can J Physiol Pharmacol* 2010; 88: 369-378.
34. Silva A, Gomes O. Oxidative DNA damage protection and repair by polyphenolic compounds in PC12 cells. *Eur J Pharmacol* 2008; 601: 50-60.
35. Souto AL, Tavares JF, da Silva MS, Diniz Mde F, de Athayde-Filho PF, Barbosa Filho JM. Anti-inflammatory activity of alkaloids: an update from 2000 to 2010. *Molecules* 2011; 16: 8515-8534.
36. Szypuła W, Pietrosiuk A, Suchocki P, Olszowska O, Furmanowa M, Kazimierska O. Somatic embryogenesis and in vitro culture of *Huperzia selago* shoots as a potential source of huperzine A. *Plant Sci* 2005; 168: 1443-1452.
37. Wang J, Zhang HY, Tang XC. Huperzine A improves chronic inflammation and cognitive decline in rats with cerebral hypoperfusion. *J Neurosci Res* 2010; 88: 807-815.
38. Wilkaniec A, Strosznajder JB, Adamczyk A. Toxicity of extracellular secreted alpha-synuclein: Its role in nitrosative stress and neurodegeneration. *Neurochem Int* 2013; 62: 776-783.
39. Xiao H, Lv F, Xu W, Zhang L, Jing P, Cao X. Deprenyl prevents MPP2-induced oxidative damage in PC12 cells by the upregulation of Nrf2-mediated NQO1 expression through the activation of PI3K/Akt and Erk. *Toxicology* 2011; 290: 286-294.
40. Zhang HY, Tang XC. Neuroprotective effects of huperzine A: new therapeutic targets for neurodegenerative disease. *Trends Pharmacol Sci* 2006; 27: 619-625.
41. Zhang S, Ye J, Dong G. Neuroprotective effect of baicalin on hydrogen peroxide-mediated oxidative stress and mitochondrial dysfunction in PC12 cells. *J Mol Neurosci* 2010; 40: 311-320.

Effects of diclofenac sodium on the hippocampus of rats with acute subdural hematoma: histological, stereological, and molecular approach

Aysin Pınar Türkmen¹, Suleyman Kaplan¹, Abdurrahman Aksoy², Berrin Zuhul Altunkaynak¹, Kıymet Kübra Yurt¹, Ebru Elibol¹, Cengiz Çokluk³, Mehmet Emin Onger¹

¹Department of Histology and Embryology, Faculty of Medicine, Ondokuz Mayıs University, Samsun, ²Department of Pharmacology, Faculty of Veterinary Medicine, Ondokuz Mayıs University, Samsun, ³Department of Neurosurgery, Faculty of Medicine, Ondokuz Mayıs University, Samsun, Turkey

Folia Neuropathol 2016; 54 (2): 167-179

DOI: 10.5114/fn.2016.60808

Abstract

This study was aimed at evaluating the potential effects of acute subdural hematoma (ASDH) and diclofenac sodium (DS) therapy following ASDH on the rat hippocampus.

Twenty-four male Sprague Dawley rats were used and divided into four groups. 0.1 ml of non-heparinized autologous blood from the tail vein of the animals in the non-treatment group (NTG) and treatment group (TG) was injected into the subdural space. The TG received intramuscular diclofenac sodium at a 15 mg/kg dose daily from the postoperative second hour to the seventh day after the operation. The control group (CG) and sham group (SG) were used for control and sham operations, respectively. On the postoperative eighth day, all animals were sacrificed, and the hippocampi of all animals were stereologically and histologically evaluated. Also blood samples of the animals were biochemically analyzed.

As a result of the study, the mean number of neurons in CA1, CA2, and CA3 regions of the hippocampus and the total number of neurons were decreased in the hippocampus samples of the NTG and especially the TG subjects. When comparing the second blood samples, there was no difference between the levels of adrenaline and serotonin among the groups. However, after the operation, noradrenalin levels in the treatment group were found to be higher than those of the sham and control groups ($p < 0.05$).

In the NTG and TG, histopathological findings were observed such as Nissl condensation as well as completely dead and indistinguishable neurons with abnormally shaped, shrunken cytoplasm and nuclei. Also necrotic areas on the specimens of the TG were seen. In immunohistochemical sections, c-FOS positivity was decreased in the NTG and especially the TG. Otherwise, PGC-1 α positive cells were increased in the NTG and especially the TG.

In this study, it was shown for the first time by means of stereological techniques that using DS after ASDH caused a decrease in the number of hippocampal neurons (CA1, CA2, and CA3 regions).

Key words: acute subdural hematoma, diclofenac sodium, hippocampus, stereology, rat.

Communicating author:

Assoc. Prof. Dr. Berrin Zuhul Altunkaynak, Department of Histology and Embryology, Faculty of Medicine, Ondokuz Mayıs University, 55100 Samsun, Turkey, phone: +90 5067723379, e-mail: berrinzuhul@gmail.com

Introduction

Acute subdural hematoma (ASDH) is a life-threatening situation and generally leads to brain injury [16]. Brain damage is an important pathophysiological process in patients with ASDH [28]. The adverse effects of intracranial hematomas lead to several degenerative mechanisms, including ischemia-induced neuronal damage, clot-derived toxic factors, and edema formation [26,47]. At this point, levels of different mediators were evaluated. For example, serotonin may have protective effects on neurons [8]. Moreover, serotonin receptor agonists contribute to decrease of lesion volume and are considered as neuro-protective after ASDH [12,46]. Some researchers claim that high levels of dopamine, adrenaline, and especially noradrenaline lead to increased cerebral blood flow following brain injury [34,35]. Although there were mostly positive opinions, negative results were reported for high catecholamine levels. In a previous study, it was suggested that high adrenaline levels might have induced the apoptotic pathways in neonatal rats exposed to hypoxia [31]. Also, some researchers stated that high noradrenaline levels have potential for deleterious effects and the ability to induce apoptosis in PC12 cells, neuronal cells, and cardiac myocytes [6,51]. Therefore, in the current study we evaluated serotonin and catecholamine levels and attempted to detect their association with cell death.

In the treatment of cerebral hematomas, decompression was initially applied to minimize damage. Post-traumatic headache is one of the possible problems in the acute rehabilitation period for surviving patients [38,45]. Treatment options for the headache are non-steroidal, anti-inflammatory agents such as acetaminophen, ibuprofen, naproxen, and diclofenac sodium (DS) [5,11].

We previously reported deleterious effects of DS on the sciatic nerve, hippocampal pyramidal and granular cells, and Purkinje cells of male rats following prenatal exposure [14,32]. Also, DS has been reported to exert a neuroprotective effect by reducing the nerve root dysfunction induced by compression [10]. Additionally, several studies showed that DS did not inhibit proliferation and differentiation of neural stem cells [25].

Although these side effects have been reported, little is known about the effect of non-steroidal anti-inflammatory drugs on the brain following the

trauma caused by ASDH. The aim of the present study was therefore to investigate the effect of DS on hippocampus morphometry following ASDH and to define serotonin and catecholamine levels and their association with cell death caused by ASDH.

Material and methods

Animals

In this study, 24 adult male Sprague Dawley rats, weighing 300-350 g, were obtained from the Surgical Research Center. Adult rats were randomly divided into four groups, each consisting of six animals: control (CG), sham (SG), non-treatment (NTG), and treatment (TG). Following this, they were housed in standard plastic cages in a room air-conditioned to 20°C, under a 12/12-h light/dark cycle, and fed ad libitum.

One milliliter of autologous venous blood was collected from the tail vein of the animals belonging to all groups seven days before the experimental ASDH operation. No operation or drugs were given to the control (CG) group, but the SG, NTG, and TG were subjected to a surgical operation. On the day of sacrifice, all animals were taken to an adjacent room and decapitated, and blood was collected from the CG, SG, NTG and TG in polyethylene tubes containing 2% EDTA (0.05 ml) and stored on ice until centrifuged.

For these experiments, all procedures were approved by the Animal Experiments and Ethics Committee of Ondokuz Mayıs University.

Surgical preparation

The animals in the SG, NTG, and TG were turned to a prone position, mounted on a stereotactic frame (Fig. 1A) and intraperitoneally anesthetized with urethane 1.25 g/kg. Body temperature was measured by a rectal thermometer at 37-37.5°C by using a heating light. Following the sagittal scalp incision, a burr hole of 3 mm, placed 1 mm posterior to the coronal suture and 2 mm from the sagittal suture, was formed using a dental drill in the right parietal region under the microscope (Fig. 1). The incision of the dura mater was performed with a 30-gauge dental needle while in the subdural space another dental needle insertion was made. In the SG, only a burr hole was created and then the scalp was sutured with silk suture. No injection or insertion of the needle was made in the SG. The subdural hema-

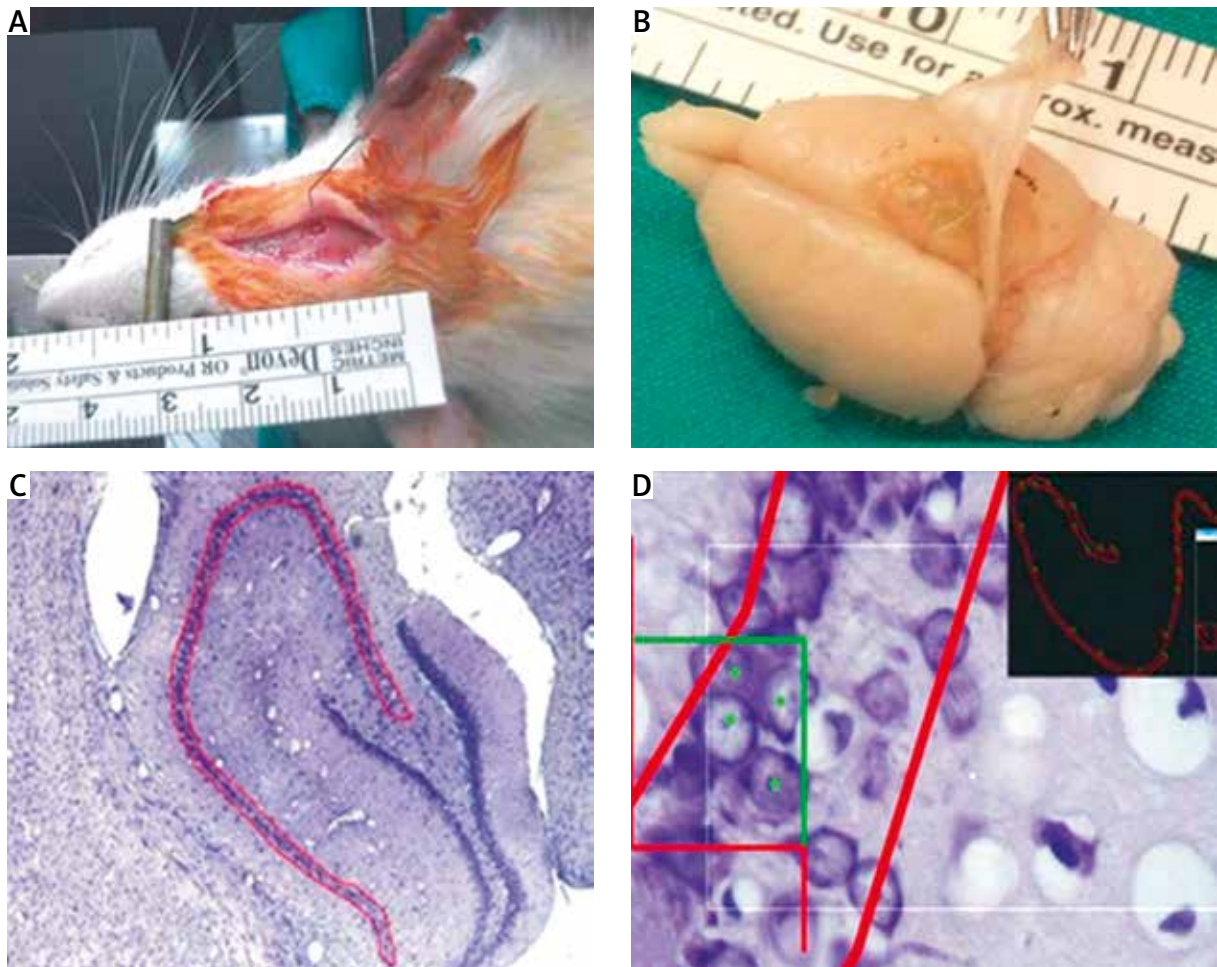


Fig. 1. Application of acute subdural hematoma model and stereological analysis procedures are shown. **A)** The animals were turned prone in a small animal stereotaxic frame and burr-hole location; also the position of the dental needle in the subdural space is seen. **B)** Macroscopic appearance of the lesion. **C)** Lining of the hippocampus boundaries during the stereological analysis. **D)** Systematic random sampling and estimation of neuron numbers in the hippocampus.

toma was produced by the slow injection of 0.1 ml non-heparinized autologous venous blood in the NTG and TG (Fig. 1A). Then, the scalp was sutured with silk suture. After waking up from anesthesia, the next seven days were spent in the normal light and dark cycle with $21 \pm 2^\circ\text{C}$ room temperature. Feed and water were supplied ad libitum [25]. The day of the operation was considered the first day of the experiment, and DS (Voltaren, 75 mg/3 ml ampoule, Novartis, Mefar İlaç Sanayi A.Ş., Kartal – Istanbul, Turkey) in a dose of 15 mg/kg daily was intramuscularly injected into the TG, beginning from the post-operative second hour to the 7th day of the experiment. Also, no treatment was used for the NTG.

Plasma collection

On the day of the operation, blood samples were collected from the tail vein of the all animals into polyethylene tubes containing 2% EDTA (0.05 ml) and stored on ice until centrifuged. The first analysis of plasma levels of serotonin, adrenaline, and nor-adrenaline was performed in these blood samples. On the day of sacrifice, after the animals were decapitated, polyethylene tubes containing 2% EDTA (0.05 ml) were used to collect the blood and the collected blood was kept on ice until the centrifugation. The isolation of the plasma from the whole blood was performed by centrifugation at 1300 RCF for

25 min. and the supernatant was collected and stored at -80°C until it is assayed. The second analysis of plasma levels of serotonin, adrenaline, and noradrenaline was performed in these blood samples of all the groups.

High performance liquid chromatography (HPLC) for detecting plasma levels of serotonin, adrenaline, and noradrenaline

The HPLC system consisted of multichannel pumps (LC 20AT), an autosampler (SIL 20A), a degasser (DGU 20A5), a diode array detector (DAD, SPD M20A) (Shimadzu, Kyoto, Japan) and an electrochemical calorimetric array detector (Coulchem III) equipped with a model 5020 guard and 5010A dual analytical cell (ESA, Chelmsford, MA). A guard column (Inertsil ODS-3, $5\ \mu\text{m} \times 20\ \text{mm} \times 4.0\ \text{mm}$, GL Science, Tokyo, Japan) and a reversed-phase C18 column (Inertsil ODS-3V, $5\ \mu\text{m} \times 250\ \text{mm} \times 4.6\ \text{mm}$, GL Science, Tokyo, Japan) were also used. The concentrations of serotonin (5-HT), adrenaline, and noradrenaline in blood samples were determined by HPLC according to the guide of the data sheet of the kits (Eureka Serotonin and Catecholamine HPLC detection KITS, Rotakim Inc., Ankara, Turkey). The detection limit was 0.03 nM for all three monoamines.

Histological procedure

At the end of the 7th day, the animals were anesthetized with ketamine (50 mg/kg) and xylazine (10 mg/kg) intramuscularly, and neutral formalin perfusion was administered intracardially. Afterwards, the brains were removed and routinely processed and embedded in paraffin. For these experiments, all procedures were approved by the Animal Experiments and Ethics Committee of Ondokuz Mayıs University.

Stereological analysis

Hippocampal sections were taken with a microtome (Leica RM 2135, Leica Instruments, Nussloch, Germany) at $20\ \mu\text{m}$ thicknesses. So, from systematic random sampling was carried by 1/6. Sampled sections in the cornu ammonis (CA 1-3) were collected and stained with cresyl violet. Optical dissector probes were placed in the marked area with random angles and evenly spaced. The stereology workstation consisted of a modified light microscope (Ste-

reo investigator 9.0., Micro Bright Field; Colchester, USA). The pyramidal cells in counting frames and the pyramidal cells on acceptable sides were counted (Gundersen, 1986; Fig. 1C, D). It is known that 15-20 sections taken from the hippocampal region is sufficient for the estimation of the total number of neurons during the application of optical fractionator method [17,49].

The total neuron number of the hippocampus was estimated by the following formula:

$$N = \Sigma Q \cdot \frac{1}{ssf} \cdot \frac{1}{asf} \cdot \frac{1}{tsf}$$

where: N – total neuron number, ΣQ – total dissector neuron number, ssf – sectioning sampling fraction, asf – area sampling fraction, and tsf – thickness sampling fraction.

The coefficient of error (CE) and the coefficient of variation (CV) of the sampling schedule of the hippocampus were validated from a pilot study [13,17,19].

Immunohistochemistry

TUNEL labeling assay

TUNEL (TdT-mediated dUTP-biotin nick end labeling) stain was applied to the hippocampus slices at the $5\ \mu\text{m}$ thickness according to the described method by Gavrieli *et al.* [32]. Followed by this process, the sections were treated with proteinase K in order to improve the antigen for 15 min and the sections were incubated in 3% hydrogen peroxidase solution prepared with 100% methanol to block endogenous peroxidase for five minutes. Slides were rinsed with PBS and incubated for 1 hour at 37°C in TdT enzyme. The samples were then washed with PBS and incubated for 30 min at 25°C with anti-digoxigenin antibody-peroxidase conjugate, rinsed with PBS, and incubated with 3,3'-diaminobenzidine (DAB) at 25°C for 5 minutes. The slides were stained in Mayer's hematoxylin. The slides were evaluated using the light microscope (Leica, LDM 4000, Wetzlar, Germany).

Immunohistochemical staining of c-FOS and PGC-1 α

Paraffin-embedded hippocampus samples were also used for c-FOS and PGC-1 α immunohistochemistry. The deparaffinization of tissue sections of $5\ \mu\text{m}$ was done in xylene and they were rehydrated in ethanol and in water and phosphate-buffered saline

respectively. The blockage of endogenous peroxidase was performed by immersion in 3% hydrogen peroxide. The tissue sections were then incubated with c-FOS and PGC-1 α antibodies (Dako, Istanbul, Turkey) at a concentration of 5 μ g/ml for 1 h at room temperature. Control sections were incubated with phosphate-buffered saline containing normal goat serum without a primary antibody. Immunostaining was then detected with a streptavidin-biotin complex kit (Dako) and developed with a di-amino benzidine tetrahydrochloride kit. The sections were counterstained with Mayer's hematoxylin followed by light microscopy.

Statistical analysis

Microsoft SPSS version 15.0 for Windows was used for statistical analyses. One-way ANOVA (Bonferroni post-hoc test) was applied to compare the results of the groups. All statistical values under 0.05 were considered significant.

Results

In this study, 24 male Sprague Dawley rats were used to create an animal model of ASDH. After sacrificing the animals, their brains were carefully removed and subdural hematomas were macroscopically observed (Fig. 1B).

Stereological results

In the study, the number of neurons in the CA1, CA2, and CA3 regions of the hippocampus and also the total numbers of neurons in all the hippocampus (Ammon's horn) were separately estimated. The number of pyramidal neurons in the CA1, CA2, and CA3 areas and the total number of neurons in the whole hippocampus of the CG, SG, NTG, and TG are shown in Figure 2. ASDH and especially DS treatment caused a significant decrease in pyramidal neurons of the hippocampus (Fig. 2).

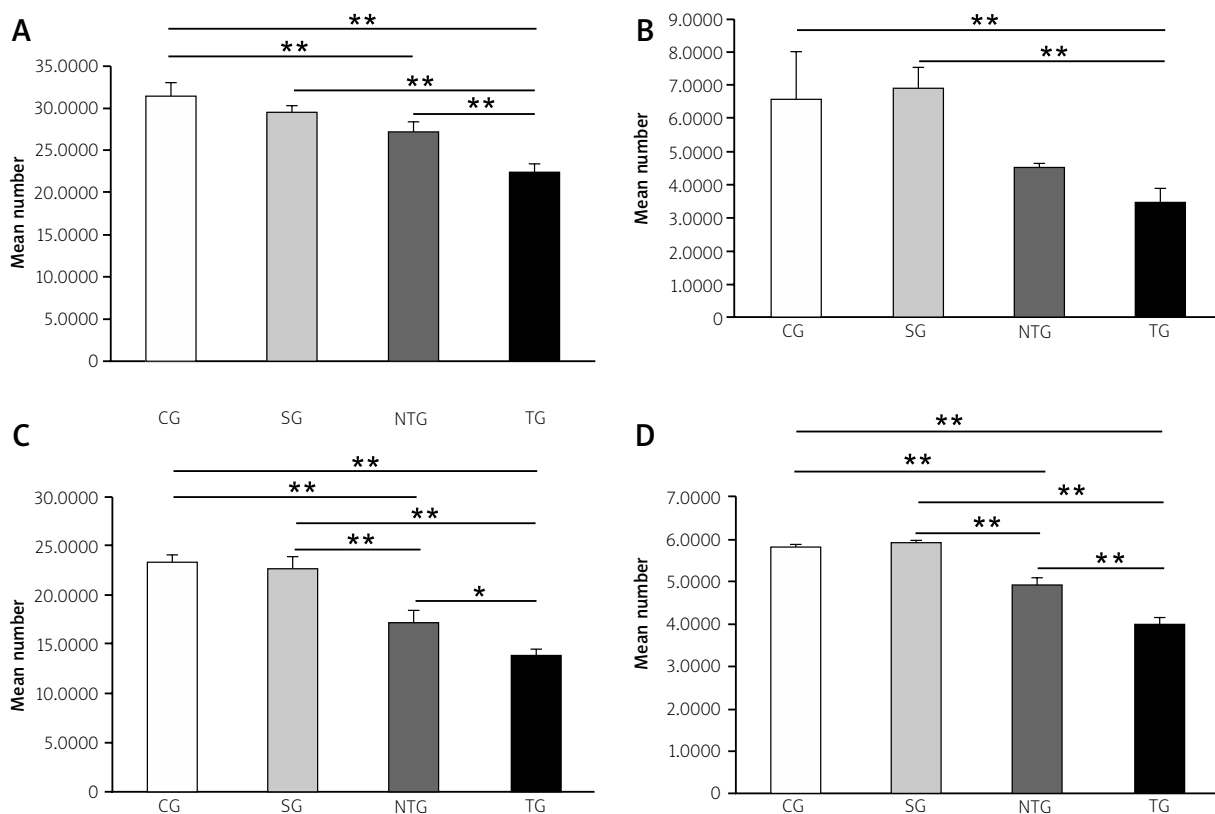


Fig. 2. Mean numerical densities of pyramidal neurons in CA1, CA2 and CA3 area of hippocampus and total number of neurons in hippocampus among CG, SG, NTG and TG are shown in **A**, **B**, **C** and **D**, respectively. * $p < 0.05$, ** $p < 0.01$ (mean \pm SEM).

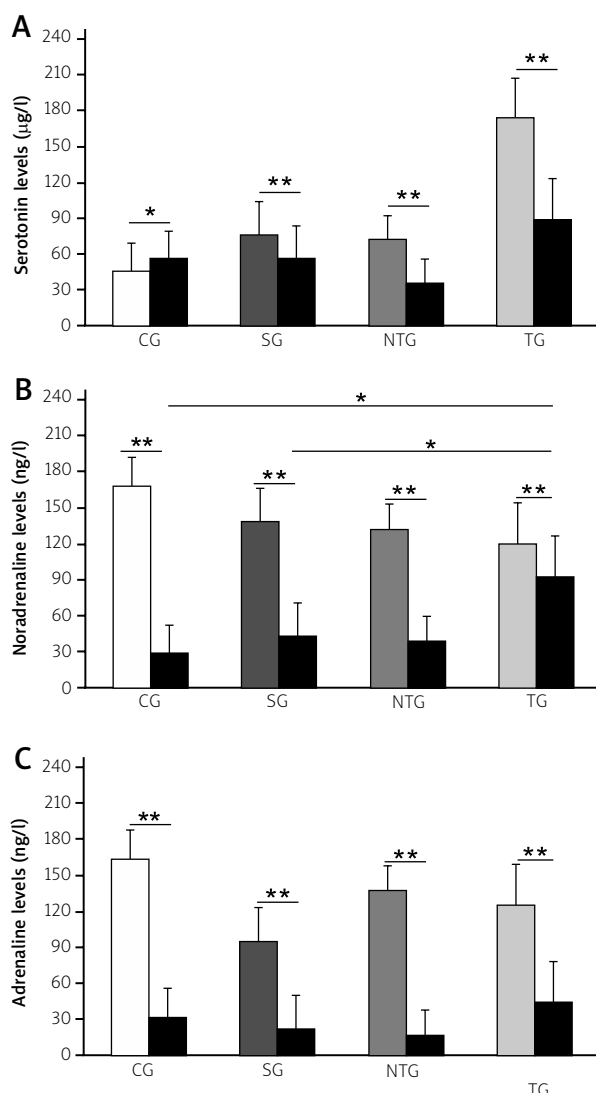


Fig. 3. Mean pre- and post-operative plasma levels of serotonin, noradrenaline and adrenaline among CG, SG, NTG and TG are shown in **A**, **B** and **C**, respectively. * $p < 0.05$, ** $p < 0.01$ (mean \pm SEM).

Biochemical results

Plasma serotonin levels

When comparing the first and postoperative serotonin levels, it was found that they were significantly reduced after the operation in the SG ($p < 0.05$) and especially in the NTG and TG ($p < 0.01$). In the control group, postoperative plasma serotonin levels significantly increased in comparison to initial levels ($p < 0.05$). However, there was no significant difference in the postoperative plasma levels of serotonin among the groups (Fig. 3A, $p > 0.05$).

Plasma noradrenaline levels

Postoperative plasma levels of noradrenaline were significantly increased after the operation, especially in the TG as compared to the other groups ($p < 0.05$). On the other hand, the plasma noradrenaline levels were significantly decreased in all groups at the second analysis (Fig. 3B, $p < 0.01$).

Plasma adrenaline levels

After the operation, plasma adrenaline levels were significantly lower than pre-operative ones in all groups ($p < 0.01$). Among the second adrenaline levels of the groups, no significant difference was found (Fig. 3C, $p > 0.05$).

Light microscopic results

Results of the control (CG) and sham (SG) group

In sections obtained from the hippocampus of rats among the CG and SG, a conventional healthy structure of the hippocampus was observed at the light microscopic level. The shape of neurons was pyramidal in the hippocampus. Furthermore, these neurons had euchromatic nuclei. The neurons and their extensions were normal. Histological structure of the CG that represented a healthy appearance is shown in Figure 4.

Results of the non-treatment group (NTG)

In the NTG, neurons included heterochromatic, pyknotic nuclei (Fig. 5, white asterisk) and dark-stained cytoplasm (Fig. 5, black-thick arrowhead). Moreover, angular displacement of pyramidal neurons was observed in the hippocampus sections of the NTG (Fig. 5, white arrow). We also examined neurons with a dark and shrunken cytoplasm, and their nuclei had some vacuoles (Fig. 5A and C). Abnormally shaped oligodendrocytes, microglia, and astrocytes were also observed (Fig. 5, white arrowhead). Trunks of the primary dendrites were dilated and pale stained compared to those in the other groups (Fig. 5, black-thin arrowhead). Chromatolysis was detected in degenerated neurons in the hippocampus samples of this group (Fig. 5, black arrow). Moreover, in hippocampal slices of the NTG, some neurons were at the initial stage of degeneration, but some of the neurons were fully degenerated or dead.

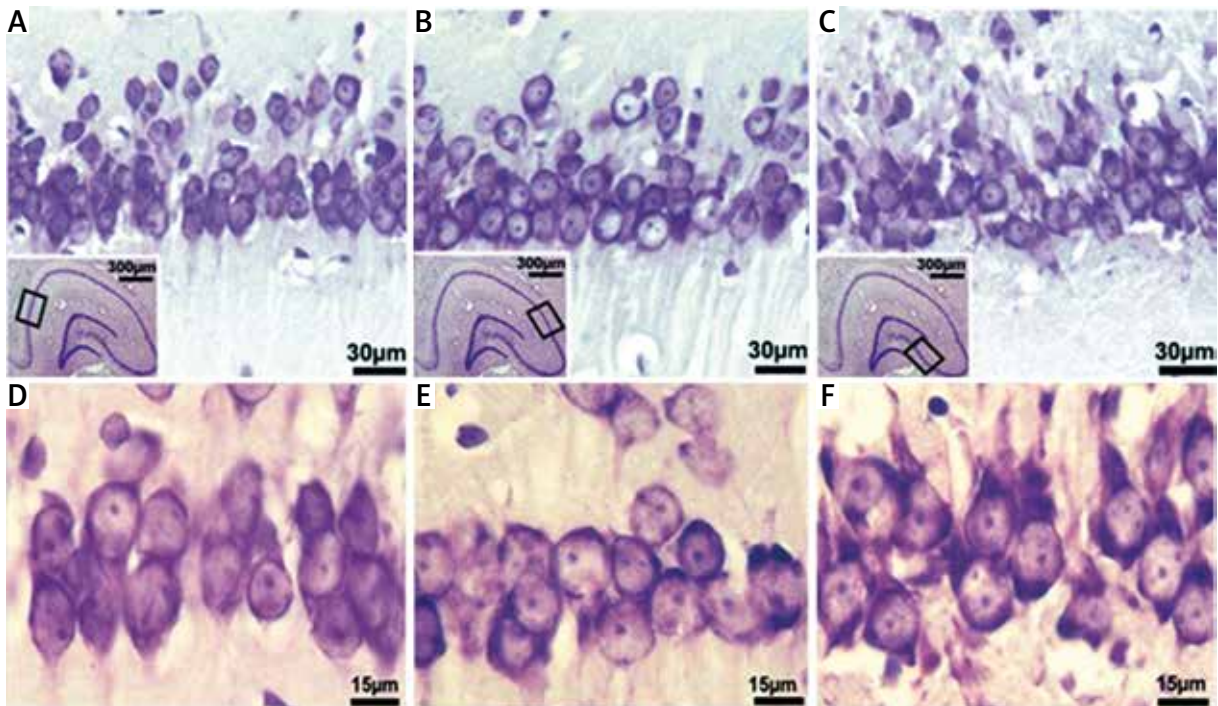


Fig. 4. Light microscopic sections obtained from the hippocampus of the control group. In A-C and D-F, specified portions of CA1, CA2, and CA3 regions are observed at low and high magnification, respectively. Thumbnails in the framed areas show hippocampal regions at the lowest magnification. In D-F, healthy neurons are clearly seen in CA regions. Cresyl violet.

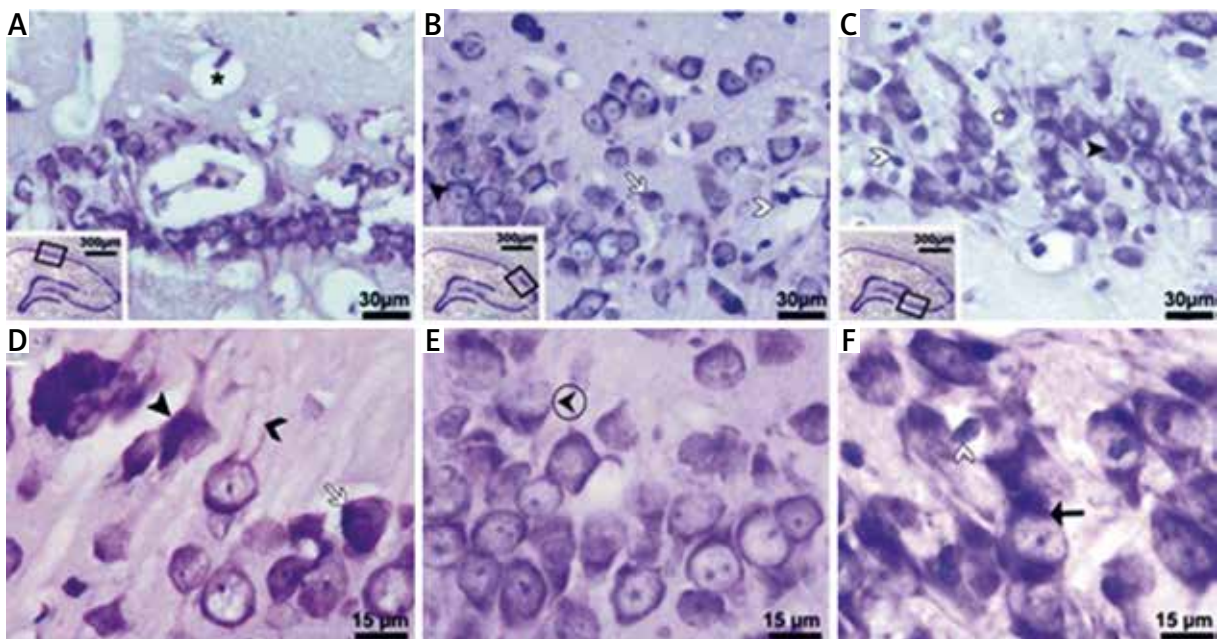


Fig. 5. Light micrographs obtained from the hippocampi of NTG. White asterisk – pycnotic neurons; white arrows – neurons with dark-stained cytoplasm; white arrowheads – glia cells; thick-black arrowhead – neurons with indistinguishable cytoplasm and nucleus; black asterisk – vacuole; black ringed arrowhead – swelled nucleus with pale chromatin; thin black arrowhead – enlarged and pale stained trunks of primary dendrites; black arrows – concentrated Nissl granule containing areas. Cresyl violet.

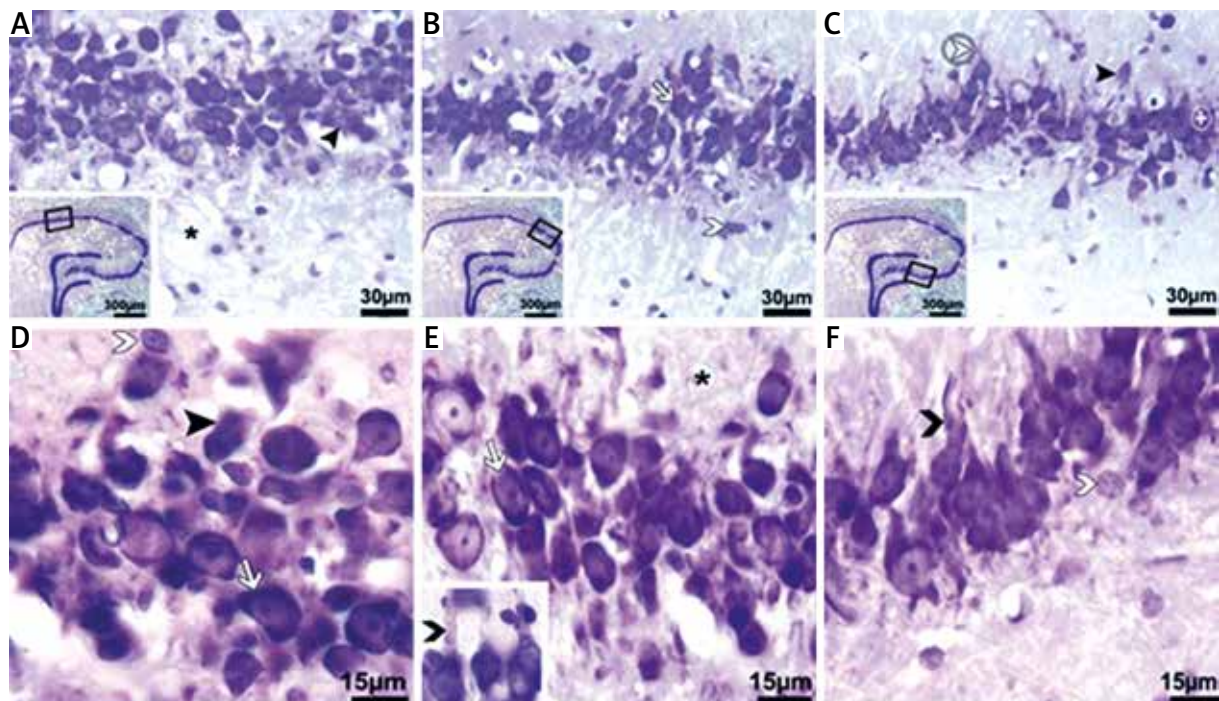


Fig. 6. Light micrographs obtained from the hippocampi of TG. White asterisk – pycnotic neurons; white arrows – neurons with dark-stained cytoplasm; white arrowhead – glia cells; white ringed arrowhead – wavy appeared axon terminals; white ringed plus – necrotic area; thick-black arrowhead – neurons with indistinguishable cytoplasm and nucleus; black asterisk – vacuole; thin-black arrowhead – enlarged and pale stained trunks of primary dendrites. Cresyl violet.

Results of the treatment (TG) group

In the light microscopic sections that were obtained from the TG, axonal extension was observed such that trunks of the primary dendrites were enlarged and pale stained in comparison to those of the CG (Fig. 6, thin-black arrowhead). Also, in the peripheral part of some degenerated neurons, Nissl condensation occurred, meaning that chromatolysis was defined (Fig. 6; black arrow). Some neurons are indistinguishable with their pale nuclei and swollen cytoplasm (Fig. 6, black ring arrowhead). In addition to neurons at the early stage of cellular damage, completely dead and indistinguishable neurons with abnormally shaped, shrunken cytoplasm and nuclei were also found (Fig. 6, thick black arrowhead). In white matter, edema, degenerated axon remains, and micro-vacuolization were observed (Fig. 6, black asterisks).

Some structures were observed as necrotic areas on certain specimens (Fig. 6, white ring + sign). It is noteworthy that chromatin in the nucleus was decreased, and dark-stained cytoplasm of pyramidal

neurons was detected (Fig. 6, white arrow). Furthermore, the axons of pyramidal neurons were wavy in appearance (Fig. 6, white ring arrowhead).

Immunohistochemical results

No positive cell was seen in TUNEL-stained hippocampus sections of all the groups (Fig. 7). In the control and sham groups, neurons in the hippocampus were well stained with c-FOS, and immune reactivity was decreased following the ASDH procedure and especially DS treatment (Fig. 8C and D). However, in the NTG and TG, positivity of PGC-1 α was increased after ASDH operation and especially DS treatment (Fig. 9C and D).

Discussion

In recent years, despite improvements in the imaging and treatment modalities used in the diagnosis of head trauma, related morbidity and mortality are still high [11]. Traumatic brain injury may lead to serious complications such as intracranial

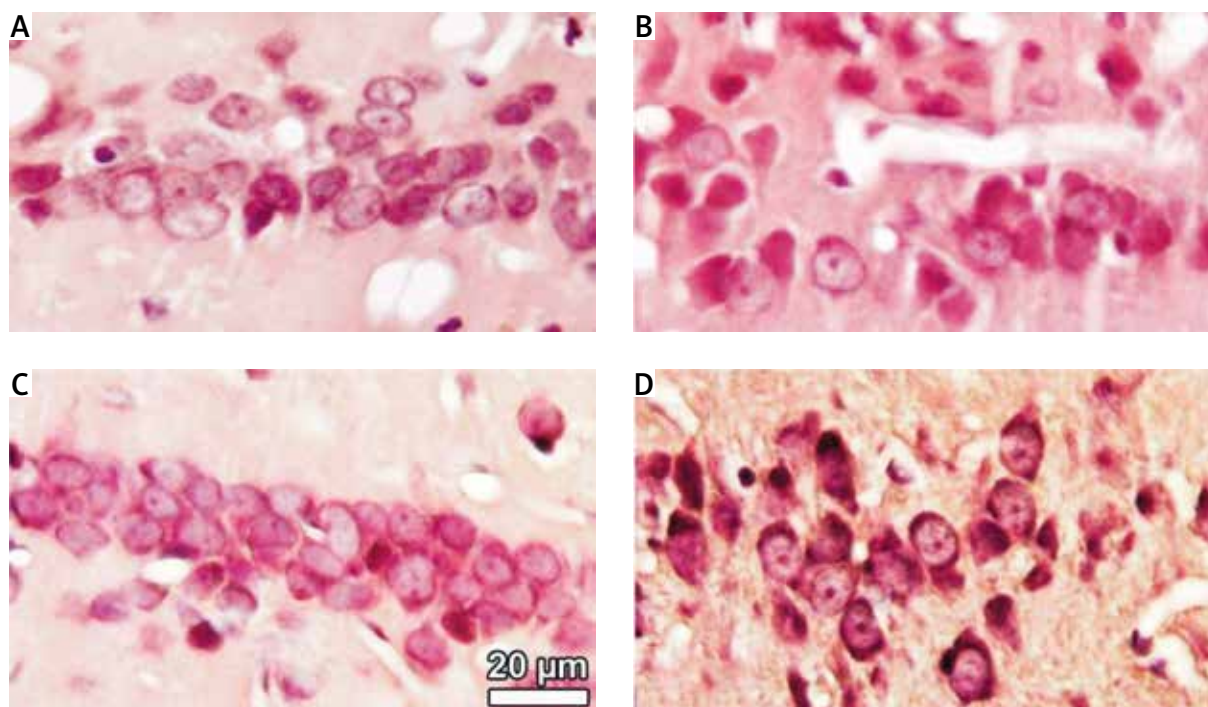


Fig. 7. Light micrographs showing TUNEL immune reactivity at 40× magnification for CG (A), SG (B), NTG (C) and TG (D). No TUNEL positivity was seen in the groups. For all micrographs, magnification bars are the same, with 20 µm.

hematomas. Subdural hematomas constitute 50 to 60% of traumatic intracranial hematomas [52]. The most frequent symptom of acute subdural hematoma is the sudden onset of severe headaches. Diclofenac sodium (sodium-(o-[(2,6-dichlorophenyl)-amino]-phenyl)-acetate) (DS) is a non-steroidal, anti-inflammatory drug characterized by a relatively low molecular weight [25,41]. It has a role in inhibiting the cyclooxygenase (COX) enzyme, reducing arachidonic acid release and improving its uptake [41]. It is a strong analgesic and has an antipyretic role. Hence, it is commonly used for treatment of headaches caused by traumatic brain injury. In this study, we aimed to detect the effect of ASDH and DS treatment on the hippocampus.

In the literature, a number of studies of traumatic brain injury have been conducted in animal models, and fluid percussion, vacuum deformation, and weight reduction methods were used [43]. Since these methods can lead to severe, primary diffuse brain damage, Sasaki and Dunn's model was used in our study [39]. So, the model is specific for presenting the effects of ASDH.

Also, experimental animal models of traumatic brain injury have generally focused on necrotic and apoptotic neuronal cell death. As a result of the studies, axonal damage, memory, and learning defects were reported [20,21]. According to Hausmann *et al.*, following the brain injury, neurons are subjected to apoptotic cell death. However, in our study we detected apoptosis by TUNEL stain after the ASDH in neither the NTG nor the TG. Therefore, we suspected that occurrence of cell death after ASDH may have been caused by ischemic necrosis. However, several papers have suggested that c-FOS-triggered AP-1 might mediate apoptosis through transcriptional regulation of expression of the FasL gene to start the extrinsic apoptotic pathway [23, 24]. Our data indicate that c-FOS may be related to neuronal proliferation, because we did not detect increasing c-FOS immune reactivity or an apoptotic signal with the TUNEL stain following ASDH in either the NTG or the TG. Also, we thought that c-FOS immune reactivity decreased following ASDH because of the decreased cellular activity. Our data on PGC-1 α immune reactivity indicated that PGC-1 α positivity was higher in the NTG and TG than in the control and sham groups.

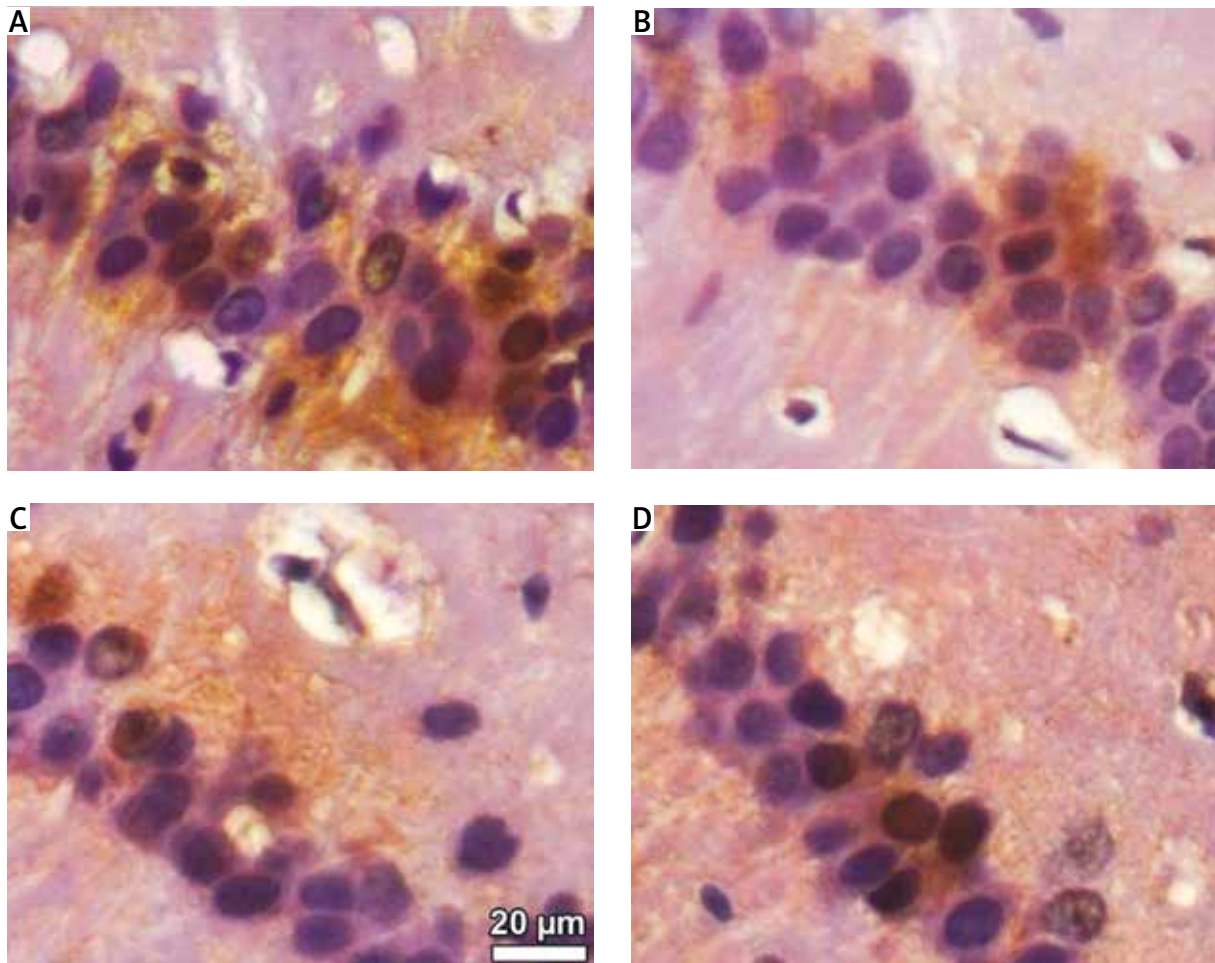


Fig. 8. Light micrographs showing c-FOS immune reactivity at 40× magnification for CG (A), SG (B), NTG (C) and TG (D). Particularly, c-FOS positive cells were noted in CG and SG. These positive cells were decreased in NTG and especially TG. For all micrographs, magnification bars are the same, with 20 µm.

Therefore, we suggest that PGC-1 α -mediated upregulation of the antioxidant defense system could promote cell death following ASDH.

In the study of Tran *et al.* (2006), a lateral perfusion model was used, and they studied the contralateral hippocampus area using the optical fractionator method seven days after brain injury. According to their results, the number of neurons significantly decreased compared to that of the sham group [48].

According to our findings, the number of neurons in the CA1 region of the NTG was significantly decreased at seven days after ASDH ($p < 0.01$). The number of neurons in the CA2 region showed no significant change compared to the control group ($p = 1.135$), because the CA2 region is variably sized, and generally no significant difference

could be determined between study groups in terms of the number of neurons in this region [36]. Like in the CA1 region, the number of neurons in the CA3 region of the NTG was significantly reduced compared to the control group ($p < 0.01$). When we evaluated the total number of neurons, it was found to be significantly lower in the NTG than the control group ($p < 0.01$). In the sham group, the number of neurons in the CA3 region was significantly different than the number in the control group ($p < 0.01$). This reduction in the number of neurons of the subjects in the sham group may be caused by stress during surgical procedures and skull defects [44]. Indeed, in a previous study, saline injection stress was shown to reduce the number of neurons [3].

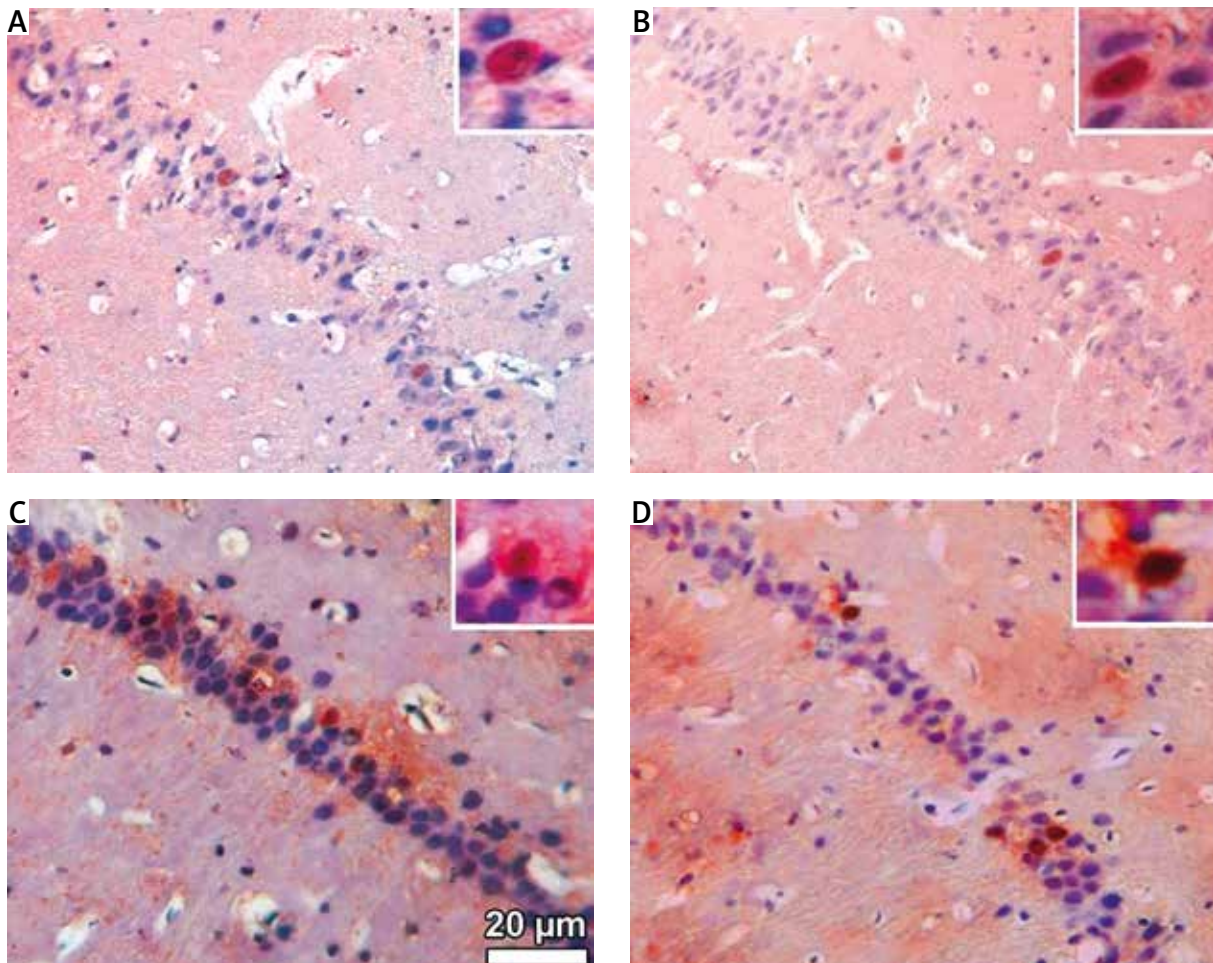


Fig. 9. Light micrographs showing PGC-1 α immune reactivity at 40 \times magnification for CG (A), SG (B), NTG (C) and TG (D). PGC-1 α positivity was increased in NTG and especially TG. Small pictures show PGC-1 α -positive neurons at $\times 100$ magnification in all groups. For all micrographs, magnification bars are the same, with 20 μ m.

Adverse effects of DS on the CNS have been clearly shown [3,33]. DS inhibits the differentiation and proliferation of neural cells in the hippocampus [14]. In the literature, 20-week-old male rats that were prenatally exposed to DS exhibited a reduction in the number of hippocampal neurons [14,18]. As a result of analysis by our stereological findings, DS treatment caused a decrease in the number of neurons compared to control and sham groups ($p < 0.01$). However, DS treatment in the TG did not cause significant changes in the number of neurons as compared to the NTG ($p > 0.05$).

In our study, histopathological findings were similar to the findings of ischemia and necrosis [4]. In our histological examination of the hippocampus after acute unilateral hematoma, neuronal shrink-

age, pycnotic neurons, and vacuolar degenerations were detected in the NTG. Also, DS application increased the degeneration of the neurons, and more neuron death was seen in the TG than in the NTG. Also DS treatment caused a decrease of the c-FOS and PGC-1 α activity. Therefore cellular loss was higher in the TG than that of the NTG.

Previous studies of acute stress showed an increased rate of serotonin metabolism in the brain. The lower level of serotonin that results is not helpful in overcoming stressful situations in the future. This reduction leads to changes in sleep patterns and eating habits, and impairs sensitivity to pain [22]. In previous studies, low serum levels of serotonin have been identified in migraine patients [30]. In our study, the first measurements of the serotonin levels showed

large differences, because the control group was not subjected to the operation on the operation day, so the level was low in that group. Because the TG was subjected to the operation and drug injection, it had the highest level. Serotonin levels of the other two groups were approximately the same as each other, higher than those of the controls, but lower than that of the TG. This situation resulted from their stress level being between the CG and TG. When comparing the second plasma levels of serotonin, a significant difference was found between the first and second levels of the groups. Also, the second serotonin levels were significantly reduced after the operation in the NTG and TG ($p < 0.01$). This reduction may be due to an inability to cope with the physical stress of the operation [22].

Stress may cause an increase of noradrenaline and adrenaline [27], but DS application may cause a reduction in stress in the TG. The second plasma levels of noradrenaline were found to be significantly increased in the TG in comparison to those of the other groups. In addition, adrenaline levels were increased in comparison to those of the other groups (not significant).

In conclusion, the results presented here show cell loss in the hippocampus due to exposure to ASDH by using stereological methods. Moreover, after ASDH, DS treatment caused a further increase in cell loss. Therefore, further studies are required to confirm this and to refine the effect mechanism and treatment alternatives to DS so as to decrease pain and prevent cell loss in patients with ASDH.

Acknowledgments

This study was supported by Scientific Research Foundation of Ondokuz Mayıs University (PYO.TIP.1904.12.028).

Disclosure

Authors report no conflict of interest.

References

1. Altunkaynak BZ, Ozbek E, Unal B, Aydın N, Aydın MD, Vuraler O. Chronic treatment of haloperidol induces pathological changes in striatal neurons of guinea pigs: a light and electron microscopical study. *Drug Chem Toxicol* 2012; 35: 406-417.
2. Altunkaynak BZ, Unal D, Altunkaynak ME, Halici Z, Kalkan Y, Keles ON, Aksak S, Selli J, Unal B. Effects of diabetes and ovariectomy on rat hippocampus (a biochemical and stereological study). *Gynecol Endocrinol* 2012; 28: 228-261.
3. Aygün D, Kaplan S, Odaci E, Onger ME, Altunkaynak ME. Toxicity of non-steroidal anti-inflammatory drugs: a review of melatonin and diclofenac sodium association. *Histol Histopathol* 2012; 27: 417-453.
4. Brierley JB, Meldrum BS, Brow AW. The threshold and neuropathology of cerebral "anoxic-ischemic" cell change. *Arch Neurol* 1973; 29: 367-374.
5. Burdan F, Starostawska E, Szumiło J. Prenatal tolerability of acetaminophen and other over-the-counter non-selective cyclooxygenase inhibitors. *Pharmacol Rep* 2012; 64: 521-528.
6. Burke WJ, Schmitt CA, Miller C, Li SW. Norepinephrine transmitter metabolite induces apoptosis in differentiated rat pheochromocytoma cells. *Brain Res* 1997; 760: 290-293.
7. Canan S, Aktaş A, Ulkay MB, Colakoglu S, Rağbetli MC, Ayyıldız M, Geuna S, Kaplan S. Prenatal exposure to a non-steroidal anti-inflammatory drug or saline solution impairs sciatic nerve morphology: a stereological and histological study. *Int J Dev Neurosci* 2008; 26: 733-738.
8. Cifariello A, Pompili A, Gasbarri A. 5-HT receptors in the modulation of cognitive processes. *Behav Brain Res* 2008; 195: 171-179.
9. Communal C, Singh K, Pimentel DR, Colucci WS. Norepinephrine stimulates apoptosis in adult rat ventricular myocytes by activation of the β -adrenergic pathway. *Circulation* 1998; 98: 1329-1363.
10. Cornefjord M, Olmarker K, Otani K, Rydevik B. Effects of diclofenac and ketoprofen on nerve conduction velocity in experimental nerve root compression. *Spine (Phila Pa 1976)* 2001; 26: 2193-2200.
11. Crooks CY, Zumsteg JM, Bell, KR. Traumatic brain injury: a review of practice management and recent advances. *Phys Med Rehabil Clin N Am* 2007; 18: 681-710.
12. Dooley AE, Pappas IS, Parnavelas JG. Serotonin promotes the survival of cortical glutamatergic neurons in vitro. *Exp Neurol* 1997; 148: 205-214.
13. Dursun H, Albayrak F, Uyanik A, Keleş NO, Beyzagül P, Bayram E, Halici Z, Altunkaynak ZB, Süleyman H, Okçu N, Ünal B. Effects of hypertension and ovariectomy on rat hepatocytes Are amlodipine and lacidipine protective? (A stereological and histological study). *Turk J Gastroenterol* 2010; 21: 387-395.
14. Gokcimen A, Rağbetli MC, Baş O, Tunc AT, Aslan H, Yazici, AC, Kaplan S. Effect of prenatal exposure to an anti-inflammatory drug on neuron number in cornu ammonis and dentate gyrus of the rat hippocampus: a stereological study. *Brain Res* 2007; 1127: 185-192.
15. Graham DI, McIntosh TK, Maxwell WL, Nicoll JA. Recent advances in neurotrauma. *J Neuropathol Exp Neurol* 2000; 59: 641-651.
16. Greenberg MS. Head trauma. In: *Handbook of Neurosurgery*. Thieme, New York 2001; 626-686.
17. Gundersen HJ, Jensen EB. The efficiency of systematic sampling in stereology and its prediction. *J Microsc* 1987; 147: 229-263.
18. Gurtskaia G, Tsiklauri N, Nozadze I, Nebieridze M, Tsagareli MG. Antinociceptive tolerance to NSAIDs microinjected into dorsal hippocampus. *BMC Pharmacol Toxicol* 2014; 15: 10.
19. Güven D, Altunkaynak BZ, Ayrancı E, Kaplan S, Bildircin ED, Kesim Y, Rağbetli MC. Stereological and histopathological evaluation of ovary and uterine horns of female rats prenatal-

- ly exposed to diclofenac sodium. *J Obstet Gynaecol* 2013; 33: 258-321.
20. Hausmann R, Biermann T, Wiest I, Tübel J, Betz P. Neuronal apoptosis following human brain injury. *Int J Legal Med* 2004; 118: 32-36.
 21. Hensler JG. *Handbook of the Behavioral Neurobiology of Serotonin* 2010; 21: 367-378.
 22. Jesberger JA, Richardson JS. Neurochemical aspects of depression: The past and the future? *Int J Neurosci* 1985; 27: 19-47.
 23. Kasibhatla S, Brunner T, Genestier L, Echeverri F, Mahboubi A, Green DR. DNA damaging agents induce expression of Fas ligand and subsequent apoptosis in T lymphocytes via the activation of NF-kappa B and AP-1. *Mol Cell* 1998; 4: 543-551.
 24. Kolbus A, Herr I, Schreiber M, Debatin KM, Wagner EF, Angel P. c-Jun-dependent CD95-L expression is a rate-limiting step in the induction of apoptosis by alkylating agents. *Mol Cell Biol* 2000; 20: 575-582.
 25. Kudo C, Kori M, Matsuzaki K, Yamai K, Nakajima A, Shibuya A, Niwa H, Kamisaki Y, Wada K. Diclofenac inhibits proliferation and differentiation of neural stem cells. *Biochem Pharmacol* 2003; 66: 289-295.
 26. Lacut K, Bressollette L, Le Gal G, Etienne E. VICTORI Ah (Venous Intermittent Compression and Thrombosis Occurrence Related to Intra-cerebral Acute hemorrhage) Investigators Prevention of venous thrombosis in patients with acute intracerebral hemorrhage. *Neurology* 2005; 65: 865-874.
 27. Manunta Y, Edeline JM. Noradrenergic induction of selective plasticity in the frequency tuning of auditory cortex neurons. *J Neurophysiol* 2004; 92: 1445-1463.
 28. McClelland S, Mackey SJ, Kim SS. The dangerous gamble of heparinization within two weeks of non operative traumatic acute subdural hematoma in patients with increased stroke risk: a case series. *J Postgrad* 2014; 60: 194-201.
 29. Merens W, Vander Does AJW, Spinhoven P. The effects of serotonin manipulations on emotional information processing and mood. *J Affect Disord* 2007; 103: 43-62.
 30. Nagata E, Shibata M, Hamada J, Shimizu T, Katoh Y, Gotoh K, Suzuki N. Plasma 5-hydroxytryptamine (5-HT) in migraine during an attack-free period. *Headache* 2006; 46: 592-596.
 31. Noh JS, Kim EY, Kang JS, Kim HR, Oh YJ, Gwag BJ. Neurotoxic and neuroprotective actions of catecholamines in cortical neurons. *Exp. Neurol* 1999; 159: 217-241.
 32. Odaci E, Cihan OF, Aslan H, et al. Prenatal diclofenac sodium administration increases the number of Purkinje cells in female rats: a stereological study. *Int J Dev Neurosci* 2010; 28: 145-196.
 33. Ozyurt B, Kesici H, Alici SK, Yilmaz S, Odaci E, Aslan H, Rağbetli MÇ, Kaplan S. Prenatal exposure to diclofenac sodium changes the morphology of the male rat cervical spinal cord: A stereological and histopathological study. *Neurotoxicol Teratol* 2011; 33: 282-287.
 34. Patel NJ, Chen MJ, Russo-Neustadt AA. Norepinephrine and nitric oxide promote cell survival signaling in hippocampal neurons. *Eur J Pharmacol* 2010; 10: 633-636.
 35. Pfister D, Strebler SP, Steiner LA. Effects of catecholamines on cerebral blood vessels in patients with traumatic brain injury. *Eur J Anaesthesiol Suppl* 2008; 42: 98-103.
 36. Rağbetli MC, Aydinlioğlu A, Koyun N, Yayici R, Arslan K. Total neuron numbers in CA1-4 sectors of the dog hippocampus. *Indian J Med Res* 2010; 131: 780-785.
 37. Rağbetli MC, Ozyurt B, Aslan H, Odaci E, Gokcimen A, Sahin B, Kaplan S. Effect of prenatal exposure to diclofenac sodium on Purkinje cell numbers in rat cerebellum: a stereological study. *Brain Res* 2007; 1174: 130-135.
 38. Safaz I, Alaca R, Yaşar E, Tok F, Yılmaz B. Medical complications, physical function and communication skills in patients with traumatic brain injury: a single center 5-year experience. *Brain Inj* 2008; 22: 1-7.
 39. Sasaki M, Dunn L. A model of acute subdural hematoma in the mouse. *J Neurotrauma* 2001; 18: 1241-1246.
 40. Schmitz C. Variation of fractionator estimates and its prediction. *Anat Embryol* 1998; 198: 371-397.
 41. Scholer DW, Ku EC, Boettcher I, Schweizer A. Pharmacology of diclofenac sodium. *Am J Med* 1986; 80: 34-46.
 42. Simon E, Bánk J, Gál J, Siro P, Novak L, Fulesdi B, Molnarc C. Administration of preemptive analgesia by diclofenac to prevent acute post craniotomy headache. *Iddeggyogy Sz* 2012; 65: 302-306.
 43. Siu SSN, Yeung JHK, Lau TK. A study on placental transfer of diclofenac in first trimester of human pregnancy. *Hum Reprod* 2000; 15: 2423-2425.
 44. Sorrells SF, Sapolsky RM. An inflammatory review of glucocorticoid actions in the CNS. *Brain Behav Immun* 2007; 21: 259-272.
 45. Staltnacke BM. Post concussion symptoms in patients with injury-related chronic pain. *Rehabil Res Pract* 2012; 528: 265.
 46. Sun ZL, Feng DF. Biomarkers of cognitive dysfunction in traumatic brain injury. *J Neural Transm* 2014; 121: 79-90.
 47. Tanweer O, Boah A, Huang PP. Risks for hemorrhagic complications after placement of external ventricular drains with early chemical prophylaxis against venous thromboembolisms. *J Neurosurg* 2013; 119: 1309-1322.
 48. Tran LD, Lifshitz J, Witgen BM, Schwarzbach E, Cohen AS, Grady MS. Response of the contralateral hippocampus to lateral fluid percussion brain injury. *J Neurotrauma* 2006; 23: 1330-1342.
 49. Tunç AT, Aslan H, Turgut M, Ekici F, Odaci E, Kaplan S. Inhibitory effect of pinealectomy on the development of cerebellar granule cells in the chick: a stereological study. *Brain Res* 2007; 1138: 214-234.
 50. West MJ, Slomianka L, Gundersen HJ. Unbiased stereological estimation of the total number of neurons in the subdivisions of the rat hippocampus using the optical fractionators. *Anat Rec* 1991; 231: 482-497.
 51. Zilkha-Falb R, Ziv I, Nardi N, Offen D, Melamed E, Barzilai A. Monoamine-induced apoptotic neuronal cell death. *Cell Mol Neurobiol* 1997; 17: 101-119.
 52. Zwienerberg-Lee M, Muizelaar JP. *Clinical pathophysiology of traumatic brain injury in humans neurological surgery*. HR Saunders, Philadelphia 2004; pp. 5039-5064.

Natural apoptosis in developing mice dopamine midbrain neurons and vermal Purkinje cells

Joaquín Martí-Clúa

Departament de Biologia Cel·lular, de Fisiologia i d'Immunologia, Unidad de Citologia i d'Histologia, Facultat de Biociències, Universitat Autònoma de Barcelona, Barcelona, Spain

Folia Neuropathol 2016; 54 (2): 180-189

DOI: 10.5114/fn.2016.60385

Abstract

Natural cell death by apoptosis was studied in two neuronal populations of BALB/c, C57BL/6 and B6CBA-A^{w-j}/A hybrid stock mice: (I) dopaminergic (DA) neurons in choosing coronal levels throughout the anteroposterior extent of the substantia nigra pars compacta (SNc), and (II) Purkinje cells (PCs) in each vermal lobe of the cerebellar cortex. Mice were collected at postnatal day (P) 2 and P14 for the midbrain study, and at P4 and P7 for the analysis of the cerebellum. No DA cells with morphologic criteria for apoptosis were found. Moreover, when the combination of tyrosine hydroxylase and TUNEL or tyrosine hydroxylase and active caspase-3 immunohistochemistry were performed in the same tissue section, no DA cells TUNEL positives or active caspase-3-stained DA neurons were seen. On the other hand, when PCs were considered, data analysis revealed that more dying PCs were observed at P4 than at P7. Values of neuron death were highest in the central lobe; this was followed by the posterior and anterior lobes and then by the inferior lobe. To determine if apoptotic death of PCs is linked to their time-of-origin profiles, pregnant dams were administered with [³H]TdR on embryonic days 11-12, 12-13, 13-14 and 14-15. When TUNEL and [³H]TdR autoradiography or active caspase-3 immunohistochemistry and [³H]TdR autoradiography were combined in the same tissue section, results reveal that the naturally occurring PC death is not related to its time of origin but, rather, is random across age.

Key words: postnatal, dopamine, substantia nigra pars compacta, cerebellar cortex, Purkinje cells, neurogenetic timetables, apoptosis.

Introduction

An important principle of neural development is that cell populations are generated in higher numbers during embryogenesis and undergo a natural cell death that determines their final counts in adults [7,39]. When neurons die following a stereotyped series of molecular and cellular events, it is termed apoptosis [11,18]. Apoptosis serves for a joint of

critical processes including the withdrawal of aberrant axon projection, the elimination of ectopic neurons and the refinement of neural circuits [10]. It has been proposed that excess of neuronal elements is regulated by competition among members of the neuronal population for the trophic support that they receive from their postsynaptic targets and from afferent projections [3,23,40].

Communicating author:

Dr. Joaquín Martí, Departament de Biologia Cel·lular, de Fisiologia i d'Immunologia, Unidad de Citologia i d'Histologia, Facultat de Biociències, Universitat Autònoma de Barcelona, 08193 Bellaterra, Barcelona, Spain, e-mail: joaquim.marti.clua@uab.es

Dopaminergic (DA) neurons of the midbrain are involved in several neurologic and psychiatric diseases including schizophrenia, addictive behaviors and satiety disorders [8,42]. They are especially vulnerable to degeneration in human dopamine deficiency diseases [44]. It has been proposed that an inappropriate amplification of basal physiological cell death in nigrostriatal DA neurons may have an impact on later susceptibility to disorders such as Parkinson's disease [34].

The natural occurring neuron death in the substantia nigra pars compacta (SNc) has been reported in rats [6]. The time course of this phenomenon is largely postnatal, with important roles for glial cell line-derived neurotrophic factor and brain-derived neurotrophic factor [20,37,38]. In the striatum, the principal input component of the basal ganglia, apoptotic dying cells occur within the first month of postnatal development [32].

In mice, on the other hand, natural death of SNc DA neurons has been studied with contradictory results. This is because several authors observed evidence of neuroapoptosis during the early postnatal development of this motor nucleus [14], whereas Lieb *et al.* [22] and Blum [5] did not find any DA neurons with signs of apoptosis. To address this issue, we examined histologically, at P2 and P14, series of BALB/c, C57BL/6 and B6CBA-A^{w-j}/A hybrid stock brains for signs of apoptosis in midbrain DA cells at several anatomical levels throughout the antero-posterior axis of the SNc. In the present study, we used the TUNEL method in conjunction with morphological analysis at the light microscopic level, and immunohistochemistry for active caspase-3, aiming to determine and quantify apoptotic neuron death in the SNc during normal development.

In the cerebellar cortex, on the other hand, PCs are also involved in processes of apoptosis [17,26]. Two time windows have been reported: in the first of these, apoptotic figures have been found at E15 [2]. In the second, dying PCs are seen from birth until P10 [16,19,25]. Thus, whereas the timing and extent of dying PCs have been addressed [16], to our knowledge, no attempts have been made to determine whether physiological PC death is related to its time of origin. We know from previous autoradiographic studies that, in mice, cerebellar PCs are generated according to precise neurogenetic timetables [27,29]. Consequently, terminal deoxynucleotidyl transferase-mediated dUTP nick end-labeling method (TUNEL)

and [³H]TdR autoradiography, and active caspase-3 immunohistochemistry and [³H]TdR autoradiography were combined in the same tissue section to determine, at P4 and P7, if apoptotic PCs death in the region of the vermis is linked to their time of origin.

Material and methods

Animal preparation and experimental design

BALB/c and C57BL/6 mice were provided by Autonomous University of Barcelona animalarium. B6CBA-A^{w-j}/A hybrid stock mice were obtained from the mouse colony at Indiana University School of Medicine. The experimental animals were the offspring of pregnant dams injected subcutaneously between 8:00 a.m. and 9:00 a.m. on two consecutive days with [³H]TdR (5 µCi/g of body weight, New England Nuclear, no. NET-027) according to the following time-window: embryonic day (E)11-12, E12-13, E13-14 and E14-15. For staging of animals, E1 was the day after mating. The day of birth was defined as P0. Seven animals were used for each experimental group and data time point. Standard laboratory conditions (food and water *ad lib*, 22 ± 2°C, 12 h light: dark cycle starting at 08:00) were used and all the experiments were performed in accordance with the Ethical Committee of our University.

Following anesthesia with sodium pentobarbital (50 mg/kg of body weight, i.p.), pups were perfused intracardially with 10% neutral buffered formalin. Tissue processing was developed as regular procedures from our laboratory. The blocks containing the midbrain and the cerebellum were sectioned at 10 µm in coronal and sagittal planes, respectively. Only one of every fifth section was placed on microscopic slides previously coated with poly-(L-lysine).

Immunocytochemistry for tyrosine hydroxylase and TUNEL, and tyrosine hydroxylase and active caspase-3

Sections were immunostained for tyrosine hydroxylase. They were deparaffinized and rehydrated through a graded series of ethanol and distilled water, as in routine processing. After this, sections were washed twice for 15 min in PBS, soaked in a solution containing absolute methanol plus 3% H₂O₂ for 20 min. Sections were then washed in PBS, blocked for 30 min with 10% normal goat serum in PBS, followed by washes with 0.5% Triton X-100/PBS

and finally PBS. Afterwards, sections were incubated with a monoclonal mouse anti-tyrosine hydroxylase (1 : 1000, Sigma, St Louis, MO, USA) for 90 min at room temperature. After rinsing with PBS during 15 min, sections were incubated for 1h at room temperature with the secondary antibody (Sigma biotinylated anti mouse IgG diluted 1 : 300 in PBS) and extravidin-peroxidase (Sigma). Immunoreactive sites were detected by submerging the slides in 0.05% diaminobenzidine tetrahydrochloride (DAB) plus 3% H₂O₂ in TBS 0.05 M (pH 7.6) supplemented with 2 ml of CoCl₂ (1%) for 5 min. With this color modification of DAB, we yield a distinct dark-blue color that is easily distinguished from brown DAB [13].

After immunocytochemical evaluation, the slides were processed for TUNEL for visualizing the 3'-OH ends of DNA fragments in apoptotic cells or for active caspase-3. For TUNEL, sections were incubated with 20 µg/ml of proteinase K during 20 min at room temperature. They were then soaked in the TdT buffer (30 mM Tris-HCl, pH 7.2, 140 mM sodium cacodylate, 1 mM CaCl₂) for 15 min and then incubated at 37°C for 75 min with the TdT buffer containing 0.3 eu/µl terminal deoxynucleotidyl transferase and 0.04 nmol/µl biotin-16-deoxyuridine triphosphate. The reaction was stopped by soaking the sections in Tris buffer. The biotinylated dUTP molecules incorporated into nuclear DNA were visualized by incubation with horseradish peroxidase-conjugated streptavidin (Dako, Glostrup, Denmark) diluted 1 : 100 at 37°C for 30 min. After further rinsing of the sections in PBS, the peroxidase coloring reaction was performed by immersing the sections for 5 min in 0.05 M Tris-HCl buffer, pH 7.4, containing 30 mg/dl DAB, 65 mg/dl sodium azide, 10 mM imidazole, and 0.005% H₂O₂, yielding the characteristic brown color. Sections were counterstained with hematoxylin. For positive control of TUNEL labeling, histological sections were incubated with DNase (5 µg/ml) at 37°C during 10 min to induce DNA strand breaks. For negative control, terminal deoxynucleotidyl transferase was replaced with distilled water.

To immunostain active caspase-3, after TH immunohistochemistry, sections were processed for microwave-mediated antigen retrieval, in 0.01M citrate buffer (pH 6). Sections were heated at 750 W for 5 min. They were then cooled for 20 min at room temperature. Nonspecific binding was blocked for 30 min with 10% normal goat serum in PBS containing 0.5% Triton X-100. Afterwards, sections were incubated

in primary antibody to active caspase-3 (polyclonal rabbit anti-active caspase-3, 1 : 100; Chemicon International) diluted in PBS and incubated for 75 min at room temperature. This was followed by rinses with PBS during 15 min. Sections were then incubated for 1h at room temperature with the secondary antibody (Sigma biotinylated anti rabbit IgG diluted 1 : 500 in PBS) and extravidin-peroxidase (Sigma). Slices were treated with 0.05% DAB plus 3% H₂O₂ in TBS 0.05 M (pH 7.6) for 5 min.

Sections were counterstained with hematoxylin, dehydrated and cover-slipped. The specificity of the antibodies was tested by omission of the primary antibodies.

TUNEL, active caspase-3 immunohistochemistry and [³H]TdR autoradiography

When TUNEL or active caspase-3 immunohistochemistry had been completed (see previous section), the slides were processed for autoradiography following a previously described method [28]. This consisted of coating the slides with liquid photographic emulsion (undiluted Kodak NTB3) in a dark-room illustrated by Kodak Series 2 dark-red safelights, drying them in a humidified atmosphere, and storing them in light-tight boxes in the refrigerator for an exposure period of 12 weeks. The slides were developed in Kodak D-19, and were then post-stained with hematoxylin, dehydrated, and cover-slipped with Permount. Labeled PCs could be identified by the cluster of reduced silver grains (black granules) over their nuclei. Neurons with ten grains or more per nucleus were considered labeled.

Quantitative analyses

All of the histological quantifications were performed blindly. Two neuronal populations were studied: the SNc DA neurons and the vermal PCs. DA cells were separately analyzed in plates 46, 50, 54 and 60 along the anteroposterior axis of the SNc [30,31,43]. PCs were studied in each cerebellar cortex lobe (anterior, central, posterior and inferior) at the level of the vermis. Their names and boundaries are those assigned by Altman and Bayer [1].

For quantification, a DA neuron was considered as apoptotic only if it fulfilled the morphologic criteria for apoptosis (characteristic basophilic, rounded and intranuclear chromatin clumps) reported previ-

ously [15,36]. On the other hand, to be considered as an apoptotic PC, the structure observed had to fulfill the following criteria: (a) one or more fragments of highly condensed chromatin (within or reminiscent of a pyknotic nucleus) and distinct from the PC nucleolus, and (b) position within the PC layer [16].

Frequency of [³H]TdR-labeled PCs was calculated as a percentage by dividing the number of neurons labeled by the total number of neurons scored. To infer PCs neurogenetic timetables, a modification of the progressively delayed comprehensive labeling procedure was used [4]. The rationale of this method is based on the fact that ³H-TdR will only be incorporated by those neuroblasts engaged in the DNA synthesis during isotope supply. Whether the onset of the injections with the radioactive agent is progressively delayed by 24 hours, the percentage of labeled cells decreases reflecting the production of neurons from their precursor cells. Thus, the proportion of PCs originating between two injection series is equal to the daily decline in the percentage of labeled neurons.

Statistical treatment

Two-way ANOVAs with “age” and “strain” as the main between-subject factors were used to analyze the number of dying cells as well as the proportion of labeled neurons. When appropriate, further decomposition of the interaction was performed. Levene’s test was used to test homogeneity of variances. When necessary, data were log transformed to achieve homogeneity of variances. If only two means were available, Student’s *t*-test or Mann-Whitney *U* test were utilized. A *p* value less than 0.05 was considered statistically significant.

Photographic material

Photographic material presented in this report was digitally captured by a CCD-IRIS color video camera (Sony, Japan) coupled to the microscope. The digitized images were processed with the Adobe Photoshop software.

Results

Neuroapoptosis in the midbrain

The gross overall morphology of the SNc appeared similar in BALB/c, C57BL/6 and B6CBA-A^{w-j}/A hybrid stock mice. In order to perform a detailed analysis of

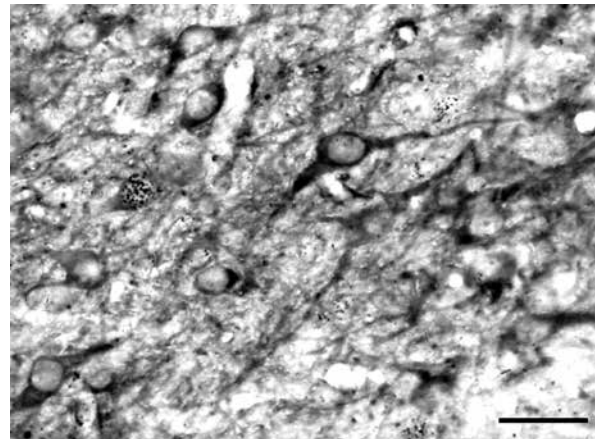


Fig. 1. High-magnification of a TH-immunostained section through the substantia nigra pars compacta of a B6CBA-A^{w-j}/A hybrid stock mouse sacrificed at P14. Scale bar: 50 μm.

physiological cell death, light microscopic observations of the midbrain were made through the antero-posterior axis of the SNc. After a meticulous study based on an extensive collection of sections, no DA cells with morphologic criteria for apoptosis were seen. When the combination of tyrosine hydroxylase and TUNEL or tyrosine hydroxylase and active caspase-3 immunohistochemistry were performed in the same tissue section, no DA cells TUNEL positives or active caspase-3-stained DA neurons were observed in any level of the studied midbrain. This has been taken into account in all of the examined mice. Figure 1 shows examples of tyrosine hydroxylase-stained neurons in the SNc from B6CBA-A^{w-j}/A hybrid stock mice.

Purkinje cell death in the cerebellar cortex

The cerebellum showed the characteristic pattern of fissures and foliar crowns. Cardinal fissures determining the limits among the four lobes of the cerebellar cortex were present and distinguishable. This occurred in all of the studied mice. Apoptotic PCs were confirmed by DNA fragmentation, the TUNEL method or active caspase-3. TUNEL positive macroneurons in the developing cerebellum were selectively labeled among numerous hematoxylin-stained PCs. Dying PCs were distributed throughout the cerebellar cortex lobes at both ages examined. As a secondary marker of apoptosis, selected cerebellar cortex sections were tested for immunore-

Table I. Number of TUNEL positives Purkinje cells per section in each lobe of the cerebellar cortex

Age	Strain	LA	LC	LP	LI
P4	BALB/c	6.1 ± 0.9*	12.3 ± 1.4*	6.5 ± 0.7	3.8 ± 0.8*
P7	BALB/c	3.1 ± 0.8*	4.9 ± 0.9*	2.2 ± 0.6*	1.5 ± 0.9*
P4	C57BL/6	6.4 ± 0.9*	11.2 ± 1.5*	7.4 ± 0.8*	3.4 ± 0.5*
P7	C57BL/6	2.7 ± 0.7*	4.5 ± 0.9*	2.6 ± 0.9*	1.3 ± 0.6*
P4	B6CBA-A ^{wj} /A hybrid stock	7.2 ± 0.8*	11.7 ± 1.3*	7.0 ± 0.8*	4.1 ± 0.5*
P7	B6CBA-A ^{wj} /A hybrid stock	3.4 ± 0.7*	5.9 ± 1.1*	2.3 ± 0.7*	1.4 ± 0.5*

Means ± S.E.M (n = 7) per section are indicated

*Student's t-test or Mann-Whitney U test, p < 0.05 vs. P4

P – postnatal day, LA – anterior lobe, LC – central lobe, LP – posterior lobe, LI – inferior lobe

Table II. Number of active caspase-3-immunoreactive Purkinje cells per section in each lobe of the cerebellar cortex

Age	Strain	LA	LC	LP	LI
P4	BALB/c	2.4 ± 0.4*	5.1 ± 0.7*	3.4 ± 0.5*	3.4 ± 0.5*
P7	BALB/c	1.6 ± 0.5*	2.3 ± 0.4*	1.5 ± 0.3*	1.7 ± 0.4*
P4	C57BL/6	2.6 ± 0.4*	4.7 ± 0.5*	3.7 ± 0.4*	3.2 ± 0.9*
P7	C57BL/6	1.3 ± 0.2*	2.4 ± 0.4*	1.6 ± 0.3*	1.6 ± 0.5*
P4	B6CBA-A ^{wj} /A hybrid stock	2.2 ± 0.5*	4.5 ± 0.5*	3.5 ± 0.4*	3.5 ± 0.5*
P7	B6CBA-A ^{wj} /A hybrid stock	1.3 ± 0.5*	2.5 ± 0.5*	1.6 ± 0.2*	2.4 ± 0.3*

Means ± S.E.M (n = 7) per section are indicated

*Student's t-test or Mann-Whitney U test, p < 0.05 vs. P4

P – postnatal day, LA – anterior lobe, LC – central lobe, LP – posterior lobe, LI – inferior lobe

activity to activated caspase-3. Immunoreactivity to active caspase-3 occurred in the PC cytoplasm.

Numbers of TUNEL positive neurons and active caspase-3-reactive PCs quantified at P4 and P7 in the anterior, central, posterior and inferior lobes are presented in Tables I and II. Results of the two-way ANOVA are depicted in Table III. Data analysis demonstrated significant effects of the “age” in all lobes of the cerebellar cortex. No effect of the main factor “strain” was observed. The interaction of “age X strain” was not statistically significant. Post hoc comparisons of means revealed that mice collected at P4 always presented more apoptotic PCs than those killed at P7. Moreover, data analysis indicated that numbers of TUNEL positives and active caspase-3-immunoreactive PCs were highest in the central lobe; this was followed by the posterior and anterior lobes and then by the inferior lobe.

Developmental timetables of PCs at P4 and P7 were inferred at the four, previously indicated, lobes of the cerebellar cortex. Initially, the frequency of

tagged PCs was estimated by sequential [³H]TdR-labeling embryonic windows as graphically displayed in Figure 2. Statistical analysis of the results showed that at any given time within this generation period, and both for the P4 and P7, the percentage of labeled PCs remains constant within each lobe studied. In a subsequent analysis, profiles of PCs origin were constructed. In Figure 3, the frequencies of newly generated PCs at each selected lobe are plotted against time. Data analysis indicated that the birth sequences of postmitotic neurons for both survival times within each cerebellar cortex lobe are closely similar. Figure 4 shows examples of PCs labeled with [³H]TdR.

Discussion

Neuron death in the substantia nigra pars compacta

The physiological loss of SNc DA cells has been convincingly demonstrated in rats [6] and non-hu-

Table III. Results of the two-way ANOVA of the dying, TUNEL and active caspase-3-reactive Purkinje cells number per section in each lobe of the cerebellar cortex

	Dying	TUNEL	Caspase-3
Anterior lobe			
Age (A)	[$F_{1,36} = 61.4, p < 0.00001$]	[$F_{1,36} = 16.6, p < 0.0002$]	[$F_{1,36} = 12.2, p < 0.001$]
Strain (S)	NS	NS	NS
A × S	NS	NS	NS
Central lobe			
Age (A)	[$F_{1,36} = 96.1, p < 0.00001$]	[$F_{1,36} = 43.8, p < 0.00001$]	[$F_{1,36} = 34.6, p < 0.00001$]
Strain (S)	NS	NS	NS
A × S	NS	NS	NS
Posterior lobe			
Age (A)	[$F_{1,36} = 92.1, p < 0.00001$]	[$F_{1,36} = 45.3, p < 0.00001$]	[$F_{1,36} = 16.8, p < 0.001$]
Strain (S)	NS	NS	NS
A × S	NS	NS	NS
Inferior lobe			
Age (A)	[$F_{1,36} = 62.5, p < 0.00001$]	[$F_{1,36} = 33.4, p < 0.00001$]	[$F_{1,36} = 12.51, p < 0.001$]
Strain (S)	NS	NS	NS
A × S	NS	NS	NS

NS – not significant

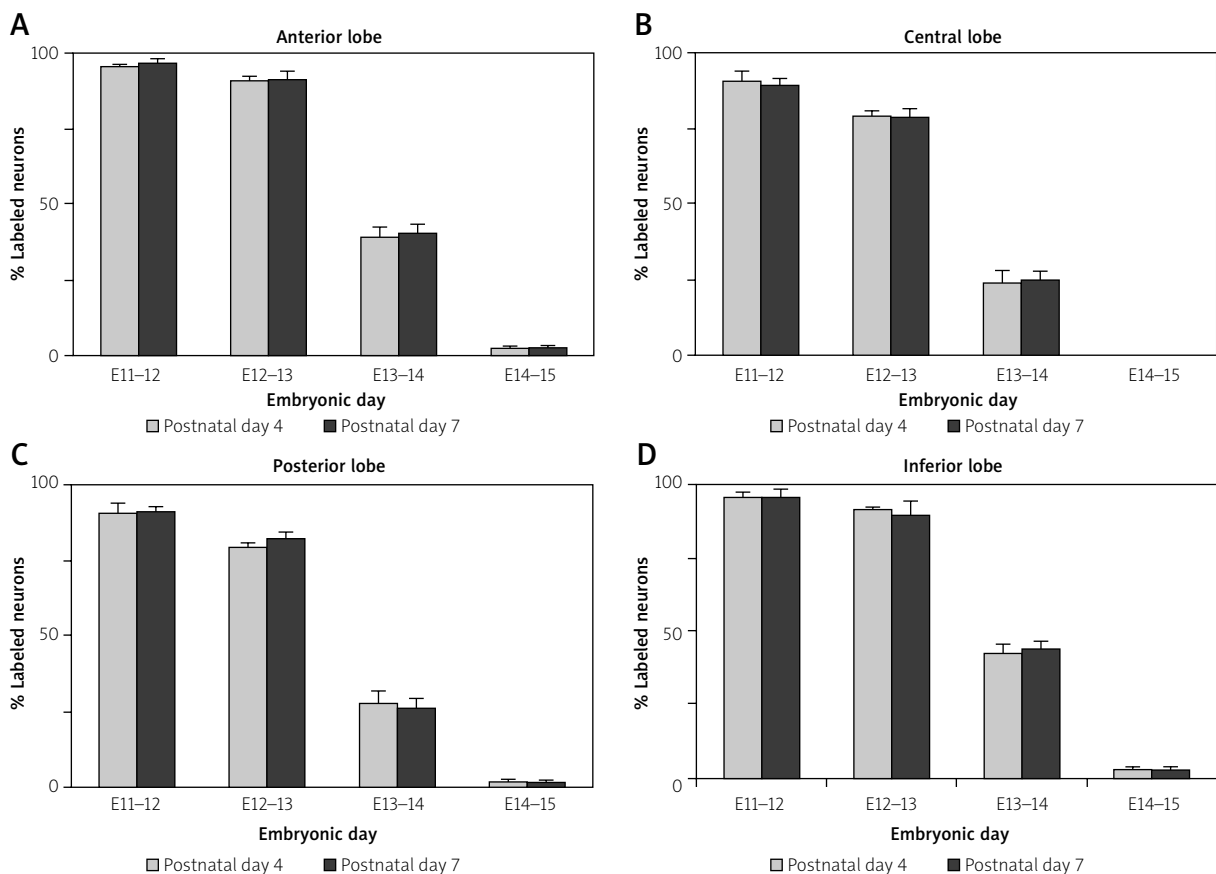


Fig. 2. Comparison of [³H]TdR-labeling patterns in each lobe of the cerebellar cortex. Frequency histograms of Purkinje cells labeled with [³H]TdR on two consecutive days of the embryonic period (abscissa) and survival until P4 (empty columns) and P7 (solid columns). Percentages are expressed as mean ± SEM.

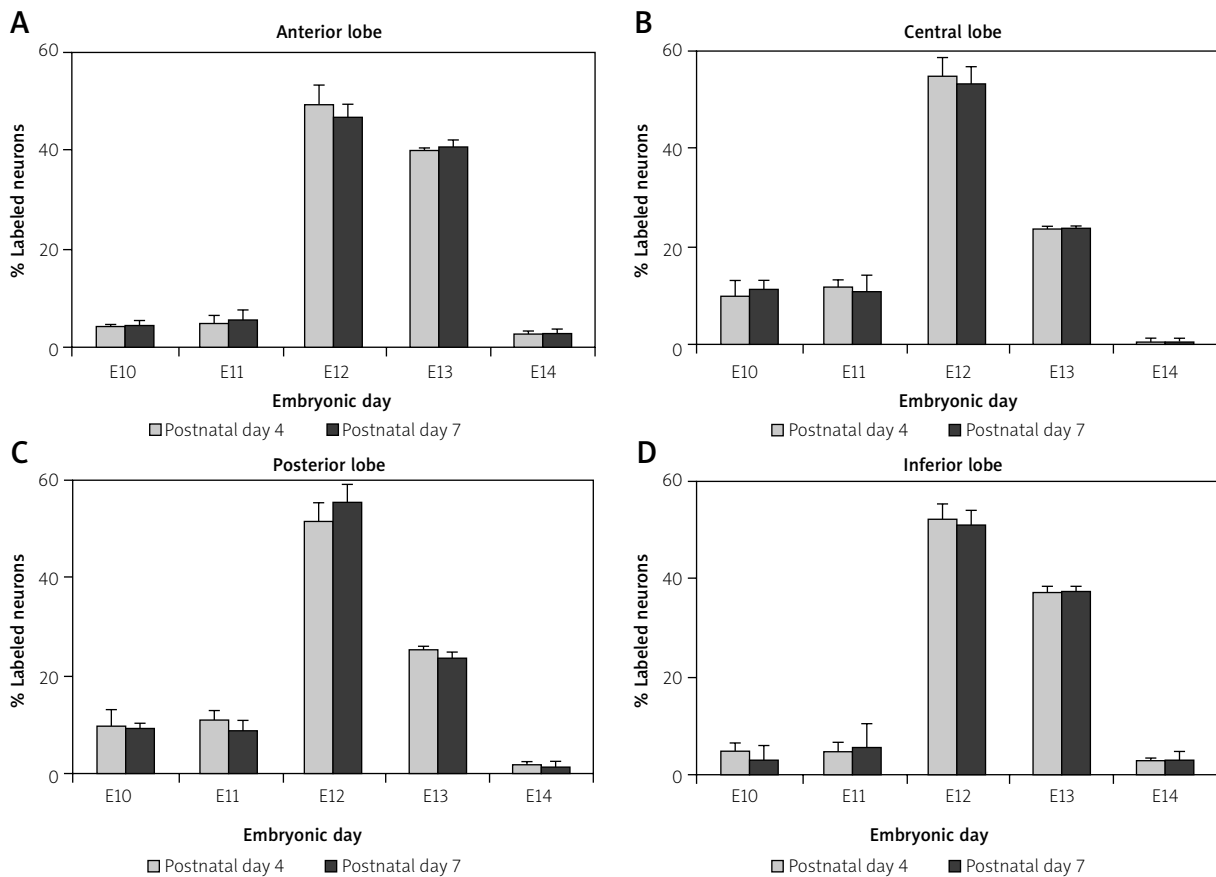


Fig. 3. Generative profiles for Purkinje cells within each cerebellar lobe examined. The inferred frequencies (ordinate) of newly generated neurons for P4 empty columns and P7 solid columns are plotted against the relative embryonic time-period (abscissa). Percentages of newborn Purkinje cells were determined by the rate of decline in $[^3\text{H}]\text{TdR}$ -labeled cells at that time point.

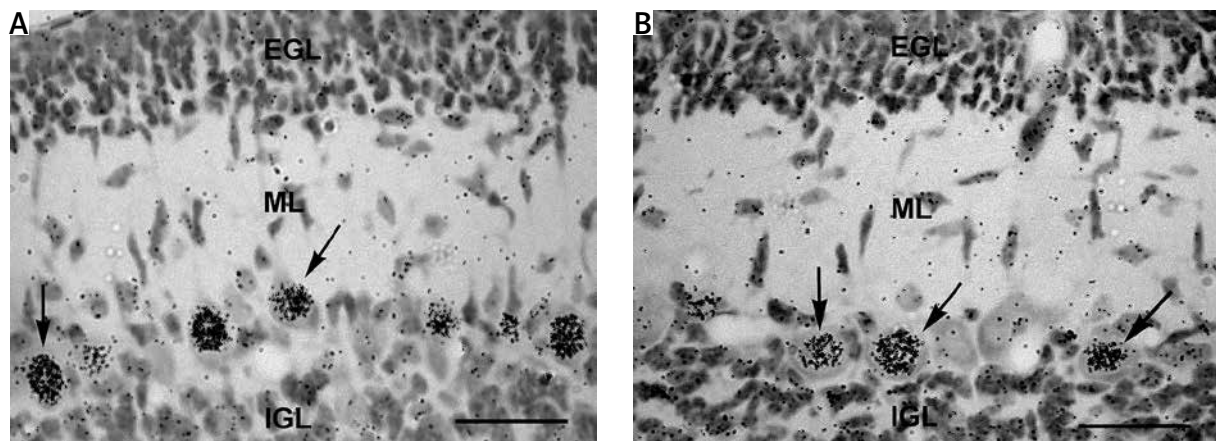


Fig. 4. Representative photomicrograph at the level of the lingula (posterior lobe) from mice exposed to $[^3\text{H}]\text{TdR}$ on E12-13 (A) or on E13-14 (B) and killed at P7. Note that many Purkinje cells are labeled on E12-13, while on E13-14 the percentage of tagged cells declines reflecting the production of postmitotic neurons by their precursor cells. EGL – external granular layer, ML – molecular layer, IGL – internal granular layer. Arrows show examples of Purkinje cell labeled. Scale bars: 30 μm .

man primates [34]. In mice, this event has been analyzed with contradictory results [5,14,22]. The current study reveals that in mice collected at P2 or at P12, no tyrosine hydroxylase-reactive cells with signs of apoptosis were found in the SNc. We do not know the reasons for these discrepancies but they may derive from biological differences among the mice strains studied, e.g. Lieb *et al.* [22] utilized CBA/J, Blum [5] used F2 littermates from a C57Bl/6 X 129 cross breeding, and C57/bl and CD-1 are used by Jackson-Lewis *et al.* [14]. BALB/c, C57BL/6 and B6CBA-A^{w-j}/A hybrid stock are used in the present work.

From the present results, it is proposed that the naturally occurring DA-neuron apoptosis in the early postnatal life is an event that might be restricted to certain strains of mice. Another possibility is that the natural loss of DA cells occurs in all strains of mice but neurons die in some of these strains through a nonapoptotic mechanism. In this regard, there is evidence indicating that the nature of cell death in the SNc of the *weaver* homozygotes is not apoptotic [33,35]. This fact may be relevant to the pathogenesis of neurodegenerative diseases such as Parkinson's disease, in which the role of apoptosis has been questioned [41].

Apoptotic natural cell death in PCs

We show that PCs apoptosis occurs within the first postnatal week. Our data demonstrate that the most important number of apoptotic PCs was seen in the central lobe; this was followed by the posterior and anterior lobes and then by the inferior lobe. In addition, the estimated values of active caspase-3-immunoreactive PCs was lower than that of TUNEL positives nuclei, at all cerebellar cortex lobes examined. These results are in agreement with the findings from other investigations, which have shown that caspase-3 activation occurs early in the course of apoptosis and precedes DNA fragmentation [9,32,45]. Moreover, at the time of degeneration, we did not observe any differences in the cytoarchitecture of the cerebellar cortex at the light microscopic level, which suggests that the migration and settling of postmitotic PCs in the Purkinje cell layer was normal.

Generative timetables of PCs were inferred at the four, previously indicated, lobes through the antero-posterior axis of the cerebellar cortex. Our basic information is that the onset of PCs neurogenesis, its pattern of peaks and valleys, and its total span

were close between P4 and P7. The experiments using ³[H]TdR autoradiography were designed to answer the question of whether the PCs apoptosis in the early postnatal period is related to neurogenetic patterns. If apoptosis of PCs is random across age, there should be no significant differences in the neurogenesis of PCs between P4 and P7. On the other hand, if apoptosis is systematic across age, the neurogenetic patterns of PCs should be different at P4 with respect to P7. The data reported here support the first possibility; no divergences were seen in PCs time-of-origin profiles. To our knowledge, this is the first report that links PCs neurogenetic timetables with the naturally occurring neuronal death of these macroneurons.

This report indicates that the times of origin for a given PC may not predispose it to start a developmental program of cell death. The same may occur in other neurons of the cerebellar system, which would ensure the organization and refinement of corticonuclear circuits. In this way, there is evidence showing climbing-fiber elimination [12] and loss of young granule cells [24] in the developing cerebellum. Moreover, alteration of basal neuron death in the human cerebellar system may be involved in sudden unexplained perinatal death; previous studies have found defects in both PCs and inferior olivary nuclei neurons in victims of sudden intrauterine unexplained death and sudden infant death syndromes [21].

Acknowledgments

The author is very grateful to Drs. Shirley A. Bayer and Bernardino Ghetti for providing B6CBA-A^{w-j}/A hybrid stock mice.

Disclosure

Author reports no conflict of interest.

References

1. Altman J, Bayer SA. Development of the Cerebellar System: In Relation to its Evolution, Structure and Functions. CRC Press, Inc., Boca Raton 1997.
2. Ashwell K. Microglia and cell death in the developing mouse cerebellum. *Dev Brain Res* 1990; 55: 219-230.
3. Barde YA. Trophic factors and neuronal survival. *Neuron* 1989; 2: 1525-1534.
4. Bayer SA, Altman J. Directions in neurogenetic gradients and patterns of anatomical connections in the telencephalon. *Prog Neurobiol* 1987; 29: 57-106.

5. Blum M. A null mutation in TGF- α leads to a reduction in mid-brain dopaminergic neurons in the substantia nigra. *Nature Neurosci* 1998; 1: 374-377.
6. Burke RE. Ontogenic cell death in the nigrostriatal system. *Cell Tissue Res* 2004; 318: 63-72.
7. Clarke PGH. Neuronal death in the development of the vertebrate nervous system. *Trends Neurosci* 1985; 8: 345-349.
8. Collo G, Cavalleri L, Spano P. Structural plasticity in mesencephalic dopaminergic neurons produced by drugs of abuse: critical role of BDNF and dopamine. *Front Pharmacol* 2014; 5: 259.
9. Davoli MA, Fourtounis J, Tam J, Xanthoudakis S, Nichoson D, Robertson GS, Ng GY, Xu D. Immunohistochemical and biochemical assessment of caspase-3 activation and DNA fragmentation following transient focal ischemia in the rat. *Neuroscience* 2002; 115: 125-136.
10. Dekkers MP, Nikolettou V, Barde YA. Cell biology in neuroscience: death of developing neurons: new insights and implications for connectivity. *J Cell Biol* 2013; 203: 385-393.
11. Dikranian K, Ishimaru MJ, Tenkova T, Labruyere J, Qin YQ, Ikonomidou C, Olney JW. Apoptosis in the in vivo mammalian forebrain. *Neurobiol Dis* 2011; 8: 359-379.
12. Hashimoto K, Kano M. Functional differentiation of the multiple climbing fiber inputs during synapse elimination in the developing cerebellum. *Neuron* 2003; 381: 785-796.
13. Hsu SM, Soban E. Color modification of diaminobenzidine (DAB) precipitation by metallic ions and its application for double immunohistochemistry. *J Histochem Cytochem* 1982; 30: 1079-1082.
14. Jackson-Lewis V, Vila M, Djaldetti R, Guegan C, Liberatore G, Liu J, O'Malley K, Burke RE, Przedborski S. Development cell death in dopaminergic neurons of the substantia nigra of mice. *J Comp Neurol* 2000; 424: 476-488.
15. Janec E, Burke RE. Naturally occurring cell death during postnatal development of the substantia nigra of the rat. *Mol Cell Neurosci* 1993; 4: 30-35.
16. Jankowski J, Miething A, Schilling K, Baader SL. Physiological Purkinje cell death is spatiotemporally organized in the developing mouse cerebellum. *Cerebellum* 2009; 8: 277-290.
17. Jankowski J, Miething A, Schilling K, Oberdick J, Baader SL. Cell death as a regulator of cerebellar histogenesis and compartmentation. *Cerebellum* 2011; 10: 373-392.
18. Kalinichenko SG, Matveeva NY. Morphological characteristics of apoptosis and its significance in neurogenesis. *Neurosci Behav Physiol* 2008; 38: 333-344.
19. Kitao Y, Hashimoto K, Matsuyama T, Iso H, Tamatani T, Hori O, Stern DM, Kano M, Ozawa K, Ogawa S. ORP150/HSP12A regulates Purkinje cell survival: a role for endoplasmic reticulum stress in cerebellar development. *J Neurosci* 2004; 24: 1486-1496.
20. Kholodilov N, Yarygina O, Oo TF, Zhang H, Sulzer D, Dauer W, Burke RE. Regulation of the development of mesencephalic dopaminergic systems by the selective expression of glial cell line-derived neurotrophic factor in their targets. *J Neurosci* 2004; 24: 3136-3146.
21. Lavezzi AM, Corna MF, Repetti ML, Matturri L. Cerebellar Purkinje cell vulnerability to prenatal nicotine exposure in sudden unexplained perinatal death. *Folia Neuropathol* 2013; 51: 290-301.
22. Lieb K, Andersen C, Lazarov N, Ziener R, Urban I, Reisert I, Pilgrim C. Pre- and postnatal development of dopaminergic neuron numbers in the male and female mouse midbrain. *Dev Brain Res* 1996; 94: 37-43.
23. Linden R. The survival of developing neurons: a review of afferent control. *Neuroscience* 1994; 58: 671-682.
24. Lossi L, Mioletti S, Merighi A. Synapse-independent and synapse-dependent apoptosis of cerebellar granule cells in postnatal rabbits occur at two subsequent but partly overlapping developmental stages. *Neuroscience* 2002; 112: 509-523.
25. Lossi L, Gambino G. Apoptosis of the cerebellar neurons. *Histol Histopathol* 2008; 23: 367-380.
26. Madolosso SH, Pérez-Villegas EM, Armengol JA. Naturally occurring neuronal death during the postnatal development of Purkinje cells and their precerebellar afferent projections. *Brain Res Rev* 2005; 49: 267-279.
27. Martí J, Wills KW, Ghetti B, Bayer SA. Regional differences in the Purkinje cells settled pattern: a comparative autoradiographic study in control and homozygous weaver mice. *Exp Neurol* 2002; 175: 168-181.
28. Martí J, Wills KW, Ghetti B, Bayer SA. A combined immunohistochemical and autoradiographic method to detect midbrain dopaminergic neurons and determine their time of origin. *Brain Res Protoc* 2002; 9: 197-205.
29. Martí J, Santa-Cruz MC, Bayer SA, Ghetti B, Hervás JP. Purkinje cell age-distribution in fissures and in foliar crowns: a comparative study in the weaver cerebellum. *Brain Struct Funct* 2007; 212: 347-357.
30. Martí J, Santa-Cruz MC, Bayer SA, Ghetti B, Hervás JP. Generation and survival of midbrain dopaminergic neurons in weaver mice. *Int J Dev Neurosci* 2007; 25: 299-307.
31. Martí J, Santa-Cruz MC, Molina V, Serra R, Bayer SA, Ghetti B, Hervás JP. Regional differences in the vulnerability of substantia nigra dopaminergic neurons in weaver mice. *Acta Neurobiol Exp* 2009; 69: 198-206.
32. Mellios K, Zacharaki T, Sophou S, Latsari M, Antonopoulos J, Dinopoulos A, Parnavelas JG, Dori I. Natural and lesion-induced apoptosis in the rat striatum during development. *Brain Res* 2009; 1252: 30-44.
33. Migheli A, Piva R, Wei J, Attanasio A, Casolino S, Hodes ME, Dlouhy SR, Bayer SA, Ghetti B. Diverse cell death pathways result from a single missense mutation in weaver mice. *Am J Pathol* 1997; 151: 1629-1638.
34. Morrow BA, Roth RH, Redmond DE, Sladek JR, Elsworth JD. Apoptotic natural cell death in developing primate dopamine midbrain neurons occurs during a restricted period in the second trimester of gestation. *Exp Neurol* 2007; 204: 802-807.
35. Oo TF, Blazeski R, Harrison SM, Henchcliffe C, Mason CA, Roffler-Tarlov SK, Burke RE. Neuron death in the substantia nigra of weaver mouse occurs late in development and is not apoptotic. *J Neurosci* 1996; 16: 6134-6145.
36. Oo TF, Burke RE. The time course of developmental cell death in phenotypically defined dopaminergic neurons of the substantia nigra. *Dev Brain Res* 1997; 98: 191-196.

37. Oo TF, Kholodilov N, Burke RE. Regulation of natural cell death in dopaminergic neurons of the substantia nigra by striatal glial cell line-derived neurotrophic factor in vivo. *J Neurosci* 2003; 23: 5141-5148.
38. Oo TF, Marchionini DM, Yarygina O, O'Leary PD, Hughes RA, Kholodilov N, Burke RE. Brain-derived neurotrophic factor regulates early postnatal developmental cell death of dopamine neurons of the substantianigra in vivo. *Mol Cell Neurosci* 2009; 41: 440-447.
39. Oppenheim RW. Cell death during development of the nervous system. *Ann Rev Neurosci* 1991; 14: 453-501.
40. Oppenheim RW, Johnson JE. Programmed cell death and neurotrophic factors. In: *Fundamental Neuroscience*. Squire LR, Bloom FE, McConnel SK, Roberts JL, Spitzer NC, Zigmond JM (eds.). Elsevier Academic Press, San Diego 2003; 499-532.
41. Perry G, Nunomura A, Smith MA. A suicide note from Alzheimer disease neurons? *Nat Med* 1998; 4: 897-898.
42. Ries V, Cheng H-C, Baohan A, Kareva T, Oo TF, Rzhetskaya M, Bland RJ, During MJ, Kholodilov N, Burke RE. Regulation of the postnatal development of dopamine neurons of the substantia nigra in vivo by Akt/protein kinase B. *J Neurochem* 2009; 110: 23-33.
43. Sidman RL, Angevine JB, Taber-Pierce E. *Atlas of the Mouse Brain and Spinal cord*. Harvard University Press, Cambridge 1971.
44. Sulzer D, Surmeier DJ. Neuronal vulnerability, pathogenesis and Parkinson's disease. *Mov Disord* 2013; 28: 715-724.
45. Zacharaki T, Sophou S, Giannakopoulou A, Dinopoulos A, Antonopoulos J, Parnavelas JG, Dori I. Natural and lesion-induced apoptosis in the dorsal lateral geniculate nucleus during development. *Brain Res* 2010; 1344: 62-76.

Lhermitte-Duclos disease with neurofibrillary tangles in heterotopic cerebral grey matter

Daniel Rusiecki¹, Boleslaw Lach²

¹Department of Pediatrics, McMaster University, ²Department of Pathology and Molecular Medicine, McMaster University and Hamilton Health Sciences, Hamilton, Canada

Folia Neuropathol 2016; 54 (2): 190-196

DOI: 10.5114/fn.2016.60434

Abstract

We report a 46-year-old patient with Lhermitte-Duclos disease (LDD) who underwent a successful surgery but died of other causes four years later. The autopsy revealed Lhermitte-Duclos disease asymmetrically affecting both cerebellar hemispheres. The subcortical white matter of both cerebral hemispheres contained several foci of grey matter heterotopia. Only heterotopic neurons contained tau-positive neurofibrillary tangles (NFT), displaying characteristic ultrastructural features of paired helical filaments (PHF). Neither senile plaques nor NFTs were found in other areas of the central nervous system. The brain also showed other developmental abnormalities such as megalencephaly, numerous foci of meningeal glial heterotopia and multifocal telangiectasia. Although some of these findings were previously described in LDD, this is the first case of this disease with NFTs selectively accumulating in the neuronal heterotopic tissue.

Key words: Lhermitte-Duclos disease, grey matter heterotopia, neurofibrillary tangles, PTEN, macrocephaly.

Introduction

Lhermitte-Duclos disease (LDD), a disorder first described by French physicians Lhermitte and Duclos in 1920 [25], is a benign, slow growing dysplastic gangliocytoma of the cerebellum, characterized by replacement of the granule cell layer by abnormal granule and Purkinje like cells. The most frequent presenting signs and symptoms are megalencephaly, increased intracranial pressure, nausea, hydrocephalus, ataxia, gait abnormalities, and intermittent headaches, all of which are attributed to the mass effect [6,11,25]. Many cases are associated with a mutation in the phosphatase and tensin homolog or *PTEN* gene which is also involved in numerous

otherwise unrelated central nervous system abnormalities, namely Cowden syndrome [1,6,11], autism spectrum disorder [18], cerebral cortical dysplasia [11,30] and Bannayan-Riley-Ruvalcaba syndrome [30]. The presence of cortical heterotopia has been reported in a small number of LDD cases [3,5,17,32]. We describe a unique case of LDD with cerebral cortical heterotopic grey matter containing neurofibrillary tangles.

Clinical history and autopsy findings

This 42-year-old male with a large head and partial left ocular paresis since childhood, presented with headaches, neck pain, ataxia and signs of raised

Communicating author:

Boleslaw Lach, MD, PhD, Department of Pathology and Molecular Medicine, McMaster University, 237 Barton St. East, L8L 2X2 Hamilton (Ontario), Canada, e-mail: lach@hhsc.ca

intracranial pressure. Magnetic resonance imaging (MRI) scan showed left cerebellar mass and obstructive hydrocephalus. A ventriculo-peritoneal shunt was inserted. A posterior fossa craniectomy was carried out and multiple biopsies of the diffusely enlarged left cerebellar hemisphere were performed. Post-operatively the patient made a good recovery and returned to full employment until his sudden death from myocardial infarction and right parietal "stroke" four years later. He had no other significant past medical history. He was a university graduate and worked as an accountant. Post-mortem examination confirmed massive myocardial infarction with endocardial thrombi and systemic atherosclerosis.

The brain weighed 2,220 grams after formalin fixation. The combined weight of the cerebellum and brainstem was 250 grams. The left cerebellar hemisphere was enlarged and measured approximately 6.5 × 5.5 × 7.0 cm. The right (grossly normal) hemisphere measured 5.0 × 4 × 5.0 cm. The lateral and inferior aspects of the affected hemisphere displayed coarse, broad, firm and more numerous gyri, measuring from 5 to 10 mm in width. The brainstem was normal.

Coronal sections of the cerebral hemispheres confirmed a recent haemorrhagic infarct in the posterior parietal area. Both frontal lobes contained subcortical foci of heterotopic grey matter, each measuring approximately 2 cm in the largest diameter. Similar, smaller heterotopic nests were also present in the temporal and parietal lobes on each side.

Material and methods

Large hemispherical blocks of the cerebellum and frontal lobes as well as an additional set of brain tissue samples removed from all representative areas of the left cerebral hemisphere, were formalin fixed and routinely processed for paraffin embedding and staining with hematoxylin and eosin (H&E), Luxol Fast blue combined with Periodic Acid Schiff (PAS & LFB) as well as Kluver-Barrera method, and Palmgren stain for axons. Selected sections of the hippocampus, amygdala and frontal cortex with heterotopic foci were immunostained for Tau protein (Tau, rabbit polyclonal antibodies, 1 : 200), neurofilaments (NF, monoclonal antibody, 1 : 400), glial fibrillary acidic protein (GFAP, polyclonal antibody, 1 : 500) and ubiquitin (UBQ, 1 : 300), all from DAKO as previously reported [20,28]. Glutaraldehyde fixed biopsy specimen from the cerebellar tumour was routinely

processed for plastic embedding and ultrastructural study as previously reported [28]. Small fragments of heterotopic grey matter tissue in the frontal lobe were carefully removed from the large paraffin block, deparaffinised, washed in several changes of distilled water, post-fixed in 2% glutaraldehyde for 24 hrs, and re-embedded in epoxy-resin. Routinely stained thin sections were examined in a Phillips 200 electron microscope as previously reported [28].

Results

Microscopically, the cerebellar folia showed striking "inverted" architecture with a thickened molecular layer markedly enriched in the myelinated axons (Fig. 1). Normal Purkinje and granule cells were replaced by dysplastic ganglionic cells of various sizes, often reminiscent of abnormal Purkinje cells (Fig. 2A). Intermediate zones between the normal and abnormal cerebellar tissues showed gradual transitions of a steadily increasing number of large dysplastic cells replacing the small granule cells. Dysplastic areas showed rich vascularization and numerous interstitial vacuoles. Subcortical white matter was markedly reduced in volume and displayed loss of axons and myelin. Scattered intraparenchymal and meningeal vessels contained dusty mural calcifications. The dentate nucleus was abnormal in shape but otherwise not remarkable. The right cerebellar hemisphere contained several, small subpial foci of gangliocytoma composed of dysplastic neurons as well as a disorganized network of

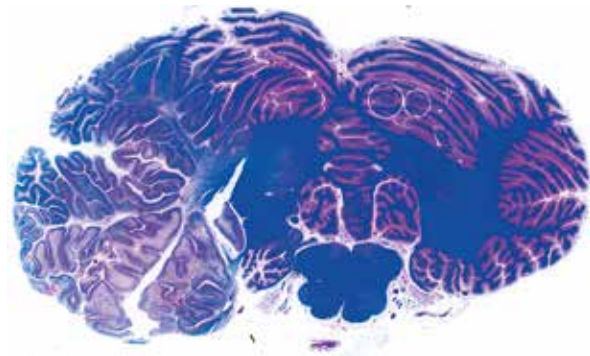


Fig. 1. Whole mount of cerebellum and brainstem showing massive enlargement of the left cerebellar hemisphere. Broadened and abnormal folia show myelination of the molecular layer and loss of myelin in the underlying white matter. Two independent small foci of gangliocytoma are present in the contralateral cerebellar hemisphere (encircled) (LFB&PAS stain).

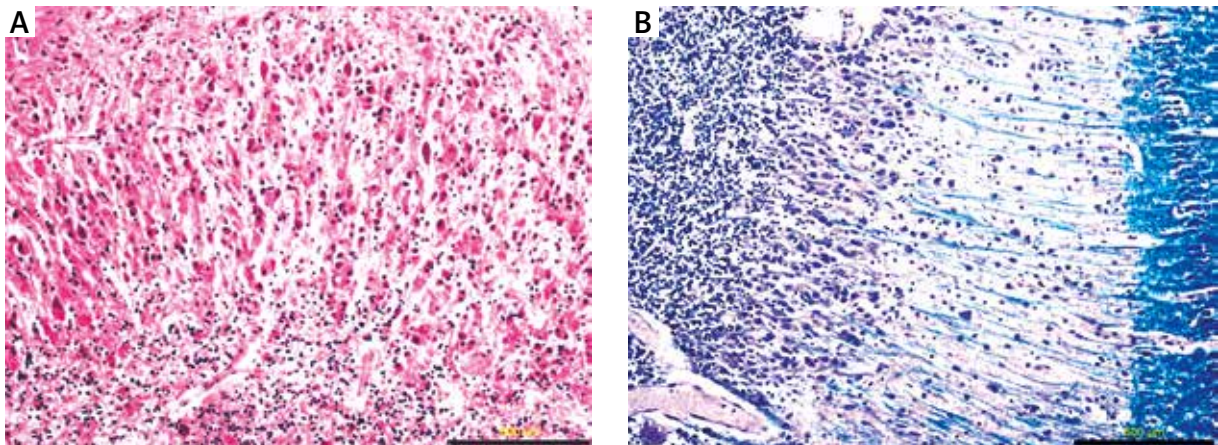


Fig. 2. Tumour in the left cerebellar hemisphere. Replacement of the molecular and Purkinje cell layers by dysplastic neurons (A). Contralateral hemisphere. Dysplastic ganglionic cells streaming from the Purkinje cells layer to the molecular layer. Granule cells are reduced in number. The broad band of subpial myelination of the molecular layer is on the right hand side.

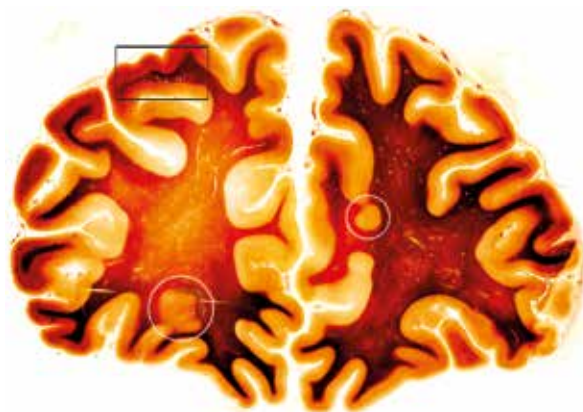


Fig. 3. Palmgren stain of the whole mount of frontal lobes. Subcortical foci of heterotopic grey matter in each hemisphere (encircled). Marked area in the left superior frontal gyrus contains capillary telangiectasia illustrated in Figure 6. The white matter of both lobes displays increased vascular markings due to a large number of telangiectatic capillaries.

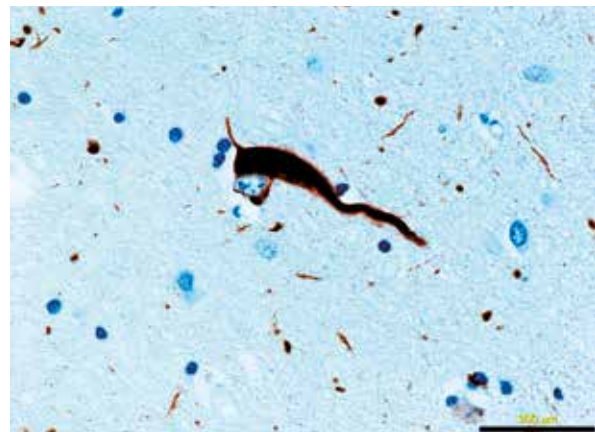


Fig. 4. Tau positive neurofibrillary tangle and multiple neuritic threads in the neuropil of heterotopic grey matter tissue from the frontal lobe.

myelinated axons and glia. Many folia showed dysplastic neurons overlying depleted granule cells and accompanied by dense myelination of the molecular layer (Fig. 2B), a change indistinguishable from that in the contralateral, main tumour mass.

The heterotopic grey matter of the frontal lobes (Fig. 3) contained scattered neurons with neurofibrillary tangles (NFT) as well as neuritic threads, both strongly positive for Tau (Fig. 4) and UBQ. Electron microscopic examination revealed tight collections

of paired helical filaments (PHF) in the perikaryon and myelinated axons in the background (Fig 5A). They measured approximately 20 nm and displayed periodic constrictions (Fig. 5B). However, the diameters deviated upwards and downwards of these values, most likely due to suboptimal processing of the tissue. In addition, there was an almost equal number of long straight 15 nm tubules without constrictions (Fig. 5B). The neuropil of the heterotopic foci as well as the adjacent white matter displayed a moderate degree of gliosis. The cortex overlying heterotopia did not demonstrate architectural abnormalities. However, cortical disorganization with marked gliosis was present in the left superior and middle

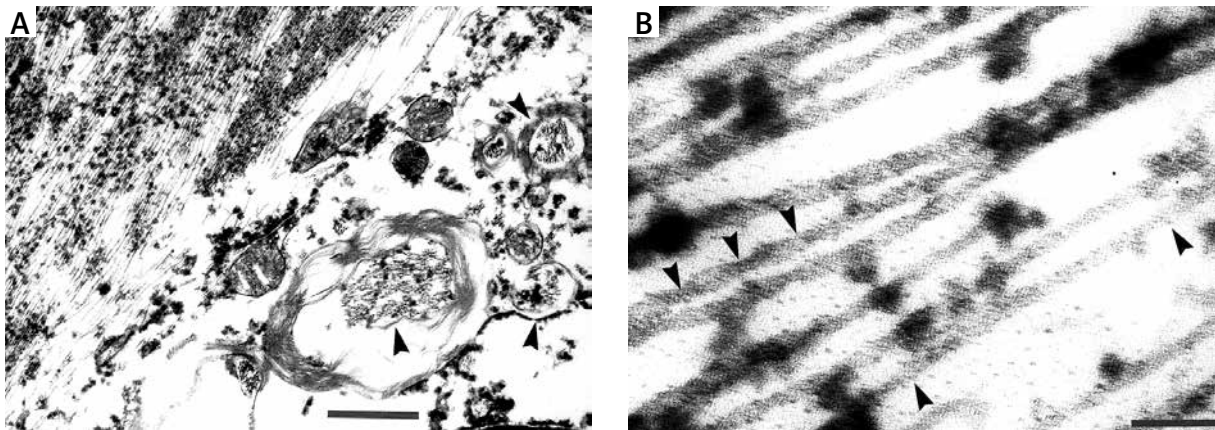


Fig. 5. Low power electron micrographs showing accumulation of paired helical filaments in neurofibrillary tangle. Arrows point to myelinated axons filled with PHFs. Bar = 250 nm (A). High power view of neurofibrillary tangle showing twisted filaments (three arrows pointing downwards) and straight filaments (two arrows). Bar = 65 nm (B).

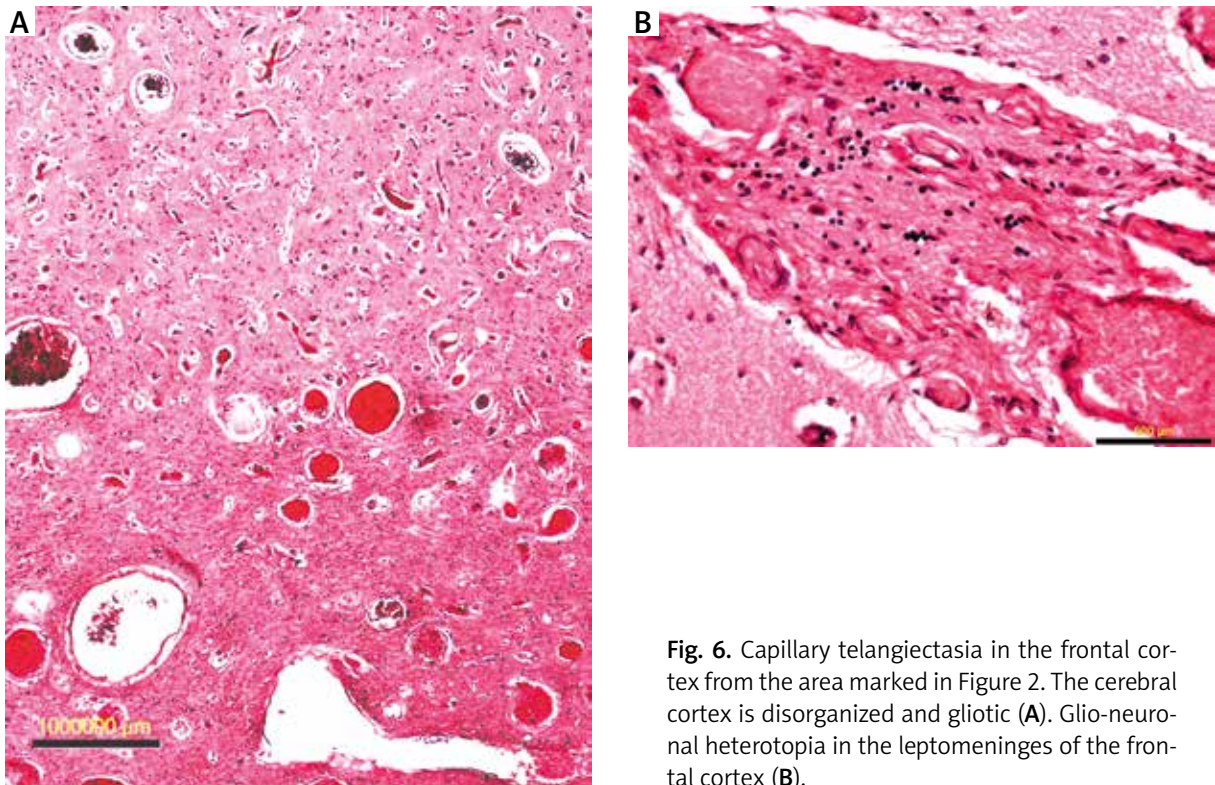


Fig. 6. Capillary telangiectasia in the frontal cortex from the area marked in Figure 2. The cerebral cortex is disorganized and gliotic (A). Glio-neuronal heterotopia in the leptomeninges of the frontal cortex (B).

frontal gyri involved by capillary telangiectasia (Fig. 6A). An increased number of telangiectatic capillaries was noticeable in the white matter of both cerebral and cerebellar hemispheres. Meningeal nests of heterotopic, glio-neuronal and glial tissue were very frequent in all cerebral cortical areas (Fig. 6B) as well as in the leptomeninges overlying the non-tumorous

cerebellar folia. There was no evidence of NFTs, amyloid angiopathy or senile plaques in any other part of the brain, including hippocampal formations. Re-examination of the surgical specimen of the tumour biopsy revealed no PHFs in the neuronal or glial cells. The tumour tissue was not available for additional molecular or immunohistochemical testing.

Discussion

Lhermitte-Duclos disease is characterized by thickened cerebellar folia due to replacement of the granule cell layer by enlarged neurons of various sizes, most often reminiscent of Purkinje cells [10,25]. Other key features include the absence or reduction in numbers of Purkinje and granule cells, and myelination of the molecular layer, creating appearance of inverted folia. The lack or very low proliferative activity indicates that LDD may represent a malformation rather than the tumour [25]. However, progression to malignant and other benign tumours such as anaplastic ganglioglioma [36] and DNET [24] has been reported in a few cases. The new tumour is usually discovered many years after the initial LDD diagnosis [24,36].

Most cases of LDD present unilaterally, with no preference of side. However, bilateral LDD has been reported in five patients [5,7,32,34,39]. Four cases exhibited large bilateral lesions [7,32,34,39], the other had foci of LDD-like changes such as inverse myelination and dysplastic changes in the contralateral hemisphere [5]. Our case was similar to the latter, displaying several small nests of gangliocytic tumour and multifocal aberrant myelination of the molecular layer in the contralateral hemisphere.

Lhermitte-Duclos disease is often associated with macrocephaly and other developmental abnormalities such as subcortical grey matter heterotopia, meningeal glial heterotopia and vascular malformations [25]. Macrocephaly is found in approximately half of LDD cases and is usually present in other PTEN-related conditions such as Bannayan-Ruvalcaba-Riley syndrome [14,25]. However, this number may be higher as Mary Ambler suggested that isolated macrocephaly might be a sign of subclinical LDD [3]. Leptomeningeal glial nests result from an over-migration of glia beyond the pia limitans to the subarachnoid space [8,12]. Experimental studies have revealed that these heterotopia occur after damage to the pial basal lamina [23]. Physical injury to the pial basal lamina during the development, or the dysfunctions as well as deficiencies of proteins comprising the basal lamina, such as laminin, can result in an over-migration of glia [23]. To our best knowledge, there is no known link between LDD or PTEN mutations and any of these conditions. However, PTEN mutations are associated with a high rate of vascular malformations [37] and several studies demonstrated cavernous and venous angiomas [22] as well

as other developmental vascular abnormalities in LDD [2,27,41]. An association of this mutation with LDD may explain striking hypervascularisation of gangliocytomas observed in one large study [1], and possible contribution to the widespread presence of telangiectasias in our patient. Multifocal, clinically silent cerebral subcortical grey matter heterotopia is the most unique finding among the constellation of brain abnormalities in our patient. Cortical heterotopia is a malformation caused by an arrest in neuronal migration from the ventricular zone in the developing brain [4,38]. Heterotopia are often associated with malformations in the overlying cortex that may display dyslamination and the presence of abnormal neurons [38]. Lhermitte-Duclos disease and other diseases with heterotopic grey matter or other forms of aberrant neuron migration, share many features such as formation of dysplastic and hypertrophic neurons [19,21], as well as predisposition to megalencephaly in carriers [31].

The presence of Tau-positive neuritic threads and neurofibrillary tangles (NFT) with the ultrastructural PHF characteristics has not been reported in association with LDD. Paired helical filaments in this patient were present only in the heterotopic neurons and not detected in the neoplastic cells or glia in the biopsy tissue, or any other part of the post-mortem brain. Although tau-positive neurons have been found in other forms of cortical dysplasia [16], tau immunoreactivity does not infer presence of NFTs or PHFs [9]. Hyperphosphorylated tau NFTs are typically associated with Alzheimer's disease [40]. They may also develop at any age in other unrelated conditions such as subacute sclerosing panencephalitis, ALS, certain heavy metal poisoning, dementia pugilistica, Down syndrome, tuberous sclerosis [15,40] and gangliogliomas [26]. It is unknown if the etiological factors responsible for the given disease are also responsible for the production of PHF or whether the environment of chronically diseased brain predisposes to NFT formation [40]. It has been suggested that the presence of NFT-like inclusions in neurons in cortical dysplasia could be secondary to pre-existing cytoskeletal abnormalities [16]. Sen *et al.* [33] reported absence of NFTs in paediatric cases with cortical dysplasia, while older patients with similar cortical anomalies had classical NFTs. Therefore, it is very plausible that abnormal neurons in dysplastic foci are much more prone to degeneration and premature aging than histologically normal neurons [33].

Lhermitte-Duclos disease is genetically linked to a mutation in PTEN, which acts as a tumour suppressor protein for diverse pathways. The defective function of PTEN can cause excessive mTOR activation that can lead to cell proliferation, hypertrophy, and improper migration [19]. Disrupting PTEN in the cerebellum and cortex of murine models created pathology resembling human LDD and cortical dysplasia, respectively [19,21]. This model had all the features of LDD with hypertrophic neurons, loss of Purkinje cells, and symptoms of increased intracranial pressure [19]. The development of NFT in conjunction with LDD can also be traced to the PTEN pathway. However, the mechanisms that cause dysplastic neurons to accumulate NFTs are uncertain [29]. A study by Griffen *et al.* [13] has revealed a negative correlation between PTEN levels and the severity of tau tangles in AD brains. It has been subsequently confirmed that PTEN accumulates in NFTs, most likely as a consequence of deregulation of downstream signalling and nuclear dysfunction of PTEN in AD neurons [35]. Unfortunately, this is an archival case from the period when molecular studies for detection of this mutation were unavailable and possible relation between occurrence of NFT and PTEN gene mutation in our patient remains unknown.

Disclosure

Authors report no conflict of interest.

References

- Abel TW, Bake SJ, Fraser MM, Tihan T, Nelson JS, Yachnis AT, Bouffard JP, Mena H, Burger PC, Eberhart CG. Lhermitte-Duclos disease: a report of 31 cases with immunohistochemical analysis of the PTEN/AKT/mTOR pathway. *J Neuropathol Exp Neurol* 2005; 64: 341-349.
- Akiyama Y, Ikeda J, Ibayashi Y, Nonaka T, Asai Y, Houkin K. Lhermitte-Duclos disease with cervical paraspinal arteriovenous fistula. *Case report. Neurol Med Chir* 2006; 46: 446-449.
- Ambler M, Pogocar S, Sidman R. Lhermitte-Duclos disease (granule cell hypertrophy of the cerebellum) pathological analysis of the first familial cases. *J Neuropathol Exper Neurol* 1969; 28: 622-647.
- Barkovich JA, Kuzniecky RI. Gray matter heterotopia. *Neurology* 2000; 55: 1603-1608.
- Beuche W, Wickboldt J, Friede RL. Lhermitte-Duclos disease – it's minimal lesions in electron microscope data and CT findings. *Clin Neuropathol* 1983; 2: 163-170.
- Boonpipattanapong T, Phuenpathom N, Mitarnun W. Cowden's syndrome with Lhermitte-Duclos disease. *Br J Neurosurg* 2005; 19: 361-365.
- Bozbuga M, Gulec I, Suslu HT, Bayindir C. Bilateral Lhermitte-Duclos disease. *Neurol India* 2010; 58: 309-311.
- Choi BH, Matthias SC. Cortical dysplasia associated with massive ectopia of neurons and glial cells within the subarachnoid space. *Acta Neuropathol* 1987; 73: 105-109.
- Duong T, De Rosa M, Poukens V, Vinters H, Fisher R. Neuronal cytoskeletal abnormalities in human cerebral cortical dysplasia. *Acta Neuropathol* 1994; 87: 493-503.
- Eberhart C, Wiestler O, Eng C. Cowden disease and dysplastic gangliocytoma of the cerebellum/Lhermitte-Duclos disease. In: WHO Classification of Tumours of the Central Nervous System. Louis D, Ohgaki H, Wiestler O, Cavenee W (eds.). 1st ed. IARC, Lyon 2007; pp. 226-228.
- Elia M, Amato C, Bottitta M, Grillo L, Calabrese G, Esposito M, Carotenuto M. An atypical patient with Cowden syndrome and PTEN gene mutation presenting with cortical malformation and focal epilepsy. *Brain Dev* 2012; 34: 873-876.
- Golden J. Lissencephaly, Type II (Cobblestone). In: Pathology and Genetics: Developmental Neuropathology. Golden J, Harding B (eds.). 1st ed. ISN Press, Basel 2004; pp. 42-46.
- Griffin R, Moloney A, Kelliher M, Johnston J, Ravid R, Dockery P, O'Connor R, O'Neill C. Activation of Akt/PKB, increased phosphorylation of Akt substrates and loss and altered distribution of Akt and PTEN are features of Alzheimer's disease pathology. *J Neurochem* 2005; 93: 105-117.
- Haskins Olney A. Macrocephaly syndromes. *Sem Pediatr Neurol* 2007; 14: 128-135.
- Hirano A, Tuazon R, Zimmerman HM. Neurofibrillary changes, granulovacuolar bodies and argentophilic globules observed in tuberous sclerosis. *Acta Neuropathol* 1968; 1: 257-261.
- Kakita A, Kameyama S, Hayashi S, Masuda H, Takahashi H. Pathologic features of dysplasia and accompanying alterations observed in surgical specimens from patients with intractable epilepsy. *J Child Neurol* 2005; 20: 341-350.
- Klisch J, Juengling F, Spreer J, Koch D, Thiel T, Buchert M, Arnold S, Feuerhake F, Schumacher M. Lhermitte-Duclos disease: assessment with MR imaging, positron emission tomography, single-photon emission CT, and MR spectroscopy. *AJNR Am J Neuroradiol* 2001; 22: 824-830.
- Kwon CH, Luikart BW, Powell CM, Zhou J, Matheny SA, Zhang W, Li Y, Baker SJ, Parada LF. PTEN regulates neuronal arborisation and social interaction in mice. *Neuron* 2006; 50: 377-388.
- Kwon CH, Zhu X, Zhang J, Knoop LL, Tharp R, Smeyne RJ, Eberhart CG, Burger PC, Baker SJ. Pten regulates neuronal soma size: a mouse model of Lhermitte-Duclos disease. *Nat Genet* 2001; 29: 404-411.
- Lach B, Joshi SS, Murty N, Huq N. Transformation of Merkel cell carcinoma to ganglioneuroblastoma in intracranial metastasis. *Human Pathol* 2014; 45: 1978-1981.
- Ljungberg MC, Sunnen CN, Lugo JN, Anderson AE, D'Arcangelo G. Rapamycin suppresses seizures and neuronal hypertrophy in a mouse model of cortical dysplasia. *Dis Model Mech* 2009; 2: 389-398.
- Lok C, Viseux V, Avril MF, Richard MA, Gondry-Jouet C, Deraumont H, Desfossez-Tribout C, Courtade S, Delaunay M, Piette F, Legars D, Dreno B, Saïag P, Longy M, Lorette G, Laroche L, Caux F.

- Brain magnetic resonance imaging in patients with Cowden syndrome. *Medicine* 2005; 84: 129-136.
23. Mooney SM, Siegenthaler JA, Miller MW. Ethanol induces heterotopias in organotypic cultures of rat cerebral cortex. *Cer Cortex* 2004; 14: 1071-1080.
 24. Nair P, Pal L, Jaiswal AK. Lhermitte-Duclos disease associated with dysembryoplastic neuroepithelial tumor differentiation with characteristic magnetic resonance appearance of "tiger striping". *World Neurosurg* 2011; 75: 699-703.
 25. Nowak DA, Trost HA. Lhermitte-Duclos disease (dysplastic cerebellar gangliocytoma): a malformation, hamartoma or neoplasm? *Acta Neurol Scand* 2002; 105: 137-145.
 26. Oberc-Greenwood MA, McKeever PE, Kornblith PL, Smith BH. A human ganglioglioma containing paired helical filaments. *Hum Pathol* 1984; 15: 834-838.
 27. Okunaga T, Takahata H, Nakamura M, Iwasaki K. A case report of Lhermitte-Duclos disease with systematic AVMs. *No To Shinkei* 2003; 55: 251-255.
 28. Omulecka A, Lach B, Alwasiak J, Gregor A. Immunohistochemical and ultrastructural studies of stromal cells in haemangioblastoma. *Folia Neuropathol* 1995; 33: 41-45.
 29. Ortiz O, Bloomfield S, Schochet S. Vascular contrast enhancement in Lhermitte-Duclos disease: case report. *Neuroradiology* 1995; 37: 545-548.
 30. O'Rourke DJ, Twomey E, Lynch S-A, King MD. Cortical dysplasia associated with the PTEN mutation in Bannayan Riley Ruvalcaba syndrome: a rare finding. *Clin Dysmorphol* 2012; 21: 91-92.
 31. Pang T, Atefy R, Sheen V. Malformations of cortical development. *Neurologist* 2008; 14: 181-191.
 32. Perez-Nunez A, Lagares A, Benitez J, Urioste M, Lobato RD, Ricoy JR, Ramos A, González P. Lhermitte-Duclos disease and Cowden disease: clinical and genetic study in five patients with Lhermitte-Duclos disease and literature review. *Acta Neurochir* 2004; 146: 679-690.
 33. Sen A, Thom M, Martinian L, Harding B, Cross JH, Nikolic M, Sisodiya SM. Pathological tau tangles localize to focal cortical dysplasia in older patients. *Epilepsia* 2007; 48: 1447-1454.
 34. Shanley DJ, Vassallo CJ. Atypical presentation of Lhermitte-Duclos disease: preoperative diagnosis with MRI. *Neuroradiol* 1992; 34: 103-104.
 35. Sonoda Y, Mukai H, Matsuo K, Takahashi M, Ono Y, Maeda K, Akiyama H, Kawamata T. Accumulation of tumor-suppressor PTEN in Alzheimer neurofibrillary tangles. *Neurosci Lett* 2010; 471: 20-24.
 36. Takei H, Dauser R, Su J, Chintagumpala M, Bhattacharjee MB, Jones J, Adesina AM. Anaplastic ganglioglioma arising from a Lhermitte-Duclos-like lesion. *J Neurosurg* 2007; 107: 137-142.
 37. Tan W-H, Baris HN, Burrows PE, Robson CD, Alomari AI, Mulliken JB, Fishman SJ, Irons MB. The spectrum of vascular anomalies in patients with PTEN mutations: implications for diagnosis and management. *J Med Genet* 2007; 44: 594-602.
 38. Thom M. Epilepsy Part I: Cortical Dysplasia. In: *Pathology and Genetics: Developmental Neuropathology*. Golden J, Harding B (eds.). 1st ed. ISN Press, Basel 2004; pp. 61-66.
 39. Tuli S, Provias JP, Bernstein M. Lhermitte-Duclos disease: literature review and novel treatment strategy. *Can J Neurol Sci* 1997; 24: 155-160.
 40. Wisniewski K, Jervis GA, Moretz RC, Wisniewski HM. Alzheimer neurofibrillary tangles in diseases other than senile and presenile dementia. *Ann Neurol* 1979; 5: 288-294.
 41. Wolansky LJ, Malant G, Heary R, Maniker AH, Lee HJ, Sharer LR, Patel UJ. Preoperative MRI diagnosis of Lhermitte-Duclos disease: case report with associated enlarged vessel and syrinx. *Surg Neurol* 1996; 45: 470-476.

Instructions to Authors

This instruction is based upon *Uniform Requirements for Manuscripts Submitted to Biomedical Reviews* (the complete document appears in *N Engl J Med* 1997; 336, 309-315).

Aims and scope

Folia Neuropathologica is an official journal of the Mossakowski Medical Research Centre Polish Academy of Sciences and the Polish Association of Neuropathologists. The journal publishes original articles and reviews that deal with all aspects of clinical and experimental neuropathology and related fields of neuroscience research. The scope of journal includes surgical and experimental pathomorphology, ultrastructure, immunohistochemistry, biochemistry and molecular biology of the nervous tissue. Papers on surgical neuropathology and neuroimaging are also welcome. The reports in other fields relevant to the understanding of human neuropathology might be considered.

Publication charge

Please note that there is an obligatory charge (25[^] Euro) for the manuscript being accepted for publication in *Folia Neuropathologica*. We send invoice for payment after the article is accepted for publication. There are no additional charges based on color figures or other elements.

Ethical consideration

Papers describing animal experiments can be accepted for publication only if the experiment conforms to the legal requirements in Poland as well as with the European Communities Council Directive of November 24, 1986 or the National Institute of Health Guide (National Institute of Health Publications No. 80-23, Revised 1978) for the care and use of Laboratory Animals for experimental procedure. Authors must provide a full description of their anesthetics and surgical procedures. Papers describing experiments on human subjects must include a statement that experiments were performed with the understanding and consent of each subject, with the approval of the appropriate local ethics committee.

Submission of manuscripts

Articles should be written in English. All new manuscripts should be submitted through the online submission at <http://panel2.termedia.pl/fn>

For authors unable to submit their manuscript online, please contact with Prof. E. Matyja, Editor-in-Chief of *Folia Neuropathologica*, ematyja@imdik.pan.pl

The Editorial Board reserves the right to reject a paper without reviewers' opinion if the content or the form of the paper does not meet minimum acceptance criteria or if the subject of the paper is beyond the aims and scope of the journal.

Legal aspects

In sending the manuscript the author(s) confirm(s) that (s)he has (they have) not previously submitted it to another journal (except for abstracts of no more than 400 words) or published it elsewhere. The author(s) also agree(s), if and when the manuscript is accepted for publication, to automatic and free transfer of copyright to the Publisher allowing for the publication and distribution of the material submitted in all available forms and fields of exploitation. The author(s) accept(s) that the manuscript will not be published elsewhere in any language without the written consent of the copyright holder, i.e. the Publisher.

All manuscripts submitted should be accompanied by an authors' statement including signed confirmation of the above and confirming that this publication has been approved by all co-authors (if any), as well as by the responsible authorities at the institution where the work has been carried out. The authors' statement should be signed by ALL co-authors. Additionally, the author(s) confirm(s) that (s)he is (they are) familiar with and will observe the "Instruction to Authors" included in *Folia Neuropathologica* and also that all sources of financial support have been fully disclosed. Materials previously published should be accompanied by written consent for reprinting from the relevant Publishers. In the case of photographs of identifiable persons, their written consent should also be provided. Any potential conflict of interest will be dealt with by the local court specific to the Publisher. Legal relations between the Publisher and the author(s) are in accordance with Polish law and with international conventions binding on Poland.

Authors agree to waive their royalties.

Anonymous review

All manuscripts will be subject to a process of anonymous editorial review.

Preparation of manuscripts

Articles must be written in English, with British spelling used consistently throughout. Authors not entirely familiar with English are advised to correct the style by professional language editors or native English speakers.

- The length of original article should not exceed 20 printed pages including text, illustrations, tables, and references.

- Manuscripts should be typed using 12pts.font, double-spaced, and fully corrected. Allow a margin at least 2.5 cm at the top, bottom and left side of the page. Text should not be justified.
- The title page should contain: the author's full names, title of the paper, all authors' affiliations, full name and address of the communicating author (including e-mail address and fax number), running title (not exceed 40 characters including spaces).
- The abstract should not exceed 350 words. A list of 3–10 key words is recommended below the abstract.
- The manuscript body should be organized in a standard form with separate sections: Introduction, Material and Methods, Results, Discussion, and References. Review articles should be divided into sections and subsections as appropriate without numbering.
- Do not underline in the text. Avoid footnotes.
- All dimensions and measurements must be specified in the metric system.
- The source of any drug and special reagent should be identified.
- Particular attention needs to be paid to the selection of appropriate analysis of data and the results of statistical test should be incorporated in the results section.
- The nomenclature used should conform to the current edition of the Nomina Anatomica or Nomina Anatomica Veterinaria.
- Acknowledgements should be made in a separate sheet following Discussion and before References. These should contain a list of dedications, acknowledgements, and funding sources.
- Legends of figures and tables should be typed on separate pages.
- The editor reserves the right to make corrections.

Tables

- Tables numbered in Roman numerals require a brief but descriptive heading.
- The major divisions of the table should be indicated by horizontal rules.
- Explanatory matter should be included in footnotes, indicated in the body of the table in order of their appearance.
- Tables must not duplicate material in the text or in illustration.

Illustrations

All figures should be supplied electronically at resolution 300dpi in all standard formats (tiff, jpg, Adobe Photoshop, Corel Draw, and EPS). Name your figure files with "Fig" and the figure number, e.g., Fig1.tif

- The maximum figure size is 84 mm or 174 mm for use in a single or double column width, respectively.
 - When possible, group several illustrations on one block for reproduction. Like all other figures, block should be prepared within a rectangular frame to fit within a single or double column width of 84 and 174 mm, respectively, and a maximum page height of 226 mm.
 - Each figure should include scale magnification bar; do not use magnification factors in the figure legends.
 - All figures, whether photographs, graphs or diagrams, should be numbered using Arabic numerals and cited in the text in consecutive numerical order
 - **Immunohistochemical study requires color illustrations of very good quality. The papers with white and black immunohistochemistry will not be accepted.**
 - **For the paper accepted before 01.04.2016 the publication charge includes only the expense of color illustrations.** The cost of color print for every successive 8 pages is 200 euro irrespective of the number of color pages, i.e., the price remains the same whether there is one or eight pages.
- The Publisher makes out the bill to the communicating Author.

References

The list of references (written on a separate page) should include only those publications that are cited in the text. Avoid citation of academic books, manuals and atlases. References may be arranged alphabetically and numbered consecutively. References should be given in square brackets with no space between the comma and the consecutive number, e.g. [3,4,6-12].

References should be written as follows:

Journal papers: initials and names of all authors, full title of paper, journal abbreviation (according to Index Medicus), year of publication, volume (in Arabic numerals), first and last page (example below):

1. Valverde F. The organization of area 18 in the monkey. *Anat Embryol* 1978; 154: 305-334.
2. Uray NJ, Gona AG. Calbindin immunoreactivity in the auricular lobe and interauricular granular band of the cerebellum in bullfrogs. *Brain Behav Evol* 1999; 53: 10-19.

Book and monographs: initials and names of all authors, full title, edition, publisher, place, year (examples below):

1. Pollack RS. Tumor surgery of the head and neck. Karger, Basel 1975.
2. Amaral DG, Price JL, Pitkanen A, Carmichael ST. Anatomical organization of the primate amygdaloid complex. In: Aggleton JP (ed.). *The amygdala*. Wiley-Liss, New York 1992; pp. 1-66.

Reference to articles that are accepted for publication may be cited as „in press” or Epub.

Proofs

Corrections to the proofs should be restricted to printer's errors only; other alterations will be charged to the authors. In order to maintain rapid publication, proofs should be returned within 48 hours, preferably by e-mail, fax or courier mail. If the Publisher receives no response from the authors after 10 days, it will be assumed that there are no errors to correct and the article will be published.

Subscription information

The journal is published in one volume per year consisting of four numbers. The annual subscription price is 160 PLN for Institutions from Poland and 80 PLN for individual subscribers from Poland and 140 Euro for foreign Institutions and 70 Euro for foreign individual subscribers.

Payment should be made to:

Termedia sp. z o.o., ul. Kleeberga 8, 61-615 Poznan
BZ WBK III O/Poznan PL 61 1090 1359 0000 0000 3505 2645
SWIFT: WBKPPLPP

The publisher must be notified of a cancellation of a subscription not later than two months before the end of the calendar year. After that date the subscription is automatically prolonged for another year.

Publishing, Subscription and Advertising Office:

TERMEDIA Publishing House
ul. Kleeberga 2
61-615 Poznan, Poland
phone/fax +48 61 822 77 81
e-mail: termedia@termedia.pl
<http://www.folianeuro.termedia.pl>

Folia

Neuropathologica



AUTHOR'S STATEMENT

Title of the article

.....

.....

.....

The author(s) hereby confirm(s) that:

- The above-mentioned work has not previously been published and that it has not been submitted to the Publishers of any other journal (with the exception of abstracts not exceeding 400 words).
- All co-authors named and the relevant authorities of the scientific institutions at which the work has been carried out are familiar with the contents of this work and have agreed to its publication.
- In sending the manuscript together with illustrations and tables agree(s) to automatic and free transfer of copyright to the Publisher allowing for the publication and distribution of the material submitted in all available forms and fields of exploitation, without limits of territory or language, provided that the material is accepted for publication. At the same time the author(s) accept(s) that the submitted work will not be published elsewhere and in whatever language without the earlier written permission of the copyright holder, i.e. the Publisher.
- (S)he (they) agree to waive his(her)(their) royalties (fees).
- (S)he (they) empower(s) the Publisher to make any necessary editorial changes to the submitted manuscript.
- All sources of funding of the work have been fully disclosed.
- The manuscript has been prepared in accordance with the Publisher's requirements.
- (S)he (they) is (are) familiar with the regulations governing the acceptance of works as published in *Folia Neuropathologica* and agree(s) to follow them.
- (S)he (they) agree to accept appropriate invoice from the Publisher in case colour illustrations are implemented.

Date

Signatures of **all authors**

The covering letter formula can be found at: www.folianeuro.termedia.pl

-The covering letter should be sent to Associate Editor:

Milena Laure-Kamionowska

-Editorial Office of Folia Neuropathologica

Mossakowski Medical Research Centre, Polish Academy of Sciences

Poland Medical Research Centre

ul. Pawinskiego 5

02-106 Warszawa, Poland

CONTENTS

Can neurodegenerative disease be defined by four 'primary determinants': anatomy, cells, molecules, and morphology?_89

Richard A. Armstrong

High expression of DNA methyltransferases in primary human medulloblastoma_105

Tímea Pócza, Tibor Krenács, Eszter Turányi, János Csáthy, Zsuzsanna Jakab, Peter Hauser

Assessment of candidate immunohistochemical prognostic markers of meningioma recurrence_114

Tamás Csonka, Balázs Murnyák, Rita Szepesi, János Bencze, László Bognár, Álmos Klekner, Tibor Hortobágyi

Ultrastructural pathology of human peritumoural oedematous cerebellar cortex_127

Orlando José Castejón

Survival in the pre-senile dementia frontotemporal lobar degeneration with TDP-43 proteinopathy: effects of genetic, demographic and neuropathological variables_137

Richard A. Armstrong

The topography of cortical microbleeds in frontotemporal lobar degeneration: a post-mortem 7.0-tesla magnetic resonance study_149

Jacques De Reuck, Florent Auger, Nicolas Durieux, Vincent Deramecourt, Claude-Alain Maurage, Florence Lebert, Didier Leys, Charlotte Cordonnier, Florence Pasquier, Régis Bordet

Potent effects of alkaloid-rich extract from *Huperzia selago* against sodium nitroprusside-evoked PC12 cells damage via attenuation of oxidative stress and apoptosis_156

Anna Magdalena Lenkiewicz, Grzegorz Arkadiusz Czapski, Henryk Jęsko, Anna Wilkaniec, Wojciech Szypuła, Agnieszka Pietrosiuk, Aneta Marta Uszynska, Agata Adamczyk

Effects of diclofenac sodium on the hippocampus of rats with acute subdural hematoma: histological, stereological, and molecular approach_167

Aysin Pinar Türkmen, Suleyman Kaplan, Abdurrahman Aksoy, Berrin Zuhâl Altunkaynak, Kıymet Kübra Yurt, Ebru Elibol, Cengiz Çokluk, Mehmet Emin Onger

Natural apoptosis in developing mice dopamine midbrain neurons and vermal Purkinje cells_180

Joaquín Martí-Clua

Lhermitte-Duclos disease with neurofibrillary tangles in heterotopic cerebral grey matter_190

Daniel Rusiecki, Boleslaw Lach